



International Conference on Nuclear Energy Technologies and Sciences (2015)

15-16 October 2015

ISSN 2413-5453



**ICoNETS Conference Proceedings
International Conference on Nuclear Energy Technologies
and Sciences (2015), Volume 2016**

Conference date: 15–16 October 2015

Location: Bali, Indonesia

Editors: Geni Rina Sunaryo, Julwan Hendry Purba, Ir. I Nyoman Budiarsa

Sponsors: Engie, Westinghouse, Rosatom, Pt kogas driyap konsultan, Pt unitama analitika perkasa, Nucadvisor

Published: 21 September 2016

ISSN: 2413-5453

Copyright © 2016 Knowledge E. All rights reserved.

This is a set of conference proceedings published in the series "KnE Energy." All articles are open access articles distributed under the terms of the latest Creative Commons Attribution License, which permits unrestricted use and redistribution provided that the original author and source are credited.

ICoNETS Conference Proceedings

Editor

1. **Dr. Geni Rina Sunaryo**, (National Nuclear Energy Agency of Indonesia, BATAN)
2. **Dr. Julwan Hendry Purba**, ST, M.App.IT, (National Nuclear Energy Agency of Indonesia, BATAN)
3. **Ir. Tagor Malem Sembiring** (National Nuclear Energy Agency of Indonesia, BATAN)
4. **Dr. Deendarlianto**, ST, M.Eng. (Gajah Mada University)
5. **Ir. I Nyoman Budiarsa**, M.T., Ph.D. (Udayana University)
6. **Prof. I Nyoman Suprpta Winaya**, Ph.D. (Udayana University)
7. **Prof. Dr.Ing. Nandy Putra** (University of Indonesia)
8. **Prof. Dr.Eng. Zaki Su'ud** (Bandung Institute of Technology)
9. **Dr. rer.nat. Ayi Bachtiar**, S.Si (Padjajaran University)
10. **Prof. T.M. Indra Mahlia** (University of Technology Malaysia)
11. **Dr. Frederik Reitsma** (South Africa)
12. **Dr. Gerd Brinkmann** (Germany)
13. **Dr. Marius Fox** (South Africa)
14. **Dr. Ir. Heri Suyanto** (Udayana University)
15. **Dr. Ni Nyoman Rupiasih**, S.Si., M.Si (Udayana University)

Organized by:

1. National Nuclear Energy Agency of Indonesia, BATAN
2. Udayana University
3. HIMNI

Committee:

1. Syaiful Bakhri, Ph.D
2. Mulya Juarsa, M.Sc
3. Drs. Sahala Maruli Lumban Raja
4. Topan Setiadipura, S.Si, M.Si
5. Marini Landina, SE
6. Sofia Loren Butar-Butar, ST
7. Anik Purwaningsih, S.Si
8. Dr. R. Mohammad Subekti
9. Ir. Sriyono
10. Restu Maerani, ST
11. Nurul Huda, S.Si
12. Helmi Setiawan, S.Sos
13. Drs. Heru Santosa

Sponsored by:

1. GOLD SPONSOR: ENGIE
2. WESTINGHOUSE
3. ROSATOM
4. PT KOGAS DRIYAP KONSULTAN
5. PT UNITAMA ANALITIKA PERKASA
6. NUCADVISOR

Table of Contents

EFFECT OF Ti-ION IMPLANTATION ON THE MECHANICAL AND CORROSION PROPERTIES OF THE FeCrNi SUPER ALLOY

Ari Handayani, Bernadus Bandriyana, Tjipto Sujitno, Arbi Dimyati

EFFECT OF β -QUENCHING ON OXIDATION RESISTANCE OF ZIRCONIUM ALLOY ZrNbMoGe FOR FUEL CLADDING MATERIAL

B. Bandriyana, M. Nevinggo, Abu Khalid R., A. Dimyati

EFFECT OF U- 99 Mo/AI FUEL DENSITIES ON NEUTRONIC AND STEADY STATE THERMAL HYDRAULIC PARAMETERS OF MTR TYPE RESEARCH REACTOR

Surian PINEM, Lily SUPARLINA, Tukiran SURBAKTI

THE EFFECT OF BORIC ACID ON CORROSION OF SS 304 AS PWR PRESSURIZER MATERIAL

Febrianto

FATIGUE STRENGTH EVALUATION OF PRESSURIZER WALL STRUCTURE IN PRESSURIZED WATER REACTOR

Roziq Himawan

STRENGTH BASED NUMERICAL APPROACH CONSTITUTIVE MATERIAL PREDICTION OF SPOT WELDED JOINTS OF STEEL

I Nyoman Budiarsa

EVALUATION OF OPERATING PERFORMANCE OF THE REACTOR COOLANT SYSTEM OF RSG-GAS USING CHEMCAD6.1.4

Sukmanto Dibyo, Ign.Djoko Irianto, Santosa Pujiarta

LOSS OF FLOW EVENT ANALYSIS OF THE RRI-50 CONCEPTUAL DESIGN

Endiah Puji Hastuti, Surip Widodo

COMPARISON OF UNCERTAINTY METHODS FOR PIPE DEFLECTION CALCULATION

Nursinta Adi Wahanani, Entin Hartini, Roziq Himawan

THE EFFECT OF TURBULENCE MODELS ON COOLANT TEMPERATURE AND VELOCITY FOR THE PEBBLE-BED TYPED HIGH TEMPERATURE REACTOR

Muhammad Subekti

PROPOSED TESTING QUALITY OF SILICON NITRIDE IN NUCLEAR APPLICATION BY CERAMOGRAPHY

Tjokorda Gde Tirta Nindhia

INVESTIGATION OF ROD CONTROL SYSTEM RELIABILITY OF PWR REACTORS

Deswandri and Syaiful Bakhri

RADIONUCLIDE DISPERSE TO ENVIRONMENT FROM PWR REACTOR ON SEVERE ACCIDENT CONDITION USING MACCS PROGRAM

Sri Kuntjoro, Pande Made Udiyani

APPLICATION OF TREND ANALYSIS METHOD FOR EMERGENCY RESPONSE IN NPP ACCIDENT

Pande M.U., Kuntjoro S.

EVALUATION OF RADIONUCLIDE RELEASE ESTIMATION OF POWER REACTOR USING SCDAP/RELAP

Jupiter Sitorus Pane, Surip Widodo

APPLICATION OF ^{99m}Tc RADIOISOTOPE IN DIAGNOSTIC PROCEDURES AND INTERNAL RADIATION DOSE ESTIMATION

Nur Rahmah Hidayati, Basuki Hidayat

PROBABILISTIC ANALYSIS ON LEVELIZED UNIT ELECTRICITY COST (LUEC) CALCULATION OF SMALL MEDIUM REACTOR NUCLEAR POWER PLANT (SMR NPP) IN INDONESIA

Nuryanti, Suparman

THE EFFECT OF HYDRAZINE ADDITION ON THE FORMATION OF OXYGEN MOLECULE BY FAST NEUTRON RADIOLYSIS

G.R. Sunaryo, S.L. Butarbutar

ANALYSIS ON THE CHANGE IN NEUTRONIC PARAMETERS DUE TO MISPOSITIONING OF FUEL IN THE AP1000 CORE

J. Susilo, I. Kuntoro, T.M. Sembiring

ANALYSIS OF DOPPLER REACTIVITY COEFFICIENT ON TYPICAL PWR-1000 CORE WITH MOX FUEL

Rokhmadi, Suwoto, Zuhair

SEQUENCE ANALYSIS AFTER CORE DAMAGE TO DETERMINE SAFETY LEVEL OF THE AP1000

D. T. Sony Tjahyani, Deswandri

FLEXBLUE® UNDERWATER REACTOR: INTRODUCTION TO THE CONCEPT AND TO THE PASSIVE SAFETY STRATEGY FOR A STEAM GENERATOR TUBE RUPTURE ACCIDENT

Vincent GOURMEL, Fabien PUC CETTI, François REVAUD

Preface

ICoNETS, an acronym for International Conference on Nuclear Energy Technologies and Sciences, is launched in line with the National Nuclear Energy Agency of Indonesia (BATAN) objectives to give researchers and professionals from universities, research institutions and nuclear related industries the opportunities to present their latest studies, excellent ideas and thoughts related to the development of nuclear energy technologies and it's social culture aspects. It also provides exciting opportunities to all possible stakeholders to amplify their active involvements in future nuclear power plant constructions in Indonesia.

ICoNETS2015 aims at providing an international forum that brings together those actively involved in the areas of interest to the development of nuclear energy system infrastructures and sites, nuclear reactor safeties and technologies, the development of renewable energy and energy conservation, and nuclear technologies in non-energy applications.

Through a peer – reviewed process, the editor of the ICoNETS2015 will decide which of the articles submitted to the conference should be accepted and published. Peer – reviewers evaluate manuscripts for their intellectual content without regard to race, gender, sexual orientation, religious belief, ethnic origin, citizenship, or political philosophy of the authors. For confidentiality reason, the editor and any editorial staff must not disclose any information about a submitted manuscript to anyone other than the corresponding author, reviewers, potential reviewers, other editorial advisers, and the publisher, as appropriate.



Conference Paper

Effect of Ti-Ion Implantation on The Mechanical and Corrosion Properties of The FeCrNi Super Alloy

Ari Handayani¹, Bernadus Bandriyana¹, Tjipto Sujitno², Arbi Dimiyati¹

¹Center for Science and Technology of Advanced Materials, BATAN, Indonesia

²Center for Accelerator Science and Technology, BATAN, Indonesia

Abstract

Ion implantation is widely used for surface treatment to modify the near surface properties of materials especially semiconductors without changing their bulk properties. In this work an investigation on the effect of implantation by Ti-ion on the mechanical properties and the wet corrosion of the high Cr and Ni content FeCrNi alloy was performed. Because of its superior properties this alloy is also well known as super alloy and often used as structure material in nuclear reactors. The alloy containing of 55.98 wt.% Fe , 23.46 wt.% Cr, 18.23 wt.% Ni and small amount of other metal elements, was fabricated in BATAN Bandung. The alloy sample was subjected to Ti-ion implantation in anion generator with theoretical doses varied between 0.89×10^{16} , 2.68×10^{16} , 3.58×10^{16} and 10.75×10^{16} ion/cm² respectively. The hardness measurement was conducted with Vickers method and the corrosion resistance test was carried out in the borax acid (HBO₃) environment. The microstructure of the material after implantation was characterized and analyzed by means of the Scanning Electron Microscopy (SEM) equipped with the Energy Dispersive X-Ray Detector (EDX) while the surface crystal structure was identified using X-Ray Diffraction (XRD). The result showed that the Ti implantation improved the surface hardness when the dose was higher than 3.58×10^{16} ion/cm², while the corrosion resistance increased abruptly at all ion doses. However, no microstructure change could be observed on the cross section. A thin layer which is indicated by BSE image contrast was observed in the top most surface. Analysis on the EDS spectrum revealed that the layer could be considered to be the titanium oxide elucidating the increasing of hardness and exceptionally higher resistance to wet corrosion.

Keywords: Ti-Implantation, FeCrNi super alloy, hardness, corrosion resistance, SEM, EDX, XRD.

Corresponding Author: Ari Handayani; email: arihandayani@batan.go.id

Received: 29 July 2016

Accepted: 21 August 2016

Published: 21 September 2016

Publishing services provided by Knowledge E

© Ari Handayani et al. This article is distributed under the terms of the [Creative Commons Attribution License](#), which permits unrestricted use and redistribution provided that the original author and source are credited.

Selection and Peer-review under the responsibility of the ICoNETS Conference Committee.

OPEN ACCESS

1. Introduction

Ion implantation is applied for modification of material surfaces where no change of final dimension allowed. But historically ion implantation has been especially used for doping semiconductor materials because it allows reaching a high impurity filling factor in an irradiated matrix beyond the equilibrium limit of impurity solubility

compared to conventional technique such as high temperature diffusion technique [1]. It can also provides controllable synthesis of metal or semiconductor nanoparticles (NPs) at various depths under the substrate surface.

Today the mechanism of ion implantation is well establish as indicated by a large number of publication [2, 3]. However, most of them used light atoms as implanted ions. It is widely accepted by many researchers, that due to high acceleration energy the ion implantation causes both impurity incorporation and material defect or amorphization. These could lead to changing of chemical and physical properties of material in the near surface. In most cases defects can be healed by annealing at high temperature [4]. Didyk et al. used deuterium ion implantation by low energy ion irradiation beam line technique to create high hydrogen concentration in the subsurface area of some pure metals (Cu, Zr, Pd, Ti, V) and Pd-alloys [5]. They observed nanosized defects on all samples as revealed by small angle X-ray scattering. Nitrogen or other ions can be implanted into a tool steel target. The structural change caused by the implantation produces a surface compression in the steel, which prevents crack propagation and thus makes the material more resistant to fracture. The chemical change can also make the tool more resistant to corrosion. In some applications, for example prosthetic devices such as artificial joints, it is desired to have surfaces very resistant to both chemical corrosion and wear due to friction. Ion implantation is used in such cases to engineer the surfaces of such devices for more reliable performance. As in the case of tool steels, the surface modification caused by ion implantation includes both a surface compression which prevents crack propagation and an alloying of the surface to make it more chemically resistant to corrosion.

Little publication about the implantation of heavy atoms such as Ti on steel or high alloyed steel. [6] studied surface modification of austenitic stainless steel by titanium ion implantation using RBS and GDOES at ion dose $2.3\text{-}5.4 \times 10^{16}$ ion/cm² and ion energy between 60 and 90 keV. The result revealed increasing of surface hardness and maximum Ti concentration in 30 – 50 nm depth at highest energy. All of the samples show increasing wear resistance due to formation of oxide layer on top surface. No information, however, about the microstructure change of the implanted sample was reported. Improved corrosion resistance in acid solution has been observed by Feng et al. in their investigation on the 316L stainless steel implanted by Ti ion at dose 2×10^{17} ion/cm² and accelerating energy up to 80 kV [7]. XPS measurement showed projected range R_p of Ti atom at the distance of 12 nm beneath the surface. But SEM image on top view revealed the severe surface roughing due to mechanical destruction of ion bombardment especially at high ion energy. Gaguk et al. reported about the implantation of stainless steel AISI 410 with TiN [8]. The study observed higher corrosion resistance in acidic solution. It showed maximum hardness at dose 10.75×10^{16} ion/cm² but no information about the Ti composition in the sample and the surface microstructure change after implantation.

In this work, ion implantation was performed on FeCrNi alloy by Ti-ion which aimed to modify surface properties of the alloy enhancing the corrosion behaviour in extrem environment especially in nuclear facilities. The stress of the work is put on the observation of structural changes and their characterization. Super alloys based on FeCrNi exhibit superior mechanical and oxidation properties at high temperature suitable for application in many field. However for application as structural material in

nuclear facilities the alloy must full fill additional requirement namely its resistance under corrosive environment.

2. Experimentals

The materials used in this work were Cr and Ni rich super alloy developed and manufactured at the center for Science and Technology of Advanced Materials PSTBM-BATAN in framework of the national program on experimental power reactor research as reported previously [9]. The chemical composition of the alloy was examined using optical emission spectroscopy (OES) and is shown in Table 1.

element	Fe	Ni	Cr	Si	Mn	C	Ti	V	Sn	P
weight %	55.98	18.32	23.46	2.55	0.075	0.073	0.003	0.037	0.006	0.002

TABLE 1: Chemical composition of used materials.

Prior to ion implantation the materials are cut to 10x10x5 mm of diameter using high precision disc cutter and subjected to grinding using sand papers down to 2000 roughness grade and fine polishing with 0,1 um diamond paste. The ion implantation is performed with ion energi 100 keV at current 20 μ A for 60, 90, 120 and 180 minutes. Ion dosis applied were calculated using the formula $D = I t / e A$, I = current, t = exposure time, e = electron charge ($1,602 \times 10^{-19}$ coulomb) and A = implant area, giving dosis 0,89 $\times 10^{16}$ ion/cm², 2,68 $\times 10^{16}$ ion/cm², 3,58 $\times 10^{16}$ ion/cm² and 10.75 $\times 10^{16}$ respectively.

After implantation the samples were transfered for hardness measurement and wet corrosion test. The Hardness was examined using micro hardness tester Shimadzu each on at least 3 position. Wet corrosion is performed using EG & G Potensiostat/ Galvanostat with the parameters; Area = 1 cm², Eq Weight = 23.38 g and density = 7.98gm/cm³. A sample coin of 1 cm of diamater and 2 mm of thickness was cut from bulk material in order to fit in the sample holder. Microstructural and chemical composition of the implanted area were examined using SEM JEOL JSM-6510LA equipped with energy dispersive X-ray detector (EDX). SEM investigation is performed at constant electron eceleration voltage 20 keV and standard work distance 10 mm fitted to EDX requirement. The imaging detector used backscattered electrons to capture phase sensitive BSE image helpfull in distinguishing between two or more in composition different thin layer. Short but basic explanation of SEM analysis was reported elsewhere [10]. For X-ray diffraction (XRD) measurement XD-610, Shimadzu was used to study the crystallographic structures of the samples. Parameter used were target Cu-K α , low angle : 20, high angle : 100, preset time : 1.0 s dan step width : 0.05 deg/step. Phase identification was approximated with help of RIETAN method.

3. Result and Discussion

Figure 1 shows the result of hardness measurement. The hardness is nearly constant over the applied ion doses which is about 140 HV25. However it slightly increases after implantation at dose higher than 3.58 $\times 10^{16}$ ion/cm² and becomes 180 HV25 at dose 10.75 $\times 10^{16}$ ion/cm². This can be concluded that at acceleration energy of

100 keV the implantation by Ti-ion can affect the mechanical property of high Cr and Ni content FeCrNi alloy only if high dosis applied. The cause of this behaviour is unclear. Possible explanations were twofold, firstly that even at the energy of 100 keV the implantation for short time were to low for Ti-ion to break the potential barrier for a penetration into the crystall lattice due the density and composition of the alloy. The Ti atoms then form very thin layer, may be consisting of some atom monolayer, which under measurement micro hardness test condition can not detectable. The total hardness were determined by the hardness of material substrate. Secondly, the increase of the hardness at high dose, therefore, simply might be related with the Ti enrichment under the sample surface which occurs when the availability of the Ti high enough due to long implantation time. This stand in fully aggreement with the measurement of [6], who confirmed this correlation. However the result of earlier study of Jatisukamto et al. about TiN implantation on AISI 410 showed continuous increasing of hardness at lower dosis which decreased at high dosis [8]. This defference might be caused by the role of much smaller Nitrogen atoms.

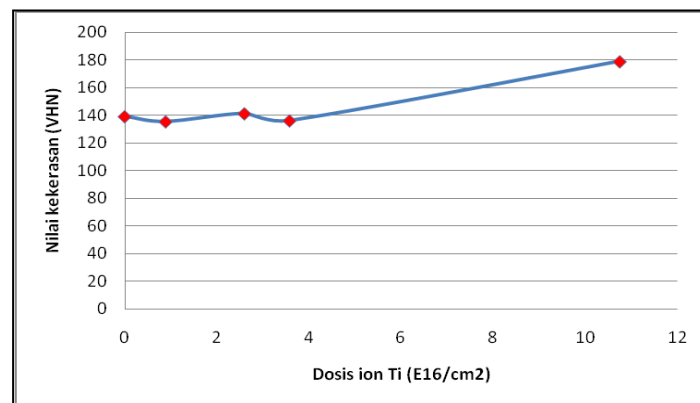


Figure 1: Hardness as a function of ion dosis.

Figure 2 shows the SEM image of the sample cross section after implantation at highest dose 10.75×10^{16} ion/cm² and its corresponding EDX spectrum taken from the near surface area as directed by arrow. The EDX spectrum indicates the existent of Ti-rich layer on the alloy surface with exceptionally high carbon content. Total concentration of Ti is 0.06%. This value is near the detection limit of EDX measurement. From the SEM cross section it is hard to get a solid statement about the thickness of this layer because it is perfectly superimposed by the bright contrast due to the edge effect. Based on the element analysis of the EDX spectrum the authors assume the Ti rich layer might consist of Ti atom clusters or tiny Ti-carbides/oxides. This layer might contribute to the slight increase of hardness on the sample surface implanted at high dose as described above. The temperature during implantation was to low to produce sufficient potential different for running a diffusion of Ti atoms toward alloy matrix. On top of the sample the EDX measurement can not detect the Ti atoms, this is might be due to the vertical detection limit of EDX much lower than lateral one. It is obvious that the number of Ti atoms in cross sectional direction must be higher than those in vertical direction.

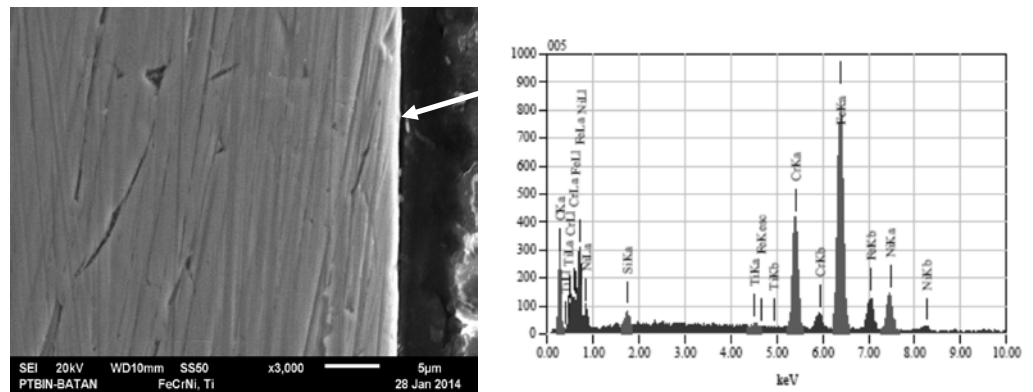


Figure 2: Cross-sectional SEM image of FeCrNi super alloy after Ti implantation at dose 10.75×10^{16} ion/cm² and corresponding EDX spectrum at position indicated by arrow.

XRD measurement confirmed the presence of Ti containing phase on the sample surface having FCC crystall structure after implantation at dose 10.75×10^{16} ion/cm² as can be seen in Fig. 3 right. From peak analysis it might be the titanium oxide of the type TiO₂.

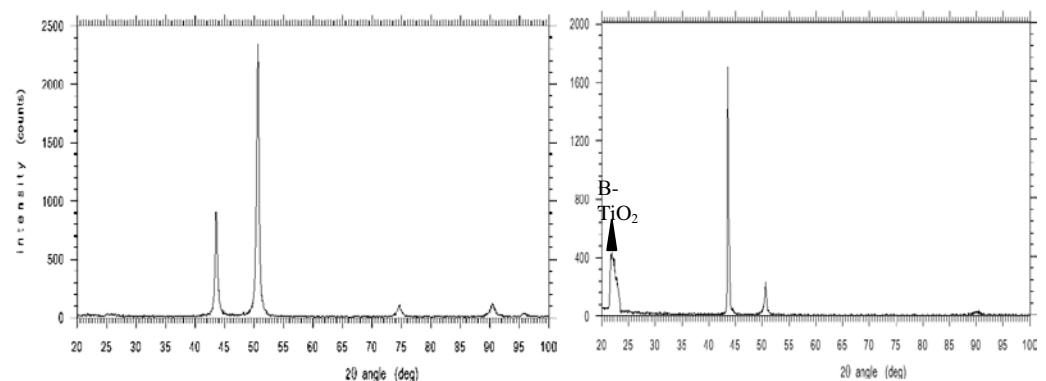


Figure 3: XRD diffraction spectrum of FeCrNi alloy before (left) and after Ti implantation (right).

The results of the wet corrosion are presented in figure 4. The corrosion rate significantly decreases as early as implantation conducted from the initial rate at 0,17 millimeter per-year (mpy) down to 0,01 mpy and remains nearly constant at all doses. This is almost 17 times of magnitude. It can be concluded that in contrast to the surface hardness, at the applied acceleration energy of 100 keV Ti implantation obviously increases the corrosion behaviour of the alloy surface for all dose applied. The sample surface become exceptionally resistant against corrosion attack. The independency of the corrosion rate on the applied dosis implies that the corrosion resistancy is pure surface effect. This stand in agreement to the SEM result as presented above. This effect is seem to be directly related with the presence of Ti rich layer on the surface. Ti build chemical barrier to the corrosion attack or mechanical effect, the impingement during implantation cause the surface damage increases the number of defects which modify its surface property as already discussed in earlier study of Feng et al. [7].

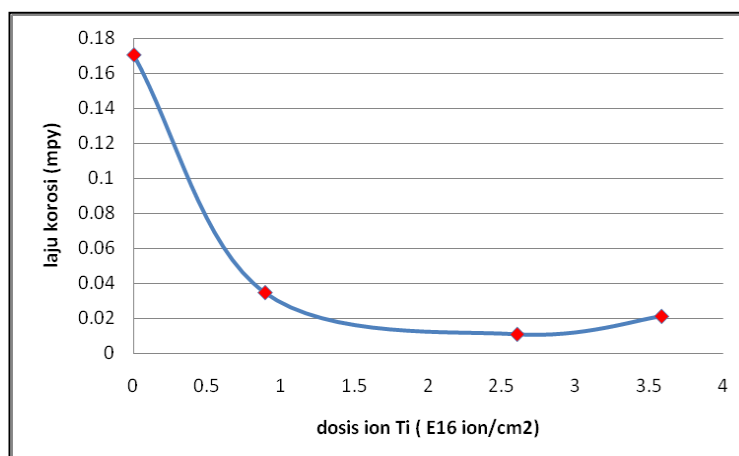


Figure 4: Corrosion rate as a function of ion dosis.

4. Conclusion

From the observation, there is no increasing of the surface hardness of high Cr and Ni content FeCrNi alloy after Ti ion implantation at lower dosis up to 3.58×10^{16} ion/cm². The hardness increase when the dose applied was higher than 10.75×10^{16} ion/cm². However, the corrosion resistance in acidic solution increased significantly and is not dependent to applied ion dosis. The depth profile of implanted Ti atoms could not measured in this study because of the detection limit of the used EDX technique. But in wide range the result stand in agreement with earlier studies.

5. Acknowledgment

The authors gratefully thanks to Center of Science and Technology of Advance Material for financial support, thanks to Sumaryo, Rohmad Salam and Agus Sujatna for technical support during this research.

References

- [1] A. L. Stepanov, Rev. Adv. Mater. Sci. 30 (2012) 150-165.
- [2] A. A. Youssef^a, P. Budzynski^b, J. Filiks^c, A. P. Kobzev^d, J. Sielanko^c, Vacuum, Vol. 77, Issue 1 (2004) P. 37-45.
- [3] N. Kumar, S. Kataria, S. Dash, S. K. Srivastava, C. R. Das, P. Chandramohan, A. K. Tyagi, K. G. M. Nair, Baldev Raj, Wear, Volumes 274-275, 27 January 2012, Pages 60-67.
- [4] D. P. Hickey, Diss, University of Florida (2007).
- [5] A. Yu. Didyk, R. Wiśniewski, K. Kitowski, V. Kulikauskas, T. Wilczynska, A. A. Shiryaev, Ya. V. Zubavichus, Depth concentrations of deuterium ions implanted into some pure metals and alloys.
- [6] P. J. Evans, J. Hyvarinen, M. Samandi, Surface and Coating Technology 71 (1995) 151-158.



- [7] K. Feng, X. Cai, Z. Li, P. K. Chu, *Mat. Letters* 68 (2012) 450-452.
- [8] G. Jatisukamto, V. Malau, M. N. Ilman, P. T. Iswanto, J. Ilmiah Teknik Mesin CakraM, Vol. 5, No.1 (2011) 14-19.
- [9] Effendi, N., *Urania*, 16(2), 2010.
- [10] A. Sujatno, R. Salam, B. Bandriyana, A. Dimiyati, *Studi Scanning Electron Microscopy (SEM) untuk Karakterisasi Proses Oksidasi Paduan Zirkonium*, Seminar Nasional X, SDM Teknologi Nuklir (2014).
- [11] M. Vigen Karimi, S. K. Sinha, D. C. Kothari, A. K. Khanna, A. K. Tyagi, *Surface and Coatings Technology* 158-159 (2004) 609-614.

Conference Paper

Effect of β -Quenching on Oxidation Resistance of Zirconium Alloy ZrNbMoGe for Fuel Cladding Material

B. Bandriyana¹, M. Nevinggo², Abu Khalid R¹, A. Dimiyati¹¹Center of Science and Technology for Advanced Material-BATAN, Puspiptek, Tangerang, Indonesia²Faculty of Science and Technology, Syarif Hidayatullah State Islamic University, Ciputat, Tangerang Selatan, Banten, Indonesia

Abstract


Effect of β -quenching of Zr-2.5Nb-0.5Mo-0.1Ge alloy used for advanced fuel cladding material of Pressurized Water Reactor (PWR) was investigated. The aim of this research is to improve the mechanical and corrosion properties through modification of the alloy with regard to high reactor burn up. The quenching process was conducted by heating the sample at temperature of 950 °C and soaking 2.5 hours, followed by quenching in water at room temperature and then continued with annealing process at 500 and 600°C. The change of hardness and oxidation resistance were characterized using optical microscope and scanning electron microscope (SEM). The effect on the oxidation resistance was investigated by the high temperature oxidation test using the MSB (Magnetic Suspension Balance) at 700 °C for 5 hours. The hardness increased from 217 VHN to 265 VHN after quenching due to grain refinement and precipitation hardening. The oxidation rate followed the typical parabolic growth characteristic. The formation of thin layer was considered to be a stable oxide ZrO₂ that influenced the oxidation characteristic and increasing the hardness of the alloy.

Keywords: cladding material, zirconium alloy, quenching, hardness, oxidation.

Corresponding Author:
B. Bandriyana, email:
bandri@batan.go.id

Received: 29 July 2016
Accepted: 21 August 2016
Published: 21 September 2016

Publishing services
provided by Knowledge E

 B. Bandriyana, et al.
Santosa Pujiarta. This article
is distributed under the terms
of the [Creative Commons
Attribution License](#), which
permits unrestricted use
and redistribution provided
that the original author
and source are credited.

Selection and Peer-review
under the responsibility of
the ICoNETS Conference
Committee.

 OPEN ACCESS

1. Introduction

The advanced fuel cladding materials based on ZrNbMoGe alloy which termed for high performance for reactor application with high burn up has been investigated at PSTBM-BATAN. The niobium containing zirconium alloy has been used successfully as fuel cladding material in Pressurized Water Reactor (PWR) typed nuclear power plant exhibiting high burn up [1]. Addition of Nb reduced the risk of nodular corrosion, decreased the hydrogen uptake and increased the ductility, toughness and creep resistance of the alloy [2, 3]. Molybdenum was also added to improve the hardness, phase homogeneity and corrosion resistance [4], while the addition of germanium was designed to improve the stiffness of the fuel cladding [5]. The investigation showed that the ZrNbMoGe alloy can satisfy the requirement of high material hardness and high oxidation resistance for application as reactor fuel cladding material [6]. However, a properly heat treatment process during in got production is necessary to carry out to improve the mechanical properties for subsequent manufacturing process. With regard to the workflow of fuel cladding material manufacturing both of quenching and annealing processes should be investigated [7].

Quench treatment of zirconium alloy was performed firstly by heating the material into the β -phase temperature ranges followed by rapid cooling into room temperature to produce a controlled precipitation during the subsequent aging. Based on the metallurgical consideration, during β -quenching zirconium alloy matrix transforms from a β -bcc phase to an α -hcp phase which obviously has different microstructure when treated at different cooling condition [8]. The change of microstructure was mostly indicated by the formation of a Wildman structure consisting of α -phase plates and the precipitation of small secondary phases in the grain boundaries [9]. The α to β allotropic transformation takes place at 865°C. β phase is stable up to 1860°C, while α phase exhibits strong anisotropy which plays an important role during deformation [10]. It was reported that new Nb containing Zirlo alloy is characterized by its single martensitic structure obtained by water quenching [10]. Further, β -quenching has also significantly improved the corrosion resistance of zirc alloy due to the existence of small second phase [10].

The temperature and time of the quenching and heat treatment process of the new. ZrNbMoGe alloy are the main parameter that needs further investigation. The aim of this work is to investigate the effect of β -quenching on Zr-2.5Nb-0.5Mo-0.1Ge alloy according to the microstructure, hardness and high temperature oxidation characteristics.

2. Experiments

As shown in flow chart in Fig. 1 (a) this work mainly contains the following activities: the material synthesis, the quenching and annealing, the hardness testing, oxidation experiment and the microstructure characterization. Fig. 1 (b) presents the quenching and annealing process diagrams. The annealing is performed at two different durations, 2 and 3 hours.

The ZrNbMoGe alloy was manufactured by melting of zirconium, niobium, molybdenum and germanium sponges using arc melting furnace in the argon atmosphere at temperature around 1850 °C. The mixture was 96.9 wt.%, 2.5 wt.%, 0.5 wt.%, 0.1wt.% for Zr, Nb, Mo and Ge respectively. Regarding to reach a homogeneous microstructure, the sample was remelted five times and slowly cooled in air to room temperature. The β -quenching was carried out by heating the samples 10°C/minutes, followed by soaking at 950 °C for 2.5 hours and immediately cooled in water. The sample was then annealed at 500°C and 600 °C for 2 hours to release the residual stress.

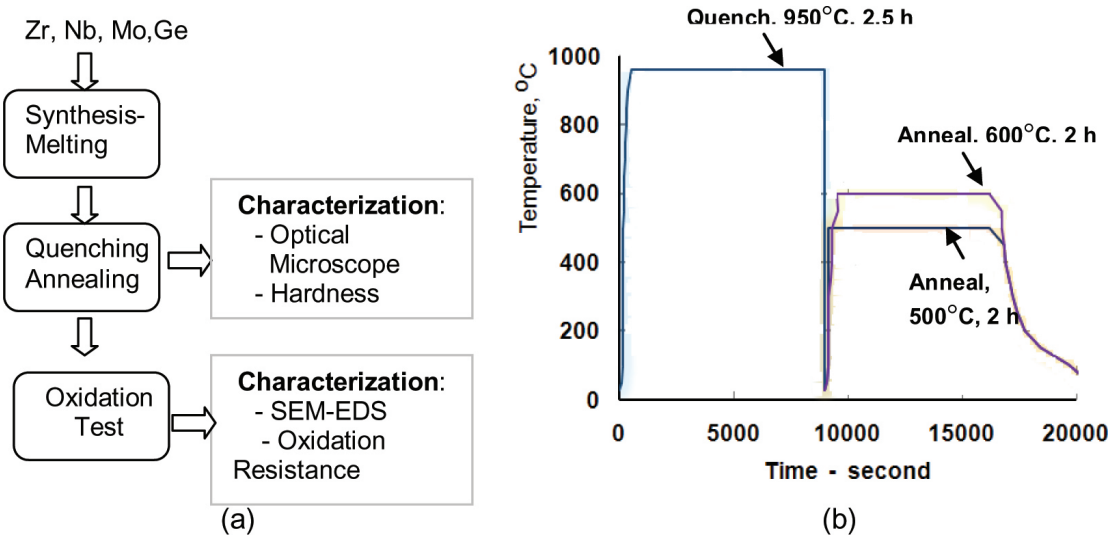


Figure 1: (a) Flow diagram and (b) quenching and annealing curve.

The sample preparation for micro structural analysis using optical microscope was performed by mechanical grinding and subsequent chemical etching in a solution of 5% H_2SO_4 , 10% HF, 30% HNO_3 and 55% H_2O by volume. The hardness measurement was carried out using Vickers Hardness tester with diamond indenter at applied load of 500 grams and indentation time 15 seconds. The high temperature oxidation test was performed in the Magnetic Suspension Balance (MSB) in the High Temperature Material Laboratory of PSTBM-BATAN. The oxidation test was carried out at temperature of 700 °C for 5 hours to simulate the operation temperature of PWR fuel cladding with the main interest on the investigation of the early stage of the oxidation. The MSB workstation consists mainly of alumina tube, electrical resistance furnace, temperature control and balancing measurement system equipped with suspension and holding magnet. The weight gains per unit area was measured in a fix time difference and displayed as characteristic oxidation curve. The sample cross section was observed using SEM JEOL JMS2605LV. For elemental analysis energy dispersive x-ray spectroscopy (EDX) attached on SEM was used.

3. Result and Discussion

The microstructures of ZrNbMoGe as cast ingot before and after quenching and annealing process taken by optical microscope are shown in Fig. 2.

The sample as cast is obviously martensitic and relatively has small amount bainitic structure due to high cooling rate after melting. The structure is homogenously distributed in

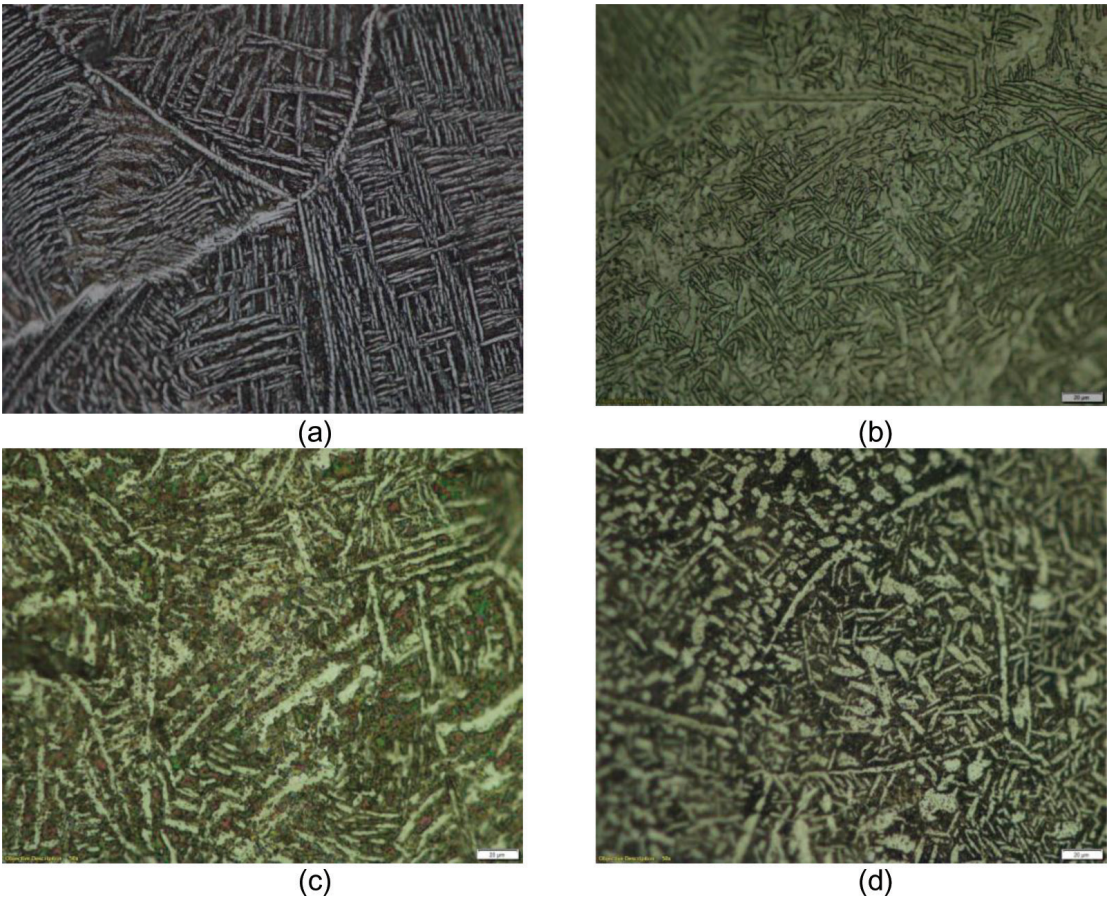


Figure 2: Microstructure of as cast in got (a), after quenching (b), after quenching continued with annealing 500°C – 2 hours (c) and 600°C – 2 hours (d).

the entire matrix volume with the characteristic lath martensite as commonly occur in Zr-Nb alloys [9,10]. After quenching, again the structure consists of martensite similar to those as cast but with more finer grains. The annealing process carried out after quenching causes a re-crystallization which leads to the grain coarsening as obvious in Fig. 2 (c) and (d). At higher annealing temperature the grain coarsening becomes faster. Previous investigation on the same alloy, the SEM-EDS analysis supported by the XRD analysis confirmed the presence of hard Zr-Ge precipitates in grains and grain boundaries [11]. This precipitation occurred during melting and significantly increase the hardness of the alloy. However, after quenching and annealing the precipitation hardening can not be observed. This could be due to applied temperature in this experiments which was lower than those during melting.

Fig. 3. shows the result of hardness measurement after and before treatment. The hardness increases significantly from 217 VHN as cast to 265 VHN after quenching process.

The change of hardness was considered to be mainly caused by the microstructure change as explained and shown above (Fig. 2). The annealing following quenching process decreases the hardness due to grain coarsening which is strongly depend on the temperature as seen in Fig.2 (c) and (d).

Figure 4 shows the oxidation characteristic curve of ZrNbMoGe in got before and after quenching and annealing process. The weight gains resulted from the oxidation in air are plotted as a function of the oxidation time.

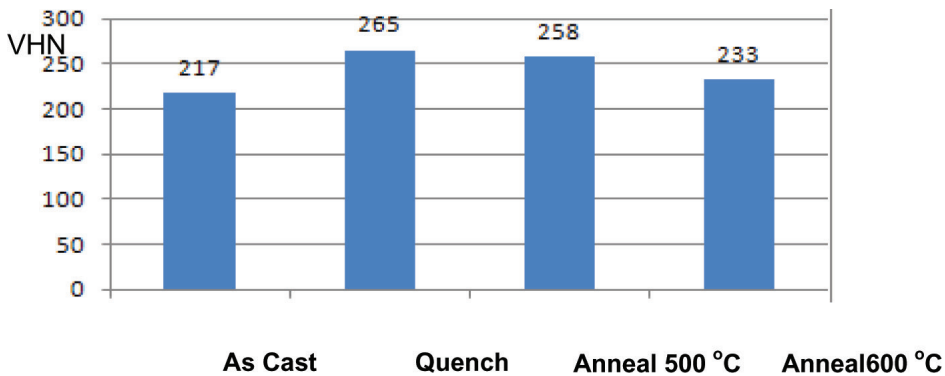


Figure 3: Hardness of ZrNbMoGe alloy before and after quenching-annealing.

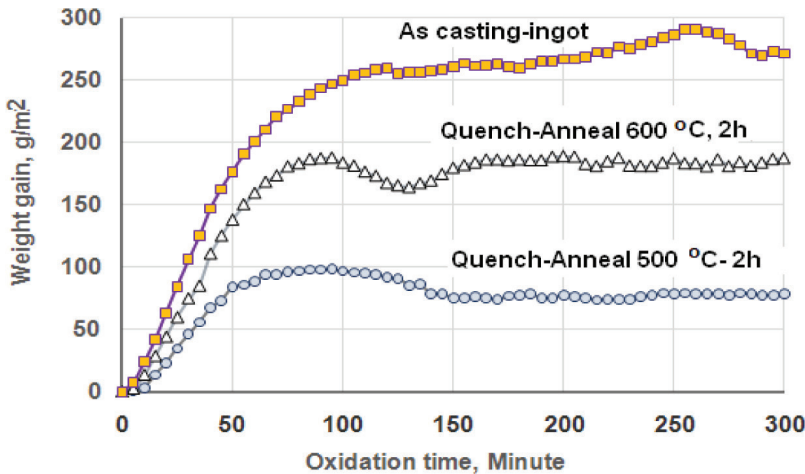


Figure 4: Oxidation characteristic curve of the ZrNbMoGe alloy oxidized in air at 700 °C.

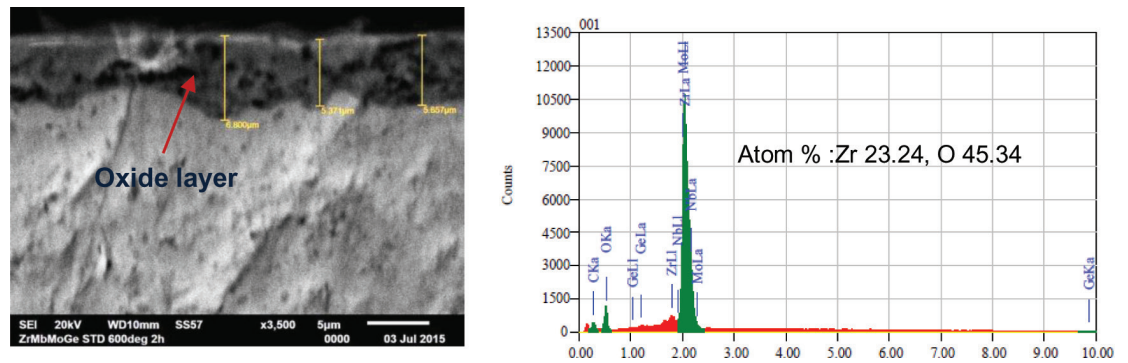


Figure 5: SEM cross section (a) and EDX spektrum (b) of ZrNbMoGe after quenching and annealing 500 °C and oxidized at 700 °C during 5 hours.

The oxidation rates of the three samples during heating up to 100 minutes follow a parabolic growth kinetics where the mass gain is proportional to the square root of time. The weight gains of all samples after 100 minutes oxidation become nearly constant. However, both samples after quenching and annealing show lower oxidation rate than those of ingot samples. Decreasing of the annealing temperature from 600 °C to 500 °C resulted in better oxidation rate, as observed by the weight gain change from 190 to 90 g/m². From the characteristic of parabolic kinetics, it is obvious that the oxide formation on the samples is oxygen inward diffusion driven process inside the oxide layer. This stands in agreement with the well known high temperature oxidation characteristics of zirconium alloy [12,13]. The mechanism of high-temperature oxidation of zirconium alloy is widely accepted to be the diffusion of oxygen anions through the ZrO₂ lattice [14,15]. The metal cations transport however is fully inhibited. The lower corrosion rate of the alloy after quenching and annealing process at the early stage of the oxidation can be considered to be caused by the effect of grain coarsening on the top most of the metal surface due to annealing which in turn decreases the number of oxide crystallites formed and so the possibilities of oxygen diffusion channeling between the oxide grains.

One result of the SEM-EDX measurements on the oxide scales formed during oxidation test, is shown in Fig. 5. On all examined specimens, the oxide layer remained on the surface. Based on the EDX result, the oxide layer was identified as zirconium-oxide ZrO₂.

After oxidation at 700 °C, SEM micrographs reveal the oxide layer thickness around 8 mm on the sample as cast and between 6 to 7 mm on the samples after quenching and annealing. These confirmed the result of oxidation measurements as discussed above (Fig. 4).

4. Conclusion

From this study, it can be concluded that quenching process increased the material hardness and decreased the oxidation during first stage of heating at 700 °C which is caused by the effect of grain refining during quenching and grain coarsening during annealing. This decreased the amount of oxygen diffusion channels and the oxide layer formed on the samples is a stable ZrO₂.

5. Acknowledgment

The authors would thank to Mr. Sumariyo, Mr. Rohmad Salam and Mr. Agus Sujatno for technical support during this research. This research has been financially supported by the SINAS Consortium 2014, the Ministry of Research and Technology of Indonesia.

References

- [1] Hyung Hoon Kim, et.al., "High-temperature Oxidation Behavior of Zircaloy-4 and Zirlo in Steam Ambient", *Journal of Material Science and Technology (JMST)*, Vol. 26, Issue 9, pp 827-832 (2010).
- [2] GuBeom Jeong, Yong Choi, Sun Ig Hong, "Mechanical Performance of Oxidized Zr-Nb-O Nuclear Cladding Tubes", *Journal of The Physics of Metals and Metallography*, Vol. 115, Issue 13, pp 1281-1284 (2014).
- [3] Sugondo, "Peningkatan Ketahanan Korosi Zircaloy-4 melalui Pemasu Timah, Tembaga dan Niobium", *Journal Teknologi Bahan Nuklir*, Vol. 7, No. 1, Januari (2010).
- [4] Yuant Tiando, Posman Manurung, Futichah, "Pengaruh Unsur Pemasu Mo dan Proses Fabrikasi Terhadap Kekerasan Plat Zirlo-Mo" *JURNAL Teoridan Aplikasi Fisika* Vol. 01, No. 01, Januari (2013).
- [5] Zhang Jinlong, et.al., "Germanium-containing zirconium-niobium alloy for fuel cladding of nuclear power station", Patent CN 102925750 A, China (2012).
- [6] B. Bandriyana, D. H. Prajitno, A. Dimiyati, "Effect of Copper Addition on the High Temperature Oxidation of Zirconium Alloy ZrNbMoGe for Advanced Reactor Fuel Cladding Material", *Advanced Materials Research*, Vol 896, pp. 617-620, February (2014).
- [7] Hans G. Weidinger, "Fabrication of Zirconium Alloy Cladding Tubes and Other Fuel Assembly Components for Water-Cooled Reactors", *Workshop on Modeling and Quality Control for Advanced and Innovative Fuel Technologies*, International Centre of Theoretical Physics, Trieste, 2005.
- [8] Tero Mangard, Ali R. Massih, "Modelling and Simulation of Reactor Fuel Cladding under Loss-of-Coolant Accident Conditions", *Journal of NUCLEAR SCIENCE and TECHNOLOGY*, Vol. 48, No. 1, p. 39-49 (2011).
- [9] Djoko Hadi Prajitno, Influence of β -quenching on The Microstructure and Microhardness of Zr₄-Nb Alloys, *International Conference on Advances in Nuclear Science and Engineering in Conjunction with LKSTN*, 351-354, (2007)
- [10] CHAI Lin Jang, LUAN Bai Feng, CHEN Jian Wei, ZHOU Jun, LIU Qing, "Effect of cooling rate on $\beta \rightarrow \alpha$ transformation during quenching of a Zr-0.85Sn-0.4Nb-0.4Fe-0.1Cr-0.05Cu alloy" *Journal of Science China Technological Sciences*, Vol. 55, Issue 10, pp 2960-2964, (2012).
- [11] Parikin, Andika Fajar, A.H. Ismoyo, B. Bandriyana, Neutron Diffraction Technique On The Structural Identification of ZrNbMoGe Alloy, *Proceedings of The International Conference on Materials Science and Technology, ICMST 2010*, 91-97, Center for Technology of Nuclear Industry Materials, 2011.
- [12] Hyun-Gil Kim, Il-Hyun Kim, Yang-Il Jung, Jeong-Yong Park And Yong-Hwan Jeong, Properties of Zr Alloy Cladding After Simulated Loca Oxidation And Water Quenching, *Nuclear Engineering And Technology*, Vol.42 No.2 April 2010.
- [13] M. Steinbruck, J. Birchley, A. V. Boldyrev, A. V. Goryachv, M. Grosse, T. J. Haste, Z. Hozer, High temperature oxidation and quench behavior of Zircaloy-4 and E110 cladding alloys, *Progress in Nuclear Energy* 52, 19-36, 2010.
- [14] Jong Hyuk Baek, Ki Bum Park, Yong Hwan Jeong, Oxidation kinetics of Zircaloy-4 and Zr-1Nb-1Sn-0.1Fe at temperatures of 700-1200C, *Journal of Nuclear Materials* 335 443-456, 2004.
- [15] M. Mihalache¹, V. Ionescu¹, T. Meleg¹, M. Pavelescu, Study of Microstructure of Oxidized Zr-2.5%Nb Subjected To Thermal Transient Treatments from, *Journ. Phys.*, Vol. 56, Nos. 7-8, P. 952-962, Bucharest, 2011



Conference Paper

Effect of U-9Mo/Al Fuel Densities on Neutronic and Steady State Thermal Hydraulic Parameters of MTR Type Research Reactor

Surian Pinem, Lily Suparlina, Tukiran Surbakti

Center for Technology and Safety of Nuclear Reactor, BATAN, Kawasan PUSPIPTK
Gd. No. 80 Serpong, Tangerang Selatan, 15310 Indonesia

Abstract

The objectives of this research work are to carry out a detailed neutronic and steady state thermal hydraulics analysis for a MTR research reactor fuelled with the low enrichment U-9Mo/Al dispersion fuels of various uranium densities. The high density uranium fuel will increase the cycle length of the reactor operation and the heat flux in the reactor core. The increasing heat flux at the fuel will causing increase the temperature of the fuel and cladding so that the coolant velocity has to be increased. However, the coolant velocity in the fuel element has a limit value due to the thermal hydraulic stability considerations in the core. Therefore, the neutronic and the steady state thermal hydraulic analysis are important in the design and operation of nuclear reactor safety. The calculations were performed using WIMS-D5 and MTRDYN codes. The WIMS-D5 code used for generating the group constants of all core materials as well as the neutronic and steady state thermal hydraulic parameters were determined by using the MTRDYN code. The calculation results showed that the excess reactivity increases as the uranium density increases since the mass of fuel in the reactor core is increased. Using the critical velocity concept, the maximum coolant velocity at fuel channel is 11.497 m/s. The maximum temperatures of the coolant, cladding and fuel meat with the uranium density of 3,66 g/cc are 70.85°C, 150.79°C and 153.24°C, respectively. The maximum temperatures are fulfilled the design limit so reactor has a safe operation at the nominal power.

Keywords: U-9Mo/Al dispersion fuel, MTR research reactor, critical velocity, high uranium density, MTRDYN

Corresponding Author: Surian Pinem, email:
pinem@batan.go.id

Received: 29 July 2016

Accepted: 21 August 2016

Published: 21 September 2016

**Publishing services
provided by Knowledge E**

© Surian Pinem et al. This article is distributed under the terms of the [Creative Commons Attribution License](#), which permits unrestricted use and redistribution provided that the original author and source are credited.

Selection and Peer-review under the responsibility of the ICoNETS Conference Committee.

OPEN ACCESS

1. Introduction

Conceptual design of innovative research reactor (RRI reactor) has been completed from aspect of neutronic and kinetic parameters [1-4]. Previous design reactor power is 20 MW (thermal), because the flux is too small so the reactor power increased to 50 MW (thermal). At the power of 50 MW with high uranium density, core power density becomes high so the active height of fuel is increased from 60 cm to 70 cm while the

other dimensions were remain fixed. RRI is a tank-in-pool type research reactor, a material testing reactor (MTR) with plate type of fuel elements and has a core grid position of neutron trap. The light water is used as the coolant and heavy water as reflector. The maximum thermal neutron flux at the reflector will be not less than $5 \cdot 10^{14} \text{n/cm}^2 \cdot \text{s}$.

RRI reactor is designed using compact core so that the heat transfer area and the amount of fuel are small, but heat flux at the fuel plate are high. Heat flux must be compensated by setting the coolant flow rate so that the reactor continued to operate safely. The flow rate of the cooling water through the channel of fuel plate is a very important parameter because instability and vibration can occur in the fuel [5]. Design criteria commonly used in determining the maximum flow rate of coolant flow is 2/3 of the critical velocity which is determined by the IAEA [6]. In this paper, the mass flow rate in the range of 750 – 900 kg/s will be analyzed.

The enhancement of cycle length of RRI reactor operation using high uranium density with the low enrichment uranium (LEU) affects neutronic and thermal hydraulic parameters. Therefore, the optimum parameter has to be obtained by varying the uranium densities of U-9Mo/Al fuel. In this work, the uranium density of the U-9Mo/Al fuel is varied for 3.66, 5.34 and 6.52 gU/cc.

The calculated neutronic parameters are excess reactivity, the maximum thermal flux, control rods worth, power peaking factor and power density. Those parameters are used for analysis of the steady state thermal hydraulic of RRI reactor. In the steady state thermal hydraulic, the temperatures of fuel, cladding and coolant are calculated. The saturation temperature of water, melting temperature of cladding as well as fuel meat are used as a limit value in optimize the parameters [8].

The WIMSD-5B code [9] is used for calculating group constants for different regions at the reactor core. Using the data from WIMSD-5B it will calculated the neutronic and steady state thermal hydraulic parameters using MTR-DYN code [9].

2. Methodology

RRI reactor has 25 core grid positions with a 5×5 core configuration. As seen in Figure 1, there are 16 standard fuel elements, 4 control rods and a central neutron flux trap position. A standard fuel contains 21 fuel plates while a follower fuel contains 15 fuel plates. The control rods are of follower type using material of AgInCd with composition of 80% Ag, 15% In, and 5% Cd. The shape of standard fuel, follower fuel and control rod are shown in Figures 2-4. In the design, the reactor might be added two safety rods if the shutdown margin of one stuck rod is less than $0.5\% \Delta k/k$. Previous research work found that the core using fuels with uranium densities of 5.34 gU/cc and 6.52 gU/cc must be added by the safety rods.

The cell calculations are carried out by using WIMS-D5 code with 69 neutron energy group of ENDF/B-VI library. The four energy groups formed are fast neutron region $0.821 \text{ MeV} < E \leq 10 \text{ MeV}$, slowing down region $5.53 \text{ keV} < E \leq 0.821, 0.625$ resonance region $< E \leq 5.53 \text{ keV}$ and thermal $0.625 < E \leq 0.0 \text{ eV}$. The WIMS-D5 will generate macroscopic absorption cross section (Σ_a), the ν -fission cross section ($\nu\Sigma_f$), the diffusion coefficient (D), the scattering matrix ($\Sigma_s, g \rightarrow g$) and the fission spectrum for all groups of core materials, which are used as input data to MTR-DYN code.

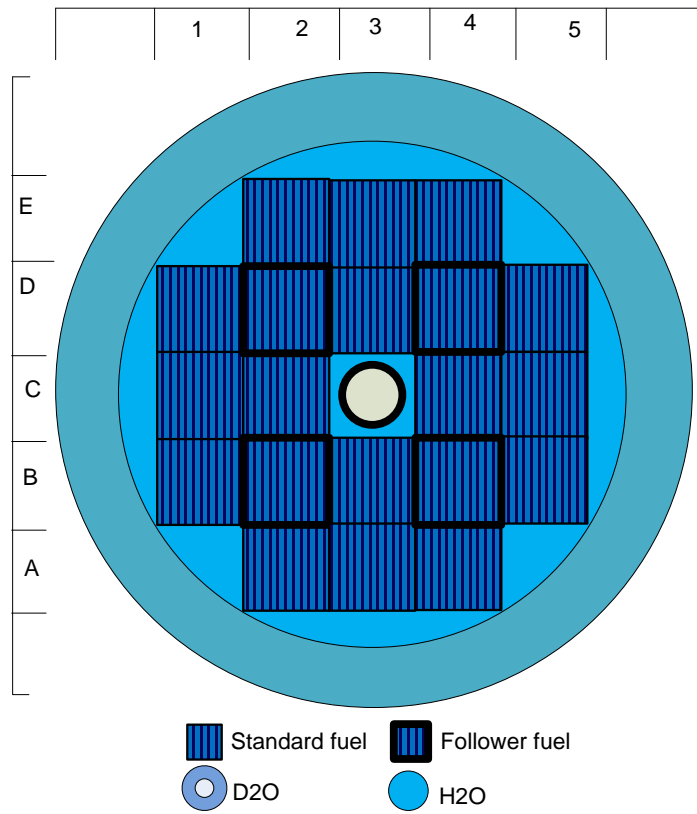


Figure 1: Core configurations of the RRI reactor [1]

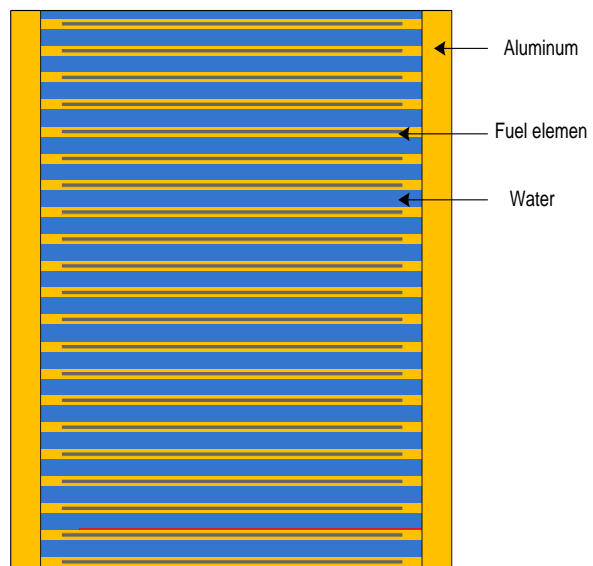


Figure 2: Standard fuel element [1]

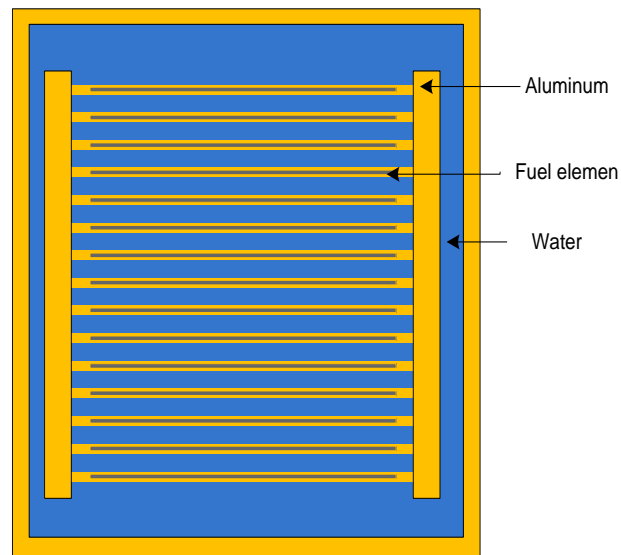


Figure 3: Fuel follower element [1]

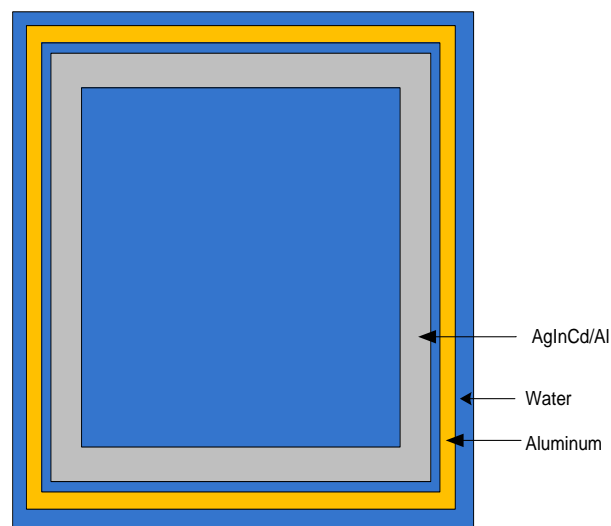


Figure 4: Control rod element

The MTR-DYN code is a coupled neutronic (N) and thermal-hydraulic (T/H) code for the MTR research reactor type. This code is developed by 3-dimensional multigroup neutron diffusion method by finite difference method. Flowchart of N and steady state T/H calculations are shown in the Figure 5.

The neutronic parameters are determined by using adiabatic models, time dependent multi group neutron diffusion problem is solved by flux factorization approach, the spatial, time-dependent neutron flux is split into time-dependent amplitude and shape function. Heat conduction equation in the fuel rods are discretized in space and time using the finite-difference method. Heat conduction is considered only in the radial direction. Fluid dynamics is modeled in a single-phase flow conditions. Mass flow rate in each cooling channel is to be determined.

Analysis of the neutronic and steady state thermal hydraulic parameter are performed at the thermal power of 50 MW. Core cooled under forced convection with

an inlet temperature is 44.5 °C. The coolant pressure is 10 atm at under surface of the water.

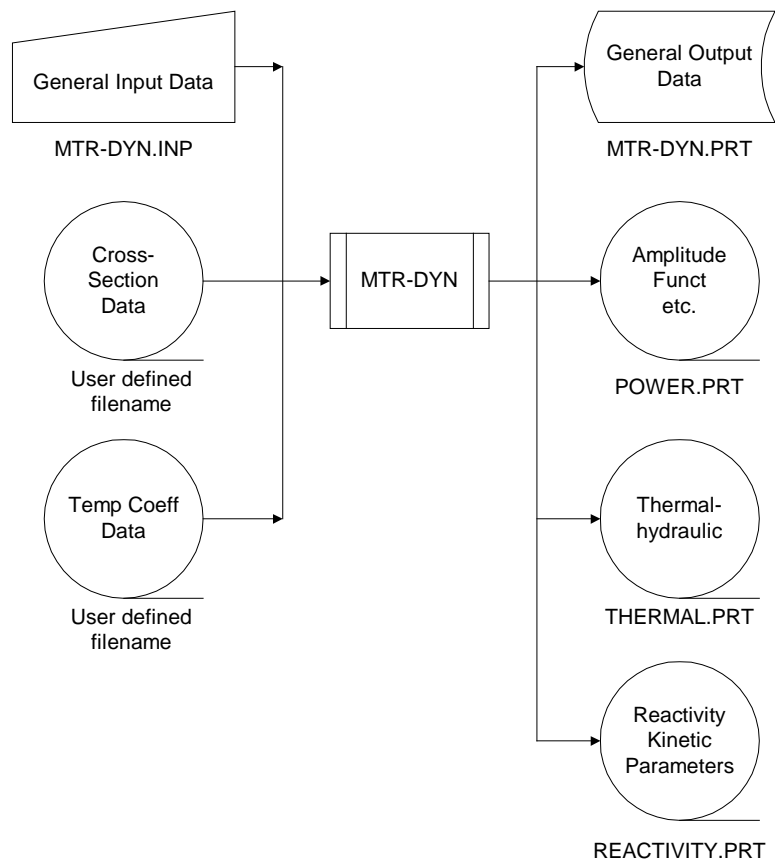


Figure 5: MTR-DYN code input/output file structure

3. Results and Discussions

The calculated neutronic parameters, such as excess reactivity, control rods worth, power peaking factor, the thermal neutron flux and power density are shown in Table 1. The excess reactivity depends on the fuel uranium density, so it is needed to select an optimum fuel uranium density in order to operate the reactor at 50 MW. Axial power peaking factor is dependent on the neutron flux distribution and effected by control rod position during operation reactor. The maximum radial and axial power peaking factor is less than the limit values of 1.4 and 1.8, respectively.

Heat flux or power density in the core depends on the reactor power operation, the burn up and the number of fuel elements in the core. Heat flux is not uniform and depends on the axial and radial position in the core reactor. Figure 6 shows axial power peaking factor for hottest channels resulting from the calculation at power of 50 MW.

No.	Parameters	Uranium density (gU/cc)		
		3.66	5.34	6.52
1.	Excess reactivity ($\% \Delta k/k$)	12.75	14.01	15.74
2.	Control rod worth ($\% \Delta k/k$)	21.69	23.22	21.80
3.	Maximum radial power peaking factor	1.1530	1.2028	1.2012
4.	Cycle length reactor operation (days)	21	35	48
5.	Maximum axial power peaking factor	1.7435	1.7435	1.7323
6.	Local power peaking factor	2.1397	1.9532	2.1080
7.	Maximum thermal neutron flux (E_{15} n/cm ² s)	1.47	1.46	1.41
8.	Power density (W/cc)	637.26	639.01	639.01

TABLE 1: Neutronic parameters with various uranium density

Heat flux or power density in the core depends on the reactor power operation, the burn up and the number of fuel elements in the core. Heat flux is not uniform and depends on the axial and radial position in the core reactor. Figure 6 shows axial power peaking factor for hottest channels resulting from the calculation at power of 50 MW.

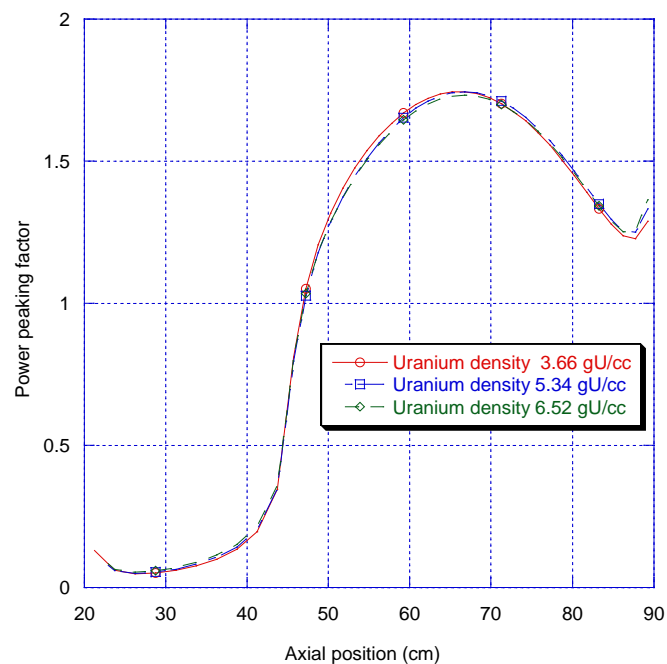


Figure 6: Axial heat flux profile of the core hot channel

The coolant mass flow rate in the RRI reactors is limited by the flow instability phenomenon. Flow instability can be happened in the reactor core with high thermal power and characterized by a flow excursion. When the flow rate and the heat flux are relative high, a small increase in heat flux causes a sudden large decrease in flow rate. For higher uranium density, the thickness of the plate or the channel width is increased so that the reactor is stable at a high flow rate. In addition to reducing the heat flux in the fuel, it can be done increasing the height of fuel so the maximum

temperature of fuel and cladding will be reduced. Calculation results of coolant velocity with various mass flows are shown in Table 2. Based on the calculation, obtained the critical velocity through the fuel channel is 17.899 m/s. By using the design criteria where the maximum coolant speed is 2/3 of criticality velocity so that maximum mass flow on the core is 800 kg/s and a maximum coolant speed at fuel channel is 10.92 m/s.

Parameters	Mass flow rate (kg/s)			
	750	800	850	900
Coolant flow rate (kg/m ² s)	6709.65	7156.96	7604.27	8051.58
Coolant velocity (m/s)	10.24	10.92	11.61	12.29

TABLE 2: Coolant velocity with various mass flow rate

Figure 6 shows that the axial hot channel conditions is resulted from the calculations for 50 MW with various fuel uranium densities. From Figure 7 shows the axial hot channel where if the uranium density increases, the temperature of the fuel also increases.

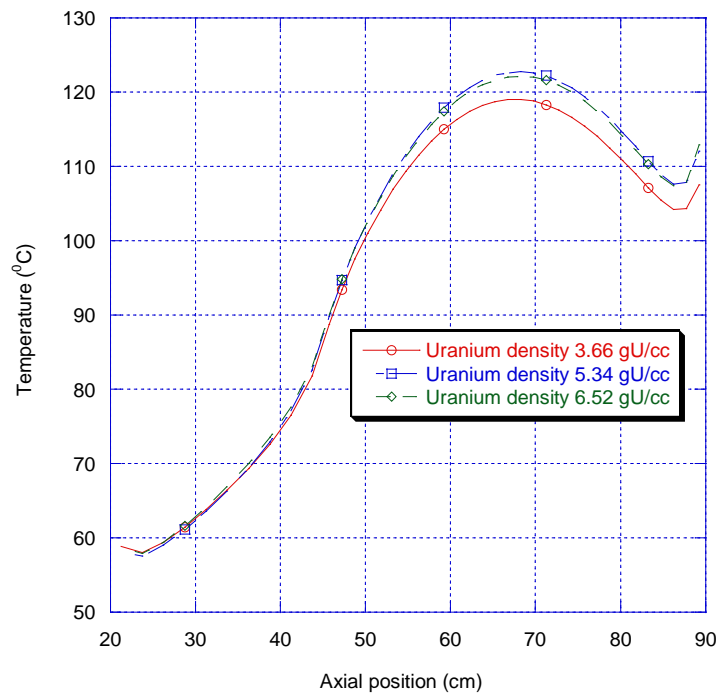


Figure 7: Fuel temperature along the axial position in the hot channel

The temperature distribution in the fuel, cladding and coolant are performed at mass flow rate of 800 kg/s. If the uranium density increasing, it makes temperature of the fuel, cladding and coolant increasing because the thermal conductivity decreases. The temperature of the fuel, coolant and cladding should be limited to maintain the integrity of the fuel. Calculation results at a steady state thermal hydraulic with various uranium densities are shown in Table 3. For the uranium densities of 3.66 gU/cc, 5.34 gU/cc and 6.52 gU/cc, with the mass flow rate

of 800kg/s, the fuel and cladding temperature are less than 170 oC so still within safe limits.

Parameters	Uranium density (gU/cc)		
	3.66	5.34	6.52
Coolant temperature at core inlet (°C)	44.5	44.5	44.5
Coolant temperature at core outlet (°C)	59.49	59.49	59.49
Maximum temperature at coolant (°C)	70.85	73.06	73.92
Maximum temperature at cladding (°C)	150.79	161.20	163.70
Maximum temperature at fuel meat (°C)	153.24	163.95	166.52

TABLE 3: Maximum temperature with various uranium density at fuel elements

Neutronic and thermodynamic calculation results indicate that the effect of fuel density in the design of the MTR type research reactor is very important for the safety of the operation and efficiency of fuel used. The higher density of fuel reactors is more efficient because the longer operating cycle but the power density will be high so that the temperature of the fuel increase. Both of these factors should be taken into account in the design of the research reactor core.

4. Conclusions

Effect of uranium densities in the neutronic and thermal-hydraulic parameters of RRI reactor have been carried out. Based on the calculation of MTR-DYN code, it is clear that all uranium densities of U-9Mo/Al fuel that are surveyed in this research work can be utilized as a candidate fuel for the RRI reactor core with thermal power of 50 MW, since the maximum temperature of cladding is less than 170 °C with the mass flow rate of 800 kg/s. However, as a future work, the transient analysis has to be carried out to obtain an optimum uranium density of U-9Mo/Al fuel for RRI reactor.

5. Acknowledgment

The authors wish to express special thanks to Tagor Malem Sembiring and Mr. Surip Widodo for his fruitfully discussions.

References

- [1] Tukiran, S. Pinem, Tagor M. S, Lily Suparlia, Jati Susilo, "Neutronics Conceptual Design of the Innovative Research Reactor Core Using Uranium Molybdenum fuel", Journal of Nuclear Reactor Technology Tri Dasa Mega, Vol. 3, Issue 3, pp. 179 – 191 (2012)
- [2] Rokhmadi, Tukiran, "Fuel Density Effect on Parameter of Reactivity Coefficient of the RRI Core", Journal of Nuclear Reactor Technology Tri Dasa Mega, Vol. 15, Issue 2, pp. 77 – 89 (2012).
- [3] Surian Pinem, Iman Kuntoro, "Effects of Density U9Mo/Al Fuel on the Kinetic Parameters of Research Reactor MTR Type", Journal of Technology Nuclear Materials, Vol. 10, Issue 1, pp. 1 – 9 (2014).

- [4] Lily Suparlina, Tukiran ,*"Analysis of Fuel Management Pattern Of Research Reactor Core Of The MTR Type Design"*, Journal of Nuclear Reactor Technology Tri Dasa Mega, Vol. 16, Issue 2, pp.:89 – 99 (2014).
- [5] Carlos Alberto de Oliviera, Miguel Mattar Neto ,*"Flow Velocity Calculation to Avoid Instability In A Typical Research Reactor Core"*, 2011 International Energy Horizonte, MG, October 24 – 28, Brazil (2011).
- [6] IAEA-TECDOC-233 ,*"Research Reactor Core Conversion From the Use of Highly Enriched Uranium to the Use of Low Enriched Uranium Fuels Guidebook"*, IAEA, Viena (1980).
- [7] Farhan Muhammad, Asad Majid ,*"Effect of High Density Dispersion Fuel Loading on Dynamics of A Low Enriched Uranium Fueled Material Test Research Reactor"*, Progress in Nuclear Energy, Vol. 51, pp. 339 – 346 (2009).
- [8] I.H. Bokhari ,*"Steady-State Thermal Hydraulic And Safety Analyses of Proposed Mixed Fuel (HEU & LEU) Core For Pakistan Research Reactor-1"*, Annals of Nuclear Energy, Vol. 31, pp. 1265 – 1273 (2004)
- [9] Roth,M.J ,*"The preparation of input data WIMSD/5"*, New York (1976)
- [10] Surian Pinem, Tagor MS, Setiyanto ,*"Transient Analysis of RSG-GAS Reactor Core When Coolant Flow Reduction Using MTRDYN Code"*, Journal of Nuclear Reactor Technology Tri Dasa Mega, Vol.11, Issue 3, pp.153 - 161(2009).



Conference Paper

The Effect of Boric Acid on Corrosion of SS 304 as PWR Pressurizer Material

Febrianto

Center for Nuclear Reactor Safety and Technology National Nuclear Energy Agency of Indonesia (BATAN) Puspiptek Complex, Building No. 80, PUSPIPTEK area, Serpong, Tangerang 15310, Indonesia

Abstract

The pressurizer is the component in the reactor coolant system which provides a means of controlling the system pressure. The pressurizer has a function to keep the operational pressure of reactor coolant system in set point condition. For controlling primary coolant system pressure, the pressurizer has pressurizer spray, heater, safety relief valve and instrumentation to control level and pressurizer. The purpose of this study is to see the effect of boric acid, lithium hydroxide and temperature on SS 304 as PWR pressurizer material. The method that used in this research is to observe the corrosion rates of pressurizer material in several boric acid and lithium hydroxide concentration at several temperature conditions using Potentiostat. Tests were conducted in 28, 60, 80, and 100 °C in 2000, 2500, 3000 ppm boric acid and addition 2.0 and 2.5 ppm lithium hydroxide. The pressurizer material corrodes in solution containing boric acid solution. The corrosion rates increased if boric acid solution concentration and temperature also increased. The results showed that that corrosion rate for the material were very small and the highest corrosion rate occurred in 3000 ppm boric acid concentration at 80 °C, that is 4.5913×10^{-1} mpy. The corrosion rates increased until temperature 80 °C, but increasing the temperature from 80 °C to 100 °C decreased the corrosion rates from 4.5913×10^{-1} to 4.5264×10^{-1} mpy. Lithium hydroxide addition in boric acid containing media generally decreased SS 304 corrosion rate as P W R pressurizer material. K.

Keywords: pressurizer, primary coolant system, boric acid, lithium hydroxide, corrosion rate

Corresponding Author:

Febrianto; email:
febrianto_bahar@yahoo.com

Received: 29 July 2016

Accepted: 21 August 2016

Publishing: 21 September 2016

**Publishing services
provided by Knowledge E**

© Febrianto. This article is distributed under the terms of the [Creative Commons Attribution License](#), which permits unrestricted use and redistribution provided that the original author and source are credited.

Selection and Peer-review under the responsibility of the ICoNETS Conference Committee.

OPEN ACCESS

1. Introduction

The pressurizer is the component in the reactor coolant system which provides a means of controlling the system pressure. The pressurizer has a function to keep the operational pressure of reactor coolant system in set point condition. The pressurizer surge line is connected to one of the reactor coolant hot legs and the spray lines are connected to two of the cold legs at the reactor coolant pump discharge. Pressurizer maintains the steam's and water's pressure are kept in thermal equilibrium. Chemical and Volume Control System controls the water level and quality.

SA -533 GR-B-CL-1 or SA-508 Grade 3, Class 1 as Vessel Base material which coated SS 304 or Ni-Cr-Fe Steel used as pressurizer vessel material. The chemical composition and mechanical properties from pressure vessel material can be seen in Table 1. This research was conducted based on consideration many corrosion problems occurred in several PWR primary coolant system components such as; steam generator tube, as well as reactor vessel head [1-5]. The chemical composition and mechanical properties are listed in Table 1.

ASME spec	SA-533		SA-508	SS-304
Type or grade	Type B		Gr. 2	
Class	1	2	1	
C (%)	≤ 0.25	≤ 0.25	≤ 0.35	≤ 0.060
Si	0.15-0.40	0.15-0.40	0.15-0.35	0.59
Mn	1.15-1.50	1.15-1.50	0.40-0.90	1.69
P	≤ 0.035	≤ 0.035	≤ 0.025	≤ 0.024
S	≤ 0.04	≤ 0.04	≤ 0.025	≤ 0.013
Ni	0.40-0.70	0.40-0.70	≤ 0.4	8.88
Cr	-	-	≤ 0.25	18.33
Mo	0.45-0.60	0.45-0.60	≤ 0.1	0.14
V	-	-	≤ 0.05	

TABLE 1. Chemical composition and Mechanical Properties [1].

In PWR, H_3BO_3 and LiOH combination is used for pH controlling. At the beginning the fuel cycle, maximum lithium concentration is 2.2 ppm. If lithium concentration higher than 2.2 ppm it will initiate fuel cladding corrosion. PWR reactor is recommended to be operated in range pH 6.9 – 7.4, with boric acid concentration around 1800 – 3000 ppm and lithium hydroxide concentration around 2.2 – 3.5 ppm. This range of pH is necessary to control the corrosion of primary system materials and also to minimize corrosion product transport within the primary system. The lithium concentration normally decreases according to decreasing boric acid concentration and is reduced to ~0.6 ppm at the end of a fuel cycle. At several US PWR reactor has found damage cause of boric acid corrosion/BAC) [1]. Boric acid addition has a negative effect to reactor primary coolant system component. Boron added in reactor coolant system in boric acid form (H_3BO_3) via Control Volume Chemical System (CVCS)

At US PWR reactor, David Besse, three CRDM nozzles had indications of axial cracking, which had resulted in leakage of the reactor’s pressure boundary. This crack had resulted in leakage reactor primary water coolant. At March, 2002, during VHP inspection, cavity was found at David Besse Reactor Pressure vessel Head adjacent to control-rod drive mechanism. These cavities caused by boric acid corrosion attack, many efforts have been under way to understand the mechanisms of BAC [6-8]. To

prevent boric acid corrosion on reactor material is necessary to reduce the leakage of reactor coolant water.

2. Theory

Boron addition to PWR reactor coolant has purpose to control reactor reactivity mainly during reactor start-up. Boron as boric acid (H_3BO_3) combination with lithium hydroxide (LiOH) has a role to control pH of reactor primary coolant. Many PWR reactor are operated in range pH 6.9 to 7.4 during fuel cycle [1-5,9-10]. PWR primary chemistry control aims to maintain primary system pressure boundary and fuel-cladding integrity, to provide for reactivity control, and to minimize ex-core radiation fields. Primary chemistry control is optimized to insure that the fuel and pressure boundary components integrity objectives are achieved. Operation at elevated pH can reduce ex-core radiation fields but the accompanying elevated lithium concentrations can lead to an increased likelihood of stainless steel corrosion, at a lower operating lithium concentration, the likelihood of stainless steel integrity problems will be minimized but an increased buildup rate of radiation fields may result. The major focus of primary chemistry programs today is pH control. Specifically, operation below pH6.9 is not desirable because of the expected more material corrosion effect will occur. At the present time, almost all plants are operating at pH(tave) = 6.9 or above. Recently, several plants operating with localized boiling in some parts of the core have experienced an axial offset anomaly (AOA), which has been attributed of high concentration of lithium and boron. AOA anomaly occurs cause of lithium boron compounds deposits at fuel surface. To solve this problem, many plant in Germany apply enrich boric acid for reducing boron in reactor coolant and reduce lithium concentration addition.

3. Methodology

SS 304 was used as specimen in this experiment. The specimen surface was polished with alumina powder. This report presents experimental data on corrosion rates of the SS 304 materials as PWR pressurizer material in boric acid, boric acid + lithium hydroxide solutions in varying concentrations and temperatures. Anodic polarization was obtained by a potential scanning from -500 mV at an open circuit potential(OCP) to 600 mV. OCP at a rate of 0.2 mV/sec after an initial delay of 30 minutes at -200 mV. A Silver/Silver chloride(Ag/AgCl) and Pt wire were used as reference electrode and a counter electrode respectively. For each condition, the boron and lithium hydroxide concentrations and temperature were changed to simulate the corrosion effect to SS 304 material. According to the purpose of this ressearch is to get related document which connected to PWR pressurizer material analysis and material corrosion evaluation. Achieving the above purpose, the experiment were performed with several steps:

- Specimen preparation

- PWR pressurizer material corrosion test use Potentiostat. The found data by Potentiostat is in corrosion current. This data will be calculated using Excel to get corrosion rate data.
- Analysis and report.

4. Result and Discussion

Corrosion rate test conducted in several boric acid concentrations and boric acid and lithium hydroxide mixture at several temperature variation using Potentiostat. There are three steps in this research, first for corrosion testing, seconds for data analysis corrosion testing , and third for reporting.

5. Effect of Boric acid addition and temperature on SS 304 Corrosion

Fig.1 shows experiment results that the increasing temperature tends to increase SS 304 corrosion rate as PWR pressurizer material eventhough is not so significant. SS 304 corrosion rate in 2000 ppm boric acid cotaining solution at 28 °C is 1.2293×10^{-2} mpy and corrosion rate increase to be 3.2937×10^{-2} mpy and 3.8859×10^{-2} mpy at temperature 80 °C, but SS corrosion rate decrease to 3.8859×10^{-2} mpy at temperature 100 °C. SS 304 corrosion rate decreased from 3.8859×10^{-2} mpy at temperature 80 °C to 3.0603×10^{-2} mpy at 100 °C. Corrosion rate decreasing cause by increasing temperature 80 to 100 °C will decrease soluble oxygen concentration in solution. Decreasing SS 304 corrosion rate from 3.8859×10^{-2} mpy at temperatur 80°C to 3.0603×10^{-2} mpy at 100°C caused by increasing temperature from 80 to 100 °C tend to reduce soluble oxygen concentration in solution. Boric acid addition to 2500 and 3000 ppm has the same effect to boric acid 2000 ppm in SS 304 corrosion rate tendency.

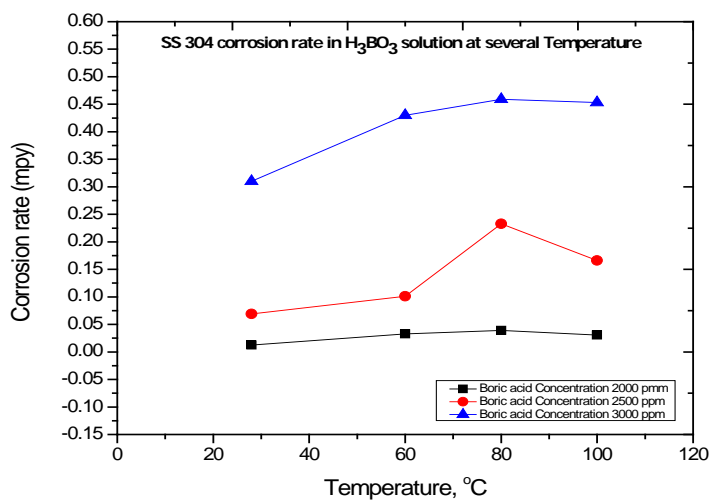


Figure 1. SS 304 corrosion rate in H₃BO₃ solution at several temperature.

6. Effect of H_3BO_3 and LiOH addition on SS 304 Corrosion at 80 °C

Fig. 2 shows SS 304 corrosion rate in boric acid at 80 °C decreased after lithium hydroxide addition

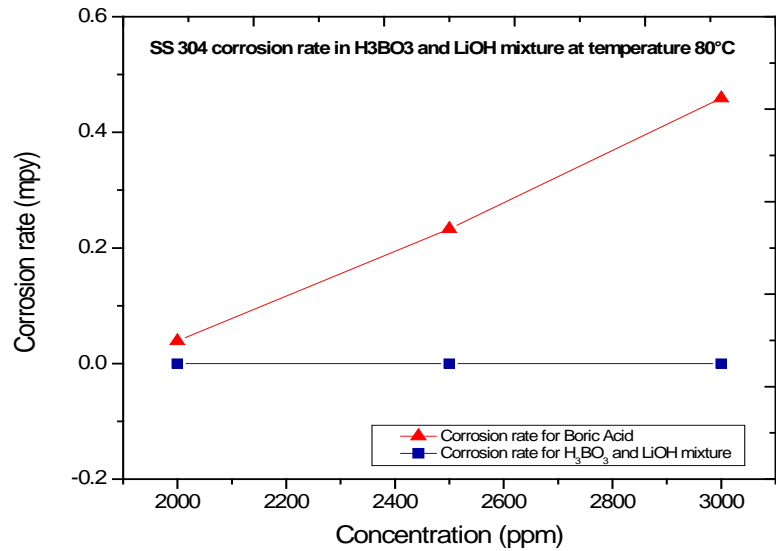


Figure 2. SS 304 corrosion rate in H_3BO_3 and LiOH mixture at 80 °C.

7. Effect of H_3BO_3 and LiOH addition on SS 304 Corrosion at temperatur 100 °C

Comparing corrosion rates data at temperature 100 °C (Fig.3) with corrosion data at temperature 80 °C (Fig. 2) shows that SS 304 corrosion rate in boric acid and boric acid + lithium hydroxide solution tend to decrease cause of increasing temperature from 80 °C to 100°C.

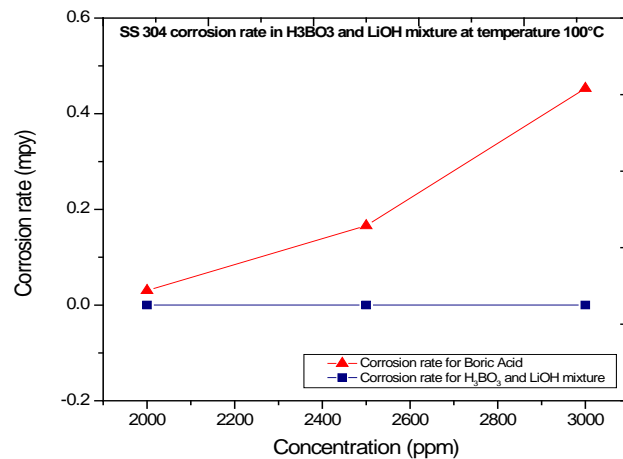


Figure 3. SS 304 corrosion rate in H_3BO_3 and LiOH mixture at 100 °C

8. Conclusion

The research was conducted at temperature 28, 60, 80, and 100 °C in 2000, 2500 and 3000 ppm boric acid concentration with 2.0 and 2.5 ppm lithium hydroxide concentration. From test result data shows SS 304 corrosion rate is relative small and the highest corrosion rate occur in 3000 ppm boric acid concentration at temperature 80 °C, namely 4.5913×10^{-1} mpy. Increasing temperature from 80 °C menjadi 100 °C decreased SS 304 corrosion rate from 4.5913×10^{-1} to 4.5264×10^{-1} mpy. Lithium hydroxide addition to boric acid containing solution generally decreased SS 304 corrosion rate as PWR pressurizer material. The corrosion experiments in solution containing H_3BO_3 and LiOH showed that the corrosion rates decreased with increasing temperature.

References

- [1] A. L. Stepanov, Rev. Adv. Mater. Sci. 30 (2012) 150-165.
- [2] A. A. Youssef^a, P. Budzynski^b, J. Filiks^c, A. P. Kobzev^d, J. Sielanko^e, Vacuum, Vol. 77, Issue 1 (2004) P. 37-45.
- [3] N. Kumar, S. Kataria, S. Dash, S. K. Srivastava, C. R. Das, P. Chandramohan, A. K. Tyagi, K. G. M. Nair, Baldev Raj, Wear, Volumes 274-275, 27 January 2012, Pages 60-67.
- [4] D. P. Hickey, Diss, University of Florida (2007).
- [5] A. Yu. Didyk, R. Wiśniewski, K. Kitowski, V. Kulikauskas, T. Wilczynska, A. A. Shiryayev, Ya. V. Zubavichus, Depth concentrations of deuterium ions implanted into some pure metals and alloys.
- [6] P. J. Evans, J. Hyvarinen, M. Samandi, Surface and Coating Technology 71 (1995) 151-158.
- [7] K. Feng, X. Cai, Z. Li, P. K. Chu, Mat. Letters 68 (2012) 450-452.
- [8] G. Jatisukanto, V. Malau, M. N. Ilman, P. T. Iswanto, J. Ilmiah Teknik Mesin CakraM, Vol.5, No.1 (2011) 14-19.
- [9] Effendi, N., Urania, 16(2), 2010.
- [10] A. Sujatno, R. Salam, B. Bandriyana, A. Dimiyati, Studi Scanning Electron Microscopy (SEM) untuk Karakterisasi Proses Oksidasi Paduan Zirkonium, Seminar Nasional X, SDM Teknologi Nuklir (2014).
- [11] M. Vigen Karimi, S. K. Sinha, D. C. Kothari, A. K. Khanna, A. K. Tyagi, Surface and Coatings Technology 158-159 (2004) 609-614.



Conference Paper

Fatigue Strength Evaluation of Pressurizer Wall Structure in Pressurized Water Reactor

Roziq Himawan

Center for Nuclear Reactor Technology and Safety – BATAN PUSPIPTK Area Building No. 80 Serpong, Tangerang Selatan 15310, Indonesia

Abstract

Fatigue strength evaluations have been performed to the pressurizer component in Pressurized Water Reactor. Fatigue is the main failure mechanism of material during system in operation. Therefore, this evaluation becomes important to be performed since the pressurizer has a very important function in the reactor's system. Analysis was performed by using Nuclear Power Plant operation data from 40 years operation and base on Miner theory. This analysis covered all stress level experienced by the reactor during the service. To determine the value of fatigue usage factor α , fatigue curve of SA 533 material was applied. Analysis results show that the cumulative fatigue damage during 40 years in operation is $4,23 \times 10^{-4}$. This value still far enough below failure criteria, which a value is 1. Therefore, the pressurizer design has already fulfilled the design qualification in term of fatigue aspect.

Keywords: pressurizer, fatigue usage factor, cumulative fatigue damage

Corresponding Author: Roziq Himawan; email: roziqh@batan.go.id

Received: 29 July 2016

Accepted: 21 August 2016

Published: 21 September 2016

Publishing services provided by Knowledge E

© Roziq Himawan. This article is distributed under the terms of the [Creative Commons Attribution License](#), which permits unrestricted use and redistribution provided that the original author and source are credited.

Selection and Peer-review under the responsibility of the ICoNETS Conference Committee.

OPEN ACCESS

1. Introduction

Primary cooling system of Pressurized Water Reactor (PWR) has a high operating pressure of about 15 MPa [1]. So that the main components in the nuclear island, that are reactor pressure vessel, pressurizer, steam generators and the primary coolant piping system should be able to retain this operating pressure. Therefore, the integrity of the mechanical structure of these components must be guaranteed for all operation condition including severe accident and transient conditions. It's known that one of the main causes of catastrophic failure of a structure is due to fatigue phenomenon [2]. Fatigue is the phenomenon in which lead into material degradation due to cyclic loading. Fatigue phenomenon may also occur in the main nuclear components during reactor service life due to transient condition such as reactor start-up and shut-down, increasing and decreasing power. These transient conditions will generate cyclic loads to the structures. These loads could be a mechanical load or/and thermal load due to temperature stratification. During normal conditions, reactor components were designed to have long fatigue life. However, the operating conditions and environment could shorten the fatigue life. Extreme environmental conditions could induce corrosion to the material. Corrosion will initiate fatigue crack prematurely [3, 4]. By these reasons, many studies related to the fatigue and fatigue

crack propagation characteristics of the reactor components and associated factors have been intensively performed [5, 6].

Pressurizer is one of the safety-related reactor components which have a function to maintain the reactor operating pressure. As a result pressurizer endures various types of loads. Therefore the structural integrity of the pressurizer should be determined through conservative stress analysis and should fulfil design requirement and stress limit which corresponds to the design conditions and additional conditions [7].

In this study, the fatigue life analysis was done for pressurizer components by calculation method. The results of the analysis are then compared with the standard design in order to determine the reliability of pressurizer.

2. Theory

Fatigue strength (it's also called as fatigue limit or endurance limit) of material is determined by performing fatigue testing using several number of specimens and varying alternating stress amplitude (σ_a) and mean stress (σ_m). The tests are performed until the specimen fracture with the cycle number of N_c or exceeds N_L [8]. Testing results then, are plotted on the graph represent the relationship between stress (σ) 'UbX' cycle number (N). This diagram is well known, as fatigue curve or Wohler diagram. In general, this diagram is drawn in $\log \sigma - \log N$ coordinate as shown in Fig. 1. Fatigue curve in $\log \sigma - \log N$ coordinate is a polygonal line. For exception, the transition part is a curve. The intersection between an oblique line and horizontal line represents theoretical limit of cycle and denoted by N_0 . In performing fatigue testing, the type of loading was determined as an actual load type in the operating system. Thus, the load type could be either tensile loads, torsional load, bending load, rotating-bending load, etc. In a detailed Wohler diagram, the diagram area is divided into three parts, namely the low-cycle fatigue strength (LCF), high-cycle fatigue strength (HCF), and sub-fatigue limit (SF) as shown in Fig. 2.

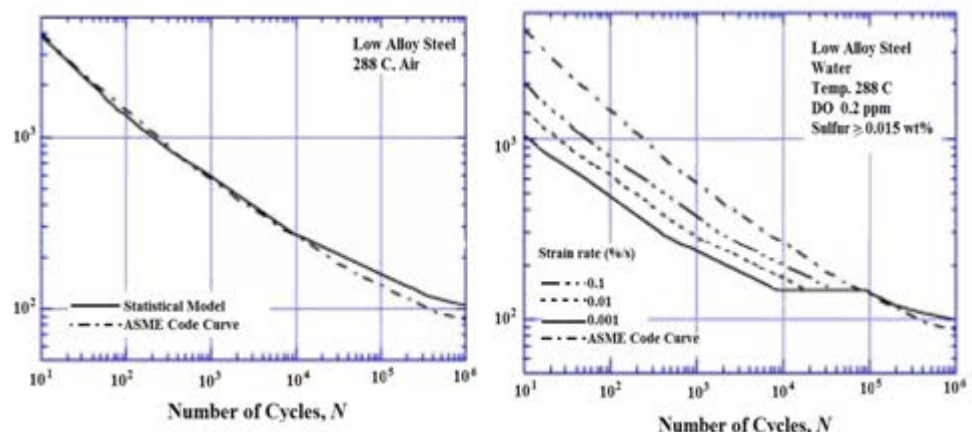


Figure 1. Fatigue diagram for Ferritic steel SA 533 B [9].

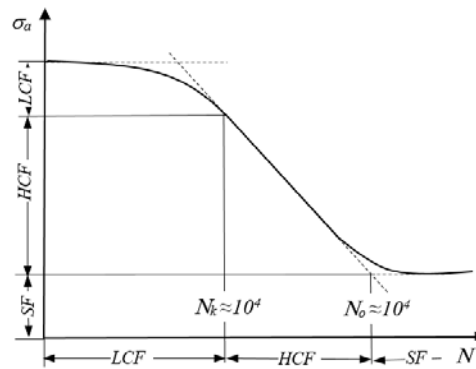


Figure 2. Wohler Diagram which include zone of low-cycle fatigue strength (LCF), high-cycle fatigue strength (HCF), and sub-fatigue limit (SF) [8]

Design of reactor components should conform to a specific standard applied in vendor countries such as ASME standards which is applicable in the United States [7]. The standard sets all the parameters or mechanical behavior of the material used in the reactor, including fatigue aspect. The ASME standard section III Division 1, Sub Division NB was applied to the design of nuclear reactor components. Therefore, in this study, the fatigue strength analysis were performed according to this standard.

Fatigue strength analysis is performed using the peak stress which is a resultant of various loads in each level of operation. Then, amplitude stress (S_a) were calculated using peak stress according to equation (1) [9].

$$S_a = \frac{S_p}{2} \tag{1}$$

The value of stress amplitude (S_a) is put in the S-N curve shown in Appendix I of ASME section III (see Figure 1) in order to determine the fatigue life of components. However, the fatigue life determined here is the life represents for one loading level, only. In fact, in the real operation, each reactor component may experience various loading levels and various cyclic numbers. To determine the accumulative fatigue life due to various loading levels, fatigue usage factor method was applied. Fatigue Usage Factor was calculated by Miner method and according to equation (2) and (3). Firstly, each ratio between loading cycles during reactor operation with the number of cycles at Wohler diagram for a certain loading level was calculated using equation (2). After all loading levels were calculated, then cumulative fatigue damage was calculated using equation (3). From this calculation, the value of the cumulative fatigue usage factor in a structure should not exceed 1. The value of 1, it means the components will experience failure due to fatigue phenomenon. Therefore, value 1 represents failure criteria.

$$\alpha = \frac{n_i}{N_i} \tag{2}$$

$$CFD = \sum \frac{n_i}{N_i} \leq 1 \tag{3}$$

with α is cumulative fatigue usage factor, n is cycle number during reactor operation for one loading level, N is cycle number in Wohler diagram for associated loading level, and CFD is cumulative fatigue damage.

3. Methodology

As described in the previous section, in this study, the fatigue strength analysis were performed to the pressurizer with a design as shown in Fig. 3. Ferritic steel of type SA 533 B was used for pressurizer material as those used in reactor pressure vessel. Design parameter of pressurizer was shown in Table 1, whilst mechanical properties and thermal properties of material were shown in Table 2.

No	Parameter	Value
1	Pressure design, MPa	17.58
2	Temperature design, °C	371
3	Normal operation pressure, MPa	15.82
4	Normal operation temperature, °C	344
5	Vessel volume, m ³	68
6	Water volume under normal operation, m ³	31.4
7	Steam volume under normal operation (full capacity), m ³	36.5
8	Installed heater capacity, kW	2,400

TABLE 1. Design parameter of pressurizer

No	Sifat Material	Nilai
1	Young Modulus E (GPa)	191
2	Poisson Ratio; ν	0.3
3	k (W/m °C)	40.9
4	ρ (kg/m ³)	7784
5	α (m/m °C)	12.5×10^{-6}
6	Yield Stress ;MPa	345
7	Ultimate tensile strength, MPa	550 - 690

TABLE 2. Mechanical and thermal properties of SA 533 B material

In the analysis of fatigue strength, the stress values which occur during reactor operation (for a specific load level) and cycle number were needed. In the operation of nuclear power reactors, the operating level is divided into five levels, namely the operating conditions level A, level B, level C, level D and testing conditions [7]. For each level there are a several stress value with a certain cycle number. In this analysis of the fatigue strength, the stress value and the frequency of occurrence data are as a result from the operation of the reactor for 40 years. These data are shown in Table 3 [11].

Operation conditions Level C and Level D are not taken into account because of the frequency of occurrences are very rare. Emergency Conditions and infrequent Incidents are categorized into operating conditions Level C while faulted and Limiting Conditions Faults are categorized into operating conditions Level D. Likewise, the test

conditions are not considered in this analysis because small number of occurrences during reactor's service life.

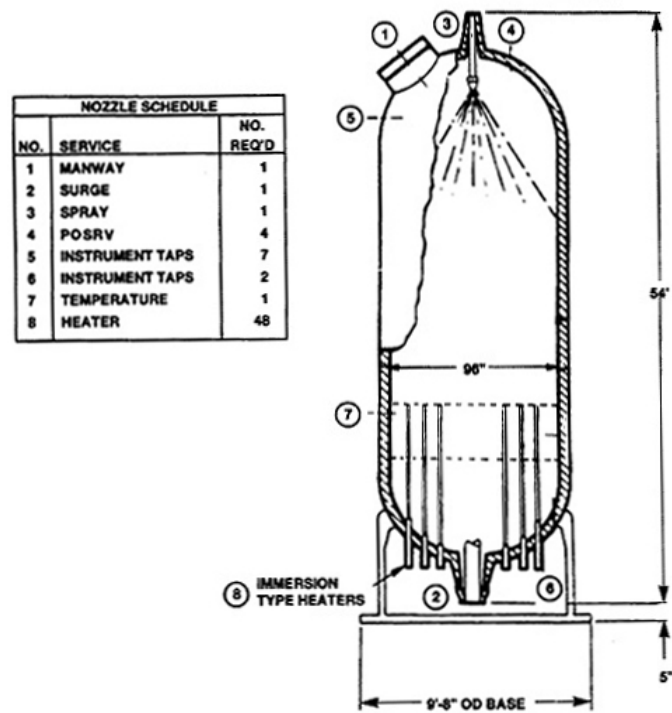


Figure 3. Schematic design of pressurizer vessel

Load No	Transient Design	Stress value (MPa)		Cycles during 40 years	
		Max.	Min.		
Level A	1/2	Heat-up/cool-down	160,9	0,0	200
	3	Unit loading/unloading	159,2	160,6	500
	4/5	Plant loading/unloading	160,7	158,0	13.200
	6/7	Step load change of 10%	164,4	157,6	2.000
	8	Steam dump	167,5	150,5	200
	9a	Steady state fluctuation (A)	160,9	158,8	1,5×10 ⁵
	9b	Steady state fluctuation (B)	161,3	160,5	3×10 ⁶
	10	Feedwater cycling	154,9	162,9	2.000
	11/12	Loop out service	167,6	160,4	80
	Level B	15	Loss of load	187,7	131,7
16		Loss of Power	176,0	132,1	40
17		Partial loss of flow	164,7	138,2	80
18a		Reactor trip A	160,9	142,7	230
18b		Reactor trip B	160,9	114,5	160
18c		Reactor trip C	160,9	114,5	10
19		Inadvertent depressurization	160,9	9,3	20
20		Inadvertent startup	167,5	142,1	10
21		Control rod drop	160,9	131,0	80
22		Inadvertent safety injection	164,0	143,7	60

TABLE 3. Load condition : Level A and Level B [7]

4. Result and Discussion

Table 4 shows CFD analysis results below. In this table, column which indicates transient conditions are removed and denoted by number which has correlation with Table 3. $\Delta\sigma$ shows the stress amplitude representing a stress difference between the maximum and minimum stress. The notation which represents number of cycles for 40 years was changed became n_i . N_i column states the fatigue life at a certain stress level, which is determined by S-N curve as shown in Figure 1. In this analysis, S-N curve of SA 533 B under water and temperature 288 °C was used. In this figure, S-N graph of ASME standard and various result from different strain rate were plotted. Furthermore, cumulative fatigue damage, α , was calculated using equation (2).

Load No.	Nilai tegangan (MPa)		(MPa)	n_i	N_i	α	
	Maks.	Min.					
Level A	1/2	160,9	0,0	160,9	200	$4,8 \times 10^4$	$4,17 \times 10^{-3}$
	3	159,2	160,6	1,4	500	$1,0 \times 10^{10}$	$1,0 \times 10^{-8}$
	4/5	160,7	158,0	2,7	13.200	$1,0 \times 10^{10}$	$1,32 \times 10^{-9}$
	6/7	164,4	157,6	6,8	2.000	$1,0 \times 10^{10}$	$2,0 \times 10^{-10}$
	8	167,5	150,5	17	200	$1,0 \times 10^{10}$	$2,0 \times 10^{-8}$
	9a	160,9	158,8	2,1	$1,5 \times 10^5$	$1,0 \times 10^{10}$	$1,5 \times 10^{-5}$
	9b	161,3	160,5	0,8	$3,0 \times 10^6$	$1,0 \times 10^{10}$	$3,0 \times 10^{-4}$
	10	154,9	162,9	8	2.000	$1,0 \times 10^{10}$	$2,0 \times 10^{-10}$
	11/12	167,6	160,4	7,2	80	$1,0 \times 10^{10}$	$8,0 \times 10^{-9}$
	Level B	15	187,7	131,7	56	80	$1,0 \times 10^{10}$
16		176,0	132,1	43,9	40	$1,0 \times 10^{10}$	$4,0 \times 10^{-9}$
17		164,7	138,2	26,5	80	$1,0 \times 10^{10}$	$8,0 \times 10^{-9}$
18a		160,9	142,7	18,2	230	$1,0 \times 10^{10}$	$2,3 \times 10^{-8}$
18b		160,9	114,5	46,4	160	$1,0 \times 10^{10}$	$1,6 \times 10^{-8}$
18c		160,9	114,5	46,4	10	$1,0 \times 10^{10}$	$1,0 \times 10^{-9}$
19		160,9	9,3	151,6	20	$5,5 \times 10^4$	$3,6 \times 10^{-4}$
20		167,5	142,1	25,4	10	$1,0 \times 10^{10}$	$1,0 \times 10^{-9}$
21		160,9	131,0	29,9	80	$1,0 \times 10^{10}$	$8,0 \times 10^{-9}$
22		164,0	143,7	20,3	60	$1,0 \times 10^{10}$	$6,0 \times 10^{-9}$
						CFD=	$4,85 \times 10^{-3}$

TABLE 4. Calculation result of Cumulative Fatigue Damage

As shown in Figure 1, curve C has endurance or fatigue limit at stress value of about 90 MPa. Thus, stress values below 90 MPa will not result damage in material due to fatigue phenomenon. However, to quantify the value of α at all stress levels in Table 4, for stress values below 90 MPa, we assume to have N_i of 1.0×10^{10} . After all of α value were calculated, then summed to obtain the CFD.

The calculation of cumulative fatigue damage from ASME Standard Curve gave a result to a value of 4.85×10^{-3} . This value is extremely small compared to the value of 1, where a value of 1 indicates that the components will fail due to fatigue phenomena. As shown in Table 4, that the value of $CFD = 4.85 \times 10^{-3}$ is accumulated during 40 years of reactor operation. Thus, it can be assumed, with the same mode of operation, the reactor is still safe from the phenomenon of fatigue even it's operated for 80 years. However, in real operation experience, a lot of reports of leaks in nuclear reactor safety component triggered by corrosion phenomena. Which resulted

in the occurrence of corrosion or pitting of the notch on the surface of the material, can spread into larger cracks due to repeated load.

No.	S-N Curve condition	CFD
1.	ASME Standard Curve	4.85×10^{-3}
2.	0.1 [%/s] strain rate	1.05×10^{-2}
3.	0.01 [%/s] strain rate	2.16×10^{-2}
4.	0.001 [%/s] strain rate	4.50×10^{-2}

TABLE 5. Calculation result of CFD using S-N Curve with various strain rate

Table 5 shows CFD calculation results from ASME standard curve and various condition with different strain rate. CFD from ASME standard curve has the smallest value, whilst the smallest strain rate has the biggest CFD value. From this table, it is known that CFD depends on the strain rate. Even for the biggest CFD value, it is still smaller than 1.

From the results of this analysis can be seen that the design of the pressurizer has fulfilled the requirements of fatigue strength aspect.

5. Conclusion

Fatigue strength analysis of pressurizer design were performed. Analysis were performed using nuclear power plant operating data to define various types of stress levels that occur in the pressurizer and cycle / frequency of the stress. Data refer to the operating history for 40 years. From the results of analysis, depends on ASME standard curve and various strain rate, show that the value of cumulative fatigue damage varies from 4.85×10^{-3} to 4.50×10^{-2} . The upper value is still smaller than 1. It can be concluded that the design meets the standards pressurizer analyzed from the aspect of fatigue strength.

References

- [1] R. Zarghami, et. al., "The Dynamic Modelling of the Pressurizer Surge Tank Transients in Light Water Reactor Nuclear Power Plants", Iranian J. of Science & Technology, Transaction B, Engineering, Vol. 29, 483 – 491, 2005
- [2] S. Suresh, "Fatigue of Materials", Cambridge University Press, 1998.
- [3] Chin-Cheng Huang and Ru-Feng Liu, "Structural integrity analyses for preemptive weld overlay on the dissimilar metal weld of a pressurizer nozzle", International Journal of Pressure Vessels and Piping, Vol. 90–91, 77–83, 2012.
- [4] W. A. Van Der Sluys and R. H. Emanuelson, "Fatigue Crack Growth In Reactor Pressure Vessel Materials And Light Water Reactor Environments", Nuclear Engineering and Design, Vol. 119, 379–388, 1990.
- [5] J. Y. Huang, et. al., "Fatigue crack growth behavior of reactor pressure vessel steels in air and high-temperature water environments", International Journal of Pressure Vessels and Piping, Vol. 85, 772–781, 2008.

- [6] C. Ensel, et. al., "Stress analysis of a 900 MW pressurizer surge line including stratification effects", Nuclear Engineering and Design, Vol. 153, 197-203, 1995.
- [7] _____, "Rules for Construction of Nuclear Power Plant Components", ASME Boiler and Pressure Vessel Code, Section III, 2004.
- [8] S. Kocanda, "Fatigue Failure of Metals", Sijthoff & Noordhoff International Publishers, 1995.
- [9] _____, Effects of LWR Coolant Environments on Fatigue Design Curves of Carbon and Low-Alloy Steels, NUREG/CR-6583.
- [10] Roziq Himawan, "Respon Panas Transien Dinding Bejana Pressurizer Pada Saat Proses Penyemprotan", Prosiding Seminar Nasional Teknologi Energi Nuklir 2014, Juni 2014.
- [11] G. Yagawa and S. Yoshimura, "A study on probabilistic fracture mechanics for nuclear pressure vessels and piping", Int. J. of Pressure Vessel & Piping, Vol. 13, 97-107, 1997.
- [12] Dixon A. G., et al., "Systematic Mesh Development for 3D CFD Simulation of Fixed Beds: Single Sphere Study", Journal of Computer and Chemical Engineering, Vol.35, Issue 7, pp.1171-1185 (2011).
- [13] Dehbi A. and Martin S., "CFD Simulation of Particle Deposition on An Array of Spheres Using an Euler/Lagrange Approach", Journal of Nuclear Engineering and Design, Vol.241, pp.3121-3129 (2011).
- [14] Kuijper J. C. et al., "HTTR-N Reactor Physics and Fuel Cycle Studies", Proceeding of 2nd International Topical Meeting on High Temperature Reactor Technology, September 22-24, Beijing (2004).
- [15] IAEA-TECDOC-1382, "Evaluation of High Temperature Gas Cooled Reactor Performace: Benchmark Analysis Related to Initial Testing of The HTTR and HTR-10", IAEA, November, Vienna (2003).

Conference Paper

Strength Based Numerical Approach Constitutive Material Prediction of Spot Welded Joints of Steel

I Nyoman Budiarsa

Mechanical Engineering, University of Udayana, Bali, Indonesia

Abstract

The deformation of spot welded joints is challenging research problem due to the complex nature of the structure. One major problem is to characterize the materials properties. The elastic-plastic material parameters and the fracture parameters of materials can be readily determined when standard specimens are available, however, for a spot welded joint, standard testing is not applicable to characterize the heat affected zone (HAZ) and the weld nugget due to their complex structure and small size. This has opened up the possibility to characterize the material properties based a dual indenter method to inversely characterize the parameters of the constitutive material laws for the nugget, HAZ and the base metals. In a mixed numerical-experimental approach, the load-deformation data of the material is used as input data to a finite element (FE) model that simulate the geometry and boundary conditions of the experiment. With indentation tests, the local plastic properties can be calculated by solving the inverse problem via finite element analysis by incrementally varying properties in 3D modeling to find a similar simulated load-displacement curve as compared with experimental one. The approach will then be used to test different welding zones and the material parameters thus predicted used to simulate the deformation of spot welded joints under complex loading conditions including tensile shear and drop weight impact tests. The evaluation based on numerical experimental data showed similar accuracy to the continuous indentation curve approach.

Corresponding Author:
I Nyoman Budiarsa;
email: nyoman.
budiarsa@unud.ac.id

Received: 29 July 2016
Accepted: 21 August 2016
Published: 21 September 2016

Publishing services
provided by Knowledge E

© I Nyoman Budiarsa. This article is distributed under the terms of the [Creative Commons Attribution License](#), which permits unrestricted use and redistribution provided that the original author and source are credited.

Selection and Peer-review under the responsibility of the ICoNETS Conference Committee.

Keywords: HAZ, finite element (FE) model, Vickers Indentation, Dual indenter

1. Introduction

In a spot welding process two or three overlapped or stacked components are welded together as a result of the heat created by the electrical resistance [1]. The welding process is a complex thermal mechanical process and the finished assembly consists of regions with significantly different microstructures and properties, including the base metal, heat affected zone (HAZ) and weld nugget. Many research has been conducted to improve the understanding on spot welded joint as the interactions between electrical, thermal, metallurgical and mechanical phenomena. [2]. One active research field is on the prediction of the dimension of spot welded joints by simulating the welding process with the finite element modeling [3]. Another active research field is on the study of microstructure development [4]. These works have resulted in several models to describe the

OPEN ACCESS

simultaneous formation that has made it possible to predict the microstructure development and transformations during spot welding process, and also to investigate the characteristics and behavior of materials, relating with the applied load conditions on the spot weld joint. The deformation of spot welded joints is challenging research problem due to the complex nature of the structure. One major problem is to characterize the materials properties. The elastic-plastic material parameters and the fracture parameters of materials can be readily determined when standard specimens are available. However, for a spot welded joint, standard testing is not applicable to characterize the HAZ and nugget due to their complex structure and small size. This has opened up the possibility to characterize the material properties based a dual indenter method. However, the method involved intensive data fitting which has to be performed based on a computational program. This work aims to further develop this method based to enable more direct parameter prediction based on analytical or semi-analytical approaches with either continuous indentation loading curve or conventional hardness tests. The approach will then be used to test different welding zones and the material parameters thus predicted used to simulate the deformation of spot welded joints under complex loading conditions. These works have resulted in several models to describe the simultaneous formation that has made it possible to predict the microstructure development and transformations during spot welding process, and also to investigate the characteristics and behavior of materials, relating with the applied load conditions on the spot weld joint.

2. Materials Behaviours and the Properties of Different Welded Zones

The plastic behavior is normally described by the constitutive material equations. In many cases, the three parameter power law hardening rule (Eq. 1) is used for steels:

$$\sigma = \sigma_0 + K\varepsilon \quad (1)$$

Where the parameter (σ_0) is the yield stress, K is the strength coefficient and ' n ' is the strain hardening exponent. These material parameters influence both the yielding strength and work hardening behavior of the spot welded joint. A measure of strain often used in conjunction with the true stress takes the increment of strain to be the incremental increase in displacement (dL) divided by the current length (L). Prior to necking, when the strain is still uniform along the specimen length, The ratio L/L_0 is the extension ratio, denoted as λ . Using these relations, it is easy to develop relations between true and engineering measures of tensile stress and strain

$$\begin{aligned} \sigma_t &= \sigma_e(1 + \varepsilon_e) = \sigma_e \cdot \lambda \\ \varepsilon_t &= \ln(1 + \varepsilon_e) = \ln \cdot \lambda \end{aligned} \quad (2)$$

These equations can be used to derive the true stress-strain curve from the engineering curve. The failure of spot welded joints can be overload failure and fracture. Gurson model is widely used in ductile fracture mechanics, in which, the fracture of material is considered as the result of void growths in the material volume. The Homogenous material surrounding the void is called matrix material. The Gurson model can realistically represent failure, provided the loading state in the coupon used to determine the Gurson parameters, is similar to that in the rupture zone of the structure. The most commonly used model based on the Gurson was called Gurson-Tvergaard-Needleman (GTN) model (ABAQUS Theory Manual

6.13), which is briefly described below. The original model developed by Gurson, assumed plastic yielding of a porous ductile material, where the yield surface was a function of a spherical void as follows

$$\Phi = \frac{3S_{ij}S_{ij}}{2\sigma_{ys}^2} + 2f \cosh\left(\frac{3\sigma_m}{2\sigma_{ys}}\right) - (1 - f^2) = 0 \tag{3}$$

Where σ_y is the yield stress of the material, σ_m is the mean stress, f is the void volume fraction. $f = 0$ implies that the material is fully dense, and the Gurson yield condition reduces to that of von Mises; $f = 1$ implies that the material is fully voided and has no stress carrying capacity. S_{ij} is the components of stress deviator ($i, j = 1, 2, 3$), defined as

$$S_{ij} = \sigma_{ij} - \sigma_m \delta_{ij} \tag{4}$$

And δ_{ij} is the Kronecher delta $\delta_{ij} = 1$ for $i=j$ and $\delta_{ij} = 0$ for $i \neq j$

3. Fe Modeling Dual Indenter and Effects of Material Properties

Figure 1(a). show the FE Models of the Vickers indentation. Only a quarter of the indenter and material column was simulated as a result of plan symmetric geometry [5]. The sample size is more than 10 time the maximum indentation depth, which is sufficiently large to avoid any sample size effect or boundary effect. The element type used is C3D8R (reduced integration element used in stress/displacement analysis). The material of interest was allowed to move and the contact between the indenter surface and the material was maintained at all the time. The Vickers indenter has the form of the right pyramid with a square base and an angle of 136° between opposite face. It is normally made of diamond with Young’s modulus of over 1000 GPa, which is significantly stiffer than steel ($E=200$ GPa). The indenter was considered as the rigid body to improve the modelling efficiency. This work is focused on the studies of plastic parameters, so only the loading curve was utilised to predict the plastic material parameters.

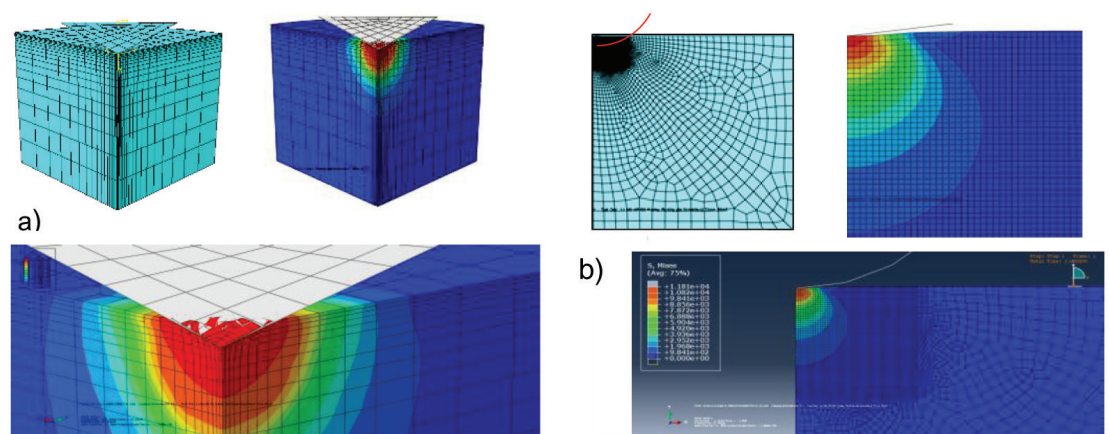


Figure 1: a). Typical Vickers indentation and b). Spherical Indentation.

Different from the Vickers indenters, spherical indenter is fully asymmetric, a typical FE model is shown in Figure.1(b). A planar specimen ($3 \times 3 \text{ mm}^2$) has been used and this specimen size is large enough to avoid potential sample size effect. The movement of the indenter

was simulated by displacing a rigid arc (rigid body) along the Z axis. The bottom line was fixed in all degree of freedoms (DOF) and the central line was symmetrically constrained. The element types used in the spherical indentation model are CAX4R and CAX3 (4-node bilinear asymmetric quadrilateral and 3-node linear asymmetric triangle element used in stress/displacement analysis without twist). A gradient meshing scheme has been developed for different regions. The mesh size is 5 μ m in the region underneath and around the indenter, while the mesh size of other regions from the nearest region to the outer edge varied from 10 μ m, 0.05 mm and 0.1mm;

A plane symmetric FE model of the spot welded joint has been established (as shown in Figure 2). The material properties used in this model will be predicted by the inverse FE modelling. An element type of C3D8R (a reduced-integration element used in stress/displacement analysis) was used. Due to symmetry the y-direction displacement at the mid-section (bottom surface) was set to zero. The left side of the specimen was fixed ($U_{x,y,z}=0$) and a displacement ($U_x=L$) was applied on the movable end. The z displacement at the mid-section was set to zero. The dimensions of the welding zones were based on the micro-hardness experimental data and optical observation. All these zones were assumed to have elasto plastic properties.

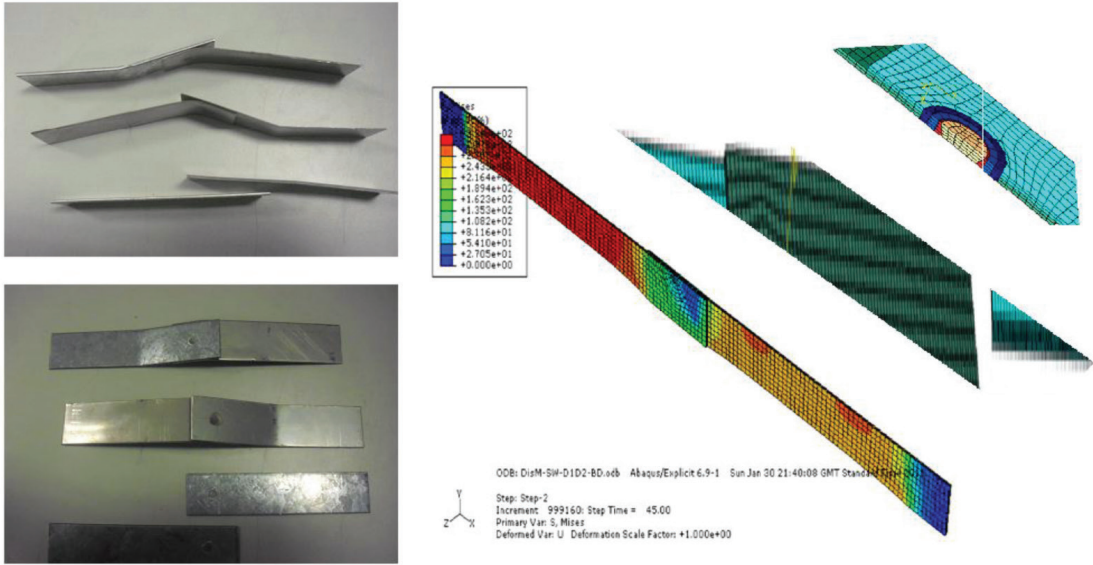


Figure 2: Specimens testing results and Typical FE to be used for simulating the tensile shear for spot welded joint.

4. Identification of Materials Parameters Based on Static Indentation

The P-h curves for both Vickers and Spherical indentation obtained the following relationship:

$$C = P/h^2 \tag{5}$$

Where P and h are the load and indentation depth on the loading curve respectively. C is the curvature coefficient with the curvature for the Vickers Indentation and spherical indenter designated as C_v and C_s respectively. The curvature is a function of the yields stress and the work hardening coefficient. The three approaches have been comparative developed to assess their suitability to predict the materials properties based on the dual indenter approach. The relationship between the curvature for both the Vickers and spherical were developed then

used a chart to predict all the material sets with the same curvature. The relationship is used to predict the material sets have the same indentation curvature. Evaluation of accuracy on the approach using 3D. The selected input data with variations in the value (n) and $\sigma_y = 100, 140, 190$ and 300 . Accuracy study chart mapping 3D-Linier on average accuracy error $\Delta n / n$ (%) is 0.1% both the prediction (n) on Vickers Indentation and on Spherical Indentation. This shows the selected predictors significantly acceptable within the limit of level confidence less than 0.5% .

Tensile-Shear test of spot weld joint has objectives for determining the elastic plastic behaviors of the welded joints being tested. Two specimen with different materials (stainless steel and Mild steel) and thickness were used. Stainless steel used is stainless steel grade 304 with a width of 25mm and thickness of 0.8mm , the other specimen is mild steel with a width of 25mm and thickness of 1.44mm . The machine has a maximum loading capacity of 30kN , with the readings being accurate to 0.5% of the force. Drop mass tests were performed in order to determine the effect of materials on deformation of welded joints under dynamic loading, which represents the crash and energy absorption characteristics of structure.

As shown in Figure 3. The modeling results showed a good agreement with the experimental data. This suggests that material laws predicted by dual indenter FE modeling of indentation test for different zones (σ_y, n) is accurate. The slight differences between numerical and experimental results on the fracture behavior suggest that detailed fracture for each material zone has to be obtained rather than using parameters from the base material, which requires further investigation.

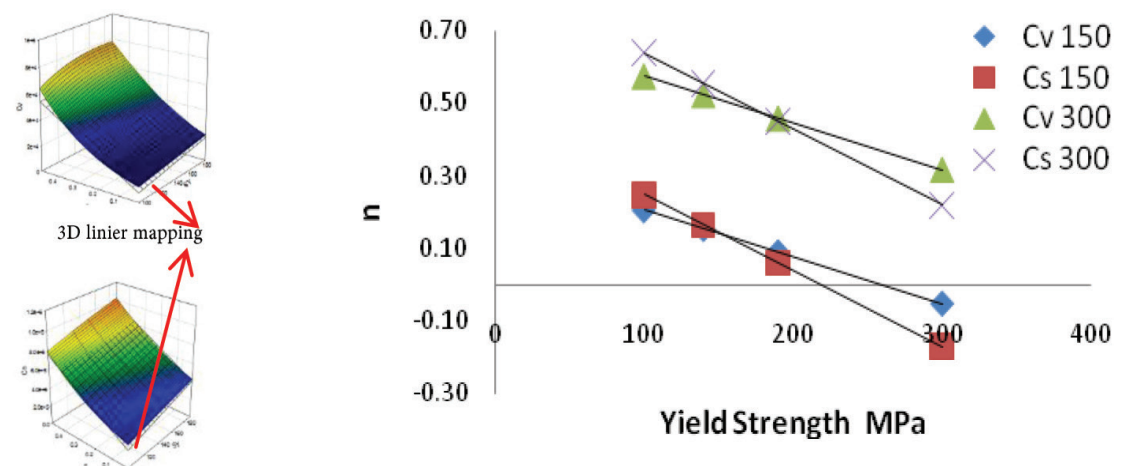


Figure 3: Typical results of inverse FE modelling on Vickers and Spherical indentation by Plotting and mapping data result from Cv and Cs chart to used predicted materials parameter.

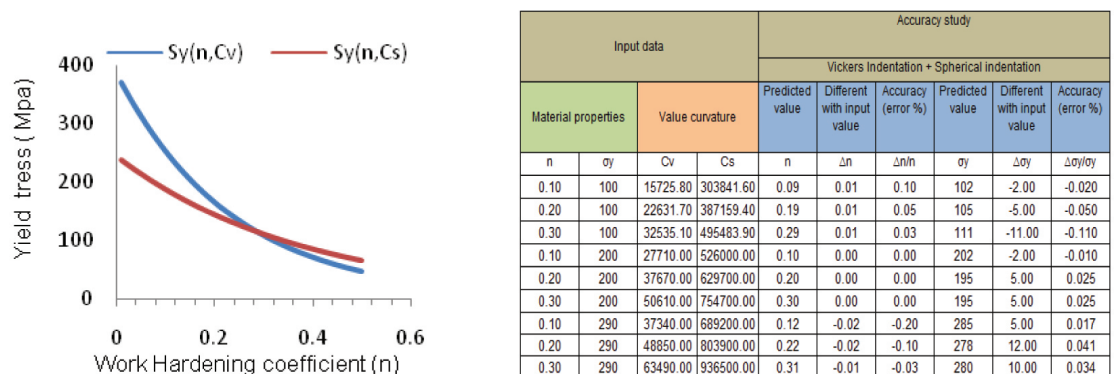


Figure 4: Typical materials parameter prediction process ($\sigma_y = 100$ Mpa, $n = 0.2$) and Accuracy study results based on the intersection between properties line for the Vickers and Spherical indentation.

5. Conclusion

A new inverse modeling using numerical approach constitutive material based on static indentation has been developed and validated. The evaluation based on numerical experimental data showed similar accuracy to the continuous indentation curve approach. The approach developed was successfully used to characterize the plastic properties of different zones in spot welded joints. These plastic material parameters were used in modeling the tensile shear deformation of the spot welded joint and showed good agreement with experimental results. The validated FE models were further used to predict the effect of nugget size and the thickness of the metal sheet on the strength of welded joints.

References

- [1] Aslanlar S., et al., 2008. Welding time effect on mechanical properties of automotive sheets in electrical RSW, *Materials and design*, vol 29, 7, pg 1427-1431.
- [2] Fan X., 2007. Simulation of distortion induced in assemblies by spot welding, *Engineering manufacture*, vol 221, 8, pg 1317-1326.
- [3] Hou Z., et al., 2007. Finite element analysis for the mechanical features of RSW process, *Journal of materials and Processing Technology*, 185, 1-3, 160-165.
- [4] Rahman M.M., et al., 2008. An Investigation into the effects of spot diameter and sheets thickness on fatigue life of spot welded structure based on FEA, *Research Journal of Applied Science*, 3(1):10-15.
- [5] Budiarsa. I N., 2013 Indentation Size Effect (ISE) of Vickers hardness in steels: correlation with H/E, *Applied Mechanics and Materials* Vol. 391 pp 23-28.

Conference Paper

Evaluation of Operating Performance of the Reactor Coolant System of RSG-GAS using ChemCad6.1.4

Sukmanto Dibyo¹, Ign.Djoko Irianto¹, Santosa Pujiarta²¹PTKRN BATAN, Gedung 80 kawasan Puspiptek Serpong²PRSG BATAN, Gedung 30 kawasan Puspiptek Serpong


Abstract

Evaluation of the operation of reactor main coolant system RSG-GAS is very important. This is related with the operation of the reactor that has been going on more than 27 years although the current reactor coolant system is still operating safely. The main coolant system RSG-GAS including both the primary and secondary cooling system. Evaluation can be conducted by calculating the coolant system performance by using the ChemCad6.1.4 software. Furthermore, this calculation result is compared with the most recent measurement in the cooling system operation. By this way it can be known the performance degradation in the Reactor Coolant System operation. The operating parameter data of primary and secondary cooling system are temperature, pressure and flow rate of coolant. The reactor operation at the power of 15 MW is used as a reference data. The calculation result shows that the temperature parameter between calculation by ChemCad and the measurement data qualitatively is no significant deviations. However in the secondary coolant system, the outlet pressure of both heat exchanger nozzles are 0.8 bar and 1.2 bar that indicate lower than the calculation results. It's may be caused by the flow disturbances through the tube-side of heat exchangers. In generally the existing operating parameters on the reactor cooling system in terms of safety aspects still under safely condition.

Corresponding Author:
Sukmanto Dibyo,
email: sukudibyo@batan.go.id

Received: 29 July 2016
Accepted: 21 August 2016
Published: 21 September 2016

Publishing services
provided by Knowledge E

 Sukmanto Dibyo, et al.
This article is distributed
under the terms of the
Creative Commons
Attribution License, which
permits unrestricted use
and redistribution provided
that the original author
and source are credited.

Selection and Peer-review
under the responsibility of
the ICoNETS Conference
Committee.

Keywords: evaluation, cooling system RSG-GAS, ChemCad6.1.4

1. Introduction

Evaluation of operating data on the reactor main cooling system RSG-GAS is very important because this is related with the operation of the reactor that has been going on since the year of 1987 [1, 2]. Analysis of cooling system for the RSG-GAS reactor has been performed by modeling of steady-state using RELAP5 several years ago [3]. To obtain the results of an evaluation of the RSG-GAS reactor operation, it can be performed using the ChemCad6.1.4 software. Although the current operating condition of reactor still meets the high safety criteria, but to ensure that the reactor remains can be operated reliably. Therefore, the evaluation of primary and secondary cooling system on steady-state is one thing that is very meaningful. In operation of Reactor Coolant System RSG-GAS, currently indicates that the reactor is operated safely [4], where the integrity of the reactor core can be maintained against damage caused by high temperature of coolant.

 OPEN ACCESS

Therefore, to obtain a high confidence to the safety aspects of such reactor operation, it is necessary also to evaluate the operation conditions of Reactor Cooling System.

The evaluation is conducted by comparing the measured data with the calculation results of operating parameters such as the temperature, pressure and flow rate of cooling systems. Recently, the reactors usually operate at a power of 15 MW, therefore the reference data of 15 MW reactor power is used.

At first step, the evaluation of operating parameters in the cooling system is to create the flow diagram of cooling system and the input parameter using the ChemCad6.1.4 Software. The input data without degradation of performance components particularly in the heat exchanger can be applied. In this case, there is any possibility of decreasing the heat transfer coefficient [5]. On the other hand, the degradation of whole cooling system commonly that caused by the aging of component may be also evaluated. Furthermore, the calculation result can be compared to the measurement data of the cooling systems. In addition, the evaluation regarding to the Reactor Cooling System RSG-GAS have also been done by previous activities [4,6].

The ChemCad6.1.4 is a program that capable to be used to design the operation, evaluation at the industry of process equipment manufacturing, analysis of unit operation, the process instalation including for the new designs (equipment sizing) of reactor cooling system [7]. The ChemCad software has been successfully applied in the design of cooling system for OPAL Research Reactor 20 MWt Australia [8]. The program can quickly configure a graphical flow-sheet, user friendly and component data completely if compared to other software such as cycle-tempo and HTRI's.

The purpose of this paper is to evaluate the operation parameter of main Reactor Cooling System RSG-GAS at the steady state operating condition. The evaluation is carried out by comparing the most recent measurement in the cooling system operation with the calculation results from the ChemCad6.1.4 SOFTWARE. Such operation parameter are primary cooling temperature, secondary cooling temperature, pressure and coolant flow rates. In the evaluation of this cooling system, the evaluation of operation parameter beyond of main Reactor Cooling System (such as emergency system, water purification system etc) are not considered.

2. Reactor CoolANT System of RSG-GAS

The main Reactor Coolant Systems consist of the primary cooling system, the secondary cooling system and the pool cooling system are shown in Figure 1, schematically. The primary and secondary cooling systems are to assure safe temperatures in the core at normal operation. During power operation of the reactor, the heat released in the core is removed by the water of the primary cooling circuit which flowing downwards through the core. The primary cooling system is cooled by two units of heat exchangers, through which heat is transferred to the secondary cooling circuit and then dissipated to the atmosphere through mechanical draft cooling towers. The main components of the cooling system consist of the primary cooling pumps, primary heat exchangers and cooling tower [9]. To monitor the operating parameter data of cooling system are provided by the measuring instrument such as flow rate, temperature, pressure and other indicators. The Flow Diagram as depicted in Figure 1, the temperature and pressure indicators are located in the position that related to the operating data of cooling systems, such as a temperature indicator is installed in the cooling flow line to the reactor, the main suction line before the primary cooling pumps, the

primary cooling inlet and outlet temperatures of each heat exchanger, secondary coolant outlet temperature from cooling towers. Further pressure indicators are located in the suction and discharge nozzles of the primary cooling pumps and secondary cooling pumps. A standard orifice is provided in the suction branch of each pump and indicates continuously the flow of each pump with analogue recorder. Furthermore, the flow of coolant pressures and temperatures that measured in each section.

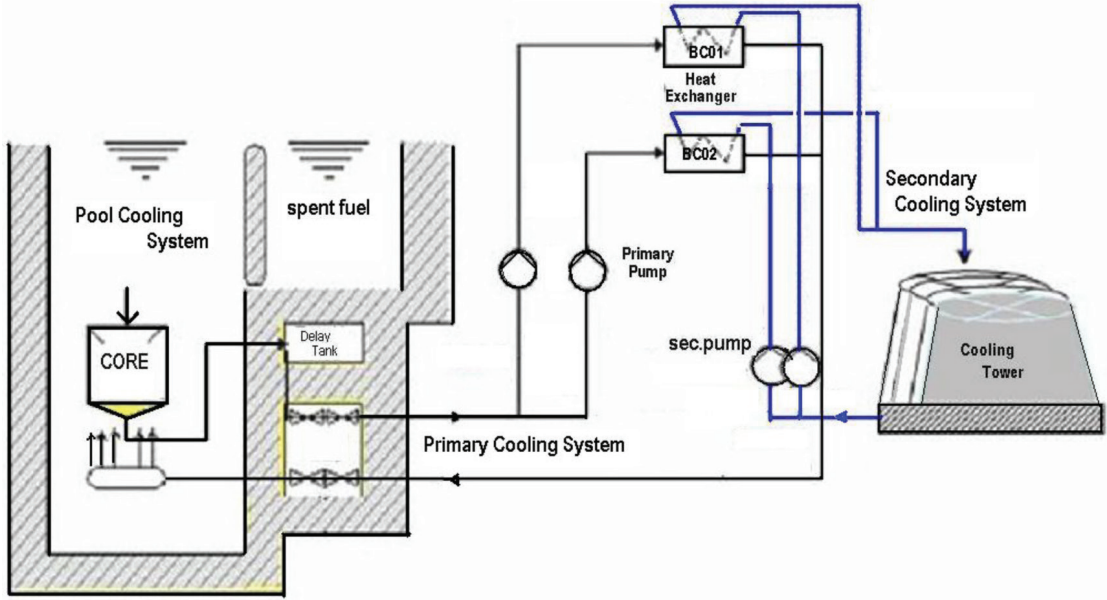


Figure 1: Flow Diagram of Main Reactor Coolant System [9].

3. Chemcad6.4.1 Software

The ChemCad software is a tool to analyze both steady-state and dynamic systems. The software uses Visual Basic Applications, and it can calculate the modeling continuous, batch, and semi-batch processes. The software is used for the design, operation, and maintenance of chemical processes in a wide variety of industries, including oil and gas production, refining, gas processing, biofuels and process equipment manufacturing [10]. Optimization calculations can also be made to the existing process, the rating on vessels, columns, heat exchangers, piping, valves and instrumentation. In the application of ChemCad, it can quickly configure a graphical flowsheet of simple or complex processes and then enter data in a Windows format to calculate the process, mass and energy balances. The software is user friendly and interactive because it directly inform less input or if an error has occurred. However, the user should have an understanding toward the principles of unit operation process.

Description of module feature contained in the ChemCad6.1.4 are as follows:

1. CC-Steady State.
The main ChemCad product, known as CC-Steady State, enables you to design new processes, rate existing processes, and optimize processes in steady state.
2. CC-Dynamics
The module known as CC-Dynamics makes it possible to design and rate existing processes using a dynamic simulation. This module is fully integrated with ChemCad to

make switching between steady state and dynamics easy and intuitive. By using CC-Dynamics, its can easily simulate everything from simple to complex control systems.

3. **CC-Batch**
This module enables to design, rate, or optimize a batch column. CCBatch includes a scheduling interface to allow an “operation step” approach to simulation of batch columns.
4. **CC-Therm**
The CC-Thermis used to design a single heat exchanger, or vet a vendor’sheat exchanger design. It is also ideal to rate existing exchangers in new service, or to perform calculations on hypothetical situations. CC-Therm can simulate shell-and-tube, air-cooled, plate-and-frame, and double-pipe exchangers. Full integration with ChemCad makes it possible to calculate exit conditions from exchanger geometry for high-fidelity simulations.
5. **CC-safety net**
The CC-Safety NET provides the capability to design or rate piping networks and safety relief devices and systems, in both steady-state and dynamic systems. The steady-state features of CC-Safety NET are included with CC steady-state. This product enables to make simultaneous flow and pressure balanced simulations even in reverse-flow situations for single or multi-phase flow.

4. Evaluation Methodology

The evaluation methods used in the analysis of Reactor Coolant System are systematically shown in Figure 2 as follows,

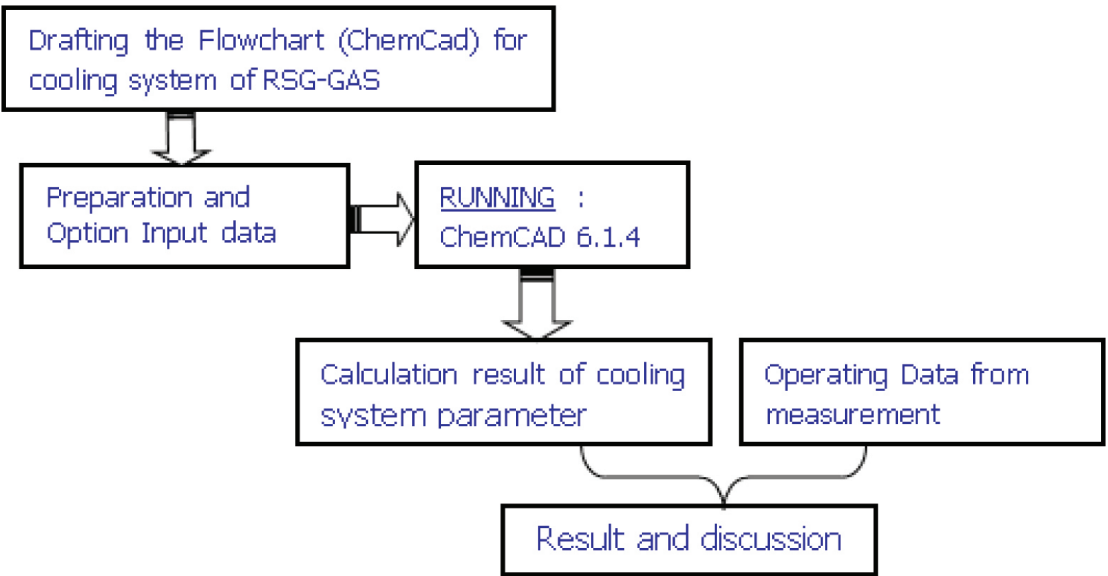


Figure 2: Schematic Flow Diagram for Evaluation.

Based on the drafting of flowchart and input data used for cooling system of RSG-GAS running the ChemCad is carried out. The running results and operating parameter of cooling system from measuring data of stream are evaluated by running the model [11].

Result and discussion focuses to the output of data analysis result and the data of operating measurement. Before running, the operating data parameters are evaluated, including temperature, pressure and flow rate. The input data of flowrate related to the coolant system are shown in Table 1 as follows:

TABLE 1. Input data of Flowrate.

No	Parameter	Nilai
1	Volumetric flowrate of primary coolant line-1, m ³ /h	1550
2	Volumetric flowrate of primary coolant line-2, m ³ /h	1600
3	Volumetric flowrate of secondary coolant line-1, m ³ /h	1950
4	Volumetric flowrate of secondary coolant line-2, m ³ /h	1950

The primary cooling system is calculated in adiabatic system, there is no heat is absorbed from the air or released into the air. Heat generated from the reactor is only released through the secondary cooling system by the cooling tower. The reactor thermal power of 15 MWt is used as a input data.

5. Results and Discussions

Based on the calculating results using the ChemCad software, the mass balance and heat balance in each of flow stream can be obtained. Mass and heat balance of the cooling system are quantitative data on the flow of coolant inlet, outlet and accumulated released in the system. At steady-state, mass and heat balance of the system components i.e inlet and outlet flow are equal [12]. So that the balance calculation is useful to evaluate the existing coolant system by analyzing the operating parameters of coolant system when the degradation of operating condition has not happened yet. By comparing the data operating parameter taken from measurement result so can be described the degradation of cooling system operating condition. In this evaluation, calculation of coolant system focuses only on the main line of primary and secondary cooling system for the parameter of temperature, pressure and flow rate. As notation here that this analysis does not involve the pool cooling system, spent fuel, emergency coolant system and purification systems.

According to the fundamental principles of the system analysis, the calculation for cooling system must be carried out together with the apparatus of the flow sheet [13]. Figure 3 depicts the flow diagram of coolant system RSG-GAS that prepared using the ChemCad6.1.4 software as an output result of calculations. In this diagram, there are two lines of primary and secondary cooling system correspond with the existing diagrams of Reactor Coolant System RSG-GAS. The Figure 3 is also provided the location of parameter indicator of temperature, pressure and mass flow rate parameters for each stream [14]. Then there are both two rectangular and circle marks that indicate the stream number and unit operation component number.

Input data used in the evaluation of this cooling system are flow rate and inlet temperature of coolant to the reactor. While in the secondary coolant system, the water temperature of the cooling tower is 34°C correspond with the measurement data as input calculations.

Simulation of the RSG-GAS coolant system at reactor power of 15 MWt has been done in which includes volumetric flowrate, temperature and pressure of coolant flow respectively. As shown in Table 2 that the parameter data available from the measurement results can be compared with the results of the analysis from the ChemCad6.1.4 software in the steady state

condition. It shows that with the assumption of adiabatic system, the temperature parameter between calculation result by ChemCad and measurement data in general is no significant differences (stream no.1, no.9, no.10, no.11, no.22 and no.27). This small difference as shown in Figure 4 is caused by the measurement data were not ignoring the existence of heat loss (< 1%) flowing out from the Reactor Coolant System to the air [15].

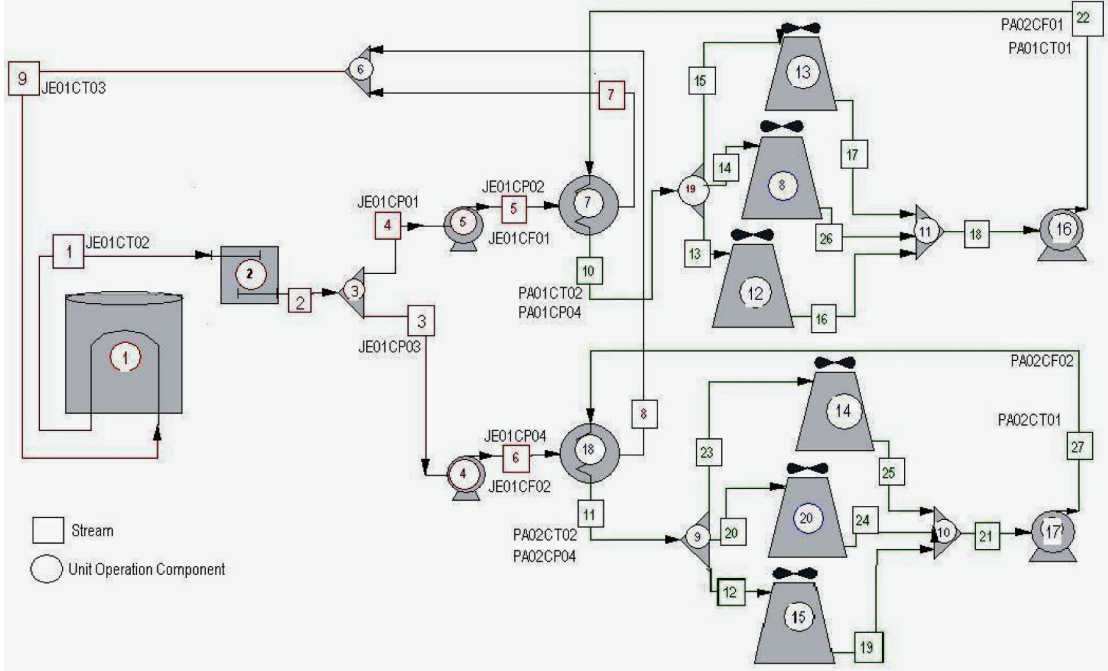


Figure 3: Flow diagram of coolant system RSG-GAS

There are differences flow pressure of primary as well as secondary system of line-1 and line-2 (as shown in Figure 4). In the suction side of the primary cooling pump (stream no.3 and no.4), the lower pressure than the calculation result occurred (Figure 5). This may be caused by pressure drop along the flow line of suction side of primary cooling pumps. Meanwhile in the secondary cooling system, the outlet pressure of both heat exchanger nozzles are 0.8 bar and 1.2 bar (stream no.10 and no.11) shows lower than calculation results. Due to this calculation assuming the heat exchangers without fouling, therefore the high pressure drop excessively is also indicates the degradation performance of heat exchanger. Blockage by impurities cause a decrease in efficiency due to reduced heat transfer area and the increase in pressure drop [16]. As note information that the secondary cooling water from the cooling tower flows pass through the tube-side of heat exchangers. Its may be caused by the flow disturbances through the tube-side of heat exchanger.

The reactor power is indicated from the reference data which uses neutronic detector and refers to data calorimetric [17]. In this case the reactor power measurement does not involve the heat energy lost out from the coolant system to the environment. Differences may occur due to the reactor power calculated by ChemCad is based on the equation of thermal energy conservation, in which heat generated from the reactor are absorbed by the cooling system and there is no heat accumulated in the system. Besides, there are many factor possibilities that could cause these differences. Nevertheless in general the existing operating parameters of Reactor Coolant System in terms of safety aspects is still under safely condition. Coolant temperature to the reactor as a operational limit parameter of Reactor Protection System (RPS) is acceptable.

TABLE 2. Operating Data of Cooling system RSG-GAS.

No	Operating Parameter	Indicator	Stream no.	Data measured	ChemCad
1	Primary coolant temp. in-core, °C	JE01CT03	9	36	36.0
2	Primary coolant temp. out-core °C	JE01CT02	1	41	41.5
3	Primary coolant pressure in-pump1, bar	JE01CP01	4	0.20	0.30
4	Primary coolant pressure in-pump2, bar	JE01CP03	3	0.15	0.30
5	Primary coolant pressure out pump1,bar	JE01CP02	5	2.60	2.60
6	Primary coolant pressure out pump2,bar	JE01CP04	6	2.65	2.60
7	Primary coolant flowrate-1, m³/h	JE01CF01	5	1550	1550
8	Primary coolant flowrate-2, m³/h	JE01CF02	6	1600	1600
9	Secondary coolant temp in-BC1 °C	PA01CT01	22	34	34.0
10	Secondary coolant temp out-BC1 °C	PA01CT02	10	38	37.5
11	Secondary coolant temp in-BC2 °C	PA02CT01	27	34	34.0
12	Secondary coolant temp out-BC2 °C	PA02CT02	11	38	37.5
13	Secondary coolant flowrate-1, m³/h	PA01CF01	18	1950	1950
14	Secondary coolant flowrate-2, m³/h	PA02CF01	22	1950	1950
15	Secondary coolant press in-pump1 bar	-	18	-	0.80
16	Secondary coolant press out-pump1 bar	PA01CP02	22	2.95	2.95
17	Secondary coolant press in-pump2 bar	-	21	-	0.80
18	Secondary coolant press out-pump2 bar	PA02CP02	27	2.95	2.95
19	Secondary coolant press out-BC1 bar	PA01CP04	10	0.80	1.30
20	Secondary coolant press out-BC2 bar	PA02CP04	11	1.20	1.80
21	Reactor power, MWt			15	16

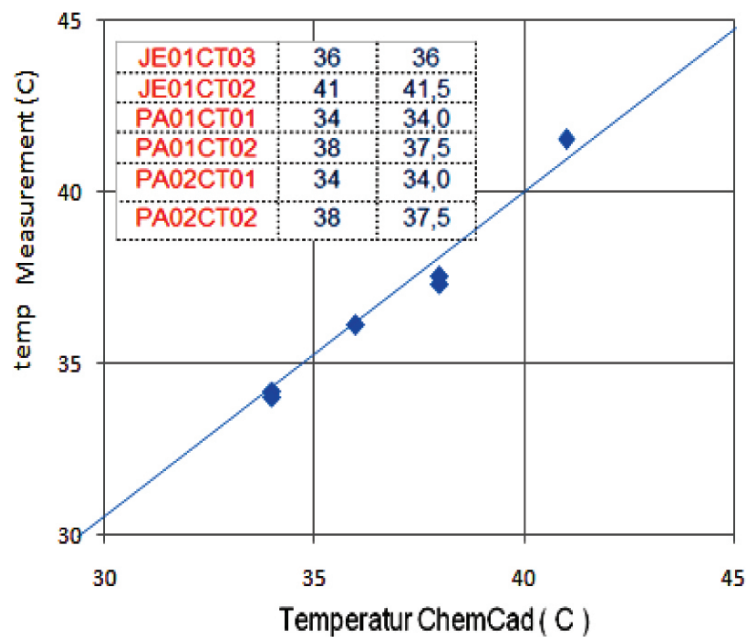


Figure 4: Curve of Temperature differences.

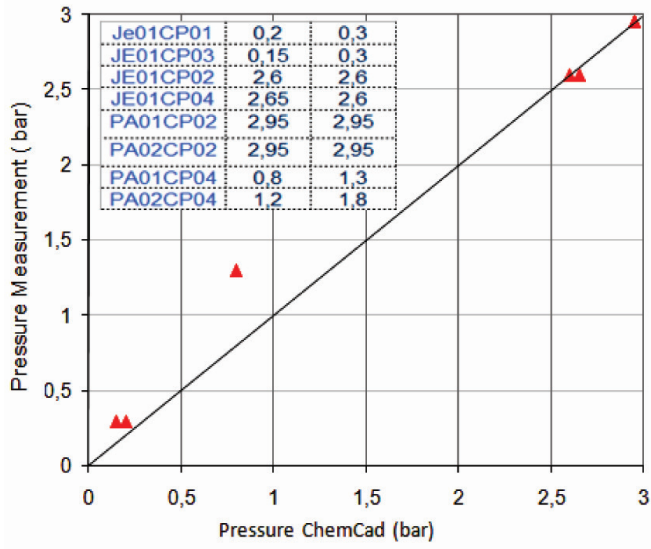


Figure 5: Curve of Pressure differences.

6. Conclusion

Based on the steady state calculation results of the reactor RSG-GAS at the power of 15 MW shows that the coolant temperature parameter between calculation by ChemCad and the measurement data in general is no significant differences. However in the secondary cooling system, the outlet pressure of both heat exchanger nozzles indicates lower than the calculation results. It might be caused by the flow disturbances through the tube-side of heat exchangers. In general the existing operating parameters on the Reactor Coolant System in terms of safety aspects is still under safely condition.

7. Acknowledgment

The authors thanks to the Mr.M.Yahya, Head of System Mechanic Reactor Operation at Center for Multipurpose Reactor of BATAN for preparing the measurement data.

References

- [1] Thantawi N, "Analysis For RSG-GAS Operation Characterictic of Reactor Cooling System", Prosiding Seminar Hasil Penelitian PRSG, p.303, 1998.
- [2] Suroso, "Comprehensive Evaluation of Secondary Cooling System of RSG-GAS", prosiding Seminar Hasil Penelitian P2TRR, p.109, 2005.
- [3] Dibyo S, "Validation of RSG-GAS Cooling System Model at Steady-State for the RELAP5. Mod3', Jurnal Teknologi Reaktor Nuklir; v.7(2); ISSN 1411-240X; Jun 2005.
- [4] Iman K, "Evaluation on the Performance of Safety Systems of the RSG-GAS Reactor during 25 Years Operation", Bulletin of Nuclear Reactor Operation, p.1-10, Vol.11, No.1 2014.
- [5] Durgesh B. et.al, "Shell and Tube Heat Exchanger Performance Analysis", International Journal of Science and Research (IJSR), Vol.3 Issue 9, Sept 2014,
- [6] Purwadi MD, "Approach to the Aging Management of RSG-GAS", Prosiding Seminar Hasil Penelitian PRSG, p.161, 2005.

- [7] Herry Hartis, "Unsteady-State Simulation Using CHEMCAD", Process Engineering Associates, LLC June 2008.
- [8] Invap, Reactor Cooling System and Connected Systems, RRRP-7225-SAR Chapter 6, ANSTO, Nov-2004.
- [9] PRSG, LAK RSG-GAS, Chapter. 6, Rev. 10, 2011.
- [10] Solanki K et.al, "Process Optimization Using ChemCad", Special Issue Azeotrope Vol:I, Issue:II Pub:2014, Page: 47-51, International Journal of Futuristic Trends in Eng. and Tech.
- [11] Bhattarai M et.al, "Design of Shell-Tube Heat Exchanger (1-shell series & 1-shell parallel)", INROADS-An International Journal of Jaipur National University, Vol3, Issue:1st, 2014.
- [12] Akram W.et.al, "Thermo-Hydraulic Behavior of Water Cooling Channel Subjected to Constant Heat Flux during Pressure Reduction Transient in its Cooling System", International Journal of Computer Applications (0975-8887) Vol 80, No 1, October 2013.
- [13] Gartman T.N et.al, "Experience in the application of the CHEMCAD program to the modeling of reactor processes", Theoretical Foundations of Chem.Engineering, Vol.43, No.6, 2009.
- [14] Sudiyono, "Cooling System of The RSG-GAS, A Study of Disabilities", prosiding Seminar Teknologi Pendayagunaan Reaktor Riset G. A. Siwabessy; 130-137, 1995.
- [15] Dibyo S, "Assessment Of Heat Loss For RSG-GAS Primary Cooling System" Prosiding Seminar Hasil Penelitian PRSG1998.
- [16] Dibyo S, "Analysis of Tube Plugging of the RSG-GAS Reactor Heat Exchangers", Jurnal Tekn. Reaktor Nuklir Vol. 9 No. 3 Oktober 2007.
- [17] Slamet W, "Influence Of Fork-Absorber Test On Core Reactivity And Power Calibration RSG-GAS", Prosiding Seminar Penelitian Dan Pengelolaan Perangkat Nuklir, PTAPB, p.323, Yogyakarta, 27 Juli 2011.

Conference Paper

Loss of Flow Event Analysis of the RRI-50 Conceptual Design

Endiah Puji Hastuti, Surip Widodo

Center for Nuclear Reactor Technology and Safety, National Nuclear Agency of Indonesia (BATAN) PUSPIPTEK Area Building No. 80 Serpong, Tangerang Selatan 15310, Indonesia

Abstract

The conceptual design of Indonesia's Research Reactor (RRI-50) core has reached the design optimization phase. RRI-50 is designed to produce the maximum neutron flux of 1.0×10^{15} n/cm²s and thermal neutron flux of 5.0×10^{14} n/cm²s. The analysis of design basis accident should have anticipated any possible accidents, one of which is loss of flow event that should be met according to the IAEA safety standard. There are many conditions that cause loss of flow accident, such as pump failure. This series of event may trigger an accident due to loss of coolant. Therefore, the event should be deeply analyzed. Loss of flow event analysis has been carried out using PARET-ANL code. The margin toward flow instability and two-phase flow becomes a design limit. The analysis was performed during initial period of event. The reactor scram occurred at 2.1 second because flow rate trip reaches 85% from its nominal value. Based on loss of flow event of the design basis accident of RRI-50 core, it can be concluded that the margin toward flow instability at the early transient, which is the worst condition, has not generated two-phase flow at a constant pressure.

Corresponding Author:
Endiah Puji Hastuti,
email: endiah@batan.go.id

Received: 29 July 2016
Accepted: 21 August 2016
Published: 21 September 2016

Keywords: Conceptual design, RRI-50, loss of flow event, simulation, code

Publishing services
provided by Knowledge E

© Endiah Puji Hastuti, et al. This article is distributed under the terms of the [Creative Commons Attribution License](#), which permits unrestricted use and redistribution provided that the original author and source are credited.

Selection and Peer-review under the responsibility of the ICoNETS Conference Committee.

 OPEN ACCESS

1. Introduction

The conceptual design of Indonesia's Research Reactor (RRI-50) has been at the design optimization stage. The RRI-50 is designed to achieve the average neutron flux as high as 1.0×10^{15} n/cm²s and thermal neutron flux of 5.0×10^{14} n/cm²s, while it is expected to operate at the lowest possible power. The reactor core components are built in 5x5 array configuration of 16 fuel elements and 4 fuel rods and 5 irradiation positions. This reactor is water (H₂O) cooled with heavy water (D₂O) moderator. The fuel used is uranium molybdenum with high uranium content (7 – 9 g U/cm³). Its core and power is in accordance with the User Criteria Document requirements and will generate high heat generation [1]. To support the design, the reactor center should be designed as compact as possible. Consequently, heat flux density at each fuel element becomes high and creates a challenge to be overcome in term of its heat removal.

In the previous research, core cooling system has been designed to indicate that heat flux generated is 590 W/cm² [1]. To prevent boiling, reactor core should be located in a pressured vessel and coolant flow rate in the parallel fuel channels is estimated high. The calculation results obtained from the previous study indicated that design criteria of $DNBR \geq 2$, ΔT_{ONB} and $V \leq 2/3$ of critical flow rate not exceeded for $P_{inlet} = 8$ kgf/cm² with flow rate of 900 kg/s [2]. Sufficient coolant design should be completed with Design Basic Accident (DBA) of

the primary coolant ensuring fuel safety in case of loss of coolant flow. To facilitate neutronic design and thermal hydraulic design, calculation of thermal hydraulic design has been carried out. As thermal hydraulic safety margin defines reactor power operation, reactor power will be in proportion with thermal neutron flux obtained.

Conceptual design of RRI-50 is considered as a research reactor with high power. This reactor concept has some similarities with China Advanced Research Reactor (CARR). The characteristics of CARR reactor have been analyzed by researchers through computer modeling. Tian et al. (2005) calculated theoretically reactor core thermal hydraulic characteristics of CARR at steady and transient state [3], while Qing Lu et al. (2009) performed a similar analysis using THAC-PRR code developed in Visual Fortran 6.5 [4]. Meanwhile, Ronghua Chen et al. (2011) carried out accidental analysis on CARR due to reactivity insertion, caused by unexpected control rod withdrawal in full power condition, using TSAC1.0 code [5]. To study the CARR thermal hydraulic safety characteristics at accident condition due to station blackout, Wenxi Tian et al. (2007) conducted an accidental analysis using TSACC code developed [6]. The use of computer codes for calculation such as PARET-ANL, RELAP-5 et cetera has proved that these codes can be used to analyze thermal hydraulic safety at steady state and transient state as carried out by Hamidouche (2009), Omar S. AL-Yahia et al. (2013), and Chatzidakis (2014) [7-9].

One of the engineered safety features (ESF) in the research reactor is residual emergency core cooling system (RECCS). The main function of RECCS is to remove heat from the core after reactor scrams and the primary cooling system does not operate, while core cooling by natural circulation is not possible. For an open pool reactor, there is an alternative design to avoid the use of such system. Passive system, such as coolant flow, fly-wheel inertia, flap valve and core chimney, is sufficient to overcome black out event. This system is not available for a research reactor with a pressure vessel in the pool, in which RCCS is provided and supplied by an onsite emergency power supply to overcome black out event [10].

The RRI-50 fuel is plate type, which is cooled by primary coolant flowing through parallel gaps and supplied by primary coolant pump. When the primary pumps inadvertently shutdowns, the core should shutdown. When the core shutdown, there is residual heat that will decrease with time. To remove this residual heat, the primary coolant pump should be designed to be able to flow the coolant for residual heat removal. The fly wheel in the coolant pump should have enough time to continuously flow the coolant. In addition, there are many cases, including pump failure, that cause loss of coolant flow. These events can initiate an accident due to loss of coolant. Therefore, they should be evaluated in depth. Loss of coolant flow event is one DBA that should be analyzed to meet IAEA safety standards. The RRI-50 primary coolant safety design should be able to anticipate black out event, in which no power is available to run the primary cooling pump, causing loss of coolant flow. The pump design should anticipate any pump failures, in which reactor core cooling safety by the primary coolant system should be ensured. Based on the previous analysis on high power research reactor such as CARR, and analysis results obtained from computation code used in the accident analysis at high power research reactor, this paper is aimed to describe an analysis on thermal hydraulic characteristics of RRI-50 core due to loss of coolant flow event during early accident, using PARET-ANL code.

2. Theory

The thermal hydraulic condition in the reactor coolant channel during transient can be outlined using mass, momentum, and energy conservation laws. The fundamental laws of mass, momentum, and energy conservation for irregular shape with constant control volume V , and surface area S , are as follows (Liepmann, 1957; Delhay, 1981) [8]:

$$\frac{\partial}{\partial t} \left[\int_v \rho dv \right] + \oint_s r \bar{u} \cdot d\bar{s} = 0 \quad (1)$$

$$\frac{\partial}{\partial t} \left[\int_v (\rho \bar{u}) dv \right] + \oint_s (\rho \bar{u}) \bar{u} \cdot d\bar{s} = \oint_s (\bar{p}) ds + \oint_v \rho \bar{\psi} dv \quad (2)$$

$$\frac{\partial}{\partial t} \left[\int_v (\rho e) dV \right] + \oint_s (\rho e) \bar{u} \cdot d\bar{s} = -\oint_s \bar{\phi} \cdot d\bar{s} + \oint_v q'' dV + \oint_s (\bar{u} \cdot \bar{p}) d\bar{s} + \int_v \rho \bar{u} \cdot \bar{\phi} V \quad (3)$$

where:

- ρ : Volume weight density for two phase coolant, (kg/m³)
- \bar{u} : Fluid flow vector, (kg/s.m²)
- p : Pressure, (Pa)
- $\bar{\phi}$: Heat flux vector, (MW/m²)
- $\bar{\psi}$: Body force vector per mass unit, (Pa)
- e : Internal energy per mass unit, including intrinsic heat (H-P/ρ); and kinetic energy $\frac{1}{2} u^2$, MW.s.
- q'' : Internal volumetric heat generation rate, (MW/m³)

Simulation of loss of coolant flow is carried out using PARET-ANL code. Before transient calculation is performed, steady state condition should be identified first where it is assumed that the reactor has been in operation for 24 hours so that equilibrium condition is achieved. Distribution of axial and radial power peak factor employs the calculation results of neutronic group, UMo-Al fuel with fuel loading of 360 gr U/cm³. The axial power peak is divided into 21 nodes, where the distribution of axial and radial power peak has considered nuclear and engineering uncertainty.

Coolant System Design

Based on the generated power, generally, research reactor can be classified into three groups: low power, medium power, and high power research reactor. Low power research reactor has power density of less than 100 kW/liter. Medium research reactor operates above 10 MW, typically about 30 – 40 MW until 70 MW with power density over 100 kW/liter. High power research reactor group is based on its core power and compactness in term of high power density and uses vessel designed in a pool. For its safety, a high power research reactor requires forced coolant flow for several hours after reactor shutdown. To ensure coolant flow availability, battery or diesel generator is needed to provide power supply to operate the emergency coolant pump. After such period, the reactor is in safe condition as long as all fuels are under the water.

RRI-50 operates with forced convection cooling mode. In shutdown operation mode where there is no more fission reaction, the fuel should always be cooled using forced convection. In a loss of coolant flow event, the residual heat is cooled using an emergency core cooling system (ECCS). The thermal hydraulic parameters in this mode are defined through steady state and transient analysis. The objectives of the analysis are to obtain reactor core responses during the postulated severe operational event or accident and to determine safety condition that can be selected at steady state and transient state. The conceptual design of RRI-50 cooling system is to remove heat generated by the fuel with nominal power of 50 MW. To

prevent boiling, RRI-50 core is designed at relatively high pressure with operational pressure at 8 kgf/cm². This system should be maintained to make the core operate at any condition. To ensure the operation of forced cooling system during normal operation, the primary cooling is equipped with 3 centrifugal pumps (two pumps operate and one pump is in standby mode). These pumps flow the primary coolant downward into reactor core through hot leg to the delay chamber. The design of the delay chamber is to decay N-16 radionuclide to safe level. The primary coolant from the delay chamber then transfers its heat to a heat exchanger and returns to the reactor pool through a distributor ring. Coolant distributor ring is installed at reactor vessel wall, 1.8 m above the core. From the distributor ring, water is sprayed to the reactor core. To ensure sufficient coolant during heat removal due to loss of flow transient, the pump is equipped with flywheel. In addition, ECCS should be able to operate automatically as decay heat is in large amount.

Postulated Initiating Events

The postulated event that might occur in case of loss of pump power supply, which is the main component in the primary cooling system, is categorized as a decrease in heat removal accident. The potential accidents that might occur are tabulated in Table 1.

TABLE 1: Potential accidents on primary coolant system [8].

No.	Potential Accident
1.	Coolant reduction due to valve failure.
2.	Leakage of the primary coolant boundary beyond the isolation valves.
3.	Leakage of the primary coolant pipe between reactor pool and primary system isolation.
4.	Leakage of the primary coolant pipe inside the reactor pool.
5.	Reactor pool leakage.
6.	Leakage of the warm water layer system.
7.	Leakage of the fuel element store purification system.
8.	Heat exchanger leakage.
9.	Rupture of a beam tube.
10.	Loss of primary pumps and flow coast down.
11.	Flow blockage to single cooling channels.

Among those potential accidents, loss of primary pumps and flow coast down is chosen as the most severe accident. If the reactor core is securely safe during this accident, then the primary cooling system design meets the required safety requirements.

3. Methodology

Loss of Flow Event Simulation

The event initiating an accident due to loss of flow is that the primary coolant pump is suddenly not functioning. This event is simulated by assuming that the reactor is in operation at nominal power of 50 MW, primary coolant flow rate of 900 kg/s, and coolant pressure of 8 kgf/cm² and power supply is suddenly lost. This event is simulated using a transient computation code,

PARET-ANL. In the simulation, the reactor is protected to scram if the coolant flow rate reaches 85% of its nominal capacity (765 kg/s) or if the power rises 114% of its nominal power (57 MW), any of which reached first will trigger reactor protection system.

Input Data

The input data use in this analysis are shown in Table 2.

TABLE 2: Input data [1].

No.	PARAMETERS	Value
1.	Reactor power, MW Power generated in fuel element, % Core flow rate, kg/s Pressure, kgf/cm ²	50 100 900 8,0
2.	Fuel element: Type Enrichment, % Geometry: Fuel element dimension, mm Fuel plate dimension, mm Fuel plate thick, mm Gap width, mm Number of plate per fuel element Number of plate per control element	U9Mo-Al 19, 75 77, 1x81 0, 54x62, 75x700 1, 3 2, 55 21 15
3.	Cladding: Type Cladding thickness, mm	AlMg ₂ 0,38
4.	Power peaking factor: Radial power peaking factor, FR F_{cool} , F_{film} , F_{hflx} , $F_{cladding}$, F_{bond} , F_{meat} Axial power peaking factor, F_A	3,000 1,167; 1,200; 1,200 1,00; 1,00; 1,00 1,2
5.	Flow area, m ²	0,07578078
	Mass flow rate, kg/s.m ² t=0	11876,36
	Mass flow rate, kg/s.m ² , t=150	819,39
6.	Power trip, Mw	57
	Flow trip, %	85

4. Results and Discussions

Steady State Condition

RRI-50 that is operating at steady state condition, before LOFT occurs, is shown in Figure 1 and 2 and Table 3. Figure 1 depicts thermal hydraulic parameters at steady state condition, in which observation is carried out at the hottest channel. As shown in Figure 1, point 0 is the fuel outlet/bottom side, while point 70 is the fuel inlet/top side. It is shown in the figure that heat flux generated is 500 W/cm² and the coolant outlet temperature at the hot channel reaches 91.38°C, making 21.24°C difference from the average channel temperature. This difference is caused by the use of uncertainty factor at the hot channel. Meanwhile, the cladding temperature distribution has the same profile with axial heat flux distribution, in which the maximum cladding temperature reaches 164.54°C. Bulk temperature and cladding temperature have not reached two-phase temperature. Compared to DNBR temperature, the margin is 47.95°C. This margin toward two-phase temperature indicates that boiling has not occurred at the steady state condition.

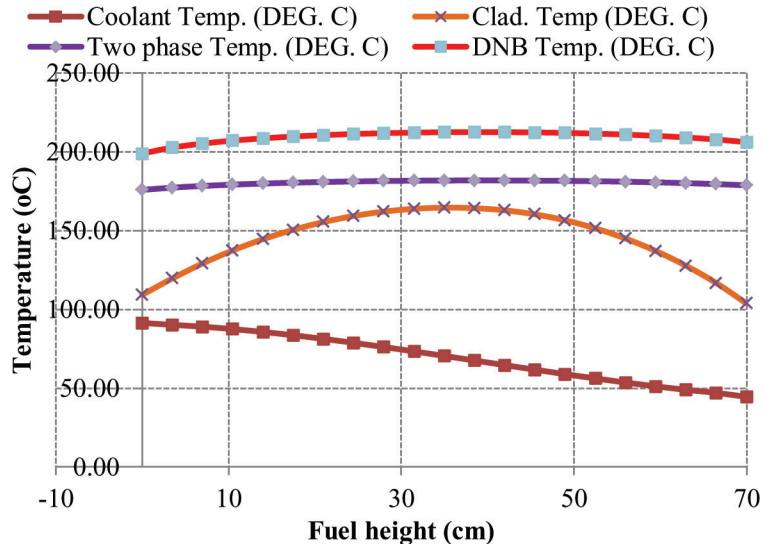


Figure 1: Thermal hydraulic parameters at steady state condition.

Figure 2 shows characteristics of heat transfer temperature at radial direction in one fuel plate, starting from the fuel central meat to the cladding and coolant. Temperature gradation patterns as a function of heat transfer process in the average channel and heat channel are indicated. There is a significant temperature difference at fuel region, between average channel and heat channel. The temperature of two-phase flow and DNBR temperature are the same for these two channels. The figure shows that there is sufficient temperature margin on two-phase temperature and DNBR temperature. Table 3 provides explanation for Figure 2 in term of figures at each region. This table outlines thermal hydraulic characteristics for RRI-50 at steady

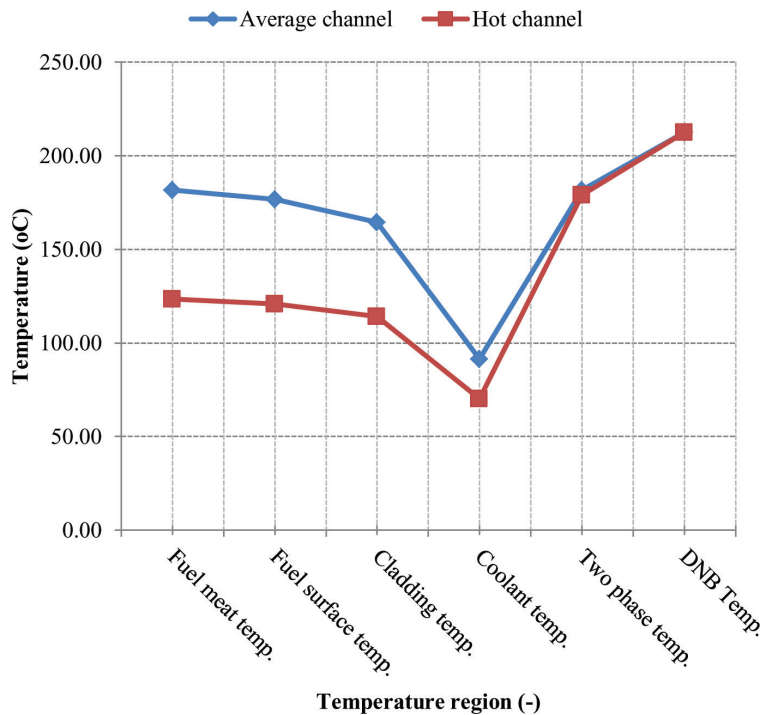


Figure 2: Thermal hydraulic parameters at fuel element regions.

TABLE 3: Comparison between hot channel and average channel at steadystate condition.

	Fuel meat temp.	Fuel surface temp.	Cladding temp.	Coolant temp.	Two phase temp.	DNB temp.
	(°C)	(°C)	(°C)	(°C)	(°C)	(°C)
Hot Channel	181,61	176,89	164,54	91,38	181,81	212,49
Ave. Channel	123,52	120,94	114,20	70,14	178,94	212,49

state in the average channel and hottest channel. The temperature difference is caused by the use of nuclear and engineering uncertainty factor in the hottest channel. On the other hand, at the average channel, both factors are assumed to 1.

Loss of Flow Event Simulation

As explained previously, LOFT event, which is anticipated at RRI-50, is one of DBA that should be considered as loss of flow event might occur any time during reactor operation. Figure 3 depicts the event at early period of LOFT. It is apparent that the decrease in flow rate occurs at 2.1th second when the flow rate reaches 85% of its normal value causing a signal due to minimum flow. The 0.5 second delay time makes the reactor scram at 4.62th second and causes the coolant and cladding temperature to decrease. Meanwhile, the flywheel of the pump provides residual flow, helping to take residual heat. At 10th second when the remaining reactor power is about 17% of the nominal power, the fuel and coolant temperatures get lower to 107°C and 73°C.

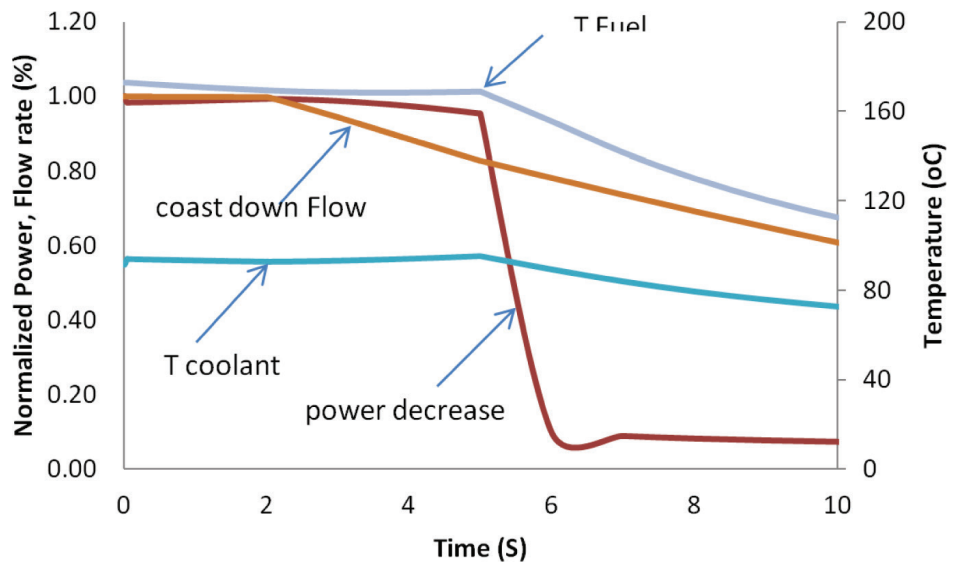


Figure 3: Normalized power and flow rate and temperature at the beginning of LOFT.

Figure 4 indicates the coolant and cladding temperature profiles at the beginning of LOFT. Significant temperature reduction is due to reactor scram. The fuel temperature decreases more rapidly than that of coolant because of the presence of cooling mode change from forced convection to natural convection. This change makes the two temperatures reach equilibrium soon after the transient.

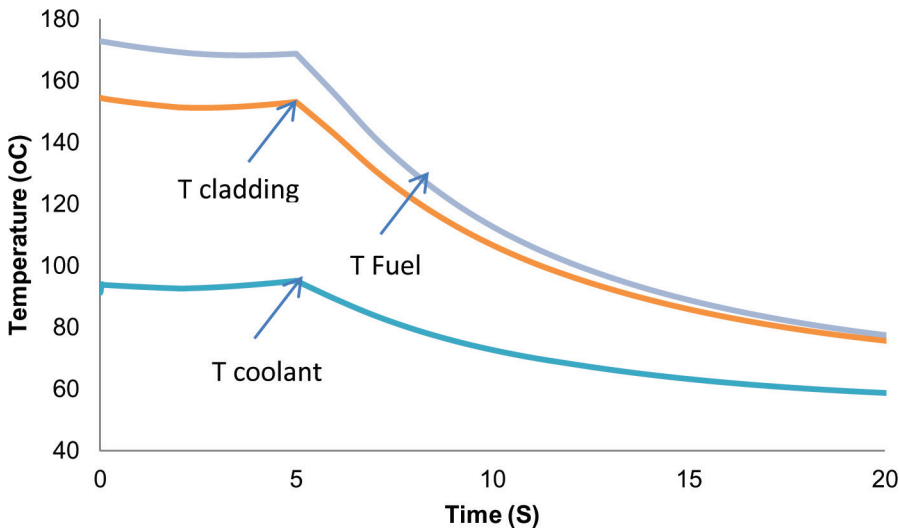


Figure 4: Coolant and cladding temperature profile at the beginning of LOFT.

Figure 5 shows the correlation among normalization of the primary coolant system, normalized power, and core reactivity during transient at early period of LOFT. It is shown that trip occurs at 4.6th second due to the flow rate of 85% of its normal value. Based on the assumption that there is a delay between trip signal and a control rod drop, scram time is 5.1 seconds. Since the reactor scrams, the reactor power drops significantly to 7.8% or 3.9 MW in 10 seconds. At the same time, core reactivity swings from -0.007\$ to -17.40\$. The presence of Doppler effect indicates that reactivity feedback occurs and causes reactor scram.

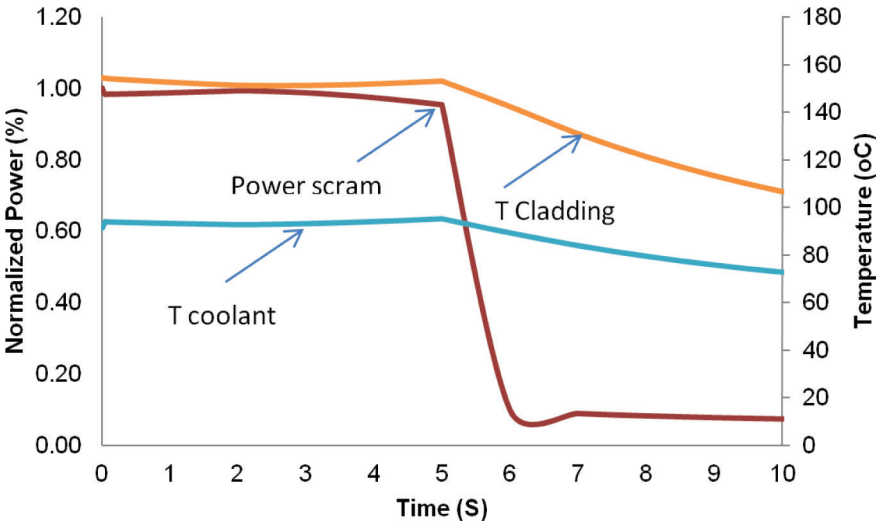


Figure 5: Fluence of reactivity and flow to power decrease.

The correlation of coolant temperature, cladding temperature and safety margin towards flow instability (S) is shown in Figure 6. The observation carried out at the first 40 seconds during loss of flow event indicates that S reaches the lowest value of 7.7 when the reactor scrams. Core reactivity change causes a decrease in cladding and coolant temperature to its respective equilibrium, i.e. 55°C and 67°C. At this equilibrium temperature, the margin towards S reaches its equilibrium value in 25 seconds, which is a safe value.

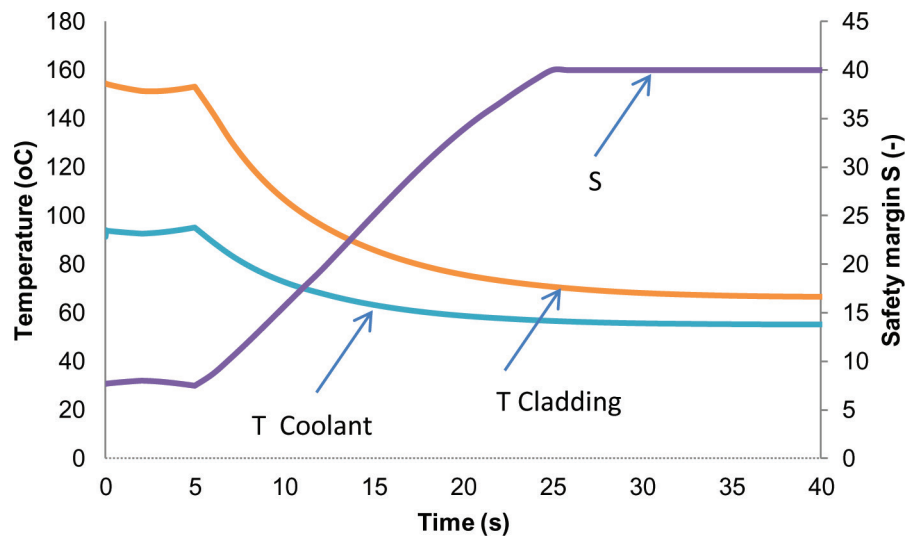


Figure 6: Corelation between coolant and cladding temperature and safety margin.

5. Conclusion

Based on the analysis results on thermal hydraulic characteristics of RRI-50 core towards loss of coolant flow transient at the beginning of accident using PARET-ANL code, it is concluded that the safety margin towards flow instability is still met at early period of LOFT and two-phase flow has not occurred at constant pressure.

6. Acknowledgment

This work has been carried out under the collaboration of RRI-50 Conceptual Design Project by PTRKN BATAN. I would like to thank you to the Neutronic Group for preparing some important parameters for this work.

References

- [1] Hastuti E. P., et al., "PTRKN 2010 Technical Document: User Criteria Document (UCD) Innovative Research Reactor", BATAN-RKN-C-2010-01-001, PTRKN-BATAN, South Tangerang, (2010).
- [2] Hastuti E. P., WIDODO S., "Thermalhydraulic Aspec Fuel element Analysis on Pre Design of High Power Innovative Research Reactor", The 19th TKPFN National Seminar Proceeding, BATAN-UIN Sunan Kalijaga, Yogyakarta, 24-25 October (2013).
- [3] W. X. Tian, S. Z. Qiu, Y. Guo, G. H. Su, D. N. Jia, "Development of A Thermal-Hydraulic Analysis Code for CARR", Annals of Nuclear Energy 32 (2005) 261-279.
- [4] Qing Lu, Suizheng Qiu, G. H. Su, "Development of A Thermal-Hydraulic Analysis Code for Research Reactors With Plate Fuels", Annals of Nuclear Energy 36 (2009) 433-447.
- [5] Ronghua Chen, G. H. Su, Wenxi Tian, Suizheng Qiu, Dounan Jia, "Development of TSAC1.0 and application to reactivity insertion accident of CARR", Nuclear Energy 53 (2011) 1-9.
- [6] Wenxi Tian, Suizheng Qiu, Guanghui Su, Dounan Jia, Xingmin Liu, Jianwei Zhang, "Thermohydraulic and Safety Analysis on China Advanced Research Reactor Under Station Blackout Accident", Annals of Nuclear Energy 34 (2007) 288-296.

- [7] Tewfik Hamidouche, Anis Bousbia-Salah, El Khider Si-Ahmed, Mohamed Yazid Mokeddem, Francesco D'Auria, "Application of Coupled Code Technique to A Safety Analysis of A Standard MTR Research Reactor", *Nuclear Engineering and Design* 239 (2009) 2104–2118.
- [8] Omar S. AL-Yahia, Mohammad A. Albati, Jonghark Park, Heetaek Chae, Daeseong Jo, "Transient Thermal Hydraulic Analysis of The IAEA 10 MW MTR Reactor During Loss of Flow Accident to Investigate The Flow Inversion", *Annals of Nuclear Energy* 62 (2013) 144–152.
- [9] S. Chatzidakis, A. Hainoun, A. Doval, F. Alhabet, F. Francioni, A. Ikonopoulou, D. Ridikas, "A Comparative Assessment of Independent Thermal-Hydraulic Models for Research Reactors: The RSG-GAS Case", *Nuclear Engineering and Design* 268 (2014) 77– 86.
- [10] Enrico Zio, Francesco DiMaio, JiejuanTong, "Safety Margins Confidence Estimation for A Passive Residual Heat Removal System, *Reliability Engineering and System Safety*", vol. 95, pp. 828–836 (2010).

Conference Paper

Comparison of Uncertainty Methods for Pipe Deflection Calculation

Nursinta Adi Wahanani, Entin Hartini, Roziq Himawan

Center for Nuclear Reactor Technology and Safety, National Nuclear Agency of Indonesia (BATAN) PUSPIPTEK Area Building No. 80 Serpong, Tangerang Selatan 15310, Indonesia

Abstract


Reliability of pipe structure is one aspect to be considered in reactor safety analysis. MSC NASTRAN is a computer code that can be used to calculate pipe deflection for reliability evaluation. MSC PATRAN can be used to generate input for this code. Uncertainty evaluation needs to be done in the input variable to understand uncertainty range in the analysis results. A computer code for evaluating structure reliability has been developed in our previous study. The code has implemented latin hypercube sampling (LHS) to assess uncertainty in the input variable, such as load and modulus of elasticity. In this study, comparison of two uncertainty methods, i.e. simple random sampling (SRS) and LHS, was carried out for the developed software. The comparison was subjected to pipe deflection calculation using 100 samples. Comparison analysis shows that LHS method produces a robust mean of variance for all sample size. The results also confirm that variance of pipe deflection using LHS is smaller by 3% than SRS one. It can be concluded that LHS is appropriate to be implemented for uncertainty analysis in the developed code.

Corresponding Author:
Nursinta Adi Wahanani,
email: sintaadi@batan.go.id

Received: 29 July 2016
Accepted: 21 August 2016
Published: 21 September 2016

Keywords: uncertainty method, pipe deflection, pipe structure, latin hypercube sampling, simple random sampling

Publishing services
provided by Knowledge E

 Nursinta Adi Wahanani, et al. This article is distributed under the terms of the [Creative Commons Attribution License](https://creativecommons.org/licenses/by/4.0/), which permits unrestricted use and redistribution provided that the original author and source are credited.

Selection and Peer-review under the responsibility of the ICoNETS Conference Committee.

 OPEN ACCESS

1. Introduction

In the design of nuclear reactor, safety factor is the most important consideration. One consideration in the safety analysis is pipe structure reliability. Computer software which are commonly used to analyze pipe structure and pressure vessel integrity in the nuclear reactor are MSC NASTRAN and ANSYS [1].

Regarding pipe deflection calculation, there are three phases that need to be completed, i.e. pre-processor, processor and post-processor phases. In the pre-processor phase, MSC PATRAN is used and uncertainty value is still not considered [2]. Output file from MSC PATRAN becomes input file for MSC NASTRAN. Analysis of the uncertainty on the final result is affected by the uncertainties of input. Therefore the addition of uncertainties in the input variables needs to be evaluated. Sensitivity analysis reflects the relationship between the uncertainty in the results and input variables [3, 4, 5].

Uncertainties in the predictions of structural strength can be calculated using simulation techniques, such as Monte Carlo simulation. The strength of structural design depends on basic strength variables of both material and geometrical aspects, such as material's yield strength, plate thickness and modulus of elasticity [6]. The probability of failure can be

caused by the uncertainties associated with the load and material properties. This probability can be estimated using a Monte Carlo simulation [3].

A computer code which has considered uncertainty factor in the input variable has been developed. Input variables in which the uncertainty are taken into account in the code are load and modulus of elasticity [2]. Uncertainty calculation in load and modulus of elasticity can also be done simultaneously using fuzzy finite element method [7]. The computer program makes it possible to communicate with MSC PATRAN in the pre-processor phase and software MSC NASTRAN in the calculation process.

Latin Hypercube Sampling (LHS) uncertainty method was used in the development of computer program. An evaluation was carried to this program using stress and deflection value resulted in MSC NASTRAN [2]. LHS method was used to increase sampling efficiency and computation time could be reduced approximately by 50% [8]. The objective of sampling is to reduce the variance in process of mean estimation. Sampling technique is useful for increasing sample availability in the function being analyzed. Reducing of simulation number in the analysis will reduce the computation process.

Simple Random Sampling (SRS) is a basic sampling technique widely used for benchmarking/ comparison. This method give random number and desired variable value according to the type of probability distribution. LHS is an evolutionary method from stratified sampling method. In case for monotonic function, this method is better than SRS, but limited for normal, triangular and uniform distribution [9]. Comparison results between SRS method and LHS method showed that under small amount of sample, there was no significant difference in prediction of mean value and variance. LHS method provided a more robust result rather than stratified sampling method [10].

In this study, comparative study using developed computer program and MSC PATRAN-MSC NASTRAN was carried out to be subjected to SRS and LHS uncertainty method. The objective of this study is to obtain an appropriate uncertainty method which match with the computer program for simulation using MSC PATRAN-MSC NASTRAN. A small variance value on deflection number was used as parameter of conformity. Comparison analysis shows that LHS method produces a robust mean of variance for all sample size.

2. Theory

The continuous increase in data size keeps challenging to estimate the characteristic of the population effective and efficient. Sampling is a standard statistical procedure to estimate or learn something from the population at low cost. Sampling is a systematic way of reducing the data size while maintaining essential characteristic of the data set [10,11].

Simple Random Sampling

Simple Random Sampling (SRS) is a basic sampling techniques are often used as the basis for the development and comparison of more complex sampling techniques. Basic principle of SRS is for each sample has the same probability to be chosen. This method is working by generating random number and obtain variable value correspond to type of data distribution. Mean is estimated according to statistical rule as shown in Eq. (1) below [10]:

$$\bar{a}_{\text{simple}} = \frac{1}{N} \sum_{i=1}^N a_i \quad (1)$$

N is multiple number of sample and a_i is generated random number. Variance value is formulated as Eq. (2) below [10] :

$$\text{Var}(a_{\text{simple}}) = \frac{1}{N-1} \sum_{i=1}^N (a_i - \bar{a}_{\text{simple}})^2 \quad (2)$$

Mean variance estimation is formulated in Eq. (3) below [10] :

$$\text{Var}(\bar{a}_{\text{simple}}) = \frac{1}{N} \text{Var}(a_{\text{simple}}) \quad (3)$$

Latin Hypercube Sampling

Latin Hypercube Sampling (LHS) is evolutionary sampling method from stratification sampling. This method is working by dividing into levels and generate samples until values from different levels were obtained [10]. LHS is one of method to obtain uncertainty. Variable with number of "k", X_1, \dots, X_k , LHS choose different value "n" on each "k". Each variable was divided into "n" interval, and for each interval, one value with same probability was chosen [12]. Mean value estimation and variance on LHS is the same as those on SRS, as describe in Eq. 4 and 5 [10].

$$\bar{a}_{\text{LHS}} = \frac{1}{N} \sum_{i=1}^N \bar{a}_i \quad (4)$$

$$\text{Var}(a_{\text{LHS}}) = \frac{1}{N-1} \sum_{i=1}^N (a_i - \bar{a}_{\text{LHS}})^2 \quad (5)$$

Mean variance estimation on LHS describe in Eq. 6 below [10].

$$\text{Var}(\bar{a}_{\text{LHS}}) = \frac{1}{N} (a_{\text{LHS}}) + \frac{N-1}{N} \text{Cov}(A_1, A_2) \quad (6)$$

$\text{Cov}(A_1, A_2)$ is covarian value between input variable.

3. Methodology

The procedure in this study is shown in Fig. 1.

There are three phases in calculation of pipe deflection. First phase is building the model, which the input file for MSC NASTRAN was built using MSC PATRAN according to spesification shown in Table 1. Value of load and modulus of elasticity according to input variable shown in Table 2. Load parameter in Table 2 has a range $\pm 10\%$ from total weight which shown in Table 1. Parameter value of elasticity modulus use varians 5% from mean value. The modulus of Elasticity used in this study referred to material of Stainless Steel Pipe based on ASTM A 312 TP 316 L [7]. Result of this process is input file with bdf extension.

The second phase is generation of variable data using value shown in Table 2. The data generation were performed by developed computer program in previous research [2]. Hundred data generated in this process then to be used for substituting load value and modulus of elasticity value in bdf file. There two sets of data generated in this process, that are one data set generated by simple random sampling and the other one by Latin Hypercube Sampling. In this process, there are two sets file for MSC NASTRAN input, each set contains 100 bdf files.

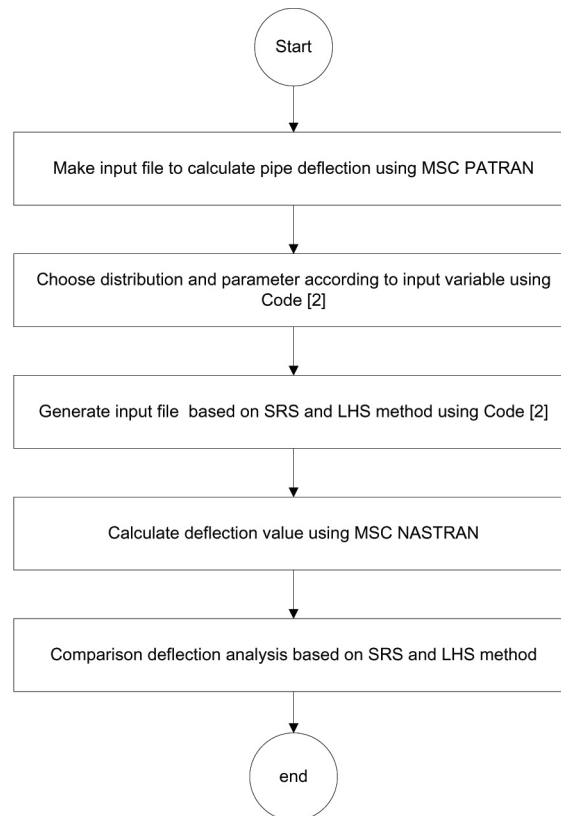


Figure 1: Research flow diagram.

The third phase is calculation phase using MSC NASTRAN to obtain pipe deflection. In this calculation, material pipe is considered as isotropic and linear elastic. While calculation mode were performed under linier static. Calculation results in this process then examined using MSC PATRAN (post processor phase).

TABLE 1: Pipe data use to simulation [7].

No	Variable	Value
1	Length	11 m
2	Inner diameter	0.3071 m
3	Outer diameter	0.3239 m
4	Total weight(Load)	1367.8 N/m
5	Elasticity Modulus	195122e06 Pa

TABLE 2: Distribution parameter.

No	Input Variabel	Distribusion	Parameter
1	Load	Uniform	[1231.02 N/m, 1504.58 N/m]
2	Elasticity Modulus	Normal	[195122e6 Pa, 98772.97 Pa]

Besides three stages as described above, in order to examine variance of data obtained by Simple Random Sampling method and Latin Hypercube Sampling method, generation data were performed three times to generate three different sample sizes, that 20, 100 and 1000. The data generation were replicated three times for each sample size. Cumulative Distribution Function was used as parameter to compare data stability in LHS method and SRS method [8].

4. Results and Discussions

Distribution of data generation in phase two, were shown in Fig. 2. Figure 2a represents result by SRS method and Fig. 2b by LHS method, respectively. These data contains 20 samples. In Fig. 2b Modulus of elasticity distributed evenly in each stratum. It can be said that LHS method provide a better distribution rather than SRS method.

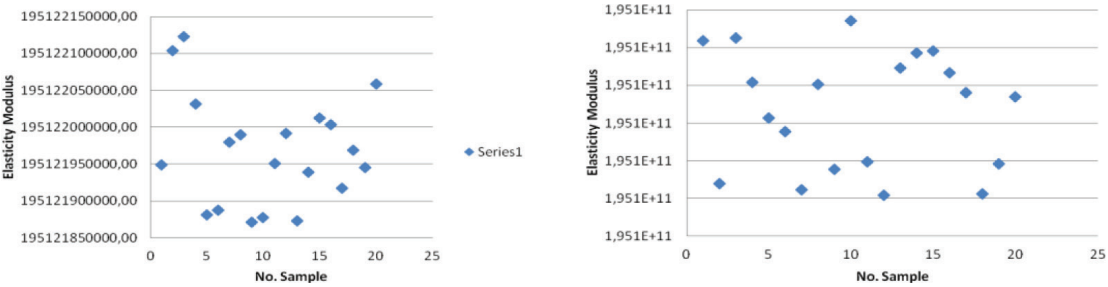


Figure 2: (a) Distribution of elasticity modulus –SRS; (b) Distribution of elasticity modulus-LHS.

Cumulativ Distribution Function (CDF) calculation results of LHS method and SRS method were shown in Fig. 3 and Fig. 4. Figure 3 and Fig. 4 represents for 20 and 100 sample size, respectively. By using 20 sample size, the variance between replication in SRS, is smaller/narrower rather than in LHS. It means, for small sample size, SRS method provides good repeatability in data generation. Variance between replication show uncertainty from sampling method. Result from replication can be used to estimate confidence interval and appropriate sample size to get robust statistic result [13].

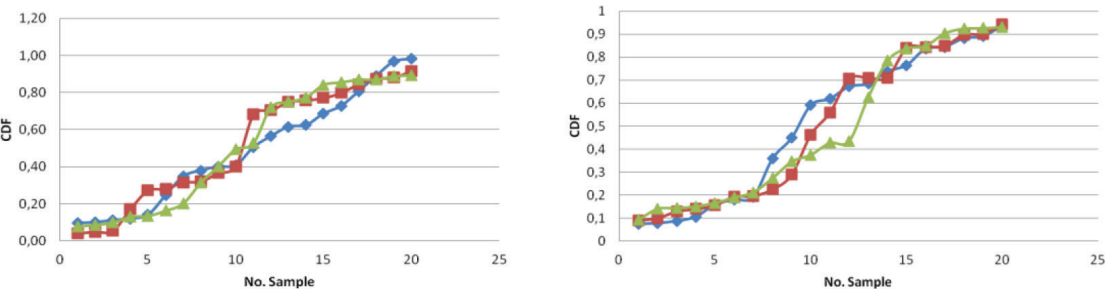


Figure 3: (a) CDF of Elasticity Modulus SRS–20 sample ; (b) CDF of Elasticity Modulus LHS–20 sample.

For larger sample size (100 samples in Fig. 4) the variance in both methods no significant difference. It means, in three replication with 100 samples, SRS and LHS method have same variance stability.

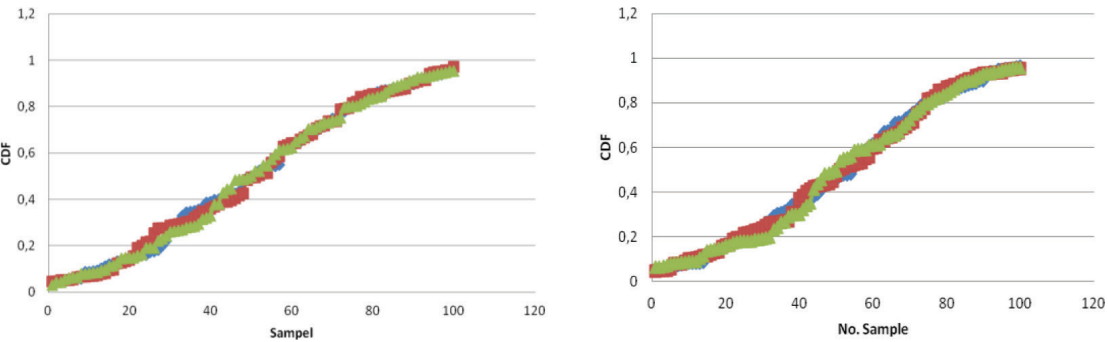


Figure 4: (a) CDF of Elasticity Modulus SRS–100 sample; (b) CDF of Elasticity Modulus LHS–100 sample.

Mean of variance for three sample sizes calculated by SRS and LHS method were shown in Table 3. For both variable, load and elasticity modulus, mean of variance of SRS method has smaller value than LHS. It occurred for all of sample size, except for 20 sample size in elasticity modulus variable, where LHS provided small variance than SRS. This result shows that LHS uncertainty method does not always give a small variance than SRS.

TABLE 3: Mean of variance of input variable.

Variable	Sample Size	Uncertainty Method	
		SRS	LHS
Load	20	4790.09	6278.89
	100	6254.40	6513.59
	1000	6178.56	6247.08
Elasticity Modulus	20	7.49E9	7.46E9
	100	5.82E9	6.56E9
	1000	6.58E9	6.59E9

Figure 5 shows the relation between mean of variance and sample size. Figure 5a shows mean of variance for load variable and Fig. 5b shows mean of variance for elasticity modulus. The sample sizes are 20,100 and 1000. For load variable (Fig. 5a), mean of variance with sample size of 100 and 1000 looks like no significant difference. Significant difference between LHS and SRS occurred for sample size of 20. Meanwhile, for elasticity modulus variable (Fig. 5b), mean of variance in LHS method has no significant difference for sample size of 100 and 1000 (remain constant). The other hand, mean of variance in SRS method decrease at sample size of 100 and then increase at sample size of 1000. It could be concluded that LHS method provide more stable mean of variance than SRS method.

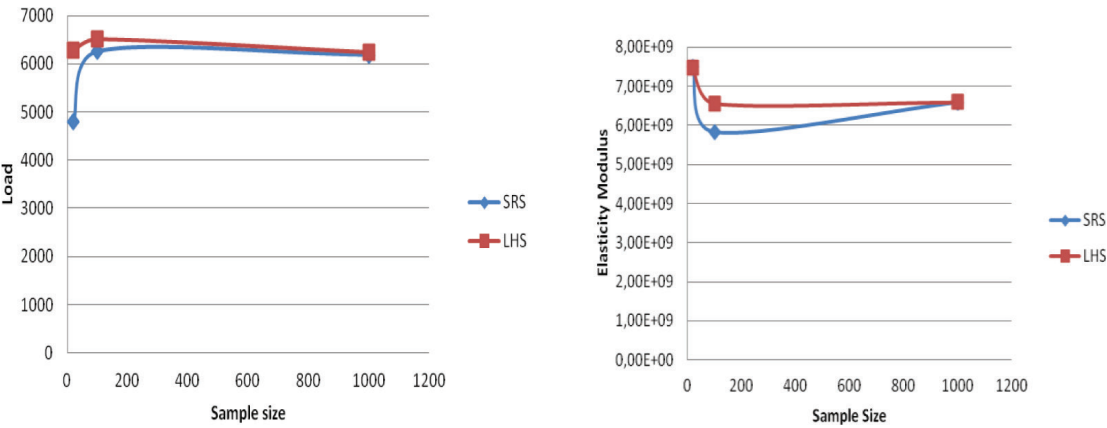


Figure 5: (a) Graph between mean of variance of load and sample size; (b) Graph between mean of variance of elasticity modulus and sample size.

Calculation results of pipe deflection using MSC NASTRAN were shown in Table 4. In the same table, result from calculation using ANSYS [7] are shown for the same case. Calculation from different software produces 0.8% differences. It could be said that no different result between MSC NASTRAN and ANSYS. Calculation result of pipe deflection with uncertainty considerations were also presented in Table 4. The calculation based on sample size of 100

using LHS and SRS method. Both methods produces variance of deflection value of $6.51E-07$ for SRS method and $6.26E-07$ for LHS method. It means, LHS' variance is 3% smaller than SRS' variance. This result show that there is no significant difference between SRS and LHS.

TABLE 4: Result of displacement calculation.

Calculation	Pipe Deflection	Variance
Without uncertainty with ANSYS [7]	12.89 mm	-
Without uncertainty with MSC NASTRAN	13.00 mm	
Uncertainty, SRS with MSC NASTRAN	13.03 mm	$6.51E-07$
Uncertainty, LHS with MSC NASTRAN	12.93 mm	$6.26E-07$

Comparison analysis of uncertainty method to calculate pipe deflection shows that LHS method produces a robust mean of variance for all sample size. The use of LHS as a uncertainty method in the developed code is appropriate.

5. Conclusion

Comparison of two uncertainty methods, i.e. simple random sampling (SRS) and LHS, has been carried out. Comparison analysis shows that LHS method produces a robust mean of variance for all sample size. The results also confirm that variance of pipe deflection using LHS is smaller by 3% than SRS one. It can be concluded that LHS is appropriate to be implemented for uncertainty analysis.

References

- [1] D. P VAKHARIA, MOHD FAROOQ A, "Determination of maximum span between pipe supports using maximum bending stress theory", *International Journal of Recent Trends in Engineering* Vol. 1, No. 6, 2009.
- [2] ENTIN HARTINI, ROZIQ HIMAWAN dan N. A Wahanani, "Pengembangan Perangkat Lunak Analisis Ketidakpastian Pada Perhitungan Struktur Material", *Prosiding Seminar Nasional MIPA 2014, Seminar Nasional MIPA 2014 FMIPA Universitas Padjadjaran*.
- [3] M. R. M AKRAMIN, A. ZULKIFLI, A. K AMIRUDIN, N. A ALANG dan M. S JADIN, "Hybrid Finite Element and Monte Carlo Analysis of Cracked Pipe, *National Conference in Mechanical Engineering Research and Postgraduate Studies (2nd NCMER 2010)*, 2010.
- [4] J. C HELTON, F. J DAVIS, J. D JHONSON, "A Comparison of uncertainty and sensitivity analysis results obtained with random and Latin hypercube sampling ", *Reliability Engineering and System Safety* 89 (2005) 305 -330.
- [5] J. C HELTON, J. D JOHNSON, C. J SALLABERRY, C. B STORLIE, "Survey of Sampling based method for uncertainty and sensitivity analysis", *Reliability Engineering and System Safety* 91 (2006) 1175 - 1209.
- [6] PAUL E. HESS, DANIEL BRUCHMAN, IBRAHIM A. ASSAKKAF, BILAL M. AYYUB, "Uncertainties in Material Strength, Geometric, and Load Variables", *Naval Engineer Journal*, Volume 114, Issue 2, pages 139-166, April 2002.
- [7] M. V RAMA RAO dan R. RAMESH REDDY, "Fuzzy finite element analysis of structures with uncertainty in load material properties", *Journal of Structural Engineering*, Vol.33 No.2, pp. 129-137, 2006.

- [8] A. OLSSON, G. SANDBERG, O. DAHLBLOM, "On Latin hypercube sampling for structural reliability analysis, *Structural Safety* 25 (2003) 47-68.
- [9] N. A. WAHANANI, A. PURWANINGSIH dan T.SETIADIPURA, "Latin Hypercube Sampling for Uncertainty Analysis, *Journal of Theoretical and Computational Studies*, Volume 8 Number 0408, ISSN 1979-3898, 2009.
- [10] IAIN A MACDONALD, "Comparison of Sampling Techniques on the Performance of Monte Carlo Based Sensitivity Analysis", Elevent International IBPSA Conference, Glasglow, Scotland (2009).
- [11] XIANGRUL MENG, "Scalable Simple Random Sampling and Stratified Sampling", Proceeding of the 30th International Conference on Machine Learning, Atlanta, Georgia, USA, 2013.
- [12] GREGORY D. WYSS, KELLY H. JORGENSEN, "A User's Guide to LHS : Sandia's Latin Hypercube Sampling Software, Risk Assessment and Systems Modeling Department Sandia National Laboratories, 1998.
- [13] CLIFFORD W. HANSEN, JON C. HELTON, CEDRIC J. SALLABERRY, " Use of Replicated Latin Hypercube Sampling to Estimate Sampling Variance in Uncertainty and Sensitivity Analysis Results for the Geological Disposal of Radioactive Waste", *Procedia Social and Behavioral Sciences* 2 (2010), 7674-7675.

Conference Paper

The Effect of Turbulence Models on Coolant Temperature and Velocity for the Pebble-Bed Typed High Temperature Reactor


Muhammad Subekti

Center for Nuclear Reactor Technology and Safety, (BATAN) Puspiptek area building No. 80 Serpong, Tangerang Selatan 15310, INDONESIA

Abstract

The 3D thermal-hydraulics analysis based on Computational Fluid Dynamics (CFD) has a role to analysis more detail the reactor safety, especially for pebble-bed typed High Temperature Reactor (HTR). A realistic pebble arrangement becomes a challenge to be modeled based on the Simple Cubic (SC), Body-Centered Cubic (BCC) and Face-Centered Cubic (FCC). Furthermore, CFD calculation could utilizes laminar model as well as turbulence model such as $k-\epsilon$, $k-\omega$ and Reynold stress model (RSM). Therefore, the objective of this reseach is to analyze the effect of turbulence model on temperature and coolant velocity distribution using FCC on pebble-bed typed HTR as well as investigation of the turbulence models. The comparison shows that all models are acceptable for HTR-10 case with the difference by the range of 0.03-0.33% for the temperature parameters, in which the minimum different is obtained by $k-\epsilon$ model.

Keywords: flow model, turbulence, temperature distribution, pebble-bed, HTRCorresponding Author:
Muhammad Subekti,
email: subekti@batan.go.idReceived: 29 July 2016
Accepted: 21 August 2016
Published: 21 September 2016**Publishing services
provided by Knowledge E**

 Muhammad Subekti.
This article is distributed
under the terms of the
[Creative Commons
Attribution License](#), which
permits unrestricted use
and redistribution provided
that the original author
and source are credited.

Selection and Peer-review
under the responsibility of
the ICoNETS Conference
Committee.

 OPEN ACCESS

1. Introduction

The safety analysis of High Temperature Reactor (HTR) based on pebble-bed fuel relies on nuclear physics calculation as well as experiment for validation. The analysis includes neutronics and thermal-hydraulics to predict the neutron flux and thermal generation values. The cooling fuel is one of the three safety concepts besides controlling reactor containing radiation. Furthermore, the temperature distribution in spherical pebble-bed fuel is determined by several parameter inputs such as coolant flow model, pressure, and temperature inlet and flow rate. In case of thermal-hydraulics one dimension (1D) calculation for characterizing the temperature distribution, the analytical codes such as THERMIX or VSOP have been utilized [1-2]. However, the three dimension (3D) calculation based on Computational Fluid Dynamics (CFD) has been carried out to study more detail the interior effect for 3D flow [3-5]. This detail analysis determines more accurate energy balance by detail model development. Therefore, the safety analysis using CFD code could inform the transient accident condition due to air ingress [4] as well as water ingress with detail temperature distribution in reactor core. The utilization of RSM has been investigated for relation of Nu number on different pebble layers under variable particle Reynold number [5], loss of coolant accident [6], and modeling height of 0.2 m [7]. Hence, RSM could be used as analysis comparator standard in this research.

In normal operation, steady state CFD calculation requires more detail boundary condition, consisted of three pebble arrangements of Simple Cubic (SC), Body-Centered Cubic (BCC) and Face-Centered Cubic (FCC). A realistic pebble arrangement for a pebble-bed reactor core is combination of different structured arrangements and it is crucial to investigate the effects of pebble arrangement on the thermal-hydraulics characteristic for safety operation [7]. Therefore the investigation of turbulence models based on different pebble arrangements is required as well to be investigated. Beside laminar model, a CFD calculation could utilize other turbulence model such as $k-\epsilon$, $k-\omega$, and Reynold stress Model (RSM). The comparison between turbulence models is relevant due to low flow rate of HTR-10 about 4.3 kg/s. The Eddy Viscosity Model (EVM) [8] and RSM has been utilized in CFD calculation with insignificant result different [9]. Hence, the further investigation is important using the turbulence model of laminar, Spalart-Allmaras, $k-\epsilon$, $k-\omega$, and RSM.

The research aims is to analyze the effect of turbulence models on temperature and coolant velocity distribution on pebble-bed typed HTR. The simplest validation was done as well using analytical analysis. For next step, the CFD calculation was carried out with FCC fuel arrangement and utilized the turbulence models of laminar, Spalart-Allmaras, $k-\epsilon$, $k-\omega$, and RSM. Finally, the analysis compared the calculation results and find a best turbulence model for HTR-10 CFD calculation.

2. Theory

HTR-10 is a high temperature gas cooled reactor with reactor power of 10 MWt. Core consists of 27,000 spherical pebble-bed fuels with diameter of 6 cm. Reactor core height and diameter are 197 cm and 180 cm, respectively, with Helium coolant flow rate of 4.3 kg/s. More technical information of the general pebble-bed fuel characteristics of HTR-10 is described in Table 1.

TABLE 1: General pebble-bed fuel characteristics of HTR-10 [4].

Parameter	Value
Core power	10 MWt
Core flowrate	5.3 kg/s
Core's heigh / diameter	197 cm / 180 cm
Fuel element (FE) number	27,000
Sphere diameter of pebble-bed fuel	6.0 cm
Wall material	Graphite
Coolant	Helium
Fluid pressure	3 MPa
Inlet / outlet Temperature	250 °C / 700 °C
Average thermal power	0.36 kW/FE

The heat transfers from pebble fuel to Helium coolant by force convection. The turbulence flow considers the Laminar, Spalart-Allmaras, $k-\epsilon$, $k-\omega$, and RSM. However, the analytical calculation still could be used for benchmarking the temperature different (ΔT) during core heating (Q) with certain flow rate (\dot{m}) in which C_p is specific heat. The classical equation for analytical calculation is described below [2]:

$$Q = \dot{m}C_p\Delta T \tag{1}$$

Laminar Model

Laminar flow through spherical-pebble bed fuel could be driven by Reynold number. The laminar model has been utilized on pebble-bed calculation [10]. In case of porous media, the calculation has utilized laminar model as well [11]. However, due to the condition of narrow gap in area contact of spherical-fuel, however the turbulence model is relevant to be utilized in CFD calculation as well.

Spalart-Allmaras Model

Spalart-Allmaras model is simple one-equation model that is originally from a low-Reynold number model for solving the turbulent viscosity. The transport equation for turbulence kinematic viscosity $\tilde{\nu}$ is described below [12]:

$$\frac{\partial}{\partial t}(\rho\tilde{\nu}) + \frac{\partial}{\partial x_i}(\rho\tilde{\nu}u_i) = G_\nu + \frac{1}{\sigma_{\tilde{\nu}}} \left[\frac{\partial}{\partial x_i} \left\{ (\mu + \sigma_{\tilde{\nu}}) \frac{\partial \tilde{\nu}}{\partial x_i} \right\} + C_{b2}\rho \left(\frac{\partial \tilde{\nu}}{\partial x_i} \right)^2 \right] - Y_\nu + S_{\tilde{\nu}} \quad (2)$$

where G_ν is the production of turbulence viscosity and Y_ν is the destruction of turbulence viscosity that occurs in the near-wall region due to the wall blocking and viscous damping. Furthermore, $\sigma_{\tilde{\nu}}$ and C_{b2} are constants, while $S_{\tilde{\nu}}$ is a user-defined source term.

k-epsilon Model

The $k-\epsilon$ (k-epsilon) model is two-equation models in which the solution of two separate transport equations allows the turbulent velocity and length scales to be independently determined. The turbulence kinetic energy k , and its rate of dissipation, ϵ , are obtained from the following transport equations [6, 12]:

$$\frac{\partial}{\partial t}(\rho k) + \frac{\partial}{\partial x_i}(\rho k u_i) = \frac{\partial}{\partial x_j} \left[\left(\mu + \frac{\mu_t}{\sigma_k} \right) \frac{\partial k}{\partial x_j} \right] + G_k + G_b - \rho \epsilon - Y_M + S_k \quad (3)$$

and

$$\frac{\partial}{\partial t}(\rho \epsilon) + \frac{\partial}{\partial x_j} \left[\left(\mu + \frac{\mu_t}{\sigma_\epsilon} \right) \frac{\partial \epsilon}{\partial x_j} \right] + C_{1\epsilon} \frac{\epsilon}{k} (G_k + C_{3\epsilon} G_b) - C_{2\epsilon} \rho \frac{\epsilon^2}{k} + S_\epsilon \quad (4)$$

where G_k is the he generation of turbulence kinetic energy due to the mean velocity gradients, G_b is the generation of turbulence kinetic energy due to buoyancy, and Y_M is the contribution of the fluctuating dilatation in compressible turbulence to the overall dissipation rate. $C_{1\epsilon}$, $C_{2\epsilon}$, and $C_{3\epsilon}$ are constants. σ_k and σ_ϵ are the turbulent Prandtl numbers for k and ϵ , respectively. S_k and S_ϵ are user-defined source terms.

k-omega Model

The $k-\omega$ model is modifications based on the Wilcox $k-\omega$ model for low-Reynolds-number effects, compressibility, and shear flow spreading. The turbulence kinetic energy k and the specific dissipation rate ω (omega) are obtained from the following transport equation [13]:

$$\frac{\partial}{\partial t}(\rho k) + \frac{\partial}{\partial x_i}(\rho k u_i) = \frac{\partial}{\partial x_j} \left(\Gamma_k \frac{\partial k}{\partial x_j} \right) + G_k - Y_k + S_k \quad (5)$$

and

$$\frac{\partial}{\partial t}(\rho \omega) + \frac{\partial}{\partial x_i}(\rho \omega u_i) = \frac{\partial}{\partial x_j} \left(\Gamma_\omega \frac{\partial \omega}{\partial x_j} \right) + G_\omega - Y_\omega + S_\omega \quad (6)$$

where G_k is the generation of turbulence kinetic energy due to the mean velocity gradients, G_ω is the generation of ω , and Γ_k and Γ_ω are the effective diffusivity of k and ω , respectively. Y_k and Y_ω are the dissipation of k and ω due to turbulence. S_k and S_ω are user-defined source terms.

Reynold Stress Model

Reynold Stress Model or RSM is a turbulence model that abandoning the isotropic eddy-viscosity hypothesis. The RSM closes the Reynolds-averaged Navier-Stokes equations by solving transport equations for the Reynolds stresses, together with an equation for the dissipation rate. The equation of RMS is similar to the research has investigated the effect of FCC[7].

3. Methodology

To investigate the effect of turbulence model on coolant temperature and velocity, the research conducts (i) coolant modeling of HTR-10 core, (ii) validation using analytical analysis, and (iii) CFD calculation. The CFD calculation is based on FCC fuel arrangement and utilizes the five turbulence model of laminar, Spalart-Allmaras, , , and RSM. Furthermore, the analysis compares the calculation results based on five models and find best turbulence model for HTR-10 CFD calculation.

TABLE 2: The property of coolant and wall at temperature of 500 °C.

	Density [kg/m ³]	Specific heat [J/kg.K]	Thermal Conductivity [W/m.K]
Helium	1.86	5195	30.28
Carbon	1790	710	86.70

The coolant modeling for pebble-bed core HTR-10 based on FCC arrangement could be describe at Fig. 1 and the property of coolant and wall at temperature of 500°C in Table 2 are calculated by using KTA standard [14]. The model size is 33.00 x 8.68 x 8.68 cm with FCC arrangement. The total coolant flow rate of 4.3 kg/s for core diameter of 180 cm is basis for the calculation that assumed flow rate through a coolant flow area of the model. In the physical model, total pebble fuel number is 28 Fuel Element (FE). The boundary wall of the coolant model limited the fuel number to 10 FE. Therefore, the total power in coolant model contained of 10 pebble fuel is 36 kW and assumed inlet temperature is 500°C. The utilization of RSM is used as analysis comparator standard in this research. Each turbulence models are compared to RSM and analyzed the temperature and velocity distribution in the coolant.

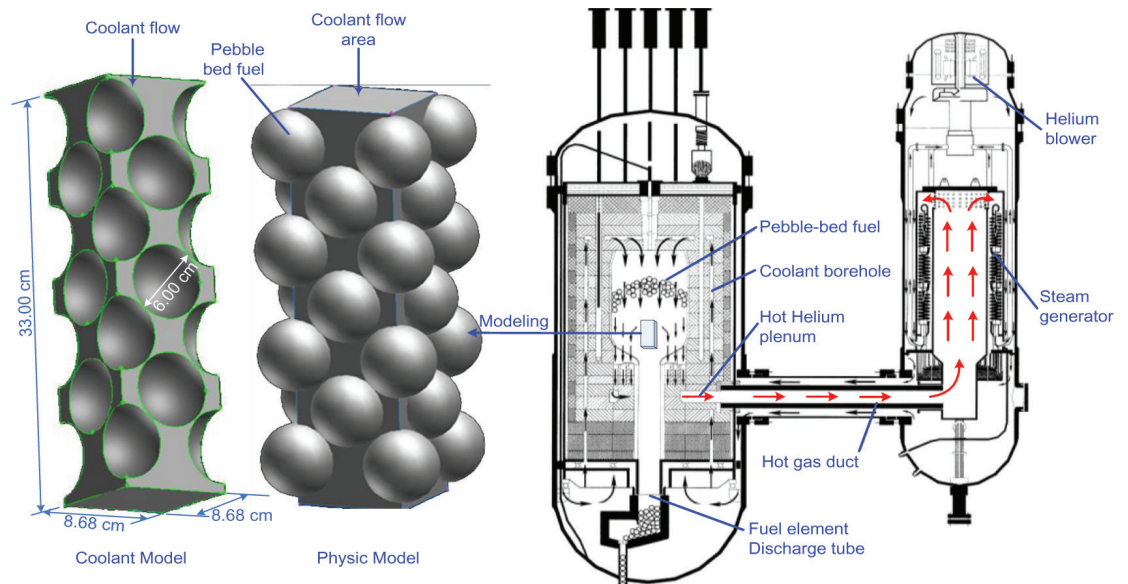


Figure 1: Coolant modeling for pebble-bed core HTR-10 based on FCC arrangement.

4. Results and Discussions

The comparison of temperature distribution to the variance of turbulence model in the Fig. 2 shows that all turbulence models have similar pattern of temperature distribution in which the coolant flows to bottom. However, the laminar model results insignificantly highest temperature distribution in bottom later due to low coolant flow-rate and short physical model height of 33 cm. Furthermore, the low coolant flow-rate impacts on low Reynolds number in HTR-10's core.

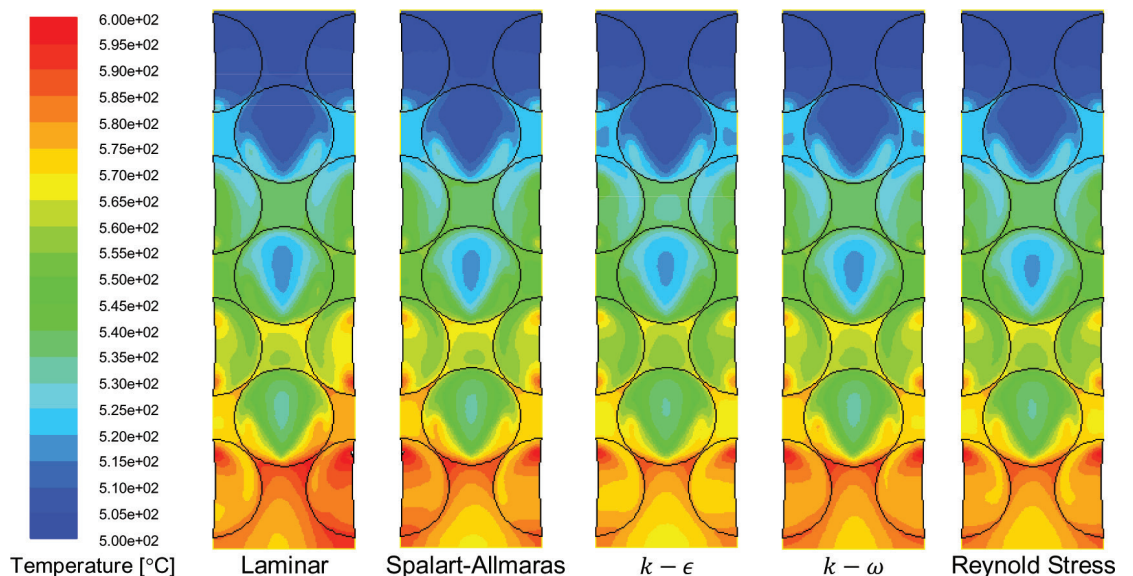


Figure 2a: Comparison of temperature distribution with variance of turbulence model.

The comparison of coolant velocity at certain position of 0.04 cm from bottom is shown in Fig. 2. The total physical model height as shown at Fig. 1 is 33 cm with inlet coolant area is 8.68 x 8.68 cm. The comparison points at certain position of 0.04 cm from bottom have

a narrowing gap between four spherical pebble-beds so that the effect of turbulent will be strong in this area. However the contour of each coolant velocity shows almost similar pattern with the velocity within 1.63 – 6.50 m/s.

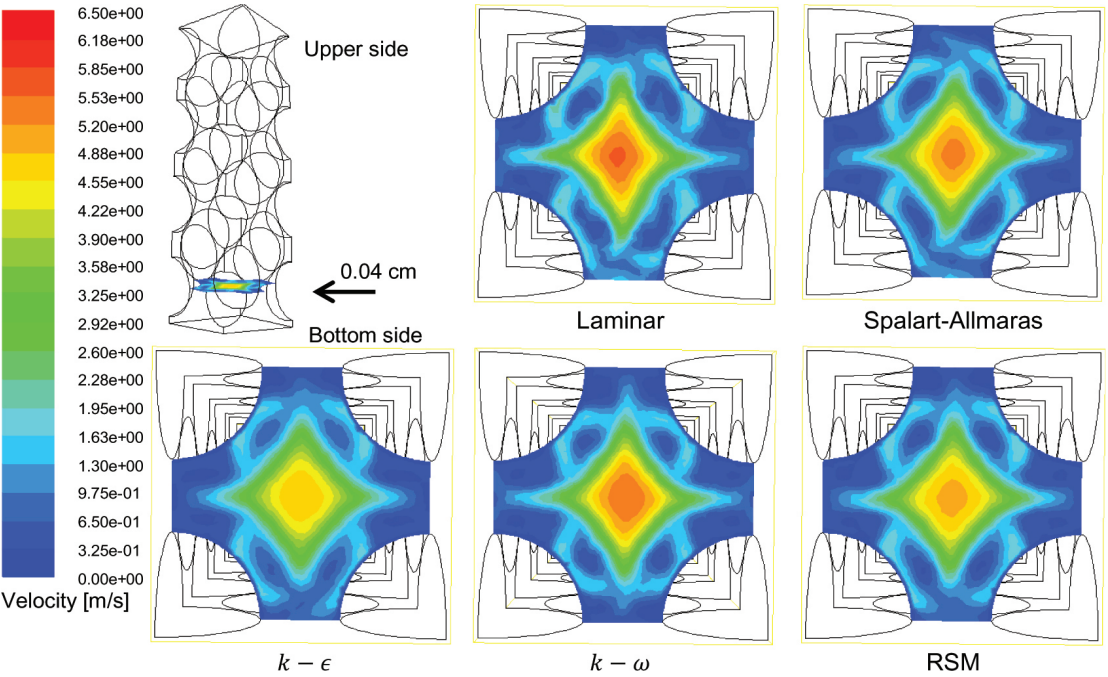


Figure 2b: The comparison of coolant velocity based on turbulence models at certain position of 0.04 cm from bottom.

Moreover, the validity of turbulence models could not be figured out before the experimental data availability. Therefore, the assessment of different choices of turbulence models could be based on analytical calculation by comparing temperature generated by CFD to the temperature generated from analytical calculation. Based on the equation (1), the temperature output of the modeling is 554.34 C. All turbulence models have average temperature results that are very close to the analytical calculation as shown in Table 3. The error varies from 0.03 to 0.33%. Therefore, all turbulence models are relevant to be utilized in CFD calculation for HTR-10.

TABLE 3: Comparison of temperature based on turbulence models.

Turbulence Models	Analytical Output [°C]	Average Output [°C]	Maximum Output [°C]
Laminar	554.34	553.86 (0.09%)	583.09
Spalart-Allmaras		553.64 (0.13%)	580.12
k-epsilon		552.49 (0.33%)	576.66
k-omega		554.15 (0.03%)	580.12
RSM		553.09 (0.23%)	579.13

For more detail comparison, Fig. 3 shows the effect of turbulence model on coolant temperature and Fig. 4 for coolant velocity at certain position of $y=0.0400$ m from bottom. The results in Fig. 3 and Fig. 4 agree to Fig. 2 that the different of turbulence models affect insignificant calculation results for temperature and velocity parameter. The calculated lines of coolant temperature and velocity for simpler laminar, Spalart-Allmaras, $k-\epsilon$, and $k-\omega$

model are close to RSM. Moreover, the closest line to RSM is $k-\epsilon$ model. The velocity peak at the coolant center in Fig. 4 shows that $k-\omega$ model is below RSM and very close to RSM. This phenomenon explains that the characteristic of $k-\omega$ model for expressing the turbulence separation line and swirl are identical to RSM.

The turbulence calculation using $k-\epsilon$ model assumes the similar ratio between Reynolds stress and mean rate of deformation (ϵ). Consequently, the $k-\epsilon$ model calculates dissipation ϵ is similar to RSM dissipation. Hence, the different of calculation result comes from other transport factors such as turbulence kinetic energy k for $k-\epsilon$ model, production, diffusion, pressure strain interaction, and rotation transport for RSM. Comparing to RSM, $k-\epsilon$ model has faster computation time due to simpler equation. The utilization of algebraic equation for calculating Reynold stress R_{ij} in RSM are not very stable and increase the computer time significantly. Therefore, the utilization of a simpler $k-\omega$ model is suggested beside an ideal RSM involving complex equation.

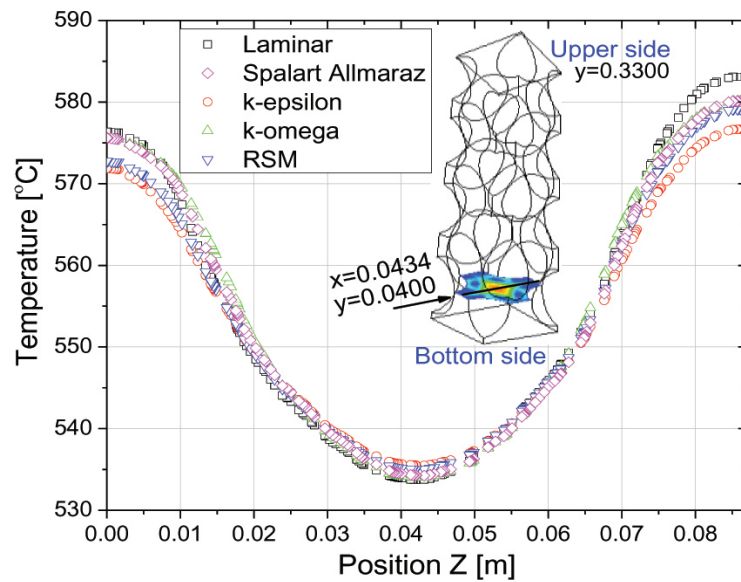


Figure 3: The effect of turbulence models on coolant temperature at certain position of 0.04 m from bottom.

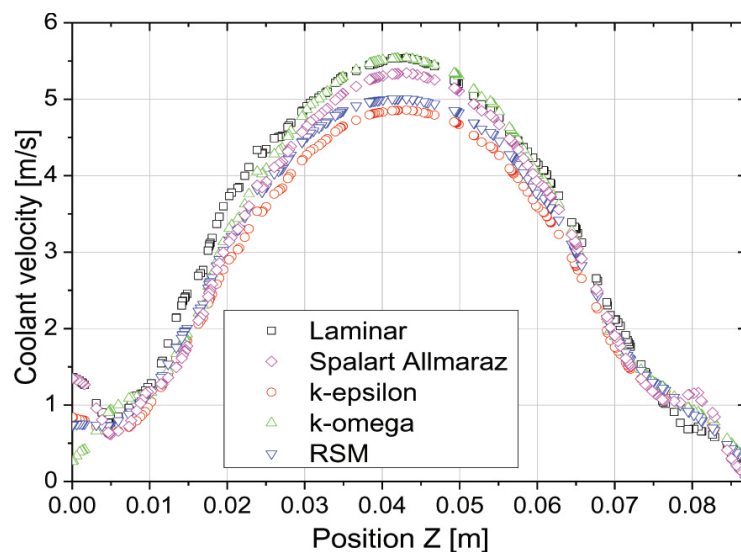


Figure 4: The effect of turbulence models on coolant velocity at certain position of 0.04 m from bottom.

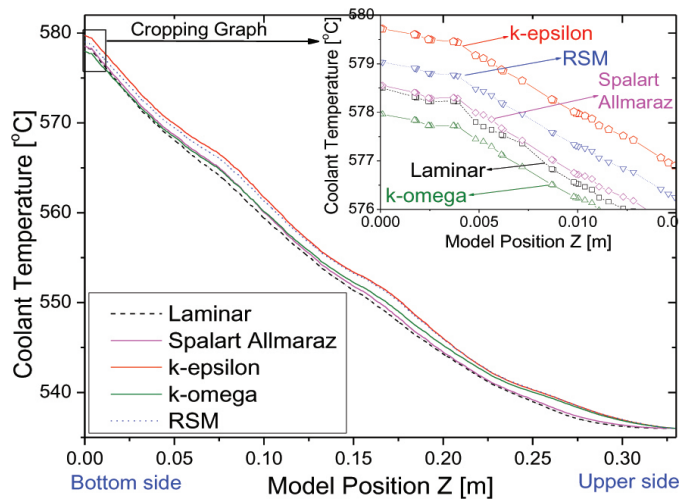


Figure 5: Effect of turbulence models on axial coolant temperature.

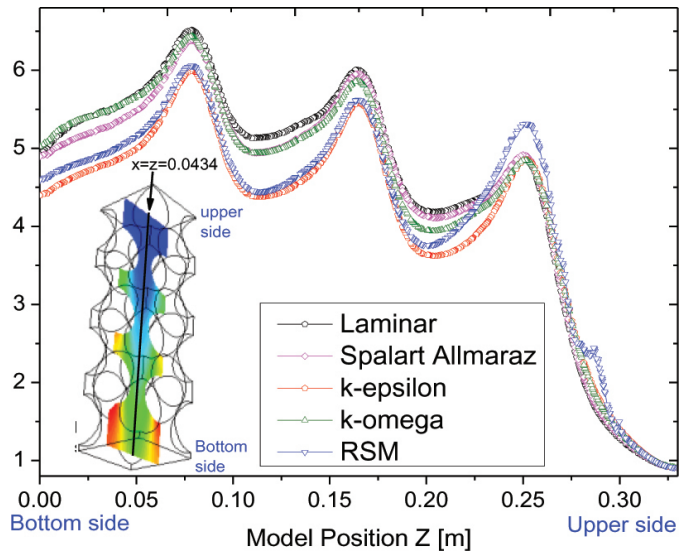


Figure 6: Effect of turbulence models on axial coolant velocity.

Furthermore, the calculation for axial temperature and velocity are analyzed as well. Fig. 5 describes the effect of turbulence model on axial coolant temperature at bottom side with position $x=z=0.0434$ and Fig. 6 for the axial coolant velocity. Peaks in Fig. 6 are due to the effect of flow-area narrowing of FCC pebble arrangement will increase the coolant velocity. In both Fig. 5 and Fig. 6, the line of each model has good agreement with Fig. 3 and Fig. 4, that all models have insignificant effect on coolant temperature and velocity, so all models are relevant to be utilized in CFD calculation for HTR-10 case. Good agreement is shown by the adjacent lines of $k-\epsilon$ and RSM. Considering the numerical stability risk and computation time of RSM, the utilization of $k-\epsilon$ model is suggested. The other models of Laminar, Spalart Allmaraz, and $k-\omega$ are acceptable to be adopt with more far space from ideal RSM. However, the characteristics of turbulence model may be different for other case based on different Reynolds number induced by fluid velocity. The different Reynolds number will affect to more significant transport factor from production, diffusion, pressure strain interaction, and rotation so that the separation line in turbulence flow could be more accurate for RSM.

5. Conclusion

The comparison shows that the effects of turbulence models are insignificant on coolant temperature and velocity for HTR-10 case. The unavailability of experimental data tends the comparison to analytical calculation with different variation of 0.03-0.33% for temperature parameters. More detail comparison shows that the $k-\epsilon$ calculation result on temperature and coolant flow distribution are closest to RSM calculation results. The detail comparison shows that the axial and horizontal calculation results have similar agreement, so all model are acceptable to be adopt in CFD calculation. However, the characteristics of turbulence model may be different for other cases based on different Reynolds number induced by different fluid velocity. Considering the numerical stability risk, computation time cost, and closest computation result to RSM, the utilization of $k-\epsilon$ model is suggested for HTR-10 case.

References

- [1] Xingqing, J. et al., "Prediction Calculation and Experiments for The First Criticality oh the 10 MW High Temperature Gas-Cooled Reactor-Test Module", Nuclear Engineering and Design, Vol.218, pp.43-49 (2002).
- [2] IAEA-TECDOC-1382, "Evaluation of High Temperature Gas Cooled Reactor Performance: Benchmark Analysis Related to Initial Testing of The HTTR and HTR-10", IAEA, November, Vienna (2003)
- [3] Du Toit, C.G. et al., "A System CFD Model of a Packed Bed High Temperature Gas-Cooled Nuclear Reactor", International Journal of Thermal Science, Vol.45, pp.70-85 (2006).
- [4] Ferng, Y.M. and Chen, C.T., "CFD Investigating Thermal-Hydraulics Characteristic and Hydrogen Generation from Graphite-Water Reaction After SG Tube Rupture in HTR-10 Reactor", Journal of Applied Thermal Engineering, Vol.31, pp.2430-2438 (2011).
- [5] Ferng, Y.M. and Lin, K.Y., "CFD Investigation of Thermal-Hydraulic Characteristics in a PBR Core Using Different Contact Treatments Between Pebbles", Annals of Nuclear Energy, Vol. 72, pp. 156-165 (2014).
- [6] Ferng, Y.M. and Chi, C.W., "CFD Investigating the Air Ingress Accident in A HTGR Simulation of Thermal-Hydraulic Characteristics", Nuclear Engineering and Design, Vol.245, pp.28-38 (2012).
- [7] Ferng, Y.M. and Lin, K.Y., "Investigating Effects of BCC and FCC Arrangements on Flow and Heat Transfer Characteristics in Pebbles Through CFD Methodology", Nuclear Engineering and Design, Vol.258, pp.66-75 (2013).
- [8] Dixon, A.G., et al., "Systematic Mesh Development for 3D CFD Simulation of Fixed Beds: Single Sphere Study", Journal of Computer and Chemical Engineering, Vol.35, Issue 7, pp.1171-1185 (2011).
- [9] Dehbi, A. and Martin, S., "CFD Simulation of Particle Deposition on An Array of Spheres Using an Euler/Lagrange Approach", Nuclear Engineering and Design, Vol.241, pp.3121-3129 (2011).
- [10] Yaser, H. and Khosrow, J., "Modeling of Laminar Forced Convection in Spherical-Pebble Packed Beds", Journal of Mechanical Science and Tech., Vol.26 (2), pp.643-649 (2012).
- [11] Pedras, M.H.J. and de Lemos, M.J.S., "Macroscopic Turbulence Modeling for Incompressible Flow through Under-formable Porous Media", Journal of Heat Mass Transfer, Vol.44, pp.1081-1093 (2001).



- [12] Najar, N.A., et al., "Comparative Analysis of $k-\epsilon$ and Spalart-Allmaras Turbulence Models for Compressible Flow through a Convergent-Divergent Nozzle", *The International Journal of Engineering and Science (IJES)*, Vol.2, Issue 8, pp.8-17 (2013)
- [13] Wilcox, D.C., "Formulation of The $k-\omega$ Turbulence Model Revisited", *AIAA Journal*, Vol. 46, No.11, pp.2823-2838 (2008).
- [14] "Reactor Core Design of High-Temperature Gas-Cooled Reactors. Part 2: Heat Transfer in Spherical Fuel Elements", KTA 3102.2, Nuclear Safety Standards Commission (KTA), Duetsch (1983).

Conference Paper

Proposed Testing Quality of Silicon Nitride in Nuclear Application by Ceramography


Tjokorda Gde Tirta Nindhia

Department of Mechanical Engineering, Engineering Faculty, Udayana University, Jimbaran, Bali, Indonesia, 80361

Abstract

The components in nuclear application should ensure the safety during operation. Testing and investigation should be performed to ensure the quality of every component. This report propose ceramography technique for testing of silicon nitride in nuclear application. Ceramic material is known brittle therefore not possible to hold by using vice as usual used in metal during cutting. Since ceramic is very hard, the cost for cutting, grinding and polishing required high cost due to utilization of diamond. Special techniques should be employed during observation bay using optical microscope because ceramic are not reflect the light. Ceramic is mainly known since their high chemical resistance therefore difficult to etching by using chemical solution. A unique respond of ceramic due to indentation make the indentation technique become part of ceramography. Indentation process requires a flat sample in order valid result to be obtained, and this can be achieved by special technique during grinding and polishing. This research introduce of ceramography process that was successfully done on Si_3N_4 , from preparation of the specimen, microstructure observation, the respond on indentation, strength, and porosity investigation. The results showed that the fluorescent dye penetrant under ultra violet source of light the defect in Si_3N_4 was easily observed therefore is suitable to be proposed as a technique for testing the quality of silicon nitride component in nuclear application.

Corresponding Author:
Tjokorda Gde Tirta Nindhia,
email: nindhia@yahoo.comReceived: 29 July 2016
Accepted: 21 August 2016
Published: 21 September 2016**Publishing services
provided by Knowledge E**

 Tjokorda Gde Tirta Nindhia. This article is distributed under the terms of the [Creative Commons Attribution License](#), which permits unrestricted use and redistribution provided that the original author and source are credited.

Selection and Peer-review under the responsibility of the ICoNETS Conference Committee.

OPEN ACCESS**Keywords:** ceramography, ceramic, silicon nitride, nuclear application, indentation

1. Introduction

Silicon nitride (Si_3N_4) is an advanced ceramic that mostly used in high-endurance and temperature applications, such as gas turbines, metal working, cutting tools and even more for application where maximum fracture toughness is required such as for seal face in nuclear application. It is also superior wear resistance, therefore excellent as bearings. Modern industry and transportation run on bearing. Bearing provide rolling contact rather than sliding contact and thus greatly decrees wear and friction. To be viable for bearing, a material must be hard and tough to resist the high Herzian contact loads to which a bearing is exposed. It must also be capable of fabrication to high smoothness and close tolerance and operate with low coefficient of friction against a mating surface. The Si_3N_4 bearing did not fail catastrophically like prior ceramics. Instead, they failed by slow development of surface spallation very similar to the failure mode of metal. The reason

for this was determined to be the higher level of fracture toughness. A very important factor compared to metals is that Si_3N_4 has approximately 40% of the specific gravity of steel that substantial reduction in stress for a given bearing size [1].

Ceramography is the art and science of preparation, examination, and evaluation of ceramic microstructure. The microstructure is the structure level approximately 0.1 to 100 μm between the wavelength of the visible light and the resolution limit of the naked eye. The microstructures include most grain, secondary phase, grain boundaries, pore, micro crack and hardness micro indentation. The 100 μm level is approximately the limit of resolution by the unaided human eye. The structure level larger than 100 μm is sometimes called the macrostructure, and some ceramic have grains and pores that are visible to the naked eye. A microscope cannot solve anything significantly smaller than the wave length of visible light 360 to 780 nm, or roughly 0.4 μm . The electron microscope, which use beam electron rather than visible light to generate image, are well suited for observation of micro structural features that are smaller than the wavelength of visible light [2].

This research introduce of ceramography process that was successfully done on Si_3N_4 , from preparation of the specimen, microstructure observation, the respond on indentation, strength, and porosity investigation. The ceramography process is expected to be used as a technique to test the quality of the silicon nitride component in nuclear applications.

2. Methodology

The material use for this research was Si_3N_4 produced by CeramTec (Plochingen, Germany) under the name SL200 B. It is a gas pressure sintered ceramic containing 3 wt.% Al_2O_3 and 3 wt.% Y_2O_3 . The material was cut by using diamond wheel (Fig. 1) with about the same thickness and mounted at upper disc of polishing machine (Fig. 2) by using thermoplastic glue (Fig. 3). For this purpose the disc should be heated by using hot plate in order to melt the glue.



Figure 1: Diamond wheel machine.

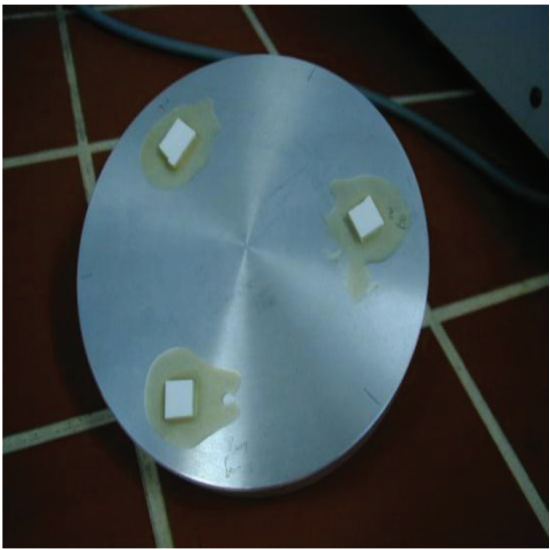


Figure 2: Mounting the specimen on upper disc of the polishing plate.



Figure 3: Example Commercial thermoplastic type of glue.



Figure 4: The polishing machine for ceramography. It is completed with upper and bottom disc to provide pressure during grinding and polishing.

The polishing was started with piano type of diamond grinding disc (Fig. 5), followed by serial polishing by using diamond powder (Fig. 6) with time and pressure variable listed in Table 1.

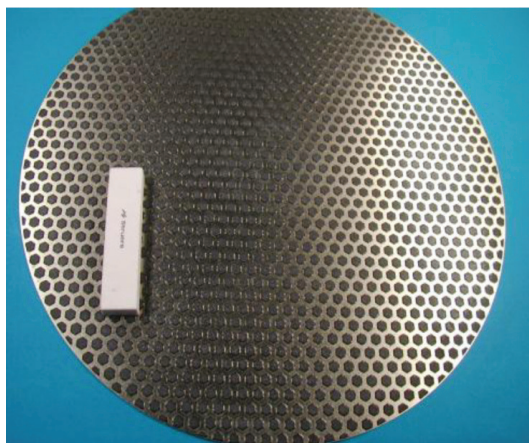


Figure 5: The piano type of diamond grinding.



Figure 6: Serial of diamond powder for polishing.

TABLE 1: Serial steps of grinding and polishing for Si_3N_4 .

Steps	Grinding/polishing method	Force level	RPM	Time (min)
1	Diamond-Piano 220	4	150	5
2	Diamond-Piano 600	6	100	2
3	Diamond powder 15 µm	8	100	30
4	Diamond powder 9 µm	8	100	60
5	Diamond powder 6 µm	8	100	90
6	Diamond powder 3 µm	8	100	30
7	Diamond powder 1 µm	8	100	30

Bright field and differential interference contrast (DIC) or so called Nomarski in optical microscope is used to observe whether the final surface still contain scratch or not. Indentation test then was performed by using Vickers (Fig. 7) and Knoop (Fig. 8) indentation. By using Vickers, the value of hardness and fracture toughness and can be provided, and from Knoop indentation the value of modulus elasticity will be obtained.

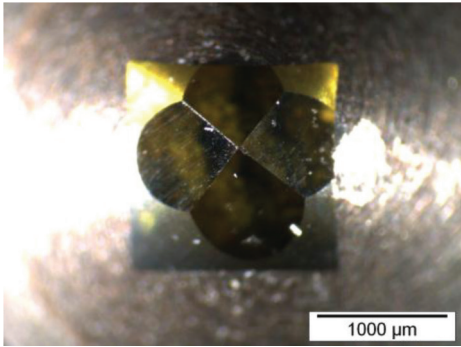


Figure 7: Vickers indenter.

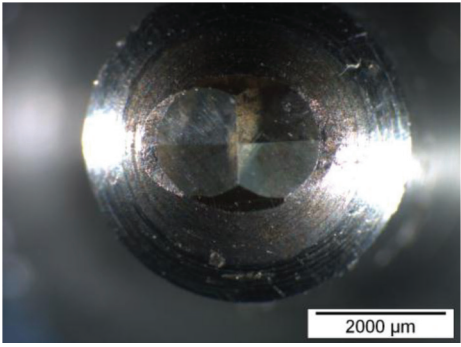


Figure 8: Knoop indenter.

Since Si_3N_4 is ceramic material, this is meaning that etching process is difficult to be performed by using chemical solution. Plasma etching (Fig. 9) was introduced in this research to reveal the microstructure. Microstructure then was revealed by using both optical microscope and scanning electron microscope (SEM). This report will be completed with successful technique in revealing the defect such as crack and porosity by utilizing fluorescence dye penetrant with ultra violet (UV) source of light.

Provide sufficient detail to allow the work to be reproduced. Methods already published should be indicated by a reference. Only relevant modifications should be described.

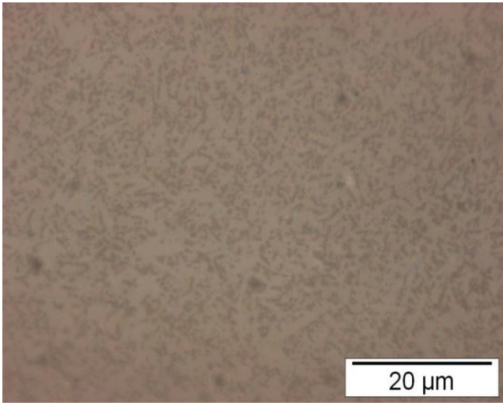


(a)

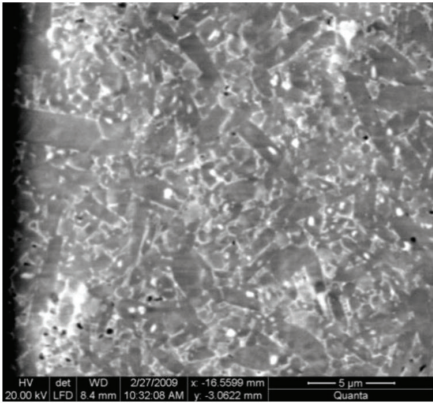


(b)

Figure 7: (a) Equipment for plasma etching, (b) Detail chamber for plasma etching.



(a)



(b)

Figure 8: Microstructure after plasma etching of Si_3N_4 (a). By using optical microscope. (b) Obtained from SEM.

3. Result and Discussion

The grinding and polishing step that was developed in this research is successfully to obtain smooth surface without scratch. The microstructure that is found as can be seen in Fig. 8. Both optical and SEM picture are presented, and indicated that there are elongated grain as a typical of β Si₃N₄ [3].

The Vickers hardness value was investigated based on ISO TC 206/SC N [4]. The load F that was applied was 10 kg. The Vickers indentation was found valid as depicted in Fig. 9, with values found was 14.2 GPa HV10, calculated by using Equation (1)[4] with d is the arithmetic mean of two diagonal Vickers indentation.

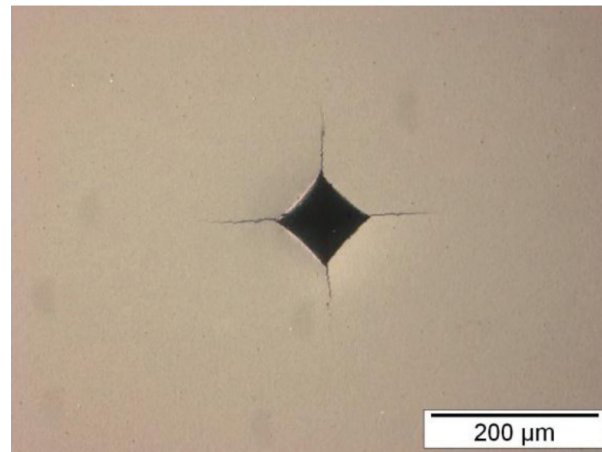


Figure 9: Vickers indentation of Si₃N₄, load applied was 10 kg.

$$HV(\text{GPa}) = 0.001 \frac{2F \sin \frac{136^\circ}{2}}{d^2} = 0.001854 \frac{F}{d^2} \tag{1}$$

The value of fracture toughness (K_{IC}) is also possible to be approached from indentation technique. The initial idea of using indentation for fracture toughness determination was introduced by Evan and Charles[5] that can be formulated from Equation (2).

$$K_{IC} \Phi / H \sqrt{a} = 0.15k(C/a)^{-3/2} \tag{2}$$

H is hardness, Φ the constrain factor (≈ 3), the indentation crack length is C should be related to the impression radius a , where k is the correction ($k=3.2$). By using the formula in Equation 2, the fracture toughness value is found 4.6 MPa.m^{1/2}.

It is interesting to be informed here that by using the result from Knoop indentation, the modulus elasticity can be approached by utilizing formula introduced by Marshal *et. al.* [5]. The method is based on measurement of elastic recovery of the in-surface dimensions of Knoop indentation. In the fully loaded state, the ratio of the diagonal dimensions, a and b of the contact area is defined by the indenter geometry $a/b=7.11$. However, on unloading, elastic recovery reduces the length of the shorter indentation diagonal, whereas the longer diagonal remains relatively unaffected. The extent of recovery depends on the hardness to modulus ratio. Therefore the distortion of the residual impression, characterized by the ratio of its dimensions, b'/a' , provide a measure H/E . The value of E then can be calculated from Equation (3).

$$b' / a' = b / a = \alpha H / E \tag{3}$$

With value of b' / a' that was obtained from Knoop indentation as depicted in Fig. 10. The value of E that is calculated from Equation (3) was obtained 189.2 GPa.

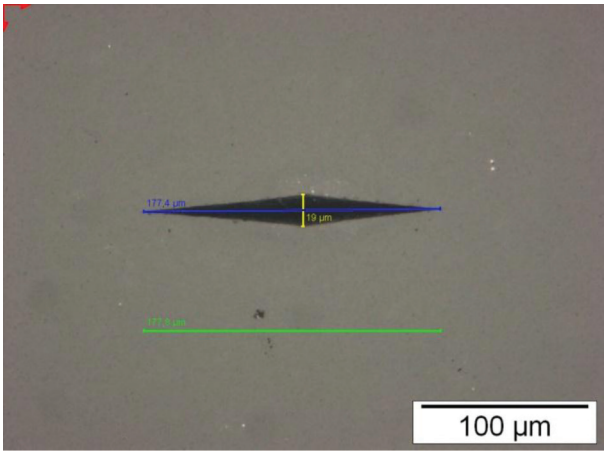


Figure 10: Measurement of long and short diagonal of Knoop indentation (HK 3) for modulus elasticity measurement.

The defect in the specimen was easily detected by using fluorescence dye penetrant as depicted in Fig. 11. Ultra violet source of light was applied for this purpose.

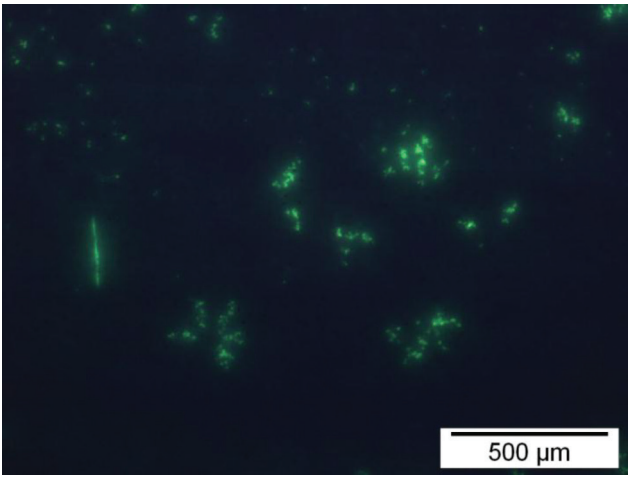


Figure 11: Illuminated green color is the defect in the specimen. This is obtained by immersed the specimen in the fluorescence dye penetrant. Observation was done with optical microscope under ultra violet source of light.

4. Conclusion

Ceramography technique on Si_3N_4 that is developed in this research is successful to reveal the microstructure and indentation respond of the material Si_3N_4 . The hardness, fracture toughness and modulus elasticity of the specimen is also possible to be determined. The results showed that the Vickers hardness values found was 4.2 GPa HV10 and the fracture toughness value

is found $4.6 \text{ MPa}\cdot\text{m}^{1/2}$. With fluorescence dye penetrant under ultra violet source of light the defect in Si_3N_4 was easily observed therefore is suitable to be proposed as a technique for testing the quality of silicon nitride component in nuclear application.

5. Acknowledgment

The author acknowledge **Univ. Prof. Dr. Robert Danzer** and **Professor Tanja Lube** of Institute for Structure and Functional Ceramic, Montanuniversitat, Leoben, Austria on supervising and facilitating this research and The Austrian Federal Ministry for Science and Research for financial support by awarding a technology grant southeast Asia (ACM-2007-01996) through program of **ASEA-UNINET**.

References

- [1] Richerson, D. W., "Modern Ceramic Engineering, Marcel Dekker Inc.", New York, (1992).
- [2] Chin, R. E., "Ceramography, ASM International, United State of America", (2001).
- [3] Lube, T. and Dusza, J., "A Silicon Nitride Reference Material-A Testing Program of ESIS TC6", Journal of The European Ceramic Society 27 (2007). pp. 1203-1209, (2007)
- [4] ISO TC 206/SC N, 2006, "Test Method for Hardness of Monolithic Ceramic at Room Temperature", (2006)
- [5] Evan, A. G. and Charles, E. A., "Fracture Toughness Determination by Indentation", Journal of The American Ceramic Society, Vol. 59, No. 7-8, pp.371-372, (1976)
- [6] Marshall, D. B., Noma T., and Evans, A. G., "A Simple Method for Determining Elastic Modulus to Hardness Ratios Using Knoop Indentation Measurements", Communications of The American Ceramic Society, pp. C175-C176, (1982)

Conference Paper

Investigation of Rod Control System Reliability of Pwr Reactors

Deswandri and Syaiful Bakhri

Center for Nuclear Reactor Technology and Safety - BATAN, Kawasan Puspiptek Gd. 80, Setu, Tangerang Selatan

Abstract

The Rod Control System is employed to adjust the position of the control rods in the reactor core which corresponds with the thermal power generated in the core as well as the electric power generated in the turbine. In a Pressurized Water Reactor (PWR) type nuclear power plants, the control-rod drive employs magnetic stepping-type mechanism. This type of mechanism consists of a pair of circular coils and latch-style jack with the armature. When the electric current is supplied to the coils sequentially, the control-rods, which are held on the drive shaft, can be driven upward or downward in increments. This sequential current control drive system is called the Control-Rod Drive Mechanism Control System (CRDMCS) or known also as the Rod Control System (RCS). The purpose of this paper is to investigate the RCS reliability of APWR using the Fault Tree Analysis (FTA) method since the analysis of reliability which considers the FTA for common CRDM can not be found in any public references. The FTA method is used to model the system reliability by developing the fault tree diagram of the system. The results show that the failure of the system is very dependent on the failure of most of the individual systems. However, the failure of the system does not affect the safety of the reactor, since the reactor trips immediately if the system fails. The evaluation results also indicate that the Distribution Panel is the most critical component in the system.

Corresponding Author:
Deswandri and Syaiful Bakhri,
email: wandri@batan.go.id

Received: 29 July 2016
Accepted: 21 August 2016
Published: 21 September 2016

**Publishing services
provided by Knowledge E**

Keywords: PWR, Control-rod, CRDMCS, Reliability Analysis, FTA

© Deswandri and Syaiful Bakhri. This article is distributed under the terms of the [Creative Commons Attribution License](#), which permits unrestricted use and redistribution provided that the original author and source are credited.

Selection and Peer-review under the responsibility of the ICoNETS Conference Committee.

 OPEN ACCESS

1. Introduction

The electricity load of a nuclear power plant is proportional with the output of the thermal power generation. The thermal output of a nuclear power plant is controlled by the insertion or withdrawal of the control-rods into and out of the reactor core. In general, PWR-type nuclear power plant employs Control-rod Drive Mechanism (CRDM) system based on magnetic stepping-type mechanism, to move the control-rods up and down [1]. This mechanism consists of a pair of circular coils and latch-style jacks with armature. By providing electric current through the coils sequentially, the control-rod which is attached to the drive shaft can be moved up or down in steps. The control system which generates these sequences is called Control-rod Drive Mechanism Control System (CRDMCS) or sometimes abbreviated to Rod Control System (RCS). The RCS is employed in PWR reactors for controlling the supply current to the coils initiated by a reactor regulating system in response to a command signal

to move the control-rods. The electromagnetic force, which is activated by the coils, causes the control-rods moving upward or downward by mechanical movement.

To ensure the safety and reliability, several researches have been carried out based on CRDM prototype or mathematical model. Simulation of the CRDM based on analytical mathematical model, numerical and finite element [1-5] have been performed to assess the behavior of the CRDM such as magnetic force, velocity of CRDM and drop analysis. Other approaches based on experiments were implemented using various prototypes to assess the reliability [6-9]. It was indicated that during the design of CRDM, the functional and performance test of the CRDM prototype have been carried out, such as drop test, impact pressure test, durability test as well as other main characteristics. Furthermore, in [10], it is demonstrated that APWR CRDM has been evaluated using FMEA and highlighted that there is no effect of single failure, which affects the actuation of the reactor protection system. Despite these previous investigations, the analysis of reliability which considers a Fault Tree Analysis (FTA) for common CRDM can not be found in any public references. This may be due to the proprietary design of the CRDM.

This paper aims to investigate the RCS reliability using the Fault Tree Analysis (FTA) method. The FTA method evaluates the system reliability by modeling the system through the fault tree-shaped diagram. In this paper, the FMEA based table of APWR CRDM in Reference [10] is used to identify basic events, which are part of developing the FTA diagram of RCS. The fault tree diagram was analyzed using the reliability analysis software ITEM TOOLKIT to obtain the minimal cutsets, which in turn can be used for the calculation of the probability and frequency of the system failures.

2. The Crdm System Description

The main function of CRDM is to adjust the position of the control-rod bank inside the reactor core. The system consists of Logic Cabinet and Power Cabinet as shown in Figure 1 [11]. The Logic Cabinet is comprised of processing part (Digital Controller) and output part. Logic function of this Cabinet is to provide command signals to control the sequential flow that will flow into each coil of Stationary Gripper, Moveable Gripper and Lift Mechanism installed on the CRDM. This signal is processed based on the input obtained automatically from the Reactor Regulating System (RRS) or manually from the operator.

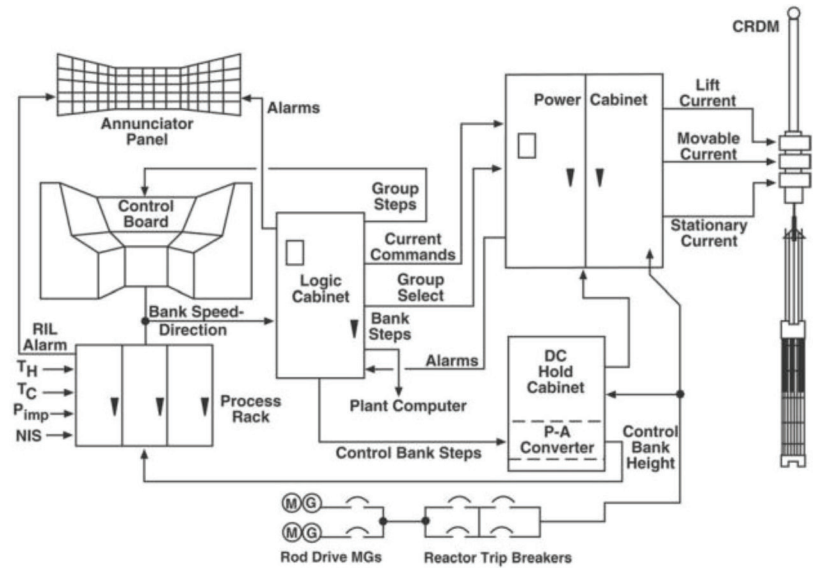


Figure 1: Diagram of CRDM Interface [11].

The Power Cabinet consists of Transformer, Molded Case Circuit Breaker (MCCB) and Current Control Unit Part. The Power Cabinet receives AC power from the motor generator through the Reactor Trip Breaker (RTB) and CRDM Distribution Panel. The Power Cabinet is employed to transform the AC voltage into DC current by using a transformer, and DC current generated is distributed to each coil in CRDM sequentially through the control process of Current Control Unit is based on a command signal from Logic Cabinet. Mechanical Control System Configuration of Control-rod Drive is shown in Figure 2 below.

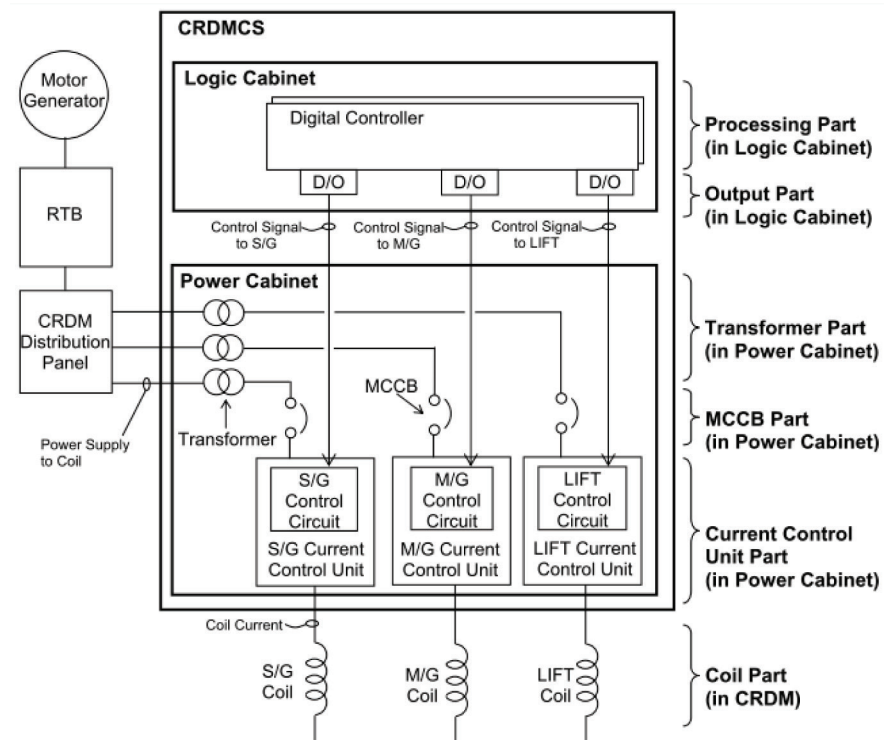


Figure 2: Mechanical control system of RCS [10].

The mechanism of insertion and withdrawal of control-rods can be described as follows [12].

1. Control-rods withdrawal:

- (a) In the initial conditions, Stationary Gripper Coil receives electrical current, while the Moveable Gripper and the lifts Coil are disconnected (do not receive any current). Because of the current flowing through the coil Stationary Gripper, the control-rod is held by Stationary Gripper (a gripped state).
- (b) Moveable Gripper Coil is energized to engage the control-rod assembly groove.
- (c) Current flow in Stationary Gripper Coil is disconnected so that the grip on the control-rod is released.
- (d) Lift Coil is electromagnetically energized to lift (pulling) moveable Gripper together with the control-rods to a new position one step to the top.
- (e) Stationary Gripper Coil is then energized to re-engage and to hold back the control-rod position staying in the position.
- (f) Current flow on moveable gripper coil is disconnected so that the grip on the control-rod is released.

- (g) Current flow in the Lift Coil is disconnected releasing the effect of electromagnetic force, then Moveable Gripper is drop to its original position one step lower than the current lifted control-rod position.
 - (h) These previous steps are repeated, so that the control-rods are upward step by step.
2. The insertion of control-rods.
- (a) Initial conditions, Stationary Gripper Coil which receives electric current will hold the control-rod, while Moveable Gripper and Lifts Coil are disconnected.
 - (b) Lift Coil is energized and then electromagnetically lift (pulling) Moveable Gripper to the position of one step upward.
 - (c) Moveable Gripper Coil is energized to engage the control-rods.
 - (d) Current flow in Stationary Gripper Coil is disconnected so that the grip on the control-rod is released.
 - (e) Current flow in the lifting Coil is disconnected, so that the influence of electromagnetic force is lost. Therefore, the Moveable Gripper including the control-rod drops downward one step.
 - (f) Stationary Gripper Coil is energized to hold the control-rod position on the position of one step higher than its earlier one.
 - (g) Current flow on Moveable Gripper Coil are disconnected disengaging the gripper from the control-rod.
 - (h) The steps are repeated, so that the control-rods are downward step by step.

3. Methodology

CRDM System is evaluated using the reliability evaluation method of Fault Tree Analysis (FTA) [13]. FTA method is applied to evaluate the reliability of the system by developing a fault-tree diagram model. The model development is started by understanding the components, the modules arrangement, its functions as well as the working procedures.

As a first step in understanding how the system and components work, this research performs assessment and rearrangement of Failure Mode and Effect Analysis (FMEA) table of the CRDM obtained from Reference [10]. The adoption of FMEA analysis results is required to assist in identifying basic events for further developed fault tree diagram.

The fault tree diagram system is then developed based on the previous understanding of the functional block, working procedure, component and module of the system. At the top of fault tree, the assumption of the system failure mode is set. Based on the modes of system failure, several intermediate events leading to a system failure are elaborated. For each intermediate event occurrence, further intermediate events causing higher intermediate events are elaborated. The development of fault tree diagram is ended up on the basic event (ie: the failure of components or modules).

Fault tree diagram is quantified using the reliability software evaluation ITEM Toolkit. The quantification results in the form of a minimum cutset and probability or frequency of system failure. Cutset minimum is the smallest combination of basic event of failure that lead to system failure. The probability or frequency of system failure is calculated based on the probability or the frequency of basic event input.

4. Results and Discussions

The Development of Fault Tree Diagram

The Modeling of system reliability is one of the techniques to evaluate the reliability and safety of a system. Among various methods to create such model, FTA is the most widely used. The FTA method is a deductive method and using diagrams to illustrate the model of system failure. The analysis begins by assuming general events (such as the failure of a system) and ends up on the basis of events, which can be the causes of the general events. In developing the fault tree diagram with FTA method, FMEA analysis is useful as an initial step in identifying the basic events. The FMEA is a method of analysis, which is conducted to identify failure modes and the effects of the failure on each individual components of the system. This step is useful for understanding the function and contribution of components to the system. In contrast to the FTA, the FMEA method only identifies the effects of the failure of individual components to the system and is unable to consider how the combined effects of the system component fail. Thus, the identification results only show the effects of a single failure. In this research, the Table of FMEA Control-rod Drive Control System in [10] is used as a reference. That table is then reprocessed according to the understanding of the study of the functions and workings procedure of the components stated in the fault tree diagram model.

Fault tree diagram for CRDM begins by assuming the system to fail for functioning. The Failure Control Systems of CRDM to function, as shown in Figure 1, can occur due to Stationary Gripper malfunction, Moveable Gripper malfunction or Elevator Coil malfunction. The cause of the failure of each gripper or coil can then be pursued further, as shown in the fault tree diagram in Figure 3, 4 and 5.

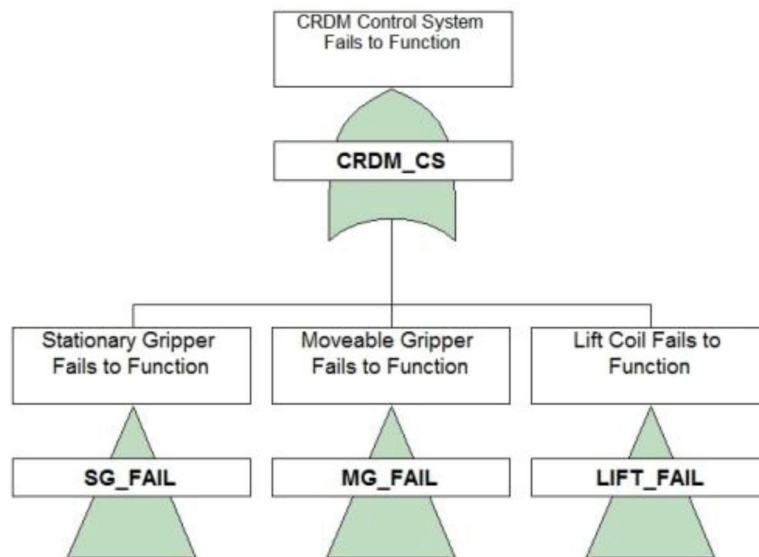


Figure 3: Top event of the CRDMCS Fault Tree Diagram System; Top Event.

As seen in Figure 4, Stationary Gripper fails to function due to damage, or sequential electric current required to generate a magnetic field fails to be supplied by Current Control Unit. This sequential current supply failure can be caused by firstly, the failure or damage Current Control Unit, MCCB, Transformer, Control Circuit inside the Current Control Unit. Secondly, the supply of electric current from the Motor Generator Unit does not reach the Power Cabinet. This type of fault can be caused by damaged Distribution Panel, spurious open of Reactor Trip Breaker or failure of the Motor Generator Unit (inoperable). Thirdly, the sequential current flow actuation

command signal for Stationary Gripper coil is not received by Logic Cabinet. This third type of failure may be caused by the Digital Controller in Part Processing (both damaged), failure of the module output in Processing Part, or Power Supply for Logic Cabinet failed, as shown on Figure 4.

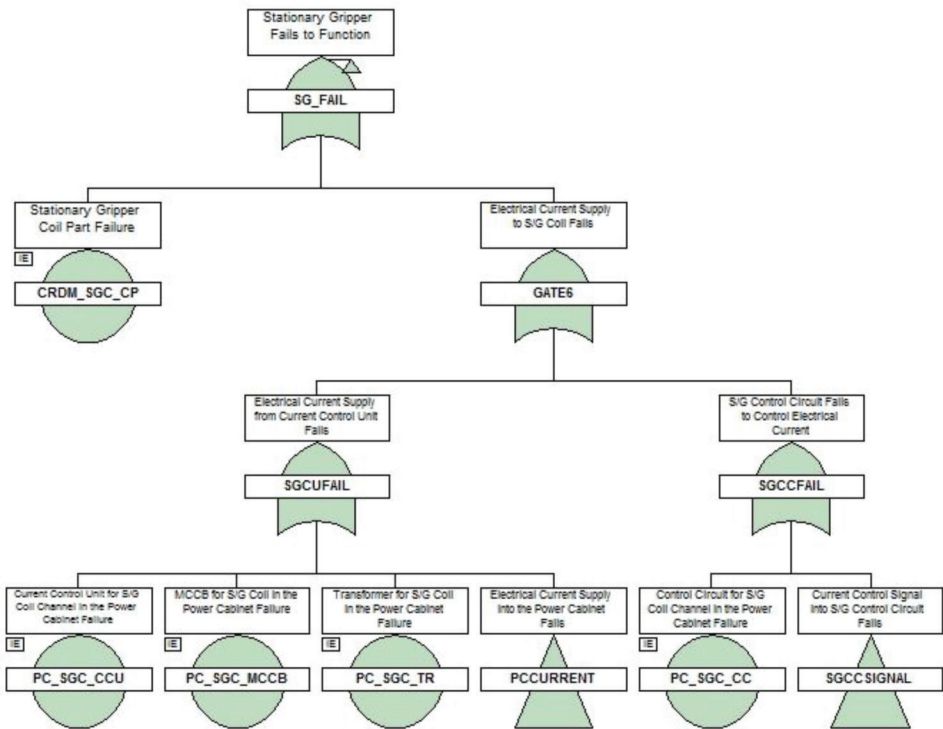


Figure 4: CRDMCS Fault Tree Diagram System; failure of Stationary Gripper.

It should be noted here, in case of Moveable Gripper failure and lifts Coil scenarios, to move the control-rod is similar to those described in Stationary Gripper as included in the fault tree. One of the critical intermediate events in CRDMCS Fault Tree is Electrical Current Supply in the Power Cabinet, because if this event occurs then all of grippers and coil become fail. The fault tree diagram for Electrical Current Supply in the Power Cabinet Fail is shown in the Figure 6.

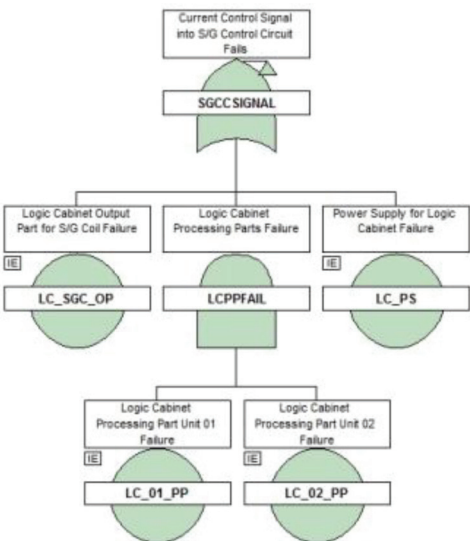


Figure 5: CRDMCS Fault Tree Diagram System; Failure of logic cabinet in Stationary Gripper line.

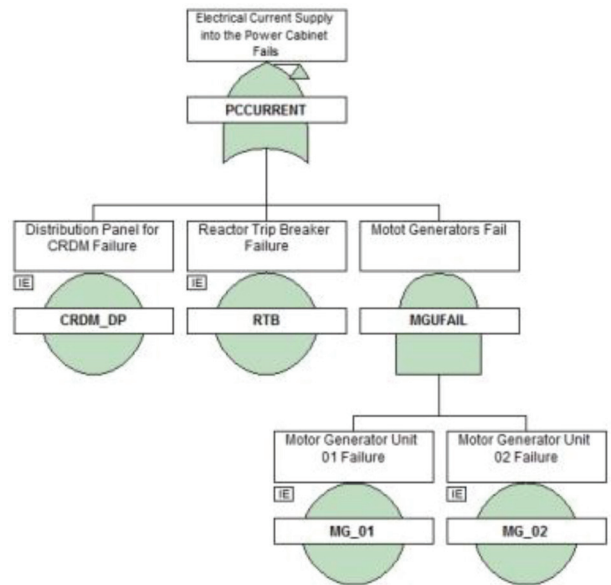


Figure 6: CRDMCS Fault Tree Diagram System; failure of power supply in Power Cabinet.

The Quantification Results and Discussion of Fault Tree Model

Fault tree diagram is quantified using reliability software ITEM TOOLKIT. Quantification goal is to obtain the least cutset which is the smallest combination of failures basic event (components) that can cause system failure. Moreover, the quantification of fault tree diagram is also intended to gain the probability or frequency of occurrence of the top event which is the assumption of a system failure. To obtain the value of the probability or frequency, data reliability of each basic event (components) which is expressed in terms of failure rate (failure rate) is required. The value of the failure rate for each basic event in this activity was obtained from several references as shown in Table 1, and the calculation result of the reliability of the system is shown in Table 2 below.

TABLE 1: Failure rate of each component.

No	Type of Component	Failure Mode	Failure Rate
1	Coil Part (CRDM_SGC_CP, CRDM_MGC_CP dan CRDM_LIC_CP)	Broken/Malfunction	9,50E-6/hr [7]
2	Current Control Unit (PC_SGC_CCU, PC_MGC_CCU and PC_LIC_CCU)	Malfunction	1,27E-5/hr[7]
3	MCCB (PC_SGC_MCCB, PC_MGC_MCCB and PC_LIC_MCCB)	Open without command/Fail to stay in closed position	1,60E-8/hr[8]
4	Transformer (PC_LIC_TR, PC_SGC_TR and PC_MGC_TR)	Malfunction	9,40E-8/hr[8]
5	Control Circuit (PC_LIC_CC, PC_MGC_CC dan PC_SGC_CC)	Malfunction	1,43E-5/hr[7]
6	Power Supply (LC_LI_PS, LC_MG_PS and LC_PS)	Fail to supply electric current	1,63E-5/hr[7]
7	Output Part (LC_MGC_OP, LC_LIC_OP and LC_SGC_OP)	Malfunction/Fail to send signals	8,40E-6/hr[9]
8	Processing Part (LC_o1_PP, LC_o2_PP, LC_MG_o1_PP, LC_MG_o2_PP, LC_LI_o1_PP and LC_LI_o2_PP)	Malfunction / Fail to process signals	8,01E-6/hr[9]
9	Distribution Panel (CRDM_DP)	Fail / Burn	2.0E-4/hr[10]
10	Trip Breaker (RTB)	Malfunction	2,50E-7/hr[11]
11	Motor Generator Unit (MG_o1and MG_o2)	Malfunction	5,20E-8/hr[8]

TABLE 2: The calculation results for system unavailability and availability.

Unavailability Q	3.8390E-04/hr
Availability	9.9962E-01/hr
No of Cut Sets	27

Table 3 shows that the cause of system failure of CRDM is dominated by the failure of the Distribution Panel. As illustrated in Chart of CRDM in Figure 2, the Distribution Panel serves to distribute the electric current supply from the Motor Generator Unit to the three coil lines (Stationary Gripper, Moveable Gripper and Lifts Coil) in the Power Cabinet. If the Distribution Panel fails, all automatic lines are also fail to function.

TABLE 3: Minimal cutset.

No	Unavailability	Minimal Cutset
1	2.0000E-04	CRDM_DP
2	1.6300E-05	LC_PS
3	1.6300E-05	LC_LI_PS
4	1.6300E-05	LC_MG_PS
5	1.4300E-05	PC_MGC_CC
6	1.4300E-05	PC_SGC_CC
7	1.4300E-05	PC_LIC_CC
8	1.2700E-05	PC_LIC_CCU
9	1.2700E-05	PC_SGC_CCU
10	1.2700E-05	PC_MGC_CCU
11	9.5000E-06	CRDM_LIC_CP
12	9.5000E-06	CRDM_SGC_CP
13	9.5000E-06	CRDM_MGC_CP
14	8.4000E-06	LC_LIC_OP
15	8.4000E-06	LC_SGC_OP
16	8.4000E-06	LC_MGC_OP
17	9.4000E-08	PC_LIC_TR
18	9.4000E-08	PC_SGC_TR
19	9.4000E-08	PC_MGC_TR
20	2.5000E-08	RTB
21	1.6000E-08	PC_MGC_MCCB
22	1.6000E-08	PC_LIC_MCCB
23	1.6000E-08	PC_SGC_MCCB
24	6.4160E-11	LC_LI_o1_PP ::LC_LI_o2_PP
25	6.4160E-11	LC_MG_o1_PP ::LC_MG_o2_PP
26	6.4160E-11	LC_o1_PP ::LC_o2_PP
27	2.7040E-15	MG_o1 ::MG_o2

In addition, Table 3 also shows that almost all minimal cutsets are basic events (23 cutsets of existing cutsets of 27). This reality suggests that the failure or success of the control-rod drive system depend on the success of each component of the basic events.

In terms of safety, the failure and the success of the CRDM are not significant, as shown in the FMEA analysis results (see Reference 10). Failure of one of the component in the system will cause a reactor trip as soon as the control-rods are not engaged properly. As described in the previous section, the function of Stationary Gripper, Moveable Gripper and Lifts Gripper are to engage and hold device control-rods alternately. If one of the components fails, the gripper in Stationary Gripper, Moveable Gripper or Lifts Gripper will also fail and the control-rods fall freely.

On the other hand, in terms of reliability, the CRDMCS failure impacts on economic factors of the reactor. The success of CRDMCS to function is required by the operator during a reactor power settings. When there is a transient in the power reactor (within normal limits), CRDMCS is required to move the control rod up and down automatically to control the reactor power remaining in stable value. CRDMCS failures which led to frequent shutdowns of the reactor will decrease the availability and the economic value of the reactor.

In the safety system, the failure of system must not happen. Therefore, the reliability of the system should be at the level close to 100% by providing redundancy of up to 4, so that the system becomes complex and expensive. However, for systems that are not related to safety such as CRDMCS, providing many redundancies for the systems will cause additional difficulties in maintenance (because the system becomes complex) and make the installation not economical (system becomes expensive). Therefore, a solution to improve the reliability of systems that are not related to safety is to provide components with very high quality for critical components.

Table 4 shows three importance values (criticality important measure) of each basic event to the occurrence of the top event (system failure). Firstly, F-Vesely Importance values demonstrates the contribution of basic event to the top event. The second important measure, i.e. The BirnBaun Importance value, shows the sensitivity of the probability of occurrence of the top event as the function of changes in the value of basic event probabilities. Meanwhile, B-Proschan Importance values indicate the probability of the top event as a result of all minimal cutsets containing critical basic events [12]. Based on the calculations results given in Table 4, it is shown that the Distribution Panel is a basic event that has the largest contribution (52%) compared with other events. The calculation results also indicate that 23 minimal cutsets, which consist of one basic event have a much higher sensitivity than other combined basic events.

TABLE 4: Importance Measure Basic Events/Components.

No	Components/Basic Events	F-Vesely	BirnBaun	B-Proschan
1	Distribution Panel (CRDM_DP)	0.5209	1	0.5209
2	Power Supply (LC_LI_PS, LC_MG_PS and LC_PS)	0.0424	1	0.0424
3	Control Circuit (PC_LIC_CC, PC_MGC_CC dan PC_SGC_CC)	0.0372	1	0.0372
4	Current Control Unit (PC_SGC_CCU, PC_MGC_CCU and PC_LIC_CCU)	0.0331	1	0.0331
5	Coil Part (CRDM_SGC_CP, CRDM_MGC_CP and CRDM_LIC_CP)	0.0247	1	0.0247
6	Output Part (LC_MGC_OP, LC_LIC_OP and LC_SGC_OP)	0.0219	1	0.0219
7	Transformer (PC_LIC_TR, PC_SGC_TR and PC_MGC_TR)	2.44E-04	1	2.44E-04
8	Trip Breaker (RTB)	6.50E-05	1	6.50E-05
9	Circuit Breaker (PC_SGC_MCCB, PC_MGC_MCCB and PC_LIC_MCCB)	4.16E-05	1	4.16E-05
10	Processing Part Module (LC_o1_PP, LC_o2_PP, LC_MG_o1_PP, LC_MG_o2_PP, LC_LI_o1_PP and LC_LI_o2_PP)	1.67E-07	8.01e-6	1.67E-07
11	Motor Generator (MG_o1 and MG_o2)	7.04E-12	5.2e-8	7.04E-12

5. Conclusion

The reliability of Control-rod Drive Control System has been evaluated using Fault Tree Analysis. During the modeling of the system, the FMEA table of CRDMCS from the reference has been used to identify the basic events based on the component failures. It is concluded that the failure of single or combined components of the system will hinder the success of the function of the complete system. Although the system fails to operate, those failures do not affect the safety system, because the system is only designed in reactor normal operation. If the system fails, the control-rods will fall freely into the reactor core immediately. Through the Fault Tree Analysis Method, a system failure is assumed and described in the form of a fault tree diagram to show basic events of the logical combination which become the cause of the system failure. It was found that the Distribution Panel is a major contributor to the cause of system failure. Quantification results also demonstrate that the majority of minimal cutsets consist of single component failure. This can be understood because the system is not a safety-related system, as well as only for normal operation purpose. Therefore, the application of redundancy can be minimized and the success of the system operation is mainly based on the implementation of high degree of reliability components.

References

- [1] Tanaka, A., et al., *Development of a 3-D simulation analysis system for PWR control rod drive mechanism*. International Journal of Pressure Vessels and Piping, 2008. **85**(9): p. 655-661.
- [2] Rajan Babu, V., G. Thanigaiyarasu, and P. Chellapandi, *Mathematical modelling of performance of safety rod and its drive mechanism in sodium cooled fast reactor during scram action*. Nuclear Engineering and Design, 2014. **278**(0): p. 601-617.
- [3] Shirazi, S. A. M., *The simulation of a model by SIMULINK of MATLAB for determining the best ranges for velocity and delay time of control rod movement in LWR reactors*. Progress in Nuclear Energy, 2012. **54**(1): p. 64-67.
- [4] Yoon, K. H., et al., *Control rod drop analysis by finite element method using fluid-structure interaction for a pressurized water reactor power plant*. Nuclear Engineering and Design, 2009. **239**(10): p. 1857-1861.
- [5] Singh, N. K., D. N. Badodkar, and M. Singh, *Numerical and experimental study of hydraulic dashpot used in the shut-off rod drive mechanism of a nuclear reactor*. Nuclear Engineering and Design, 2014. **273**(0): p. 469-482.
- [6] Rajan Babu, V., et al., *Testing and qualification of Control & Safety Rod and its drive mechanism of Fast Breeder Reactor*. Nuclear Engineering and Design, 2010. **240**(7): p. 1728-1738.
- [7] Chyou, Y. P., D. D. Yu, and Y.-N. Cheng, *Performance validation on the prototype of control rod driving mechanism for the TRR-II project*. Nuclear Engineering and Design, 2004. **227**(2): p. 195-207.
- [8] Ramesh, E. and S. Usha. *Reliability analysis of control rod drive mechanisms of FBTR for reactor startup and power control. in Reliability, Safety and Hazard (ICRESH), 2010 2nd International Conference on*. 2010.

- [9] Iida, H., et al., *Long-term stability of Sm₂Co₁₇-type magnets for control rod drive mechanism (CRDM) in a nuclear reactor*. *Magnetics, IEEE Transactions on*, 1995. **31**(6): p. 3653-3655.
- [10] Mitsubishi Heavy Industries, L. *US-APWR Technical Report. FMEA of Control Rod Drive Mechanism. Control System*. 2007.
- [11] Institute, E. P. R. *Nuclear Maintenance Applications Center: Westinghouse Full-Length Rod Control System - Life Cycle Management Planning Sourcebook*. 2006.
- [12] Roslund, C. J., et al., *Digital nuclear control rod control system*. 2012, Google Patents.
- [13] Ericson, C. A., *Hazard Analysis Techniques for System Safety*. 2005, New Jersey: John Wiley & Sons.

Conference Paper

Radionuclide Disperse to Environment from Pwr Reactor on Severe Accident Condition using Maccs Program

Sri Kuntjoro, Pande Made Udiyani

Center for Nuclear Reactor Technology and Safety - BATAN, Kawasan Puspiptek Gd. 80, Setu, Tangerang Selatan

Abstract

The atmosphere is an important pathway in the transfer of radionuclides from nuclear power plants into the environment and population. Acceptance of radiation dose to the environment and population affected by the radionuclides release and site conditions surrounding of the nuclear power plant. The radionuclides release in the atmosphere is determined by the dispersion coefficient parameter. The aim of this paper is to obtain dispersion coefficient and radionuclide released in Sebagin (West Bangka district) caused by severe accident condition from the PWR Nuclear Power Plant. Dispersion analysis of radionuclides into the environment from nuclear power PWR on severe accident conditions have been done using MACCS program. Reference for the calculation of source term fraction is selected from calculation results of the MELCOR computer code and it is implemented to PWR reactors Westinghouse 3411 MWth subject. The calculation of radionuclides release performed using MACCS program for aspiring nuclear power plant site in West Bangka. Simulation calculations for the area radius from 0.80 kmup to 20 km from the nuclear power plant site are performed. Meteorological datas used in calculation are the meteorology data from Sebagin meteorological stations for the years of 2012 period. The result is the dispersion coefficient decreases as a function of time and distance. The concentration of radionuclides through soil pathway decreases as a function of the distance, and the dominant contributor of radionuclide radiation Xe-133 and I-131. Radionuclide concentrations obtained through the air pathway decreases as a function of distance, and dominant contributors of radionuclide radiation is contributed also from I-131 and Xe-133. The presence of I-131 radionuclides are giving dangerous to humans, it is necessary to further treatment for prevent its impacts.

Keywords: dispersion coefficient, radionuclide concentration, severe accident, MACCS

Corresponding Author:

Sri Kuntjoro,
Pande Made Udiyani,
email: srikunco@batan.go.id,
pmade-u@batan.go.id

Received: 29 July 2016

Accepted: 21 August 2016

Published: 21 September 2016

**Publishing services
provided by Knowledge E**

© Sri Kuntjoro, Pande Made Udiyani. This article is distributed under the terms of the [Creative Commons Attribution License](#), which permits unrestricted use and redistribution provided that the original author and source are credited.

Selection and Peer-review under the responsibility of the ICoNETS Conference Committee.

 OPEN ACCESS

1. Introduction

Nuclear energy is one of the alternative energy being considered by the Indonesian government to maintain availability of national energy. The existence of nuclear energy implemented to build Nuclear Power Plant (NPP). According to the existence of a nuclear power plant in reactor site is requires assessment of nuclear safety to monitor and minimize the impact this may have. According to this condition, determine analysis of the consequences of radionuclides releases to the environment and population. Based on this

analysis it can be seen how big the consequences and the radiation dose to be public and the environment due to the condition of an accident on the reactor. Radionuclides release into the environment and population can result from normal and abnormal operation of nuclear power plants. The mostly radionuclide release is through to the air, which is the radionuclide release to atmosphere.

Based on radioactive exposure pathway, radionuclide dispersion in the air will be partially deposited in the ground and will culminate in the environment through the food chain to population. The distribution of radionuclides in the atmosphere is determined by the parameters of the dispersion coefficient, while the deposition parameters are influenced by the dispersion parameter. Dispersion parameters will be affected to the external and internal exposure coming from radioactive cloud, while the deposition parameters will affect to the internal and external exposure coming from radioactive deposition on the ground surface. Dispersion parameter is a parameter that is analyzed and written on the Safety Analysis Report (SAR) as part of Chapter on NPP accident analysis. Dispersion parameters can be estimated using Gaussian Plume Model (GPM) as used in computer codes TREX (Hungary), MACCS (Taiwan, USA), OSCAAR (Japan), LENA (Brazil), and using Lagrangian Plume Model (LPM) as used in computer codes HYSPLIT (USA), NAME III (UK), MINERVE-SPRAY (CEA-France)[1,2,3,4,5,6,7]. Estimation data of dispersion parameters for Muria Peninsula site plant simulation analyzed using the PC-Cosyma code has been successfully carried out[8,9]. The dispersion parameter estimation data for a potential NPP site in Indonesia is very necessary used for build of NPP SAR document, such as for prospective new site is Bangka Belitung site. Since the dispersion coefficient data for the Bangka Belitung site have not been estimated, then the research in this field will be estimated using MACCS (USA) code.

The purpose of this research is to obtain dispersion coefficient data to Seabang (West Bangka) site using MACCS2 codes. In this research, the analysis of the dispersion coefficient and concentration of radionuclide releases for severe accident conditions in nuclear power plants with a capacity of 1000 MWe PWR reactor type. Results of this analysis are the of radionuclide dispersion patterns from nuclear power plant site and it can be able to fill on reactor accident analysis chapter in the SAR reactor. Postulation selected is a severe accident condition and the specific reactor site to be chosen is Seabang-West Bangka site. The analysis was performed for the dispersion coefficient of 8th fission product groups radionuclides are released from the NPP are the noble gas, lanthanides, precious metals, halogens, alkali metals, tellurium, cerium, strontium and barium groups. Calculations using removable fraction of radionuclides in PWR reactors Westinghouse is calculated using MELCOR code [10,11].

2. Theory

Atmospheric dispersion modeling is basically an attempt to describe the functional relationship between pollutants emissions accordance pathways and resulting of radiation concentrations of radiation. Beside this is to predict radiological consequences caused by radionuclide concentration and radiological dose from various hypothetical scenarios are determined. In this study of radionuclides release through the atmospheric model using segmented Gaussian model Plume Models (GPM)[12]. Gaussian Plume Models general equations written in the following formula;

$$\chi(x, y, z) = \frac{Q}{2\pi\sigma_y\sigma_z v} \cdot \exp\left(-\frac{y^2}{2\sigma_y^2}\right) \cdot \left\{ \exp\left[-\frac{(z-H)^2}{2\sigma_z^2}\right] + \exp\left[-\frac{(z+H)^2}{2\sigma_z^2}\right] \right\} \quad (1)$$

with;

$\chi(x,y,z)$: concentration in air (χ) in axial, x premises to wind direction, y = perpendicular to wind direction, and z = high to the ground level, (Ci/m³)

Q : Radioactive release from stack, (Ci/s)

u : average wind velocity (m/s)

σ_y : segmented plume in horizontal direction (m);

σ_z : segmented plume in vertical direction (m)

H : effective high of stack (m)

y : rectangular distance from wind direction (m);

z : high distance from ground level (m);

χ/Q : dispersion factor parameter (s/m³)

Magnitude early for calculation are a plum long L, vertical and horizontal standard deviation σ_y, σ_z as follows;

$$L = \sum_i \Delta t_i \cdot v_i \quad (2)$$

$$\sigma_y(t=0) = \frac{W_b}{4.3} \quad (3)$$

$$\sigma_z(t=0) = \frac{H_b}{4.3} \quad (4)$$

with;

Δt_i : establishment time for segmentation plume

v_i : establishment velocity for segmentation plume

W_b : width of the building where the plums are formed

H_b : high of the building where the plums are formed

While the equation of the plume growth (plume are usually hot, so it will be grow up), it can be seen in the following equation;

$$\Delta h = \frac{1.6F^{1/3} X^{2/3}}{\bar{u}} \quad (5)$$

with;

Δh : magnitude of plume grow (m)

F : flux buoyancy from segmentation plume is $8.79E-05 Q$ (m⁴/s³)

Q : power distribution of heat (watt)

X : distance of radial downstream wind (m)

\bar{u} : average wind velocity (m/s)

3. Methodology

The research methodology includes a series of calculations and simulations based on postulations data, assumptions data and also based on secondary and primary data namely:

- Source term Calculation for PWR type reactor with 1000 MWe power with postulation of accident is severe accident conditions of Station Black Out (SBO), and release fraction of calculation take from MELCOR calculation results of The Westinghouse PWR reactor with power 3411 MWTh.

- Calculation of dispersion and deposition parameters using MACCS code
- Reactor site input covering meteorology and topographical conditions were wind speed, weather stability, and solar energy in 16 wind direction and 12 radius distance (800 m, 1 km, 2 km, 3 km, 4 km, 5 km, 6 km, 7 km, 8 km, 9 km, 10 km, 15 km and 20 km from the
- Nuclear power plant site. The selected topology data were taken from West Bangka data as well as the meteorological data were taken from the period of January to August 2012 with one hour interval time. The weather data is taken from 60 m from ground level and a chimney reactor height is 100 m
- The calculation is done for the fission product releases to sequences within 1-96 hours.

4. Result and Discussion

1. Source term Analysis

The analysis was first performed by calculating the reactor inventory. Further calculations was to determine reactor source term for severe accident conditions SBO using MELCOR fraction transport of severe accident SBO from PWR Westinghouse reactor with 3411 MWth power. It radionuclide fraction released results are shown in Table 1. Furthermore, in Table 2 the reactor source term assumed for this SBO accident.

TABLE 1: Fraction of radionuclide release from MELCOR calculation.

No.	Radionuclide Group	Release Fraction of Radionuclide from Reactor (MELCOR)			
		GAP	In-Vessel	Ex-Vessel	Late In-Vessel
1	Noble Gas (Xe/Kr)	1.23E-02	8.94E-01	8.19E-02	5.88E-03
2	Halogen (I)	4.58E-02	7.64E-01	6.80E-02	3.23E-03
3	Alkali Metal (Cs)	3.94E-03	6.40E-01	1.02E-01	2.41E-03
4	Te	4.97E-03	6.57E-01	2.65E-02	3.32E-03
5	Ba, Sr	4.97E-03	2.00E-03	2.35E-02	1.36E-09
6	Ru	4.97E-03	9.75E-03	2.09E-02	1.75E-05
7	Lanthium (La)	4.97E-03	1.06E-07	1.19E-04	1.93E-13
8	Ce	4.97E-03	1.01E-07	4.96E-03	1.34E-13
9	Mo	4.97E-03	4.61E-01	2.31E-10	3.44E-03

Release fraction in the reactor building depends on the type and character of fission products, and the noble gases have the largest release fraction for each place because of the nature of noble gases do not react with the material. As for fission products which is volatile type such as alkali metal (Cs) and halogen (I) has a little more fraction compare with the noble gases release. Based on released fraction of radionuclides from reactor core to the chimney (late vessel) as written in Table 1, the source term results are listed in Table 2.

Table 2 shows that radionuclide source term from the Noble Gas group (I, Xe and Kr) have a high level of radiation that is in order of 10^{12} , this is because the Noble Gas has properties that cannot be filtered, so most of the radionuclides in this group can escape to the environment. Furthermore the source term results in Table 2 are used for the calculation of dispersion parameters and radionuclides concentration are dispersed through the ground and the air.

TABLE 2: Reactor source term (Bq).

No	Radionuclides	Source term (Bq)	No	Radionuclides	Source term (Bq)
1	KR-85	4.72E+10	26	I-131	1.18E+13
2	KR-85M	9.99E+11	27	I-132	1.27E+13
3	KR-88	2.47E+12	28	I-133	2.36E+13
4	RB-86	2.26E+09	29	I-134	1.18E+13
5	SR-89	4.92E+02	30	I-135	2.04E+13
6	SR-90	4.23E+01	31	XE-133	8.55E+12
7	Y-90	4.68E-01	32	XE-135	3.61E+12
8	Y-91	2.97E-01	33	CS-134	1.91E+11
9	Y-92	1.05E+02	34	CS-137	1.11E+11
10	ZR-95	3.17E-08	35	BA-139	5.42E+02
11	ZR-97	3.00E-08	36	BA-140	8.68E+02
12	NB-95	3.19E-08	37	LA-140	1.53E+01
13	MO-99	5.21E+07	38	LA-141	2.58E-08
14	TC-99M	4.68E+07	39	LA-142	1.91E-08
5	RU-103	4.15E+07	40	CE-141	8.55E-07
16	RU-105	2.42E+07	41	CE-143	7.84E-07
17	RU-106	1.37E+07	42	CE-144	6.46E-07
18	RH-105	2.58E+07	43	PR-143	2.95E-08
19	SB-127	4.72E+10	44	ND-147	1.23E-08
20	SB-129	1.21E+11	45	NP-239	1.00E-05
21	TE-127	4.71E+10	46	PU-241	5.83E-08
22	TE-127M	6.09E+09	47	AM-241	2.40E-12
23	TE-129	1.36E+11	48	CM-242	5.63E-10
24	TE-129M	2.07E+10	49	CM-244	6.91E-11
25	TE-132	6.31E+11			

2. Weather Analysis in Sebagin Meteorology Station on West Bangka District

Weather analysis is conducted by describing the Wind Rose and it used to determine the direction and speed of the dominant wind blows from the nuclear power plant site in West Bangka district. Meteorological data are then used as input of the MACCS codes. The results of wind rose can be seen in Figure 1.

Figure 1 shows that the largest distribution of radionuclides to the South-East (zone 6 to 8), the West and the Southwest (zones 12 and 13) directions respectively. Based on Figure 1 can be determined safely zone for evacuation and relocation, which is in from the North to the North East-East (zones 1 to 3).

3. Radionuclide Dispersion Analysis

a. Dispersion Parameter χ/Q

Dispersion parameter χ/Q is influenced by radius distance and source term. Dispersion parameter χ/Q decreases with increasing source term and radius distance of release. To determine the influence of the radius distance and release time to the dispersion parameter of fission product in the Sebagin-West Bangka site are listed in Figure 2.

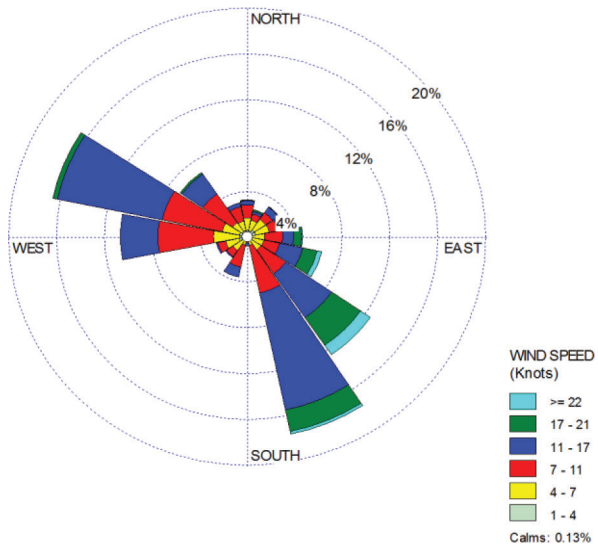


Figure 1: Anti wind rose (wind direction from NPP to Environment) of Sebagin Meteorology Station on West Bangka District.

Figure 2 shows that the dispersion parameter (χ/Q) decreases as a function of time. It is also seen that the dispersion parameter also decreases as a function of distance. The highest dispersion parameters shown in the exclusion area is within a radius of 800 m from the reactor site. While the influence of disperse time as it relates to sequences release, ie release sequences under 8 hours have dispersion parameter (χ/Q) is small, as it assumed that the source term still a small portion is released into the atmosphere. Figure 2 shows that the source term can be assumed to be whole releases to the atmosphere in the sequence of 24-96 hours.

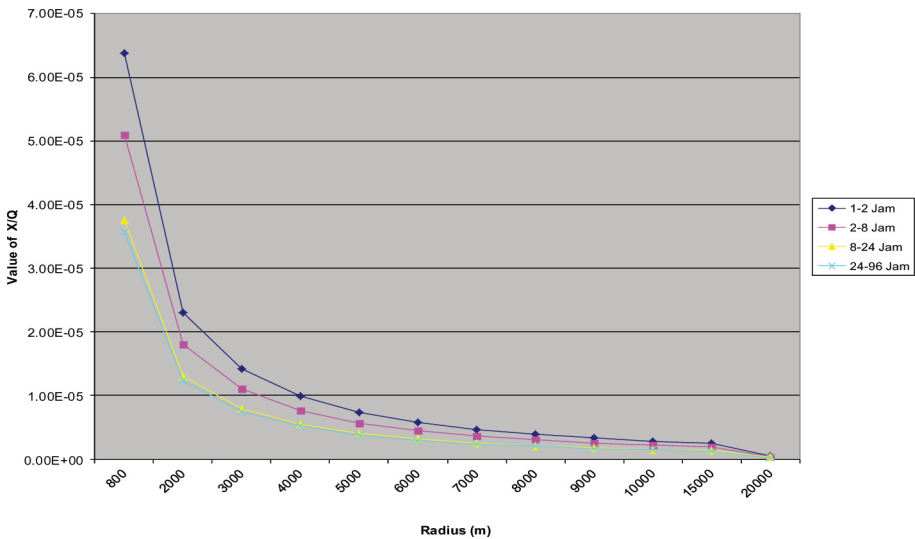


Figure 2: Dispersion Parameter (χ/Q) Fungson of Time and Radius.

b. Radionuclide Disperse Activity

Activity of radionuclide radiation dispersed through the air pathway be affected by the value of the dispersion parameter (χ/Q), it mean that, by increasing the amount of activity it will increasing the dispersion parameter (χ/Q) value as well. The calculation results of radiation activities are shown in Figure 2 and Figure 3.

Figure 3 shows the distribution of radionuclides through air pathway decreases as a function of distance and it is proportional to the decrease of dispersion parameter value (χ/Q) as shows in Figure 2. Figure 3 show that the greatest activity in a radius of 800 m in prospective nuclear power plant site which is an exclusion zone. Furthermore, from Figure 4 shows that the largest contributor of radionuclide exposure came from the I-131 at 52%, followed by Xe-133 by 40%, Cr-85M by 5% and Te-132 by 3%.

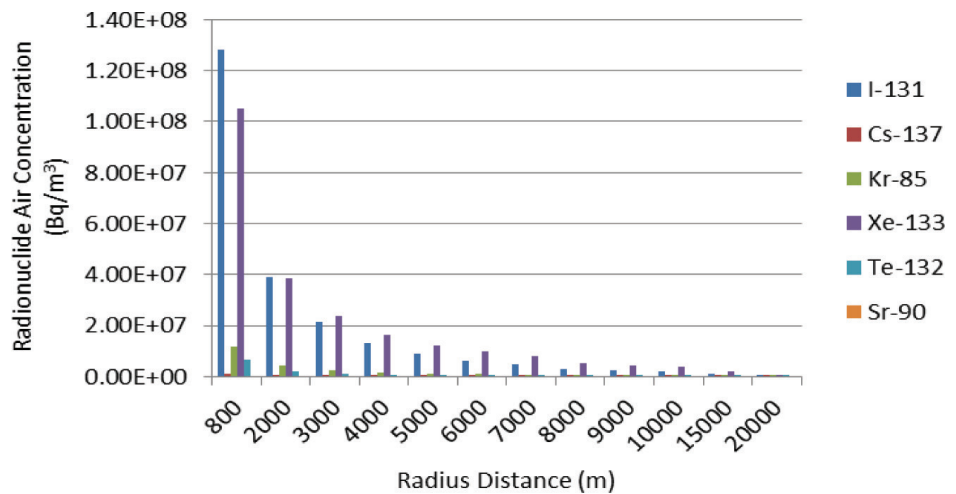


Figure 3: Radionuclide Air Concentration Function of Radius.

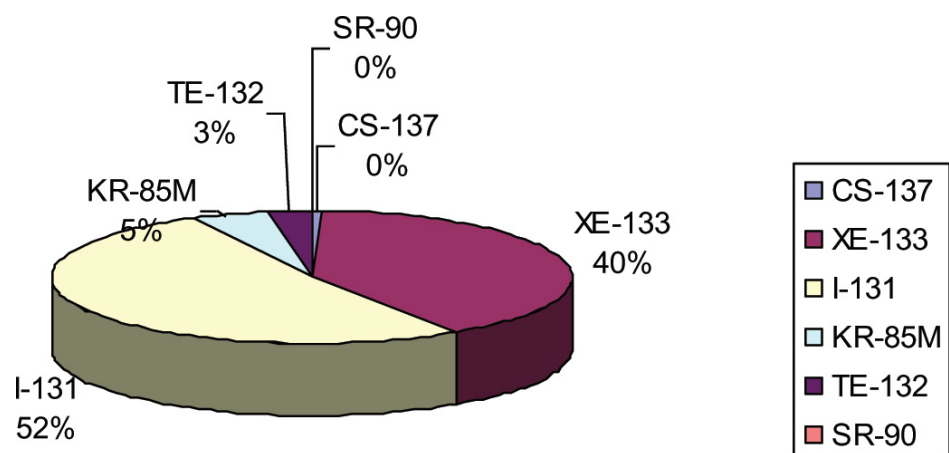


Figure 4: Percentage of Radionuclide Dispersion Release.

5. Conclusion

The dispersion analysis of the PWR to the environment on a severe accident condition using MACCS code has been done for in the Sebagin-West Bangka site. The analysis were carried out for 24 - 96 hours after the accident occur, where in that period the whole of radionuclides has been disperse from the reactor to the environment. Dispersion parameter decreases as a function of radius from the nuclear power plant site. The largest dispersion parameter is 6.30E-05 in radius 800 m from reactor site. Also obtained radionuclide activity dispersed through the air to the environment and the percentage of this radionuclides respectively. The largest

activity and percentage of radionuclide disperse to the air is come from I-131 radionuclide with value are of $1.24E+08$ Bq/m³ and 52% respectively. By obtaining dispersion factor and radionuclide activity dispersed through the air, then the purpose of this research have been achieved.

References

- [1] Robert M, Csilla V, Istvan L, Simulation of Accidental Release Using a Coupled Transport (TREX) and Numerical Weather Prediction (ALADIN) Model, Quarterly Journal of the Hungarian Meteorological Service, Vol. 114, No. 1-2, January - June 2010, pp. 101-120
- [2] Moosung J, Seok W.H, A Study on Risk Assessments Using the MACCS Code for a Nuclear Power Plant, Journal of Nuclear Science and Technology, Supplement 4, p 418-422, March 2004
- [3] Chanin D.I, Sprung J.I and colleagues MELCOR Accident Consequence Code System (MACCS) User Guides, U.S Nuclear Regulatory Commission, Washington, DC 20555, 2010
- [4] Juliana P.D, Paulo F. F, and colleagues, Atmospheric Dispersion and Dose Evaluation Due to the Fall of a Radioactive Package at a LILW Facility, International Journal of Energy Engineering, Vol 3, p 119-126, 2013
- [5] G.D. Rolpha, F. Ngana, R.R. Draxler, Modeling The Fallout from Stabilized Nuclear Clouds Using The HYSPLIT Atmospheric Dispersion Model, Journal of Environmental Radioactivity, Volume 136, Pages 41-55, October 2014
- [6] Till J. E, Rood A.S, and colleagues, Comparison of the MACCS2 Atmospheric Transport Model with Lagrangian Puff Models as Applied to Deterministic and Probabilistic Safety Analysis, Journal of Health Physics, Volume 107 - Issue 3 - p 213-230, September 2014
- [7] François V. D, Bertrand L, Vladimir S, and colleagues, Atmospheric Transport Modeling with 3D Lagrangian Dispersion Codes Compared with SF6 Tracer Experiments at Regional Scale, Science and Technology of Nuclear Installations, Volume 2007 (2007), Article ID 30863, 13 pages
- [8] Pande. M.U, dan Widodo, S. Penentuan Koefisien Dispersi Atmosferik untuk Analisis Kecelakaan Reaktor PWR di Indonesia, Jurnal Teknologi Reaktor Nuklir Vol. 14 No.2 Juni 2012, Hal. 121-132
- [9] Pande M. U, Sri K, Pane J.S., Analisis Kecelakaan Parah pada Pressurized Water Reaktor dengan Backwards Method, Jurnal Teknologi Reaktor. Nuklir Vol. 15 No.1 Februari 2013, Hal.12-26
- [10] Scott G.A, Kenneth C.W, and colleagues, Assessment of Severe Accident Source terms in Pressurized-Water Reactors with a 40% Mixed-Oxide and 60% Low- Enriched Uranium Core Using MELCOR 1.8.5, SANDIA National Laboratories, Printed April 2010.
- [11] X. Davoine and M. Bocquet, Inverse modeling-based reconstruction of the Chernobyl source term available for long-range transport, Atmos. Chem. Phys., 7, 1549-1564, 2007, p 1550-1558
- [12] Joong M.Y, Glaser R. Atmospheric Dispersion Analysis Using MACCS2, International Congress on Advances in Nuclear Power Plants, (ICAPP '04). Pittsburgh. PA; 2004; June 13- 17, United States; 2004.

Conference Paper

Application of Trend Analysis Method for Emergency Planning in NPP Accident

Pande M.U., Kuntjoro S.

Center for Reactor Technology and Nuclear Safety National Nuclear Energy Agency-BATAN, Puspisstek-Complex OB. 80, Serpong 15310, Indonesia


Abstract

A decision for emergency response should be taken based on existing nuclear preparedness assessment. However, lessons learned from the Fukushima accident revealed that emergency response personals had difficulties in estimating time duration needed for the emergency actions. For that case, it is needed an alternative way to determine the time required for a response to be implemented. The objective of this paper is to applicate the trend analysis method for an emergency planning in NPP accident, especially to estimate time duration of countermeasures such as sheltering, evacuation, and relocation. Estimation was done based on consequences and dose data of PWR-1000 MWe severe accident which was simulated for West Bangka site. Dose and consequence estimations were calculated using Pc-cosyma software, and trend analysis application was performed using statistical software. The result of simulation are: iodine tablets are to be distributed to residents in the area within radius of 20-30 km; sheltering countermeasure is needed within the radius of 20-30 km for 12 weeks; evacuation is subjected for the area of 20 km from reactor for duration of 12 weeks; relocation is subjected to radius of 10 km for 2.5 years. The trend analysis can be used for supporting the decision making, especially for emergency planning. The advantage of this method is that it can provide quicker result than past methods. Besides, uncertainties can be reduced by using accurate input data and selection of suitable computation model.

Corresponding Author:
Pande M.U., Kuntjoro S.,
email: pmade-u@batan.go.id

Received: 29 July 2016
Accepted: 21 August 2016
Published: 21 September 2016

Publishing services
provided by Knowledge E

 Pande M.U., Kuntjoro S.
This article is distributed
under the terms of the
[Creative Commons
Attribution License](#), which
permits unrestricted use
and redistribution provided
that the original author
and source are credited.

Selection and Peer-review
under the responsibility of
the ICoNETS Conference
Committee.

 OPEN ACCESS

Keywords: trend analysis, emergency response, NPP, accident

1. Introduction

The Fukushima accident, which was classified as severe accident, has caused great impacts and health consequences to people who live in the vicinity of the site [1-4]. In the early stage of the accident, the operator could not determine the severity of the impact. Emergency decision for countermeasure was taken based on emergency preparedness assessment [5-6]. However, by using existing emergency preparedness, it was difficult to estimate time duration for each countermeasure. An assessment of accident impact is necessary in order to know the severity of the consequences and to determine the actions needed. The actions of countermeasure can be divided into two types i.e. short-term countermeasures such as providing iodine tablet, sheltering and evacuation, and long-term countermeasures which include population relocation. Time duration of countermeasure is estimated based on the radiation exposure, doses, and risk assessment [7], while the in situ real time measurement

is needed to complement the estimation. By using real time doses, it is difficult to estimate time duration of countermeasure planning, such as time duration for sheltering, evacuation, and relocation. However using simulation data is also difficult because of the presence of simulation uncertainty [8,9].

Therefore, an alternative way is needed to estimate the time required for countermeasures. In statistical method, trend analysis is could be used to interpret uncertain events in the past, and to predict future events. Trend estimation is a statistical technique to aid data interpretation. When a series of measurements of a process are treated as a time series, trend estimation can be used to make and justify statements about tendencies in the data, by relating the measurements to the times at which they occur. By using trend estimation, statements about tendencies in the data can be made and justified. The objective of this paper is to applicate of trend analysis method for emergency planning in NPP accident, especially to estimate the time duration of countermeasure such as sheltering, evacuation, and relocation. Estimation was done based on consequences and dose data of PWR-1000 MWe severe accident which was simulated for West Bangka site. Dose and consequence estimations were done by using Pc-cosyma software and trend analysis application was conducted using statistical software [10].

2. Trend Analysis Methods and Applications

Trend Analysis is: the practice of collecting information and attempting to spot a pattern, or *trend*, in the information; taking past data and using it to project future results, to project how the data might appear in the future [11]. Trend analysis is could be used to estimate uncertain events in the past, in statistics, trend analysis often refers to techniques for extracting an underlying pattern of behavior in a time series, which would otherwise be partly or nearly completely hidden by noise. Although trend analysis is often used to predict future events, it could be used to estimate uncertain events in the past.

Trend estimation is a statistical technique to aid interpretation of data. When a series of measurements of a process are treated as a time series, trend estimation can be used to make and justify statements about tendencies in the data, by relating the measurements to the times at which they occurred. By using trend estimation it is possible to construct a model which is independent of anything known about the nature of the process of an incompletely understood system (for example, physical, economic, or other system). This model can then be used to describe the behavior of the observed data. In particular, it may be useful to determine if measurements exhibit an increasing or decreasing trend which is statistically distinguished from random behavior. If we are missing data for a given period of time, you can interpolate a reasonable estimate based on the figures you do have.

Regression analysis is a statistical process for estimating the relationships among variables. It includes many techniques for modeling and analyzing several variables, when the focus is on the relationship between a dependent variable and one or more independent variables. Regression analysis is widely used for prediction and forecasting, where its use has substantial overlap with the field of machine learning. Regression analysis is also used to understand which among the independent variables are related to the dependent variable, and to explore the forms of these relationships. In restricted circumstances, regression analysis can be used to infer causal relationships between the independent and dependent variables. However this can lead to illusions or false relationships, so caution is advisable; for example, correlation does not imply causation. In statistics, linear regression is an approach for modeling the relationship between a scalar dependent variable y and one or more explanatory variables denoted X . The

R-squared value indicates how closely your trend line follows your data; the closer its value is to 1, the closer it follows your data. This model can then be used to describe the behavior of the observed data.

A linear regression model assumes that the relationship between the dependent variable y_i and the p -vector of regressors x_i is linear. This relationship is modelled through a disturbance term or error variable ϵ_i – an unobserved random variable that adds noise to the linear relationship between the dependent variable and regressors. Thus the model takes the form [11]:

$$y_i = \beta_1 x_{i1} + \dots + \beta_p x_{ip} + \epsilon_i = \mathbf{X}_i^T \boldsymbol{\beta} + \epsilon_i, \dots, i = 1, \dots, n, \quad (1)$$

- Y_i is called the *regress and, endogenous variable, response variable, measured variable, or dependent variable*.
- $X_{i1}, X_{i2}, \dots, X_{ip}$ are called *regressors, exogenous variables, explanatory variables, covariates, input variables, predictor variables, or independent variables*.
- The corresponding element of $\boldsymbol{\beta}$ is called the *intercept*.
- Sometimes one of the regressors can be a non-linear function of another regressor or of the data, as in polynomial regression and segmented regression. The model remains linear as long as it is linear in the parameter vector $\boldsymbol{\beta}$.

3. Methodology

The assessment consists of several calculations, that are core inventory calculation (PWR 1000 MWe), source term calculation of severe accident, consequences calculation (individual dose), countermeasures, and risks. For estimation of countermeasure time duration use by trend analysis method.

Figure 1 shows flow chart of countermeasure assessment and estimation of countermeasure time duration. PC-COSYMA is a dose consequence and countermeasure assessment computer code according to segmented Gaussian diffusion model using source data derived from accident scenarios. Statistical computer code for trend analysis of time duration countermeasure. Estimation and simulation on West Bangka site.

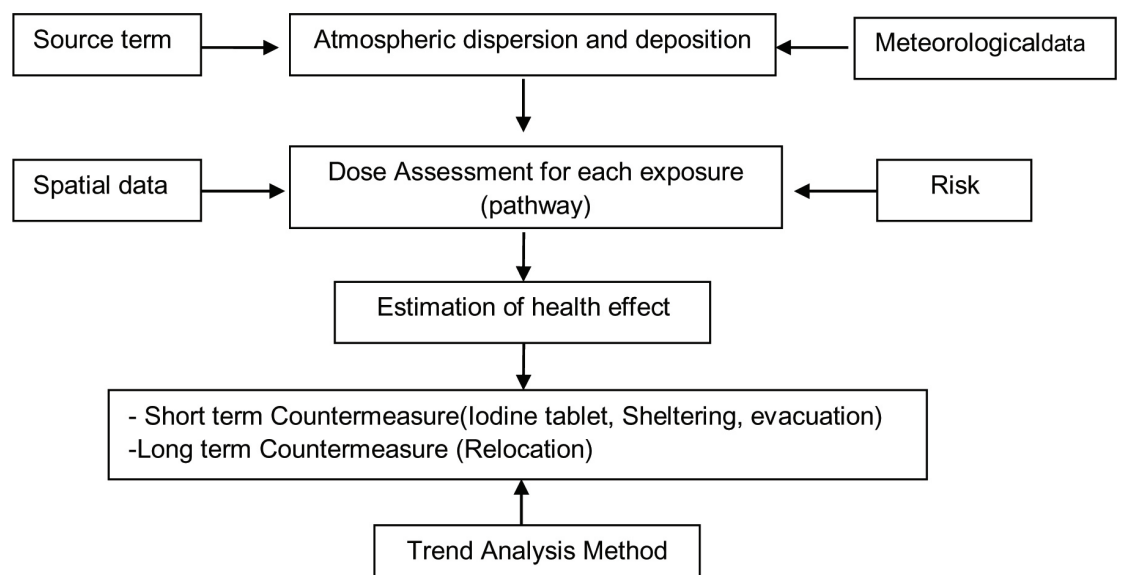


Figure 1: The assessment modelling for emergency planning.

4. Result and Discussion

Dose and Risk Calculation

Figure 2 explain the individual effective dose received as a impact of PWR 1000 MWe accident at the site of West Bangka. In Fig. 2 describe that the individual dose decreases with increasing distance. The series of dose data in Figure 2 can be used to estimate the emergency planning. The statistical relationship between the individual doses and distance approximated by the equation range of exponential trend line model. Exponential trend line used to data that rises or falls at rates that increase constantly. Use an exponential trend line for data that rises or falls at rates that increase constantly.

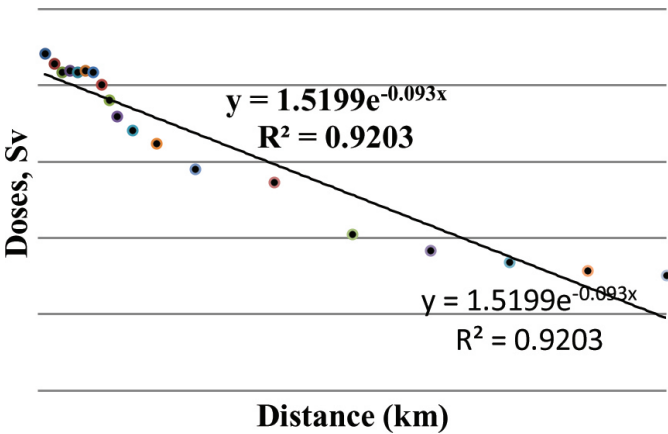


Figure 2: Individual effective dose versus distance.

This trend line can be used with such things as radioactive decay, which progressively slows down over time. This trend line represents a steady rate of increase or decrease. Trend line follow the exponential equations:

$$y = 1.519 (e^{-0.09x}), R^2= 0.920 \tag{2}$$

With y = individual dose and x = distance. The R-squared value indicates how closely your trend line follows your data; the closer its value is to 1, the closer it follows your data. With the high R-squared value indicates this model can be applied to this data set on Fig.2 and eq. (2).

According to the basic policy in the ICRP-103 recommendation [11, 12], in the emergency activities such as nuclear accident the annual dose to the people is allowed up to 100 mSv. It's defined as emergency exposure situation. Post emergency situation, the annual dose is limited within 20 mSv for the existing exposure situation for long-term exposure. Determination of counter measures are required to mitigate radiation exposure and health risks from radiation accident. Based on data in Fig. 2 and eq. (2), the countermeasure of severe accident at West Bangka was estimated. The countermeasure divided two classification are: short term (sheltering, evacuation, iodine distribution) and long term countermeasure (relocation). According to the criteria mentioned by the ICRP-63 [13], evacuation is recommended whenever the effective dose exceeds 50 mSv, and distribution Iodine tablet when the effective dose exceeds 10 mSv. The zone for sheltering is recommended when the effective dose exceeds 10 mSv, and relocation when the effective dose exceeds 100 mSv.

The result of assessment in Fig. 2 and eq. (2) are:

- **Relocation** recommended at distance below 10 km
- **Evacuation** recommended at distance 10 - 20 km
- **Sheltering** recommended at distance 20 -30 km.
- **Distribution of Iodine tablet** at distance 20 -30 km

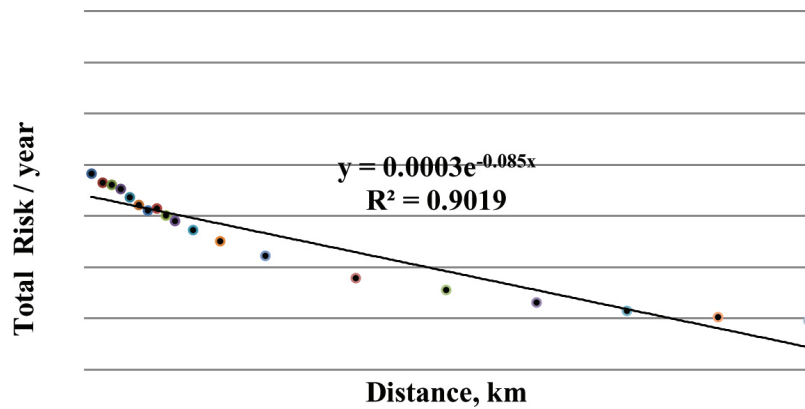


Figure 3: Total risk versus distance.

Figure 3 described the total risk will be received as a impact of PWR 1000 MWe accident at the site of West Bangka. The radiological risk will diminish with increasing distance from reactor. Total risk decreased with increased distance. Trend line follow the exponential equations:

$$y = 0.001e^{-0.08x}, R^2 = 0.901 \tag{3}$$

When y = total risk and x = distance, high R-squared value indicates this model can be applied to this data set. (Fig. 3 and eq. (3)).

Countermeasure

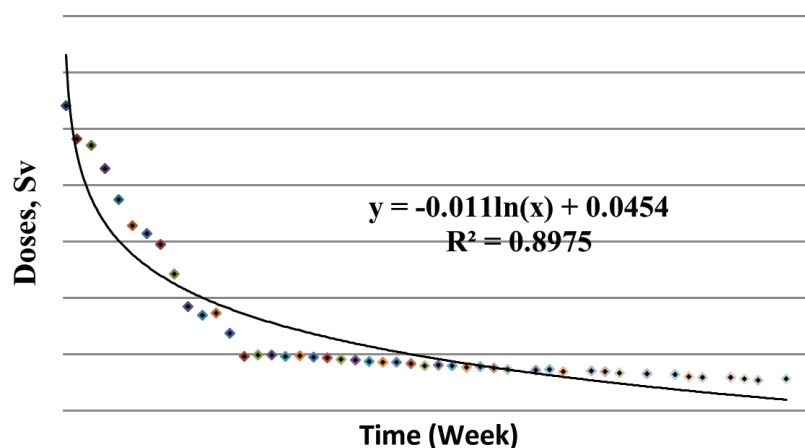


Figure 4: Effective intervention dose with time for sheltering at distance 30 km.

Figure 4 show the effective intervention dose versus time for sheltering, the effective intervention dose decreases with increasing time of sheltering. The statistical relationship between the effective intervention dose and time for sheltering approximated by the equation range of logarithmic trend line. Trend line follow logarithmic equations:

$$y = - 0.01 \ln(x) + 0,897, R^2 = 0.897 \tag{4}$$

Where y = effective intervention dose and x = time for sheltering. High R-squared value indicates this model can be applied to this data set for Fig. 4 and eq. 4. By using trend analysis and trend estimation, it can be seen how long the action performed on residents sheltering in a radius of 20-30 km (based on Fig. 2 and eq. (2), If individual effective doses for sheltering is not exceeds 10 mSv [13]. By drawing the time of Fig.2, the required to achieve a dose of 10 mSv for sheltering is 12 weeks. By using the correlation equation (4), obtained sheltering time is 10-12 weeks.

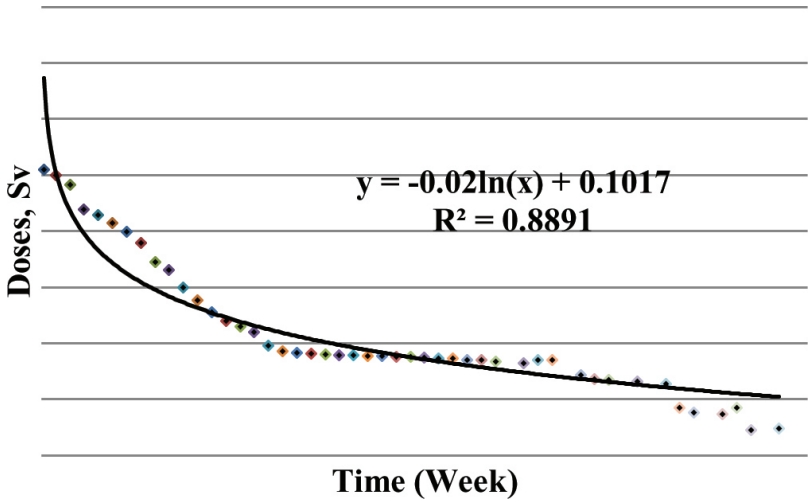


Figure 5: Effective intervention dose with time for evacuation at distance 20 km.

Figure 5 described of the relation effective intervention dose with evacuation time at distance 20 km when individual effective doses for sheltering is not exceeds 50 mSv. Fig. 5 show that the effective intervention dose decreases with increasing time of evacuation. The statistical relationship between the effective intervention dose and time for sheltering approximated by the equation range of logarithmic trend line. Trend line follow logarithmic equations:

$$y = - 0.02 \ln(x) + 0.101, R^2 = 0.897 \tag{5}$$

Where y = effective intervention dose and x=time duration for evacuation. High R-squared value on Fig. 5 and eq. (5) indicates this model can be applied to this data set. By using trend analysis and trend estimation, it can be seen how long the action performed on residents evacuation in a radius of 20 km. By drawing time on Fig. 5 required to achieve when the effective dose of evacuation is exceeds 50 mSv for 11 weeks time duration. By using the correlation on equation (5), the obtained evacuation time is 12 weeks.

Figure 6. showed the Thyroid intervention dose (IH) determining to iodine distribution. Distribution of iodine tablets do if acceptance effective dose of public at 50 mSv From Figure 6, distribution of Iodine tablet at distance 20-30 km. Iodine distribution decreases when the distance from NPP increases. Trend linein Fig. 6 is follow the exponential equations:

$$y = 5.737 (x^{-1.81}), \text{ with } R^2= 0.979 \tag{6}$$

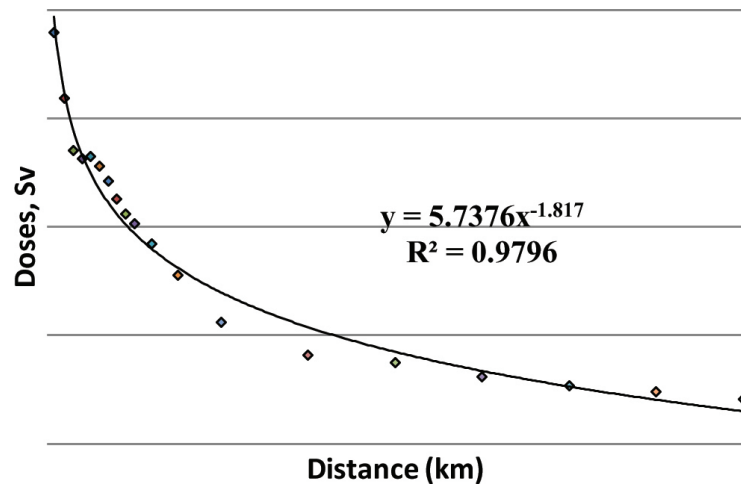


Figure 6: Thyroid intervention dose (IH) for determining Iodine distribution.

Where y = Thyroid intervention dose (IH) for determining Iodine distribution and x = distance. High R-squared value indicates this model can be applied to this data set. (Fig. 6 and eq. (6)).

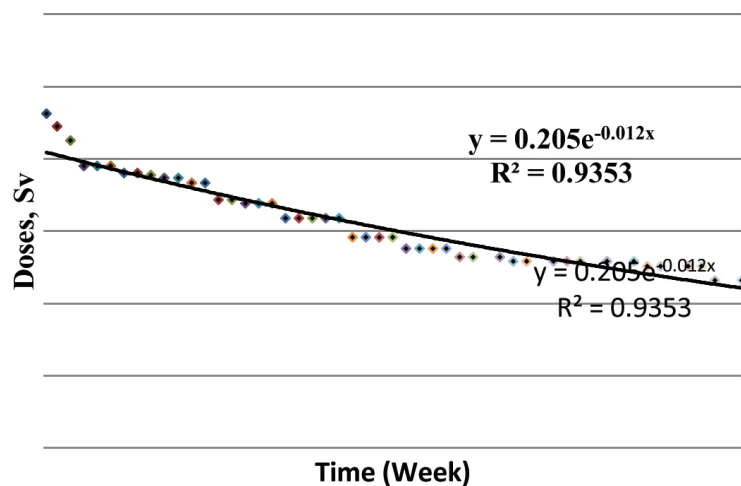


Figure 7: Effective intervention dose with time for relocation at distance 10 km.

Figure 7 explain to relation of effective intervention dose versus time duration for relocation at distance 10 km. Trend line in Fig. 7 is follow the exponential equations:

$$y = 0.205 (e^{-0.01x}), \text{ with } R^2 = 0.935 \tag{7}$$

Where y = effective intervention dose and x = time duration for relocation. By using trend analysis and trend estimation, it can be seen how long the action performed on public relocation in a radius of 10 km. By drawing time required to achieve when the effective dose exceeds 100 mSv, need the extrapolation mode. By using the correlation on equation (7) the obtained relocation time is 2.5 years.

5. Conclusion

The application of trend analysis method for emergency planning on PWR-1000 MWe accident at West Bangka has been resulted those are: iodine tablet are distributed to residents in the

area within radius 20 - 30 km; sheltering countermeasure is within the radius of 20-30 km for 12 weeks; evacuation is subjected for the area 20 km from reactor for evacuation time is 12 weeks; relocating is subjected to radius of 10 km for 2.5 years

Trend analysis can be used help for decision making, especially for the emergency planning, with the advantage in the use of trend analysis method, is faster than previous methods. Uncertainty can be reduced with accurate input data, and the selection of a suitable computation model.

References

- [1] Tanaka S., "Accident at the Fukushima Dai-ichi nuclear power stations of TEPCO outline and lessons learned", *Proc. Japan Acad. Ser. B* 88, pp. 471-473, (2012)
- [2] Nagataki S, Takamura N., Kamiya K. and Akashi M., "Measurements of individual radiation doses in residents living around the Fukushima nuclear power plant", *Radiat. Res.* 180, pp. 439-47, (2013)
- [3] Gilberto Espinosa-Paredes G. E., "Severe Accident Analysis in Nuclear Power Plants", *Science and Technology of Nuclear Installations*, Volume 1, Article ID 430471, pp 1-2, doi:10.1155/2012/430471, (2012)
- [4] Gonzalez A. J., *et al*, "Radiological protection issues arising during and after the Fukushima nuclear reactor accident", *J. Radiol. Prot.* Vol. 33, pp. 497-571, (2013)
- [5] Pande M. U., Kuntjoro S., "Penentuan Zona Kedaruratan Nuklir Off-Site (Luar Tapak) di Indonesia", *Journal of Waste Management Technology*, ISSN 1410-9565, Akreditasi No. 399/AU2/P2MI-LIPI/04/2012, Vol. 7 (2), pp. 58-65, (2014)
- [6] Pande M. U., Kuntjoro S., "PSA Level 3 dan Implementasinya pada Kajian Keselamatan PWR", *J. Tek. Reaktor. Nukl.* Vol. 16 (1), ISSN 1411-240X, No. 402/AU2/P2MI-LIPI/04/2012, pp. 31-43, (2014)
- [7] Puncher, M., "An assessment of the reliability of dose coefficients for intakes of radionuclides by members of the public", *J. Radiol. Prot.*, Vol. 34, pp. 625-643, doi:10.1088/0952-4746/33/3/573, (2014)
- [8] Preston R. J. et al., "Uncertainties in estimating health risks associated with exposure to ionising radiation", *J. Radiol. Prot.*, Vol. 33. pp. 573-588, doi:10.1088/0952-4746/33/3/573, (2013)
- [9] Boice J. D., "Uncertainties in studies of low statistical power ", *J. Radiol. Prot.* Vol 30, pp 115-20, doi:10.1088/0952-4746/33/3/573, (2010)
- [10] Shumway R. H., Stoffer, *Time Series Analysis and its Applications*, Springer Springer, ISBNo-387-00857-8, (2011)
- [11] ICRP-103, "Recommendation of the ICRP", *ICRP-103-ICRP Publication*, (2007),
- [12] Shaw P., and Croüail, P., "ALARA in Existing Exposure Situations", *J. Radiol. Prot.*, Vol. 33, pp. 487-490, doi:10.1088/0952-4746/33/3/573, (2013)
- [13] ICRP-63, *Principle for Intervention for protection of the public in a Radiological Emergency*, *ICRP-63-ICRP Publication*, (1992).

Conference Paper

Evaluation of Radionuclides Release Estimation of Power Reactor using Scdap/Relap

Jupiter Sitorus Pane, Surip Widodo

Center for Nuclear Reactor Technology and Safety, National Nuclear Energy Agency of Indonesia (BATAN), Puspptek Area Building No. 80, Serpong, Tangerang Selatan 15310, Indonesia

Abstract


Incident of radiation release to the environment is important event in reactor safety analysis. Numerous studies have been conducted using various computer codes, including SCDAP/RELAP, to calculate radionuclide releases into the reactor coolant during severe accident. This paper contains description of calculation results of radionuclide release from reactor core to primary coolant system in a 1000 MW PWR reactor with the aim to study behavior of radionuclide releases during severe accident. The calculations using SCDAP/RELAP was done by assuming that there has been a station black out which ends up with some vapor released into the containment. As a result, the water level in core was reduced up to a level where the core is no longer covered by water. The uncovered core heats up to certain temperature where the oxidation of the cladding started to occur. Afterwards the oxidation generated heat made fuel melting temperature reached and as consequences the release of radionuclide to the primary coolant. The calculations show that in parallel with the increasing of fuel temperature, the radio nuclide releases into the gap through diffusion started at time of 2000 seconds after initial simulation but with a neglected concentration. Subsequently at the time of 29200 seconds, the temperature reached more than 1000 K and the oxidation of the Zr-cladding material occurred which accelerated the fuel temperature increase and as well as radionuclide release. At 34000 seconds, maximum temperature of core reached 2800 K and radionuclide release into the primary cooling system started. At this time, accumulated dissolve fission product reached amount of 74.5 kg, while the non-condensable radionuclide reached 122 kg. However, these value need to be investigated further.

Keywords: SCDAP/RELAP, radionuclide release, severe accident

Corresponding Author:
Jupiter Sitorus Pane,
Surip Widodo,
email: jupiter_pane@batan.go.id

Received: 29 July 2016
Accepted: 21 August 2016
Published: 21 September 2016

**Publishing services
provided by Knowledge E**

 Jupiter Sitorus Pane,
Surip Widodo. This article is
distributed under the terms
of the [Creative Commons
Attribution License](#), which
permits unrestricted use
and redistribution provided
that the original author
and source are credited.

Selection and Peer-review
under the responsibility of
the ICoNETS Conference
Committee.

 OPEN ACCESS

1. Introduction

Radionuclide release of fission products into the environment is an important event for estimating the magnitude of impact from construction of nuclear installation at a particular site. This analysis is part of the Safety Analysis Report preparation. The amount of releases of radionuclide into the environment is determined by the quantity of inventory, releases of radionuclide into primary coolant system and confinement. SCADAP/RELAP developed by INEEL provides calculation method to estimate such release into primary system during severe accident [1,2,3,4].

Generally, an estimation of radionuclide releases is performed using removable fraction of radionuclide released to containment as described in NUREG 1465 [5,6]. A simple method of source term calculation has also been studied in order to obtain the relationship of radionuclide releases fraction to the temperature of the primary cooling system due to the heat up by residual heat and oxidation of the cladding material Zirconium (Zr) [7,8]. By using the code of SCDAP/RELAP one can study the mechanism of accident starting from reactor shutdown due to outage of electricity supply (Station Blackout), the increase of coolant and fuel temperature, cladding oxidation as well as heat up acceleration until the melting of fuel. As a consequences, the release of radionuclide into the gap between fuel matrix and cladding and to coolant occurred. The output of the code include fuel fission product inventory, fuel rod gap inventory, release of non-condensable gas to coolant, release of soluble fission product to coolant and fission product transport [9].

In this paper the author would like to describe the results of calculation of radionuclide releases to primary cooling system using SCADAP/RELAP code with the aim to investigate the behavior of radionuclide releases during severe accident conditions and to evaluate the capacity of SCDAP/RELAP in doing such calculation. As a case study, the author uses 1000 MW Surry PWR as the Power Reactor model.

The evaluation of radionuclide release was done by assuming that there was a station blackout at the PWR Surry and the reactor was immediately shutdown and all active safety systems failed to operate. Due to residual heat in the core, the temperature of primary coolant increased as well as its pressure. The power operated relief valve (PORV) in the Pressurizer (PZR) was set for nominal operation at 2335 psig and at 2385 psig for high pressure trip and at 2485 psig for safety valve [10]. The fluctuation of the pressure in primary system made the PORV open and close and as a result the steam generated in the primary cooling system released. This led to emptying the Pressurizer Vessel as well as the Core Vessel and called as loss of coolant [11]. This loss of coolant caused the increase of fuel temperature up to its melting point so that radionuclide could release.

An evaluation using SCDAP/RELAP to estimate inventory fission product and releases of radionuclide into the gap and primary cooling system has been performed by using an experimental device namely BOIL-OFF and by applying simple nodalization [12]. Indeed, the fuel core was modeled as one component and one node. In this analysis, the suitability of the calculation result using SCDAP/RELAP, by comparing to FASTGRASS or PARAGRASS and ORIGEN II, has been proven. However, study on source term calculation upon RINGHALS 2 PWR using SCDAP/RELAP shows an inconsistent result where calculation of the accumulated long term non-condensable radionuclide release to the coolant have huge different compared to the transport routine [13]. Therefore, in addition to evaluate the radionuclide release behavior, this study also identifies the capability of SCDAP/RELAP code in estimating radionuclide release to the coolant.

2. Theory

Accident Mechanism

In the event of Station Blackout i.e. outside power supply outages totally, the entire reactor safety function does not work completely. Although the reactor in a shutdown state as a result of reactor safety protection respond to an accident, the reactor coolant still receives heat from the fuel heat residual that causes the coolant temperature rise even reaching the melting point of the fuel if no further action taken to stop the heating. Measures to prevent the continuation

of the incidents to a more severe level referred to as the act of managing accidents or also called accident management. The increase in temperature and pressure in the primary coolant can cause the increase of pressure in PORV valve that can activate PORV valve to open. In contrast, the opening of the PORV valve causes the decrease of primary pressure up to a certain pressure limit that brings PORV back to close. These conditions, opening and closing the valve, caused the decreasing of coolant in the vessel and eventually can cause the fuel become uncovered. This condition triggers the increasing of heating up of the primary system even reaching the temperatures above 1000 K, which causes oxidation of the cladding material Zirconium (Zr). This oxidation will produce hydrogen and heat. An accumulation of residual heat and additional oxidation heat will accelerate the fuel temperature increases even it could reach the melting point of the fuel. In a solid material like fuel and cladding, the higher the temperature the faster the diffusion occurs.

Diffusion of Fission Products

In general, the fission products created in the fuel element matrix diffused in the fuel matrix through diffusion model. Especially for Xenon, Krypton, Cesium, Iodine and Tellurium the mathematical model was shown in a diffusion equation as follows [14].

$$\frac{\partial C_g}{\partial t} = \frac{1}{r^2} \frac{\partial}{\partial r} \left(D_g r \frac{\partial C_g}{\partial r} + K_g \right) \frac{\partial C_g}{\partial t} = \frac{1}{r^2} \frac{\partial}{\partial r} \left(D_g r \frac{\partial C_g}{\partial r} + K_g \right) \quad (1)$$

With,

C_g = concentration of fission product gases (fission / m³)

D_g = diffusion coefficient of atoms

K_g = atom production rate

r = radius of the fuel (m)

For less volatile fission products, the radionuclide release is modeled using CORSOR-M model. In this model the assumed rate of release at the spots for each species is formulated as [15]:

$$FP = FFP_0 \cdot (1 - e^{-FRC \cdot (TIME)}) \quad (2)$$

with,

FP = mass of the species present on the stain at the beginning of time step (Kg)

FRC = coefficient release rate

FRC value calculated by the Arrhenius equation:

$$FRC = KO(l) \cdot e^{\left(\frac{-Q}{1.502 \cdot 10^{-3} T} \right)} \quad (3)$$

with,

$KO(l)$ and $Q(l)$ = constant release of the species with the values in Tabel 1 [15].

Transfer of Radionuclide of Fission Products to the Fuel and Cladding Gap

Diffusion of fission products move towards the edge of the fuel and gap. Rate and magnitude of movement is strongly influenced by temperature, oxidation, interaction with components of the cladding and the structure of burn-up, fuel type and morphology. Fission product gases released from the fuel is assumed to reach the surface of the fuel with migration successively

from the surface of the particle (grain face) to the particle surface and ends at the edge of the particle. This model can be applied to gases derived from fission, bubble nucleation and resolution, migration of bubbles, bubble coalescence, gas bubbles and the formation of the channel on the surface of the particle (grain face), interlinked porosity on grain edges, grain boundary micro cracking and grain growth and grain boundary sweeping.

TABLE 1: Value KO(I) and Q(I).

Species	KO(min ⁻¹)	Q(kcal/mol)
UO ₂	1,46E7	143,1
Zr	2,67E8	188,2
Sn(clad)	5,95E3	70,8
Fe	2,94E4	87
Ru	1,62 E6	152,8
Zr(clad)	8,55E4	139,5
Ba	2,95E5	100,2
Sr	4,40 E5	117,0
Te	2,00E5	63,8
Ag	7,90E3	61,4
Cs*	2,00E5	63,8
I*	2,00E5	63,9

3. Methodology

The study begins with developing nodalization of core and primary system of 1,000 MW PWR reactor Surry, develop programs and inputs in accordance with the conditions and parameters of the reactor, analyze and evaluate the results of the calculation of the maximum temperature of the core and the estimated fission products in accordance with the development of the maximum temperature of the core. Table 2 shows the relevant data in the simulation calculations of Surry PWR radionuclide releases.

TABLE 2: Data Related to Surry PWR in Simulation SBO.

Parameters	Value
Power (MW)	2443
Pressure (MPa)	14,7
Operation Temperature (K)	500
Fuel element configuration	157 (15 x 15)
Active fuel element height (m)	3,66
Accumulated borated water mass (kg)	29100 (at T = 322 K)
Accumulator initial pressure (MPa)	4,24
Fuel rod number	240
Fuel pellet stack length (m)	3,6576
<i>Control rod</i>	21
Fuel pellet stack (m)	4.634
<i>Inconel spacer grid location</i>	0,0; 1,46; 1.83; 2,19; 2,93

Since the object of this study is similar to previous studies [11, 12] then nodalization, parameters value and the program calculation is also the same but with different subject. The previous studies dealt with performance of the primary system evaluation of Surry PWR but now dealt with radionuclide releases of fission product.

Nodalization of core was figure out by dividing the fuel into 5 components named component number 1, 3, 5, 7 and 9 and controls into 5 component named component number 2, 4, 6, 8, 10. Each component is divided into 10 nodes. Component 1, 3, 5, 7 and 9, each consist of 1020, 4080, 7344, 12240, 7334 rod. For the simulation, it is assumed that there has been failure on PORV valve during station black out accident. The system shutdown 100 seconds after the accident that make power decrease until 10% power.

4. Results and Discussion

The Increase in Fuel Temperature

In this simulation, the station black out accident assumed to be occurred. The reactor was shut down at 100 second after the accident so that the power reduced up to 10% from the full power. This residual heat could be accumulated reaching a very high fuel temperature if no additional cooling system operated. Figure 1 shows the increase in the maximum fuel temperature in the reactor core.

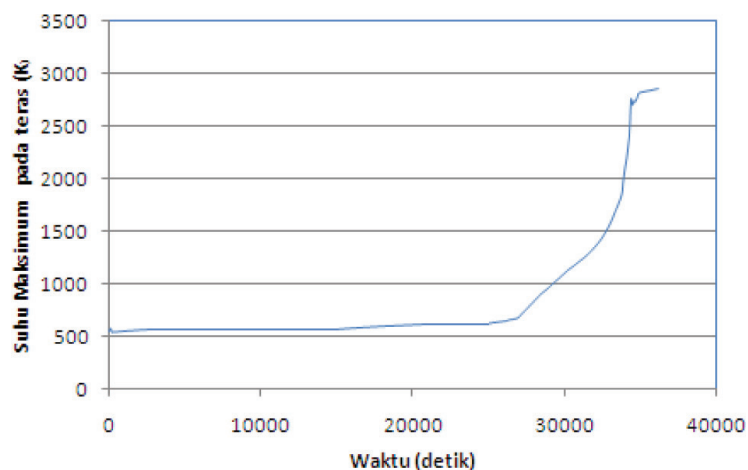


Figure 1: The maximum temperature rise of 1,000 MW reactor core.

The increase of temperature became significant starting from a few seconds to the 27200 second where the core became uncovered by the cooling and the fuel temperature reached 722 K. In parallel with the declining water levels in the core, the fuel temperature continues to rise until it reaches the temperatures above 1000 K in the second of 29200. At this temperature, Zr fuel cladding oxidation started to occur.

The Mechanism of Oxidation of the Cladding

Oxidation between vapor and Zr cladding material at temperature of 1000 K would generate heat and hydrogen gas as shown in Figure 2 and Figure 3. In these both pictures, the amount of hydrogen and heat rise due to oxidation events. The heat generated by this oxidation is accelerating fuel temperature where at the second of 34400 the fuel temperature reaches 2768 K. At this point, the heat coming from the oxidation begins to decline but still give heat

accumulation and the maximum temperature of the fuel keep rising to 2868 K. With this temperature the fuel reach its melting point. At this temperature SCDAP /RELAP can no longer continue the calculation.

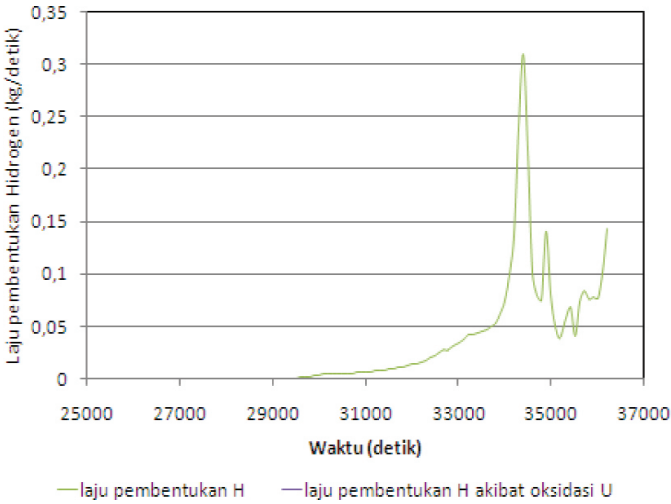


Figure 2: The rate of hydrogen formation during oxidation.

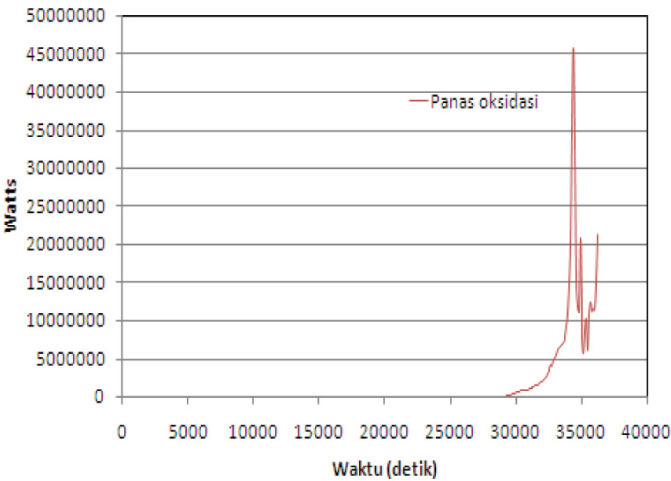


Figure 3: The heat generated during the production of Hydrogen.

Inventory of Fission Products

The fission products were formed during the fission process. Number of fission products is strongly determined by its previous reactor operating history. The code of SCDAP/RELAP provide the inventory of the core based on its operating history. Table 3 shows the fission product inventory at the nodes and components 1, 3, 5, 7 and 9 of PWR 1000 MW fuel core in the form of gas (Xe, Kr) and volatile (Cs, I, Te) with a history of being operated with a power density 3.6138e8 W / m3 within 5.9205E+7 seconds.

Release of Radionuclide and Core Damage

The inventory generated in the fuel matrix diffused with the increase of fuel temperature. From the simulation results it was detected that the diffusion output is visible from the second of 2000 with a very small of amount, for example at component 1 the diffusion of radionuclide

to the gap was about $1.79 \text{ E-}18 \text{ kg}$ and therefore it cannot be detected. This number will always be the same until it reached the seconds of 32000 in where the temperature reached the value of 1356 K. Indeed, the number of radionuclide in gap approaching $3.1 \text{ E-}09 \text{ Kg}$.

TABLE 3: Inventory of gas and volatile fission products.

Node	Xe (kg)	Kr (kg)	Cs (kg)	I (kg)	Te (kg)
1	5.9450E-04	6.6958E-05	3.4416E-04	2.3987E-05	5.5231E-05
2	8.1511E-04	9.1805E-05	4.7187E-04	3.2888E-05	7.5727E-05
3	1.0731E-03	1.2086E-04	6.2123E-04	4.3298E-05	9.9695E-05
4	1.0651E-03	1.1996E-04	6.1660E-04	4.2975E-05	9.8953E-05
5	1.0348E-03	1.1655E-04	5.9905E-04	4.1751E-05	9.6135E-05
6	1.0186E-03	1.1472E-04	5.8965E-04	4.1097E-05	9.4628E-05
7	1.0140E-03	1.1421E-04	5.8702E-04	4.0913E-05	9.4205E-05
8	1.0116E-03	1.1393E-04	5.8561E-04	4.0815E-05	9.3980E-05
9	9.8024E-04	1.1040E-04	5.6747E-04	3.9551E-05	9.1068E-05
10	7.9064E-04	8.9049E-05	4.5771E-04	3.1901E-05	7.3453E-05

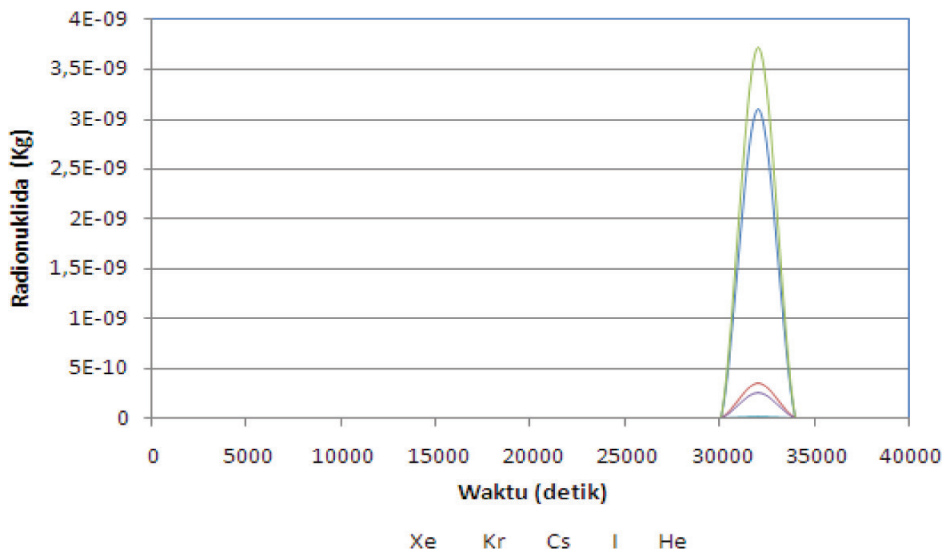


Figure 4: Removable radionuclide into fuel and cladding gap in component 1.

By increasing the temperature up to 2112 K in the second of 34000 then radionuclide not just stay in the gap but also escape to the coolant. In the second of 36200 in where temperatures reaching 2868 K, radionuclide material that reached gap will entirely migrate to cooling system with Xe and Kr are around 122 kg and CsI and CsOH of 74.5 Kg. In these conditions most of the cladding material has melted [16]. In the chart, the release of radionuclide to the cooling can be described as in Figure 5. However these numbers are out of the expected number where the values are much more than the total inventory product in gap. This condition was also identified in during performing source term calculation for RINGHALS 2 PWR [13]. This fact needs to be studied further. It is hypothesized that the problem arise due to the accumulated error of calculation, not because of the model. The longer the time, the bigger the deviations.

Nevertheless, from this analysis, it can be summarized that releases of radionuclide to the cooling depend on the size of the initial inventory from the beginning of reactor operation, type of accident, time and temperature since the accident occurred. The release of radionuclide can be stopped when the reactor can be controlled before the temperature reaches the melting temperature of the fuel cladding by equipping reactor with its protection system. Therefore, this computer code is very useful for accident managements analysis.

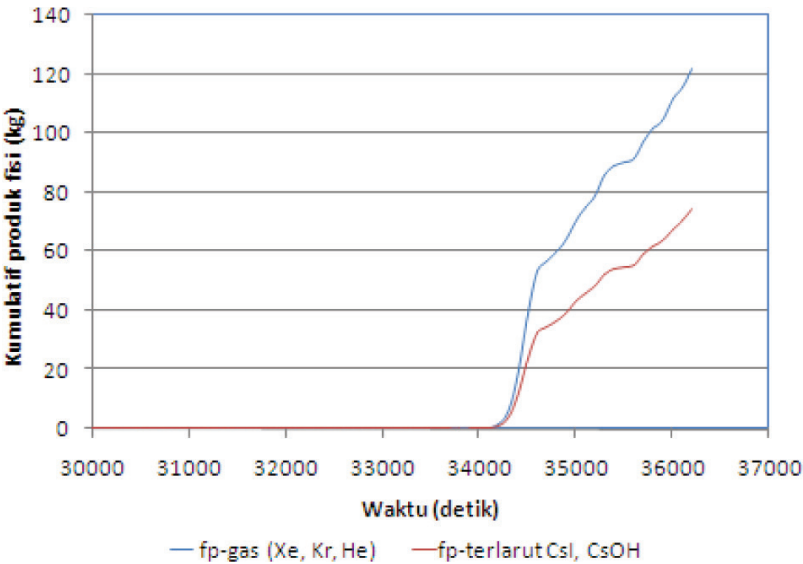


Figure 5: Radionuclide release to the primary coolant of 1000 MW reactor.

5. Conclusion

The behavior of radionuclide release of 1000 MW during severe accident highly depend on initial inventory of the core and heat up process during the period of accident. The radionuclide releases into the gap and proceed into the primary cooling system begins when the temperature has reached above 1356 K i.e. after the oxidation of Zr cladding material and hydrogen production occurred. The increase of radionuclide was rocketed when most of the cladding material melts. This release phenomenon can be used as a reference in designing a reactor accident management system of 1000 MW to mitigate releases of radionuclide into the coolant.

Further study to develop SCDAP/RELAP code capability need to be performed since the calculation result of radionuclide release to the primary cooling system of non condensable species are not as expected. It is hypothesized that the problem arise due to the accumulated error of calculation, not because of the model.

References

- [1] MEHBOOB, K., XINRONG, C., Source Term Evaluation Of Two Loop PWR Under Hypothetical Severe Accidents” *Annals of Nuclear Energy*, Volume 50, December 2012, *Pages 271-284*
- [2] KIM, S. G., GYUNO, Y, and SEONG, P. H., Prediction Of Severe Accident Occurrence Time Using Support Vector Machines, *Science Direct, Journal Elsevier, Nuclear Engineering and Technology*, 2015.

- [3] HASTE T. J., BIRCHLEY J., RICHNER M., Accident Management Following Loss-Of-Coolant Accidents During Cooldown In A Westinghouse Two-Loop PWR, *Nuclear Engineering and Design*, Volume 240, 2010, Pages 1599-1605
- [4] Urbonavičius E., Kaliatka A., Vileiniškis V. Integral analysis of large LOCA beyond design basis accident scenario in RBMK-1500, *Nuclear Engineering and Design*, Volume 240, Issue 3, March 2010, Pages 616-629
- [5] SOFFER L., BUSRON S. B., FERREL C. M., LEE R. Y., Accident Source Terms for Light-Water Nuclear Power Plants, U. S. Nuclear Regulatory Commission, NUREG 1465, Washington, DC, 1995.
- [6] Mehboob, K., Xinrong, C., Source term evaluation of two loop PWR under hypothetical severe accidents, *Annals of Nuclear Energy*, Volume 50, December 2012, Pages 271-284
- [7] Shi X, Cao, X, Liu, Z., Oxidation behavior analysis of cladding during severe accidents with combined codes for Qinshan Phase II Nuclear Power Plant, *Annals of Nuclear Energy*, Volume 58, August 2013, Pages 246-254
- [8] Wang J., Tian, W, Fan, Y., Mao, K., Lu, J., Su, G., Qiu, S., The development of a zirconium oxidation calculating program module for Module In-vessel Degraded Analysis Code MIDAC, *Progress in Nuclear Energy*, Volume 73, May 2014, Pages 162-171
- [9] SCDAP/RELAP5-3D Code Developer Team, SCDAP/RELAP5-3D Code Manual, Assessment of Modelling of Reactor Core Behaviour During Severe Accidents, INEEL/EXT-02-00589, Revision 2-2, 2003.
- [10] VEPCO, Surry Power Station Unit 1 and 2, Technical Specification, DOCKET NOS. 50-280 AND 50-281, Virginia, USA, 1991,
- [11] PANE J. S. An Evaluation of Primary System of PWR Reactor during Station Blackout Accident Using SCDAP/RELAP (Evaluasi Kinerja Sistem Primer Reaktor PWR Pada Kejadian *Station Black Out* Menggunakan Relap/Scdap), Prosiding Seminar SENTEN, Kalimantan Barat, 2014
- [12] PANE J. S., Pemodelan Dan Simulasi Lepas Radionuklida Pada Perangkat Percobaan *Boil-Off* Dengan Scdap/Relap, dipresentasikan pada Seminar Nasional Teknologi Energi Nuklir 2014, 2014.
- [13] JOHANSSON, LL, Source Term Calculation-Ringhals 2 PWR, Studsvik Eco & Safety AP Nykoping, Sweden, 1998.
- [14] HIDAKA, A., SODA, K., SUGIMOTO, J., " SCDAP/RELAP5 Analysis of Station Blackout with Pump Seal LOCA in Surry Plant, *Journal of Nuclear Science and Technology*, 2012.
- [15] BERA, B., KUMAR, M., THANGAMANI, I., PRASAD, H., SRIVASTAVA, A., MAJUMDAR, P., DUTTA, A., VERMA V., GANJU S., CHATTERJEE B., LELE H.G., RAO, V.V.S.S.. GHOSH, A.K. "Estimation of source term and related consequences for some postulated severe accident scenarios of Indian PHWR" *Nuclear Engineering and Design*, An International Journal devoted to all aspect of Nuclear Fission Energy, Elsevier, 2010.
- [16] Park, R.J., KANG, K.H., Hong, S.W. Hong, Kim HY, Detailed Evaluation of Melt Pool Configuration In The Lower Plenum Of The APR1400 Reactor Vessel During Severe Accidents, *Annals of Nuclear Energy*, Volume 75, January 2015, Pages 476-482

Conference Paper

Application of ^{99m}Tc Radioisotope in Diagnostic Procedures and Internal Radiation Dose Estimation

Nur Rahmah Hidayati¹, Basuki Hidayat²¹Center for Radiation Safety Technology and Metrology, Jl. Lebak Bulus Raya No. 49, Jakarta 12070, Indonesia²Dept. of Nuclear Medicine and molecular Imaging, School of Medicine Universitas Padjadjaran/ Dr. Hasan Sadikin General Hospital, Jl. Pasir Kaliki 162 Bandung 40161, Indonesia

Abstract


At about 70% of nuclear medicine procedures have utilized ^{99m}Tc in their clinical practices. This has lead ^{99m}Tc becoming the most convenient radioisotope in nuclear medicine diagnostic. To estimate the internal radiation dose due to the administration of ^{99m}Tc to the patients, only few documents from International Commission of Radiation Protection (ICRP) have been available. However, the calculation usually has applied Caucasian data in Standard Reference Man as a model. The objective of this study was to review the application of ^{99m}Tc in Indonesia and to compare the internal dose estimation for ^{99m}Tc procedures by using Organ Level Internal Dose Assessment/Exponential Modeling (OLINDA/EXM) software. The result of calculation was compared between Adult Caucasian model and Asian Reference Man. The result shows that ^{99m}Tc has been well applied and developed for diagnostic procedures in Nuclear Medicine Department. Moreover, in most diagnostic procedures using ^{99m}Tc in Indonesia, adult patients will receive effective dose about 1-15% higher than adult patient in foreign countries which apply the Caucasian model. Hence, to estimate the similar stochastic risk from the same procedure, the maximum value in recommended administered dose should be avoided and need to be evaluated.

Keywords: ^{99m}Tc radioisotope, diagnostic procedures, internal radiation dose, OLINDA/EXM

Corresponding Author:
Nur Rahmah Hidayati,
email: inn98@batan.go.id

Received: 29 July 2016
Accepted: 21 August 2016
Published: 21 September 2016

**Publishing services
provided by Knowledge E**

 Nur Rahmah Hidayati,
et al. This article is
distributed under the terms
of the [Creative Commons
Attribution License](#), which
permits unrestricted use
and redistribution provided
that the original author
and source are credited.

Selection and Peer-review
under the responsibility of
the ICoNETS Conference
Committee.

 OPEN ACCESS

1. Introduction

^{99m}Tc has become the most convenient radioisotope for diagnostic procedures in nuclear medicine. It has been reported that approximately 70% nuclear medicine procedures have utilized ^{99m}Tc in their clinical practices using either gamma camera or single photon emission computed tomography (SPECT). Despite the emerging nuclear medicine equipment such as Photon Emission Tomography (PET) has lead the application of molecular imaging agents, the application of ^{99m}Tc seems still to be preferred choice due to the ease of supply process [1].

The application of ^{99m}Tc radioisotopes in the world have been supplied from available methods, such as uranium fission in the research reactors using both high enriched uranium (HEU) and low enriched uranium (LEU) targets, neutron activation of ^{98}Mo in a nuclear reactor, and ^{99m}Tc production with cyclotrons. From these available options, the ^{99m}Tc production

based on uranium fission using HEU target is the favorable option regarding to consideration of several factors: the maturity of technology, production yield, available irradiation capacity, commercial compatibility, estimated unit cost, ease of nuclear regulatory approval, ease of health regulatory, and units required to supply world market [2].

With regard to its chemistry characteristic, ^{99m}Tc has major advantages for nuclear medicine procedures [3], since it has multiple oxidation states which make it is possible to be used in either single compound of ^{99m}Tc (pertechnetate), or with a labeling compound, such as ^{99m}Tc -methylene diphosphonate (MDP) for bone studies and ^{99m}Tc -Diethyl Triamine Penta-Acetic (DTPA) for renal studies. Moreover, other applications of ^{99m}Tc have been expanded into next generation of ^{99m}Tc labeling process, due to the development of research in imaging agents for cardiovascular and brain studies, such as ^{99m}Tc Tetrofosmin and ^{99m}Tc Hexamethylpropyleneamine Oxime (HMPAO), respectively [4].

Since the administration of radiopharmaceutical in those procedures will lead the patients to receive internal radiation dose, internal dosimetry should be assessed either from calculation or reference documents published by International Atomic Energy Agency (IAEA), International Commission of Radiation Protection (ICRP) and/or national regulatory authorities [5]. For example, ICRP publications no. 53, 80, and 106 provides internal dosimetry assessment for patient due to radiopharmaceutical administration in human body [6-8]. However, those documents have referred Caucasian anatomical data for the reference model.

In general, the objective of this study is to investigate the application of ^{99m}Tc in Nuclear Medicine diagnostic procedure in Indonesia, and performing internal dose estimation from related procedures. The internal dose estimation will be performed based on the calculation using OLINDA/EXM, a software from Vanderbilt University for internal dosimetry calculation in nuclear medicine. The calculation in this study will adopt the organ weight of Asian Reference Man (ARM), to be compared with Standard Reference Man in OLINDA/EXM. The result of calculation will be utilized as a tool to compare the effective dose for adult male and female of both models. It will show when the same radiopharmaceutical will be administered, how Asian model will differ from Caucasian model in terms of internal dose estimation. This study will also verify an initial assumption that, with the similar administered dose for the same radiopharmaceuticals, Asian Group will receive higher internal radiation dose because the weight of Asian Reference Model is lower than the Standard Reference Model in ICRP.

2. Theory

^{99m}Tc has been produced in a nuclear reactor as a fission product by irradiating enriched U-235. The product needs to be processed to purify ^{99}Mo from other impurities. The ^{99}Mo isotopes which are in aqueous phase, then being adsorbed into alumina (Al_2O_3) column which is contained in a radiation-shielded equipment (Fig. 1), known as technetium generators. In the generator, ^{99m}Tc is eluted by a sterile saline solution (NaCl) to recover ^{99m}Tc [9]. The elution will generate $^{99m}\text{TcO}_4$ (pertechnetate) in saline solution. The ^{99m}Tc is ready to be used either as pure pertechnetate or combined with any others labeling compounds. A typical ^{99m}Tc generator produced by Australian National Science and Technology Organisation (ANSTO) is displayed in Fig. 1. The generator can be used several times in a week by re-passing saline solution into ^{99}Mo column until the activity of eluted ^{99m}Tc is very low and unable to be applied for any diagnostic procedure. The schematic of the generator is displayed in Fig. 2.



Figure 1: Gentech, a typical of ^{99m}Tc generator produced by ANSTO.

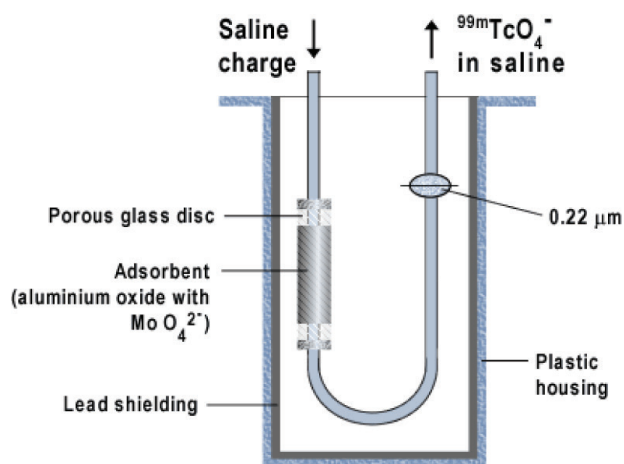


Figure 2: Schematic diagram of ^{99m}Tc generator [10].

^{99m}Tc Application for Diagnostic Procedures

^{99m}Tc application for diagnostic procedures is well known in worldwide, started from thyroid scintigrafi, perfusion studies, bone scan, and other diagnostic applications, due to its short half live, low energy, and economic consideration [11]. A report of application ^{99m}Tc in the United Stated has acknowledged that the application of nuclear medicine diagnostic in the US has increased approximately 6 million per year since early 1980 until about 20 millions in 2005. The increasing has been believed that it was due to to the application of ^{99m}Tc based agents which have replaced the use of ²⁰¹Tl in cardiac procedures from 1 % in 1973 to 57% in 2005 [12].

With regard to radiation safety practices, the administered dose of radiopharmaceutical in diagnostic procedures, ICRP has published the report regarding the administered dose to patients in ICRP Publication No. 17, then continued in 1987 by releasing the Publication No. 53: Radiation Dose to Patients from Radiopharmaceuticals, by contributing 120 radiopharmaceuticals, and the use of 71 radionuclides in 34 elements. Furthermore, with the increasing the number of new radiopharmaceuticals, the publication has been revised few times until third addendum in 2008 in Publication No.106 [8].

In 2002, IAEA has published Radiological Protection for Medical Exposure to Ionizing Radiation [5] and Nuclear Medicine Resources Manual [13], in which the administered dose of radiopharmaceuticals in diagnostic procedures have been recommended to optimize radiation protection to the patients. The first document [5] has listed the value of maximum dose to be administered to the patients in Nuclear Medicine Departments. Furthermore, the values have been adopted locally by National Nuclear Regulatory Agency (BAPETEN) into the Decree of BAPETEN head No. 17 year 2012, regarding Radiation Safety Guide in Nuclear Medicine Department in Indonesia [14]. Table 1 has presented the application ^{99m}Tc for diagnostic procedures and the standard activities of ^{99m}Tc radiopharmaceuticals [13].

Calculation of Internal Dosimetry Assessment

In previous paper, a basic concept of internal dosimetry estimation has presented a method from Medical Internal Radiation Dosimetry (MIRD) committee, which has been well applied in nuclear medicine communities [15]. Since the internal dosimetry assessment in diagnostic procedure may provide stochastic risk estimation, the assessment should be quantified to

TABLE 1: The list of ^{99m}Tc procedure and its standard activity [13].

Radiopharmaceutical	Study	Standard Activity (MBq)
^{99m}Tc -pertechnetate	Thyroid scintigraphy	80 - 200
^{99m}Tc - diethylene triamine penta acetic acid (DTPA)	Glomerular Filtration Rate	200
	Liquor Cerebro Spinalis system	185 - 370
	Gatric emptying time (liquid)	18-37
	Esophageal Reflux	37 - 74
	Esophageal Transit Time	37 - 74
	Vesico urethral Reflux	200
^{99m}Tc - 2-methoxyisobutyl isonitrile (MIBI)	Myocardial Perfusion Scintigraphy	1000 - 1110
	Tumor Imaging	555 - 740
^{99m}Tc - tetrofosmin	Myocardial Perfusion Scintigraphy	1000 - 1110
	Tumor Imaging	555 - 740
^{99m}Tc - Methylene diphosphonate (MDP)	Bone Scintigraphy	740 - 1110
^{99m}Tc – Red Blood Cell (RBC)	Ventriculography	555 - 1100
	Gastrointestinal Bleeding	370 - 1110
^{99m}Tc - macroaggregated albumin (MAA)	Pulmonary Perfusion Imaging	40 - 150
^{99m}Tc - diethylene triamine penta acetic acid (DTPA-aerosol)	Pulmonary Ventilation Imaging	900 - 1300
^{99m}Tc - nanocolloid	Lymphoscintigraphy	15 - 35
	Sentinel Node Imaging	15 - 35
^{99m}Tc - mercapto acetyl tri glycine (MAG ₃)	Renal Excretion	100
^{99m}Tc - Sulfur colloid	Gastric Emptying Time (solid)	7,4 - 14,8
	Liver scintigraphy	110 - 220
^{99m}Tc -2,6-dimethyl phenyl carbamoyl methyl) - iminodi acetic acid (HIDA)	Biliary Tract Imaging	50 - 200

estimate the effective dose for the patients [16]. Moreover, a calculation of effective dose can be done by applying a voxel based model dosimetry in computer codes, such as MIRDOSE and OLINDA/EXM. Both MIRDOSE and OLINDA/EXM have applied the organ mass in Standard Reference Man, which is adopted from Caucasian Model. Unfortunately, the distribution of MIRDOSE₃ has been withdrawn and has been being replaced by The OLINDA/EXM, since it provides more radioisotope data, modification of the organ mass, and the fitting of kinetic data [17]. The software has been approved by the Federal and Drug Administration of the USA, for internal dosimetry calculation in nuclear medicine. Since OLINDA/EXM provides a menu for organ mass modification, hence it can be used to calculate another reference model. In this study Asian Reference model has been adopted by referring the organ mass in Asian Reference Man [19].

3. Materials and Method

To calculate internal dose of ^{99m}Tc in diagnostic procedures using OLINDA/EXM, it needs the kinetic data from Technetium and the labeled compounds. These data can be found from ICRP publications, such as ICRP 53, 80 and 103 [6-8]. Other input data are the name of nuclide,

chosen body phantoms (adult male, adult female, 15 year-old, 10-year old, 5 year-old, 1-year-old, newborn, 6 month pregnant woman, 6 month pregnant woman, 9 month pregnant woman), and the kinetic data. Figure 3 shows the main menu of OLINDA/EXM.

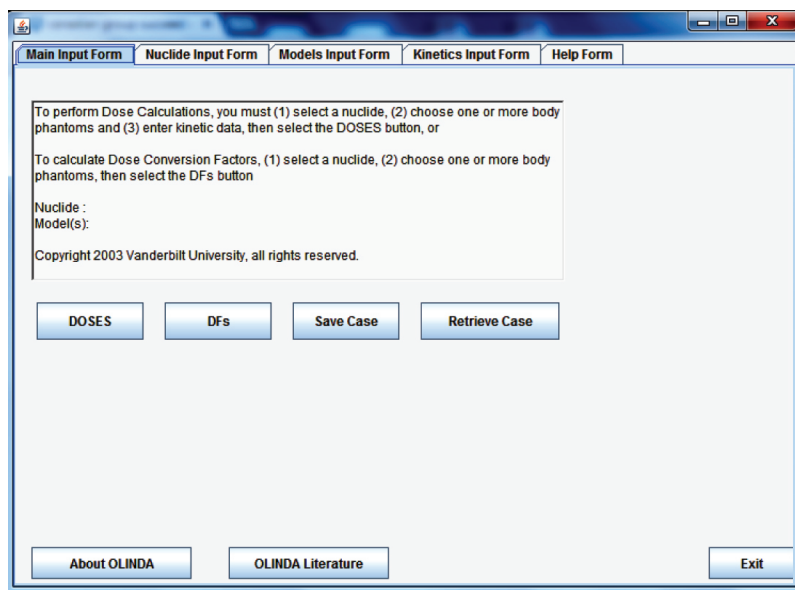


Figure 3: A sample of displayed main menu in OLINDA/EXM [18].

Tc		BIOKINETIC MODELS AND DATA
43		
Phosphonates		Biokinetic Data
	Organ (S)	\bar{A}_g/A_0
(1) Normal uptake and excretion		
	Total body (excluding bladder contents)	4.06 hr
	Bone	3.01 hr
	Kidneys	7.5 min
	Bladder contents	1.15 hr
(2) High bone uptake and/or severely impaired kidney function		
	Total body	8.69 hr
	Bone	5.84 hr

Figure 4: A sample of biokinetic data provided by ICRP [6].

In this work, the organs were selected depending on the referred organs on the kinetic data from each procedure. For example in bone scan procedure using ^{99m}Tc-MDP, the kinetic data which are available are bone, kidney, bladder and total body (Fig. 4). After the dose calculation has been done for Caucasian models [19], the effective dose due to the administration of radioisotope in those procedures can be displayed for both male and female. Furthermore, to calculate internal dose for Asian group, few organ masses need to be adopted from Asian Reference Man (ARM) [20], then it will give the effective dose. The difference of organ weight between Standard Reference Man and Asian Reference Man has been displayed on Table 2.

TABLE 2: The list of organ weights in Standard and Asian Reference Man.

ORGAN	Weight: adult male (gr)		Weight: adult female (gr)	
	SRM	ARM	SRFM	ARFM
Adrenals	16.3	14	14	13
Brain	1420	1470	1200	1320
Breasts	25	22	360	300
GB	10.5	8	8	6
LLI	167	150	160	120
SI	677	590	600	450
Stomach	158	140	140	110
ULI	220	180	200	140
Heart	316	380	240	320
Kidneys	299	320	275	280
Liver	1910	1600	1400	1400
Lungs	1000	1200	800	910
Muscle	28000	25000	17000	28000
Muscle	28000	25000	17000	28000
Pancreas	94.3	130	85	110
Red Marrow	1120	1000	1300	780
Osteogenic cells	120	120	90	90
Skin	3010	2400	1790	1800
Spleen	183	140	150	120
Testes	39.1	37	0	0
Thymus	20.9	30	20	29
Bladder	47.6	40	35.9	30
Uterus / Prostate	8	8	80	70
Fetus	0		0	0
Placenta	0		0	0
Total body	73700	60000	56912	51000

4. Result and Discussion

The purpose of this work was to review the application of ^{99m}Tc radiopharmaceutical in nuclear medicine diagnostic procedures in Indonesia, and to evaluate the internal radiation dose for ^{99m}Tc radiopharmaceuticals in related procedures. The evidences have shown that the application of ^{99m}Tc in Nuclear Medicine procedures has grown quickly in accordance with the development of research and production in radiopharmaceuticals, so that ^{99m}Tc becomes the most convenient radioisotope for diagnostic procedures in Nuclear Medicine Department due its simple characteristic to be labeled with other compounds. For example, the application of ^{99m}Tc for cardiac perfusion study, has been extended for early breast cancer detection [20] and it has shown that the early diagnosis of breast cancer using ^{99m}Tc is less painful than using mammography.

In terms of internal dose estimation, the study was intended to evaluate whether adult Standard (Caucasian) or adult Asian will receive the same number of internal radiation when

the similar procedures will be given, by applying internal dose calculation using OLINDA/EXM. As a result, in OLINDA/EXM, effective dose is produced as a unit of mSv/MBq or mSv/mCi. The result can be copied and saved in txt files for later review. This is important since an evaluation is needed to verify that the input of radionuclide, models, kinetic data, and organ weights are correct and producing an accurate result. The summary of calculation in this study has been displayed on Table 3.

From the calculation, in each MBq of ^{99m}Tc administered dose, adult Asian model receive higher effective dose than adult Caucasian model. The number is between 1% and 15% depends on the procedures has been given. This is true because each procedures has different labeled compound which means it has different biokinetic characteristic, source and target organs. Therefore, it will produce different absorbed doses in related organs and finally it will give the different effective doses. For example, in ^{99m}Tc pertechnetate for thyroid study, the effective dose estimation for adult Asian male is about 5% higher than that in adult Caucasian male. Furthermore, in ^{99m}Tc sulfur colloid for Liver scintigraphy, the difference between adult Caucasian male and adult Asian male will be about 15%. In the report of Marine, et al, it has been stated that the change of body size will result the different exposure from the targeted organ as a source and the self-absorption dose from the organ [21].

TABLE 3: The comparison of effective dose calculation for ^{99m}Tc radiopharmaceuticals for adult Asian and adult Caucasian in Standard Reference Man.

Radio-pharmaceutical	Effective Dose (mSv)/MBq					
	SRM	ARM	ARM/ SRM	SRFM	ARFM	ARFM/ SRFM
^{99m}Tc -pertechnetate	0.0087	0.0092	105%	0.0106	0.0119	112%
^{99m}Tc -DTPA	0.0052	0.0055	105%	0.0071	0.0077	109%
^{99m}Tc -MIBI	0.0074	0.0081	110%	0.0090	0.0098	109%
^{99m}Tc -tetrofosmin	0.0089	0.0094	105%	0.0110	0.0118	107%
^{99m}Tc -MDP	0.0060	0.0063	105%	0.0078	0.0089	114%
^{99m}Tc -RBC	0.0004	0.0005	105%	0.0006	0.0006	107%
^{99m}Tc -MAA	0.0108	0.0113	105%	0.0169	0.0184	109%
^{99m}Tc -DTPA (aerosol)	0.0060	0.0064	106%	0.0080	0.0081	101%
^{99m}Tc -nanocolloid	0.0091	0.0102	112%	0.0096	0.0103	107%
^{99m}Tc -MAG ₃	0.0132	0.0141	107%	0.0175	0.0193	110%
^{99m}Tc -Sulfur colloid	0.0045	0.0051	115%	0.0052	0.0054	102%
^{99m}Tc -HIDA	0.0150	0.0155	103%	0.0180	0.0194	108%

SRM : Standard Reference Man-Male, ARM : Asian Reference Man-Male,
 SRFM : Standard Reference Man-Female, ARFM : Asian Reference Man-Female

A similar study of internal dose estimation for diagnostic radiopharmaceuticals such as ^{18}F -FDG, ^{123}I -ioflupane and ^{99m}Tc -tetrofosmin has been performed to investigate the difference of internal dose across Asian model [22]. The study has presented the variation organ size within adult Chinese, Indian, Caucasian and the Caucasian female, and it has been stated that the effective dose of Caucasian female group is almost similar to the male patient in Asian group.

The finding of study has also showed that, if the administered dose for the patients has been by referring the value of administered dose from IAEA which has been adopted by BAPETEN, it will give higher effective dose to the patients in Indonesia, which means it will increase the stochastic risk. Hence, it would be better if the maximum administered dose in the Decree of BAPETEN Head No.17 year 2012 need to be either avoided or be reduced until at least, less than 15% of maximum dose to reduce the probability of stochastic risk for the patients in Nuclear Medicine Department in Indonesia.

For the future study, it would be better if the organ weight in Asian Reference Man in this study will be replaced by organ weight from of Indonesian. Then the result of study will be directly applied as Indonesian model. However, at the moment, it is hard to find the standard of anatomical data for Indonesian, since the Indonesian Reference Man has not been established yet. There was a report of anatomical data for Indonesian under IAEA project coordination, but it was not enough to represent the population [19]. Hence, temporarily, the result of this study might be useful for estimating the internal radiation dose for particular procedures in nuclear medicine despite it uses Asian Reference Man. The internal dose estimation for patients who undergo nuclear medicine diagnostic procedures will be more important when a patient also receive more radiation dose from other diagnostic modalities such as CT scan and fluoroscopy, which might add the effective dose to the patients.

5. Conclusion

The result shows that the application ^{99m}Tc has grown tremendously in accordance with the new presence of radiopharmaceutical production as well as the research in the application of ^{99m}Tc . Moreover, in most diagnostic procedures using ^{99m}Tc in Indonesia, adult patients will receive effective dose about 1-15% higher than adult patient in foreign countries which apply Caucasian model. Hence, to estimate the similar stochastic risk from the same procedure, the maximum value in recommended administered dose should be avoided and need to be evaluated.

6. Acknowledgement

A great thanks has been addressed to dr. Stephanus Massora and Prasetya Widodo for their support in the editing process of this article.

References

- [1] IAEA, (2009), Technetium- 99m Radiopharmaceuticals: Status and Trends, IAEA Radioisotopes and Radiopharmaceutical Series No.1, IAEA Publication, Vienna, pp. 1-2.
- [2] NAE-OECD, (2010), The Supply of Medical Radioisotopes: Review of Potential Molybdenum-99/Technetium- 99m Production Technologies, Nuclear Development Series, pp. 8-10.
- [3] IAEA, (2008), TECHNETIUM- 99m RADIOPHARMACEUTICALS: MANUFACTURE OF KITS, TECHNICAL REPORTS SERIES No. 466, IAEA Publication, Vienna, pp. 1-3.
- [4] IAEA, (2002), Radiological Protection for Medical Exposure to Ionizing Radiation, Safety Standard Series No. RS-G-1.5, IAEA Publication, Vienna, 2002, p.2.
- [5] FOOD AND AGRICULTURE ORGANIZATION OF THE UNITED NATIONS, INTERNATIONAL ATOMIC ENERGY AGENCY, INTERNATIONAL LABOUR ORGANIZATION, OECD NUCLEAR

- ENERGY AGENCY, PAN AMERICAN HEALTH ORGANIZATION, WORLD HEALTH ORGANIZATION, (1996), International Basic Safety Standards for Protection against Ionizing Radiation and for the Safety of Radiation Sources, Safety Series No. 115, IAEA, Vienna.
- [6] ICRP(1987), ICRP Publication 53: Radiation Dose to Patients from Radiopharmaceuticals, Oxford: Pergamon Press; 1987.
- [7] ICRP (1998), ICRP Publication 80: Radiation Dose to Patients from Radiopharmaceuticals: (Addendum 2 to ICRP Publication 53). Oxford: Pergamon Press.
- [8] ICRP (2008), ICRP Publication 106: Radiation Dose to patients from Radiopharmaceuticals. Addendum 3 to ICRP Publication 53. Oxford: Elsevier.
- [9] "Front Matter." *Medical Isotope Production Without Highly Enriched Uranium*. Washington, DC: The National Academies Press, 2009, p. 17.
- [10] IAEA website – Human Health Campus : Design principles of the $^{99}\text{Mo} \rightarrow ^{99\text{m}}\text{Tc}$ radionuclide generator, accessed from : http://nucleus.iaea.org/HHW/Radiopharmacy/VirRad/Eluting_the_Generator/Generator_Module/Design_principles/index.html
- [11] Jürgens, S., Herrmann, W. a., & Kühn, F. E. (2014). Rhenium and technetium based radiopharmaceuticals: Development and recent advances. *Journal of Organometallic Chemistry*, 751, 83–89.
- [12] Fahey, F., & Stabin, M. (2014), Dose Optimization in Nuclear Medicine, Seminars in Nuclear Medicine, Volume 44, Issue 3, May 2014, Pages 193-201.
- [13] IAEA, (2006), Nuclear medicine Resources manual, IAEA Publication, Vienna.
- [14] BAPETEN, The decree of BAPETEN head no.17 year 2012, Radiation Safety in Nuclear Medicine Department.
- [15] Hidayati, N.R, et al, (2014), Assessment of Internal Dosimetry due to the Administration of $^{99\text{m}}\text{Tc}$ -Sestamibi in Nuclear Medicine, International Conference on the Sources, Effect and Risks of Ionizing Radiation, Bali 10-11 October 2013.
- [16] Nayar, A. K., et al, (2013). Radiation Exposure and Associated Cancer Risk With Cardiac Diagnostic Imaging, 2(2), J Am Osteopath Coll Radiol 2013; Vol. 2, Issue 2.
- [17] Marine, P. M., et al. (2010). Changes in Radiation Dose with Variations in Human Anatomy: Larger and Smaller Normal-Stature Adults. *Journal of Nuclear Medicine : Official Publication, Society of Nuclear Medicine*, 51(5), 806–811.
- [18] Stabin, M. G., Sparks, R. B., & Crowe, E. (2005). OLINDA/EXM: the second-generation personal computer software for internal dose assessment in nuclear medicine. *Journal of Nuclear Medicine : Official Publication, Society of Nuclear Medicine*, 46(6), 1023–7.
- [19] IAEA, (1998), Compilation of Anatomical, Physiological and Metabolic Characteristics for a Reference Asian Man, IAEA TECDOC 1005, Volume : 1 , Data Summary and Conclusion, IAEA Publication, Vienna.
- [20] Koga, O. (2010). Accuracy of $^{99\text{m}}\text{Tc}$ - sestamibi scintimammography for breast cancer diagnosis, (1331), 205 - 209.
- [21] Marine, et al. (2010), Changes in Radiation Dose with Variations in Human Anatomy: Larger and Smaller Normal-Stature Adults, J Nucl Med. 2010 May ; 51(5): 806–811.
- [22] Hansson, E. (2012). The Internal Radiation Dosimetry of Diagnostic Radiopharmaceuticals across Different Asian Populations, MSc.Thesis University of Gothenburg, download from : http://radfys.gu.se/digitalAssets/1360/1360082_edvin-hansson-rapport.pdf.

Conference Paper

Probabilistic Analysis on Levelized Unit Electricity Cost (LUEC) Calculation of Small Medium Reactor Nuclear Power Plant (SMR NPP) In Indonesia


Nuryanti, Suparman

Center for Nuclear Energy System - National Nuclear Energy Agency (BATAN), Jl. Kuningan Barat, Mampang Prapatan, Jakarta

Abstract

SMR NPP is an alternative to overcome the dependency to diesel power plant especially in outside Java Bali system. Economic analysis is a crucial thing that should be done prior to any investment decision on the SMR NPP project and generally done by calculation of Levelized Unit Electricity Cost (LUEC). NPP projects, include SMR, are vulnerable to a number of uncertainty variables. The goal of this study was to perform economic analysis of SMR NPP project with capacity 2 x 100 MWe in Indonesia by incorporating an amount of uncertainty variables, namely the probabilistic approach. The research method is calculating LUEC with deterministic approach followed by the probabilistic approach. Probabilistic approach is done by simulating the effect of uncertainty variable on LUEC using Monte Carlo simulation technique. The results show that the deterministic approach with a discount rate of 10% obtained LUEC at 12.87 cents US\$/kWh. Whereas the probabilistic approach obtained LUEC of 13.10 plus minus 1.43 cents USD/kWh at a discount rate of 10% and amounted to 8.11 plus minus 0.88 cents USD/kWh at a discount rate of 5%. calculation in deterministic approach was 12.87 cents USD/kWh. While LUEC as the results of uncertainty variables simulation on probabilistic approach were 13.10 ± 1.43 cents USD/ kWh on discount rate 10% and 8.11 ± 0.88 cents USD/kWh on discount rate 5%. Occurrence probability of LUEC is less than 13 cents USD/kWh (benchmark value) was about 100% on discount rate of 5% and 50% on discount rate of 10%.

Keywords: Uncertainties, probabilistic analysis, LUEC, Monte Carlo technique, SMR NPPCorresponding Author:
Nuryanti, Suparman,
email: nuryanti@batan.go.idReceived: 29 July 2016
Accepted: 21 August 2016
Published: 21 September 2016**Publishing services
provided by Knowledge E**

 Nuryanti, Suparman.
This article is distributed
under the terms of the
**Creative Commons
Attribution License**, which
permits unrestricted use
and redistribution provided
that the original author
and source are credited.

Selection and Peer-review
under the responsibility of
the ICoNETS Conference
Committee. OPEN ACCESS

1. Introduction

The main characteristics of the electricity system outside Java-Bali are: limited grid (isolated areas) and still dominated by diesel power plants. Currently there are 4,640 units existing power plant, approximately 4,368 units (94.14%) were diesel with an installed capacity reached to 36.94% of the total capacity [1]. Fuel price fluctuation as well as fuel supply chain up to the diesel location become a problem that lead to the high cost of electricity power generation in this region. Small Medium Reactor (SMR) could be an alternative to overcome the dependency of isolated areas to oil-fired power plants, because this reactor type was focused on the limited grid region [2,3]. The category of SMR encompasses the

designs below 700 MWe, but new design layout and concepts are made possible by smaller size (i.e., from 350 MWe downwards) [2, 4, 5]. SMRs competitiveness lies on the higher degree of innovation implemented in their designs, improvement of safety aspects, as well as the lower initial capital costs compared to the large ones (although the unit cost USD/kWe higher at SMR NPP) [3, 6].

Economic analysis of electricity generation projects, generally done by calculating Levelized Unit Electricity Cost (LUEC), was crucial to be done prior to any investment decision on the SMR NPP project [7]. NPP project (include SMRs) are vulnerable to a number of uncertainties. Therefore an approach which is able to accommodate the possibility of these uncertainties was needed, namely probabilistic analysis [8,9].

There are many studies related to probabilistic analysis on electricity generation project [3, 10, 11, 12, 13]. This study focused on the SMR with specificity of Indonesia condition (infrastructure obstacle, payroll standard referring to PT PLN (Persero), etc.) [14]. Therefore the purpose of this study was to analyze the economics of SMR project in Indonesia considering the possibility of uncertainties. Study was conducted on SMR NPP 2 x 100 MWe. In this study, LUEC calculation performed by the deterministic approach first and then followed by the probabilistic approach. Probabilistic approach was done by simulating the effect of uncertainty variables simultaneously to LUEC. The probabilistic analysis performed by the Monte Carlo simulation techniques. Monte Carlo simulation is preceded by the development of a deterministic model that maps set of input variables to a set of output variables with some equations.

2. Methodology

Levelized Unit Electricity Cost (LUEC)

LUEC is the constant unit cost (per kWh) of a payment stream that has the same present value as the total cost of building and operating a generating plant over its life [7]. Mathematically, the calculation of NPP LUEC expressed by equation (1) [18]:

$$LUEC = \frac{\sum_t \left(\frac{Investment_t + O\&M_t + Fuel_t + Decommissioning_t}{(1+r)^t} \right)}{\sum_t \left(\frac{Electricity_t}{(1+r)^t} \right)} \quad (1)$$

With:

- Electricity_t : electricity production on year "t"
- LUEC : Levelized Unit Electricity Cost
- Investment_t : investment cost on year "t"
- O&M_t : Operation & maintenance cost on year "t"
- Fuel_t : Nuclear fuel cost on year "t"
- Decommissioning_t : Decommissioning cost on year "t"

Based on engineering economic principle, equation (1) shows that basically LUEC is the quotient between the sum of all cost component and the sum of electricity production which was discounted to present value [19].

Monte Carlo Simulation

Monte Carlo simulation is defined as a statistical sampling technique used to estimate the solutions of the quantitative problems [15]. Monte Carlo simulation is preceded by the development of a deterministic model that maps set of input variables to a set of output

variables with some equations. Furthermore, the deterministic model evaluated repeatedly with random numbers as input [16]. Repetition (iteration) is performed many times to ensure the robustness of the results [3, 17]. Because the evaluation was done repeatedly then there was an uncertainty propagation as the basic principle of Monte Carlo simulation [18]. Scheme of deterministic model and uncertainty propagation could be seen in Figure 1 and Figure 2.

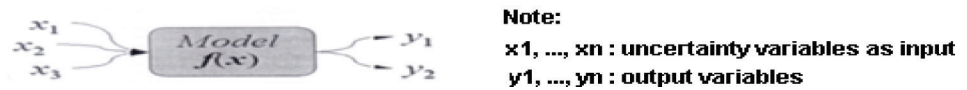


Figure 1: Deterministic Model [16].

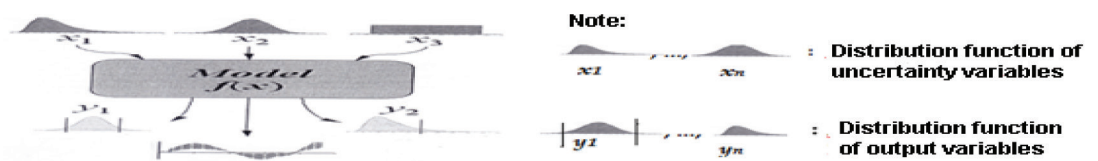


Figure 2: Uncertainty Propagation [16].

Steps of Study

The phases of study are as follows:

- Data gathering (technical and economic) that are required in the economic analysis
- Establish the necessary assumptions in the calculation
- Updating cost account data to the reference year (assumed in 2012)
- Calculating LUEC using deterministic models by using Mini G4ECONS, spreadsheet-based software from International Atomic Energy Agency (IAEA) [20].
- Distribution assignment of the uncertainty variables
- Simulating the uncertainty variables to the output (LUEC) by using @Risk [21].
- Analysis of the results and conclusion

3. Data and Assumptions

Technical and Economics Parameters of Reference NPP

Some techno-economic parameters of SMR NPP under study are shown at Table1.

TABLE 1: Techno-Economic Parameters of SMR NPP.

No	Parameters	Unit	Value
1	Capacity	MW	2 x 100
2	Capacity Factors	%	93[22]
3	Annually power production	MWh	1,629,360,000
4	Burn Up	MWd per metric tonne U ₂₃₅	60,000
5	Discount rate	%	10
6	Construction time	Year	5
7	Project lifetime	Year	40
8	Exchange rate	Rp per USD	12,000,-[23]
9	interest rate	%	3.27[24]

Structure of Electricity Generation Cost

a. Investment Cost

The investment cost of nuclear power plants is often called as Overnight Cost that consisting of: EPC costs (Engineering Procurement Construction), development costs and other costs [15]. Table 2 states the SMR NPP overnight cost from several studies that have been converted to reference year with Power Capital Cost Index (PCCI) [25].

TABLE 2: Overnight Cost (OC) of SMR from Several Studies.

No	Year	Reference	OC (USD/kWe)
1	2010	Electric Power Research Institute: 'Typical SMR' [26]	5,000 – 5,400
2	2011	Nuclear Energy Agency: '4 x PWR-335' [26]	4,900 – 5,300
3	2011	Nuclear Energy Agency: '5 x PWR-125' [26]	6,800 – 8,300
4	2010	SMR Generic Estimated Cost [27]	4,979 – 5,393
5	2009	HTR (GIF-INPRO) [28]	6,392 – 10,422

Overnight cost data in Table 2 is in the form of interval, then simulation techniques was performed to get the most probable value that can represent these values. From simulation, the most probable value is 6,288 USD/ kWe (approximation to 6,300 USD/ kWe) or overnight cost is USD 1.26 billion. It was assumed that approximately 85% of this value would be EPC Cost, which is about USD 1.07 billion. Furthermore, taking into account the infrastructure obstacle related to the construction of nuclear power plants in Indonesia, there is an expensiveness factor whose value is approximately 15% of the EPC Cost. In addition, it is also considered a number of supplementary budgets (often termed as a contingency cost) that is approximately 20% of EPC Cost. Due to the infrastructure obstacle and the contingency cost, the total investment cost obtained for SMR 2 x 100 MWe is about USD 1,634,850,000.

b. Operation & Maintenance (O&M Cost)

O & M Cost is the cost required to run the routine operation of NPP, divided into two: fixed O&M Cost and variable O&M Cost. Table 3 shows the structure of fixed O & M Cost [14, 22]. While variable O & M costs was assumed approximately to 0.6030 USD/ MWh [29].

TABLE 3: Fixed O&M Cost SMR NPP.

No	Details	Value (USD)
1	Personnel Cost	2,074,517
2	Maintenance Cost (include decommissioning cost)	15,804,792
3	Property Tax	10,553
4	Insurance Cost	488,808

c. Nuclear Fuel Cost

Table 4 shows the data of components of nuclear fuel cost. These costs are escalated to the first year of operation with escalation rate of 0,5% (assumed to begin construction in 2019) [3].

TABLE 4: Details components of Nuclear Fuel Cost (USD) [30].

Details of components	Price in 2012	Total Fuel Cost
Price of U_3O_8	130	1,386
Conversion cost (U_3O_8 to UF_6)	11	104
Enrichment	120	1,207
Fabrication	240	256
Total Fuel Cost (USD/kg U_{235})		2,953

Distribution Assignment

Several input variables that potentially cause uncertainty on LUEC, which are: investment cost, price of Natural Uranium (U_3O_8), enrichment cost, fixed and variable O&M cost, capacity factor and construction time [30]. Those variables were simulated simultaneously and furthermore their influence on LUEC could be seen.

There are three techniques in the distribution assignment. In case the historical data is available, the fitted distribution technique could be used. But, if the historical data is not available, generally researchers use literature approach and expert judgment. And if both of those techniques are not available, the final alternative used is assumption utilization [31]. Table 5 shows the result of uncertainty variables that affect the LUEC of SMR NPP.

TABLE 5: Distribution Assignment of Uncertainty Variables.

No	Uncertainty Variables	Type of Distribution	Note
1	Investment Cost	Triangular	Fitted distribution of historical data
		minimum = 4,845; most likely = 6,300; maximum = 8,469	
2	Price of natural Uranium (U_3O_8)	Pearson5	Rothwell [30]
		$\alpha = 1.5420$; $\beta = 28.437$	
3	Enrichment	Normal	Rothwell [30]
		139.740 ± 22.216	
4	Fixed O&M Cost	Extvalue	Fitted distribution of historical data
		Mean = 90.1677; Std dev = 7.2447	
5	Variable O&M Cost	Logistic	Fitted distribution of historical data
		$\alpha = 0.620609$, $\beta = 0.023733$	
6	Capacity Factor	Triangular minimum=0.88650; most likely = 0.92593; maximum = 0.99191	Fitted distribution of historical data

4. Result and Discussion

The Result of LUEC Calculation on Deterministic Model

In the calculation of LUEC using Mini G4ECONS models, the investment cost was disbursed during the construction period (investment disbursement). Furthermore, the investment cost was discounted at a certain interest rate to the Commercial Operation Date (COD). COD is

Based on Table 6 and 7, it could be seen that there was a difference on LUEC value between deterministic analysis and probabilistic analysis. In deterministic analysis (Table 6), LUEC value is in the form of single value (which is 12.87 cents USD/kWh). While in probabilistic analysis (Table 7), LUEC value is in the form of a distribution function of LUEC with a certain minimum, maximum and average value. But based on the statistical rules, LUEC value as simulation results (probabilistic analysis) can be assumed centered on the average value \pm standard deviation [33]. Therefore at discount rate of 10%, LUEC value as simulation results would be at value of 13.10 ± 1.43 cents USD/ kWh, while at a discount rate of 5% would be at value of 8.11 ± 0.88 cents USD/kWh. It means that at discount rate of 10%, LUEC value as simulation results will be centered on the value of 11.67 until 14.53 cents USD/kWh, while at discount rate of 5% will be on the value of 7.23 until 8.98 cents USD/ kWh. If the uncertainty variables aren't well monitored, then the LUEC value will be able to reach for the average plus standard deviation (14.53 cents USD/kWh at a discount rate of 10% and 8.98 cents USD/kWh at a discount rate of 5%). The LUEC value which reaches for the average plus standard deviation is termed as risk adjusted LUEC [30]. In the opposite, if the uncertainty variables are monitored properly, then the LUEC value will be able to reach for the average minus standard deviation (11.67 cents USD/kWh at a discount rate of 10% and 7.23 cents USD/kWh at a discount rate of 5%). These results indicate that if the uncertainty variables are not monitored properly, it will very likely lead to cost overruns on generation costs. Therefore, policies that allow to monitor such uncertainty variables were needed.

Figures 3 and 4 shows the tornado diagram as simulation results of the uncertainty variables to LUEC at a discount rate of 5% and 10% respectively.

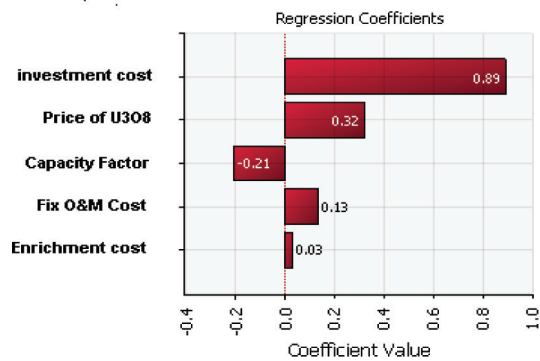


Figure 3: Tornado Diagram of SMR NPP LUEC PLTN SMR on Discount rate of 5%.

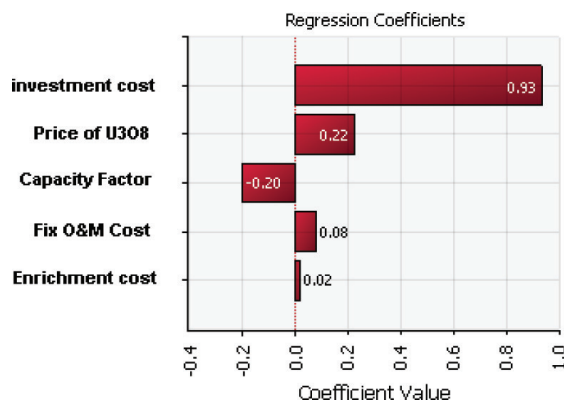


Figure 4: Tornado Diagram of SMR NPP LUEC on Discount rate of 10%.

Based on both figures, it can be seen that the investment cost has the largest coefficient value on both of the discount rate, this indicates that it is a very important variable to be monitored. Policies that allow to reduce the investment cost will contribute in lowering the LUEC value of SMR, for example by increasing the portion of national industrial participation in the project.

Figure 5 shows the cumulative distribution function (CDF) of simulation results of the uncertainty variables to SMR LUEC (in unit of mills USD/kWh) at discount rate of 10% and 5%. The CDF in Figure 5 is used to determine the probability of occurrence that LUEC value is less than the benchmark value. The benchmark value is the LUEC value that will be assigned as the selling price of electricity from NPP company to utility company (PT PLN (Persero)) as agreed in the PPA (Power Purchase Agreement). SMR NPP is projected to be built in isolated area, as an alternative solution for the high cost of generation (generally diesel power plants were used) due to the high price of oil. Based on information from PLN, it is known that the price of electricity in isolated areas generally is about 12 cents USD/ kWh. Taking into account SMR is a relatively new technology for Indonesia, it is assumed that the benchmark value of LUEC for SMR is slightly more expensive at 13 cents USD/ kWh or 130 mills USD/kWh.

Based on Figure 5 shows that the occurrence probability of SMR LUEC is less than 13 cents USD/kWh for discount rate 5% is approximately 100%, while at the discount rate of 10% the occurrence probability of LUEC is less than 13 cents USD/kWh is only about 50%. These results indicate a need for a strong commitment from the government to provide a government guarantee on SMR NPP project, such as manifested by using low/ social discount rate. By decreasing in discount rate (from 10% to 5%), the occurrence probability of SMR LUEC is less than benchmark value will increase (from 50% to 100%) so it is expected that SMR NPP can compete with other power plants in outside Java-Bali System.

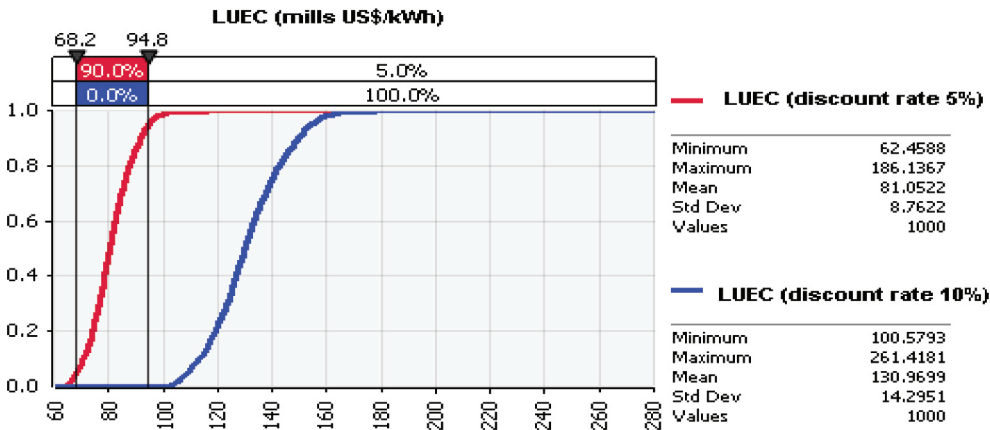


Figure 5: Cumulative Distribution Function (CDF) of SMR NPP LUEC as Result of Simulation on Uncertainty Variables.

5. Conclusion

Probabilistic analysis was proved to be able in accommodating the possibility of an amount of uncertainty variables occurrence in the SMR NPP project. The result of LUEC calculation with deterministic approach was amounted to 12.87 cents USD/ kWh. While the LUEC value as simulation results of uncertainty variables (probabilistic approach) was amounted to 13.10 ±1.43 cents USD/ kWh at a discount rate of 10% and of 8.11 ± 0.88 cents USD/kWh at a discount

rate of 5%. Variables that affect LUEC uncertainties should be monitored properly so that the occurrence of cost overruns on electricity generation cost could be avoided. The occurrence probability of LUEC is less than 13 cents USD/kWh (benchmark value) is approximately 100% at a discount rate of 5% and 50% at a discount rate of 10%.

6. Acknowledgment

The research was granted by the IAEA in the form of Coordinated Research Project (CRP) entitled "Financing Model Considering Risk Analysis for Nuclear Power Plant In Indonesia" in 2014. An acknowledgement was submitted to Ir. Suroso Isnandar (PLN) and Dr. Sudi Ariyanto (BATAN) for intense discussion during the research accompany.

References

- [1] PT PLN (Persero), "Statistik PLN 2013", Sekretariat Perusahaan PT PLN (Persero), Jakarta, ISSN No. 0852-8179, (Mei 2014)
- [2] IEA/NEA, "Current Status, Technical Feasibility and Economics of Small Nuclear Reactors", OECD, Paris, (Juni 2011)
- [3] LOCATELLI, G. dan MANCINI, M., "Small-medium Sized Nuclear, Coal and Gas power plant: A Probabilistic Analysis of Their Performances and Influence of CO₂ Cost", *Energy Policy*, 38, pp. 6360-6374, (2010).
- [4] PETROVIC, B., RICOTTI, M., MONTI, S., CAVLINA, N. dan NINOKATA, H., "Pioneering Role of IRIS in the Resurgence of Small Modular Reactors", *Nuclear Technology*, Vol. 178, No. 2, pp. 126-152, (2012).
- [5] REYES, J. dan LORENZINI, P., "NuScale: A Modular, Scalable Approach to Commercial Nuclear Power", *Nuclear News*, (2010).
- [6] BOARIN, S. dan RICOTTI, M., "Research Article: An Evaluation of SMR Economic Attractiveness", Hindawi Publishing Corporation, *Science and Technology of Nuclear Installations*, Volume 2014, Article ID 803698, (2014).
- [7] BLACK & VEATCH, "Levelized Cost of Energy Calculation, Methodology and Sensitivity", http://csep.efchina.org/Levelized Cost of Energy Calculation_BV_EN.pdf. Accessed on 18 February 2014.
- [8] RODE, et al., "Montecarlo Methods for Appraisal and Valuation: A Case Study of a Nuclear Power Plant", CEIC Working Paper 01-01, Carnegie Mellon Electricity Industry Center, Carnegie Mellon University, Pittsburgh, (2001).
- [9] FITRIANI, H. et al., "Kajian penerapan model NPV-at-risk sebagai alat untuk melakukan evaluasi investasi pada proyek infrastruktur jalan tol", *Jurnal Infrastruktur dan Lingkungan Binaan* Vol. II No. 1, Hal. 1-12 (Juni 2006).
- [10] FERETIC, D., & TOMSIC, Z., "Probabilistic analysis of electrical energy cost comparing: Production costs for gas, coal and nuclear power plants", *Energy Policy*, 33, pp. 5-13, (2005).
- [11] Roques, A. et al., "Using probabilistic analysis to value power generation Investment under uncertainty", EPRG 065, Electricity Policy Research Group (EPRG), University of Cambridge, England, (2006).
- [12] NURYANTI, "Studi Kelayakan Finansial Proyek PLTN di Indonesia dengan Memasukkan Unsur Ketidakpastian", Thesis, Fakultas Teknik Universitas Indonesia, (2012).

- [13] NURYANTI, dkk., "Analisis Probabilistik Pada Perhitungan Biaya Pembangunan Listrik Teraras PLTN", *Jurnal Pengembangan Energi Nuklir*, Volume 14 No. 1 Hal. 23-33, Jakarta (2012).
- [14] PUSLITBANG PT PLN (Persero) dan PPEN-BATAN, "Laporan Akhir: Studi Ekonomi, Pendanaan dan Struktur Owner dalam Rangka Rencana Persiapan Pembangunan PLTN Pertama di Indonesia", PLN, Jakarta (2006).
- [15] HOLTON, Glyn A., *Value-at-Risk: Theory and Practice*, 2nd ed, E-book at <http://value-at-risk.net>, Accessed on 4 February 2012
- [16] SRIDADI, B., "Pemodelan dan Simulasi Sistem: Teori, Aplikasi dan Contoh Program dalam Bahasa C", Penerbit Informatika, Jakarta, (2009).
- [17] TJONG, W., F., "Aplikasi Statistik Ekstrim dan Simulasi Monte Carlo dalam Penentuan Beban Rencana pada Struktur dengan Umur Guna Tertentu", *Dimensi Teknik Sipil*, Vol. 3, No. 2, September 2001, Hal. 84-88 (2001), ISSN 1410-9530.
- [18] IEA/NEA, "Projected Cost of Generating Electricity (2010 Edition)", OECD, Paris, (2010)
- [19] BLANK & TARQUIN, "Engineering Economy", 6th, Mc Graw Hill, Singapore, (2008)
- [20] IAEA, "Mini G4 Econs Software", IAEA, Vienna, (2008)
- [21] PALISADE CORPORATION, "Guide to using @Risk: Risk Analysis and Simulation Add-In for Microsoft Excel Version 5.5", (May 2009)
- [22] PT PLN (Persero), PT LAPI ITB & JAPC, "Feasibility Study for Bangka Nuclear Power Plant Project – Non Site aspect", (2013)
- [23] BANK INDONESIA, "Foreign Exchange Rate in Year 2012", <http://www.bi.go.id/> [Accessed on 01 June 2014]
- [24] OECD, "Commercial Interest Reference Rate (CIRRs)", www.oecd.org/tad/xcred/cirrs.pdf. [Accessed on 01 June 2014]
- [25] _____, "Power Capital Cost Index (PCCI) North America", <http://www.ihscera.com/> [Accessed on 05 Mei 2014]
- [26] ABDULLA, A. & AZEVEDO, I. L., "Developing a Range of Levelized Cost Estimates for Integral Light Water Small Modular Reactor", www.andrew.cmu.edu, [Accessed on Mei 2014]
- [27] US DEPARTMENT OF ENERGY, "SMR Financing and Economics, The Nuclear Option: Is Small Scale Nuclear Energy an Option for Alaska?", December 2010
- [28] ONO, K., "Generation IV International Forum Economics Assessment Methodology and Application", GIF-INPRO Interface Meeting, Vienna, March 1, 2013
- [29] ROTHWELL, G., "The Economics of Future Nuclear Power: An Update of The Economic Future of Nuclear Power (2004), a Study Conducted at the University of Chicago", Stanford University, (2011)
- [30] _____, "The Economics of Nuclear Power, Updated August 2013", <http://www.world-nuclear.org/info/inf02.html> [Accessed on 15 Desember 2013]
- [31] YE, S. & TIONG, R., "NPV at risk method in infrastructure project investment evaluation, *Journal of Construction Engineering and Management*, Vol. 126, No. 3 pp. 227-233 (May/ June 2000), ISSN 0733-9634/00/0003-0227-0233.
- [32] THOMAS, S., "The economic of nuclear power: An update", Berlin: Heinrich-Böll-Stiftung, March 2010, <http://www.psir.org/> [Accessed on 03 Februari 2012]
- [33] SUPRANTO, J., "Statistik: Teori dan Aplikasi, Jilid 1", Edisi 7, Penerbit Erlangga, Jakarta, (2009)

Conference Paper

The Effect of Hydrazine Addition on the Formation of Oxygen Molecule by Fast Neutron Radiolysis

G.R. Sunaryo, S.L. Butarbutar

Center for Nuclear Reactor Technology and Safety, National Nuclear Energy Agency, Puspiptek Area, Tangerang Selatan 15314, Indonesia


Abstract

Hypothetically speaking, hydrazine could suppress the oxygen formation as a major of corrosion initiator. In this work, we developed a calculation model to understand the effect of hydrazine addition toward the oxygen under PWR condition. Our great interest is to study whether this strategy would also be effectively applied in PWRs. In the present work, the effect of hydrazine on suppressing the molecule oxygen under neutron irradiation is described. The simulation was done by using FACSIMILE. The variation dose applied assuming a batch system and at high dose $\sim 10^4$ Gy s^{-1} . Three different temperatures were applied, which are room temperature, 250 and 300 °C at two system oxygenated water, which are aeration and deaeration. At room temperature, for deaerated condition, added hydrazine under a range of 10^{-6} – 10^{-4} M into primary coolant were not effective to suppress O_2 form since the effect was similar as in the pure water system since for 10^{-3} M hydrazine addition, a large produce of O_2 were obtained. In reverse, for deaerated condition, hydrazine concentrate about 10^{-3} M can suppress O_2 form significantly, while hydrazine add in the range between 10^{-6} – 10^{-4} M is again confirmed to be the same as in pure water system. For high temperature, at 250 and 300 °C, the results showed that in deaerated condition, hydrazine addition can suppress O_2 form proportionally to its concentration while in aerated condition, hydrazine add with concentration of 10^{-6} and 10^{-5} M were not effectively to suppress O_2 form, a slightly decrease of O_2 occurred due to the addition of 10^{-4} M hydrazine and 10^{-3} M of hydrazine can suppress the formation of O_2 significantly.

Corresponding Author:
 G.R. Sunaryo,
 email: genirina@batan.go.id

Received: 29 July 2016
 Accepted: 21 August 2016
 Published: 21 September 2016

**Publishing services
 provided by Knowledge E**

 G.R. Sunaryo. et al.
 This article is distributed
 under the terms of the
 Creative Commons
 Attribution License, which
 permits unrestricted use
 and redistribution provided
 that the original author
 and source are credited.

Selection and Peer-review
 under the responsibility of
 the ICoNETS Conference
 Committee.

 OPEN ACCESS

Keywords: radiolysis, fast neutrons, hydrazine, O_2 , Facsimile

1. Introduction

Pressurized Water Reactors (PWRs) use light water (H_2O) both as a coolant and as a moderator [1]. In the reactor core, water is circulated under extreme conditions such as high pressure, high temperature and heavy mixed neutron/ γ -radiation fields results in chemical decomposition of water (radiolysis) [2]. By means of radiolysis of water, various species such as free radicals (e^-_{aq} , H^\cdot , $\cdot OH$, and HO_2^\cdot/O_2^\cdot) and molecular products (H_2 , H_2O_2 and O_2 (as a secondary product)) are generated continuously. These species can lead to corrosion, cracking, and hydrogen pickup both in the core and in the associated piping components of the reactor [2-5]. As this issue has been an important consideration in PWRs, thus optimal water chemistry control is expected to play important role to mitigate the corrosion caused by radiolysis of water.

Recently, chemical compound being added into primary systems of PWRs such as: 1) dissolved hydrogen to suppress the oxidizing radicals and molecular products formation, 2) boron in form of boric acid to control the neutron reactivity and to suppress the oxygen concentration that play role on corrosion process [6]. While Ishida et al. (2006) have developed a selected method to mitigate stress corrosion cracking in boiling water reactors (BWRs) named hydrazine and hydrogen co-injection (HHC) [7], which is injected through feed water system. Hypothetically speaking, hydrazine could suppress the oxygen formation as a major of corrosion initiator. In this work, we developed a calculation model to understand the effect of hydrazine addition toward the oxygen under PWR condition. Our great interest is to study whether this strategy would also be effectively applied in PWRs.

In this work, FACSIMILE computer code were used to investigate the effect of hydrazine to suppress the oxidator, O_2 , on primary cooling water radiolysis at temperatures between 25 and 350 °C under neutron irradiation. We considered that G-values, the number of species produced (or consumed) per unit of energy absorbed, and rate constant of all species involved that we used in this calculation would be acceptable up to 350 °C. How far is the effects of hydrazine addition toward the formation of oxygen were discussed in this work.

2. Methodology

The absorption of ionizing energy by the coolant results in coolant radiolysis which can generate continuously free radical species and molecular products (where free radical species react with each other). In this study, we assumed a continuous radiation in a homogeneous chemical stage batch system, as coolant radiolysis is categorized in this type. It has been described in detail previously [8] that radiation chemical simulation is an analysis of simultaneous chemical reactions and is in effect the integration of time-dependent multivariable simultaneous differential equations. Therefore, in this present work, FACSIMILE was used to solve differential equations.

The important key parameters to evaluate the chemical effects of ionizing radiation are temperature dependence of the radiation-chemical yields or G-values of the species (in this case for fast neutrons), and the rate constants for all of the reactions involving these species in pure water. These two parameters are needed as inputs for our code. In addition to that, high dose rate of neutrons 10^4 Gy/s, aeration and deaeration system, and the reaction set of a hydrazine system. Details information were discussed as follow.

G-value is given in the units of "molecule per 100 eV"; for conversion into SI units (mol/J), 1 molecule/100 eV \approx 0.10364 μ mol/J. In this work, we need G-values of reactive radical species, molecular product and water itself by fast neutron irradiation. G-value of fast neutrons were taken from Ref. [9] (Table 1), it is a combination of measurements and computer modeling; irradiations carried out using the YAYOI fast-neutron source reactor at the University of Tokyo, with an average energy for fast neutrons of \sim 0.8 MeV. G-values measured at 250 °C were adopted for temperature above 250 °C. In order to provide the reaction set and rate of reaction as one of important parameter for one to understand radiolysis process, we use the self-consistent radiolysis database that recently compiled by Elliot and Bartels [10] (the reactions set not shown in this work). This new database provides recommended values to use in high-temperature modeling of light water radiolysis over the temperature range between 20-350 °C. In addition to that, the reactions set of hydrazine is also necessary in order to know the effect of hydrazine addition. Table 1 provides a numbered list of reactions and corresponding rate constants used in this work. The mechanism reaction of hydrazine with free radicals and molecular products, also with O_2 radicals is quite complex.

TABLE 1: Main chemical reactions of hydrazine and their corresponding rate constants (k) at 25 °C used in our FACSIMILE. For first-order reactions (indicated by the symbol †), the value of k is given in s^{-1} .

Reaction	Symbol	$k(M^{-1}s^{-1})$
R1	$e^-_{aq} + N_2H_5^+ \rightarrow H^\cdot + N_2H_4$	1.60×10^8
R2	$H^\cdot + N_2H_4 \rightarrow H_2 + N_2H_3$	1.30×10^5
R3	$H + N_2H_5^+ \rightarrow H_2 + N_2H_4^+$	1.30×10^5
R4	$OH + N_2H_4 \rightarrow N_2H_3 + H_2O$	5.40×10^9
R5	$OH + N_2H_5^+ \rightarrow N_2H_4^+ + H_2O$	8.20×10^7
R6	$N_2H_4^+ + N_2H_4^+ \rightarrow N_4H_8^{2+}$	1.00×10^8
R7	$N_2H_3 + N_2H_3 \rightarrow N_4H_6$	6.00×10^8
R8	$N_4H_8^{2+} \rightarrow NH_4^+ + N_3H_4^+$	$1.00 \times 10^4 \text{ †}$
R9	$N_4H_6 \rightarrow NH_3 + N_3H_3$	$7.20 \times 10^4 \text{ †}$
R10	$N_2H_4 + H_2O_2 + H_2O_2 \rightarrow N_2 + 4H_2O$	2.43×10^8
R11	$N_2H_3 + H_2O_2 \rightarrow OH + N_2H_2 + H_2O$	1.00×10^9
R12	$N_3H_4^+ \rightarrow N_2 + NH_4^+$	$1.30 \times 10^4 \text{ †}$
R13	$N_2H_4 + O_2 \rightarrow H_2O + H_2O + N_2$	7.00×10^3
R14	$N_2H_3 + O_2 \rightarrow O_2^- + H^\cdot + N_2H_2$	3.80×10^8
R15	$N_2H_2 + N_2H_2 \rightarrow N_2 + N_2H_4$	2.00×10^4
R16	$H^\cdot + N_2H_4 \rightarrow N_2H_5^+$	1.00×10^1
R17	$N_2H_5^+ + H \rightarrow NH_2 + NH_4^+$	1.30×10^5
R18	$H^\cdot + N_2H_3 \rightarrow N_2H_4^+$	1.00×10^1
R19	$N_3H_2^- \rightarrow N_2 + NH_2^-$	$7.70 \times 10^3 \text{ †}$
R20	$OH + NH_3 \rightarrow NH_2 + H_2O$	7.52×10^8
R21	$NH_2 + NH_2 \rightarrow N_2H_4$	1.00×10^{10}
R22	$NH_2 + N_2H_4 \rightarrow N_2H_3 + NH_3$	1.00×10^7
R23	$NH_3 + H \rightarrow NH_4^+ + e^-_{aq}$	7.00×10^6
R24	$H + N_2H_3 \rightarrow N_2H_4$	7.00×10^9
R25	$N_2H_5^+ \rightarrow H^\cdot + N_2H_4$	$7.88 \times 10^2 \text{ †}$
R26	$N_2H_4^+ \rightarrow H^\cdot + N_2H_3$	$7.88 \times 10^3 \text{ †}$
R27	$N_3H_4^+ \rightarrow H^\cdot + N_3H_3$	$1.00 \times 10^1 \text{ †}$

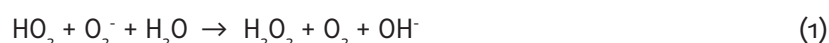
In this work, the concentration of hydrazine added to the system is under a range (10^{-6} to 10^{-3} M) and using a well-accepted mechanism for radiolysis in the presence or absence of air. Dose rate is also one of the input data to perform radiolysis simulation. Dose rate of neutrons are assumed as high dose rate conditions, a typical condition in reactor core (10^4 Gy s^{-1}). Once again, the purpose of this study is to understand the best estimation of hydrazine addition to suppress the O_2 formation in primary coolant water system.

3. Result and Discussion

The effect of hydrazine on coolant radiolysis at temperature range between 25-300 °C, high neutron dose rate condition and in the presence or absence of air were carried out using computer code FACSIMILE. Our code has been validated with other calculation in pure and other solution. The validity of the simulation is checked from the aspect of mass balance and numbers of hydrogen and oxygen atoms in major products are approximately 2:1 [8]. For the sake of comparison, the time evolution of O_2 concentration were calculated in pure water system (black lines) and by varying the concentration of hydrazine added to our system under a range, 10^{-6} , 10^{-5} , 10^{-4} , and 10^{-3} M (magenta, blue, green and red lines, respectively).

1. Simulation at room temperature

Figure 1 shows the time evolution of $[O_2]$ as reproduced by our simulation at 25 °C in deaerated (a) and aerated (b) condition. For deaerated condition, the varying concentration of added hydrazine in the range between 10^{-6} – 10^{-4} M has no effect in reaching the steady state concentration of O_2 which is similar as in the pure water system. However, a striking feature of our simulated results obtained at 10^{-3} M hydrazine addition, where it increases with time, was the large produce of O_2 . Our hypothesis for this result is that there are two reactions contribute to the formation of O_2 (based on the importance) at longer time:



Reaction (2) is much slower with a rate constant about 3 order of magnitude lower than for reaction (1). In reverse the concentration of hydrazine about 10^{-3} M can suppress the formation of O_2 significantly pass through a minimum point then reach the steady state concentration at very low level $\sim 5 \times 10^{-9}$ M, while the addition of hydrazine in the range between 10^{-6} – 10^{-4} M is confirmed in Figure 1(b) as the same as in pure water system.

The results for the concentration of O_2 in aerated aqueous 10^{-3} M hydrazine solutions show that this long-lived molecular species are decreased compared to those in deaerated solutions. The reactions of oxygen consumption, reaction R13 and R14 are much faster than the reactions of oxygen formation such as reaction (1) and (2), thereby cannot protect the oxygen molecule from further reactions with these species in the homogeneous stage of radiolysis, or in other words, this phenomena leads to a decrease in the concentration of O_2 . Indeed, as can be seen in Figure 1, the steady state concentration of O_2 in aerated hydrazine solutions are six magnitudes lower than in deaerated solutions.

2. Simulation at 250 °C and 300 °C

Figure 2(a), (b) and Figure 3(a), (b) show time variations of the oxygen molecule as a function of time in pure water and hydrazine solution at deaerated and aerated condition respectively. Overall, in all case, steady state concentrations of O_2 are lower than those in Figure 1 both in the presence or absence of air. In deaerated condition, Figure 2(a) and Figure 3(a), shows obviously how each concentration of hydrazine addition suppress the formation of O_2 . It is readily explained that the higher the concentration of hydrazine the lower the generation of O_2 . This explanation is described in combination of reaction R.. and R.. that convert the N_2H_4 and N_2H_3 into water, N_2H_2 and N_2 .

In the other side, the highest concentration of hydrazine which is 10^{-3} M can suppress the formation of O_2 until it becomes negligible $\ll 10^{-20}$ M. Figure 2(b) and Figure 3(b) show that in absence of hydrazine addition give the same result with 10^{-6} and 10^{-5} M of hydrazine

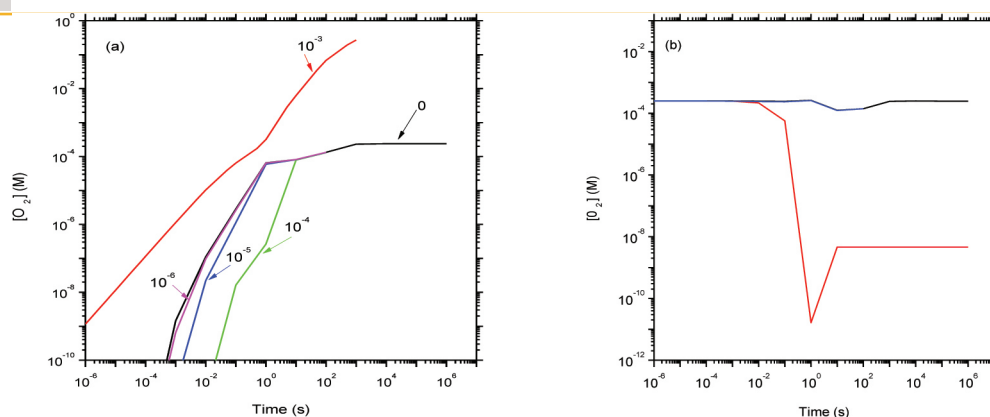


Figure 1: Time evolution of $[O_2]$ (in Molar) of pure water (black lines) and aqueous hydrazine solutions at 25 °C, calculated using our FACSIMILE in deaerated (a) and aerated (b) condition at the assumption of dose rate 10^4 Gy s^{-1} . and by varying the concentration of hydrazine added to our system under a range, 10^{-6} , 10^{-5} , 10^{-4} , and 10^{-3} M (magenta, blue, green and red lines, respectively).

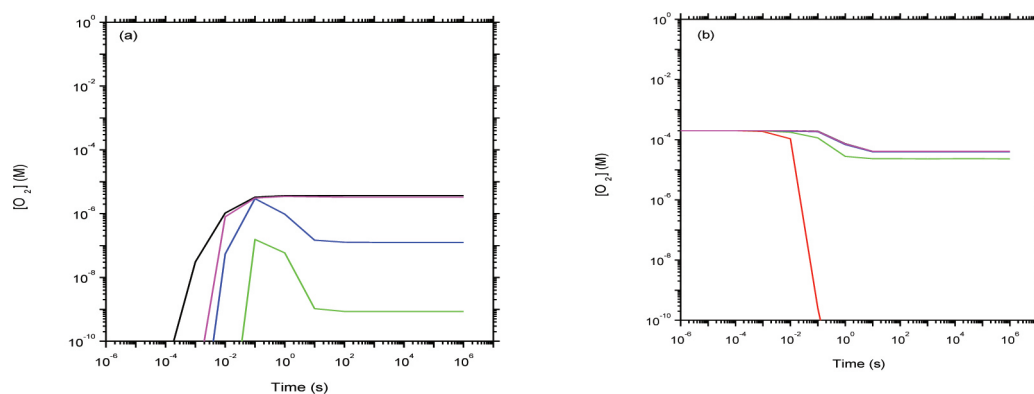


Figure 2: Time evolution of $[O_2]$ (in Molar) of pure water (black lines) and aqueous hydrazine solutions at 250 °C, calculated using our FACSIMILE in deaerated (a) and aerated (b) condition at the assumption of dose rate 10^4 Gy s^{-1} . and by varying the concentration of hydrazine added to our system under a range, 10^{-6} , 10^{-5} , 10^{-4} , and 10^{-3} M (magenta, blue, green and red lines, respectively).

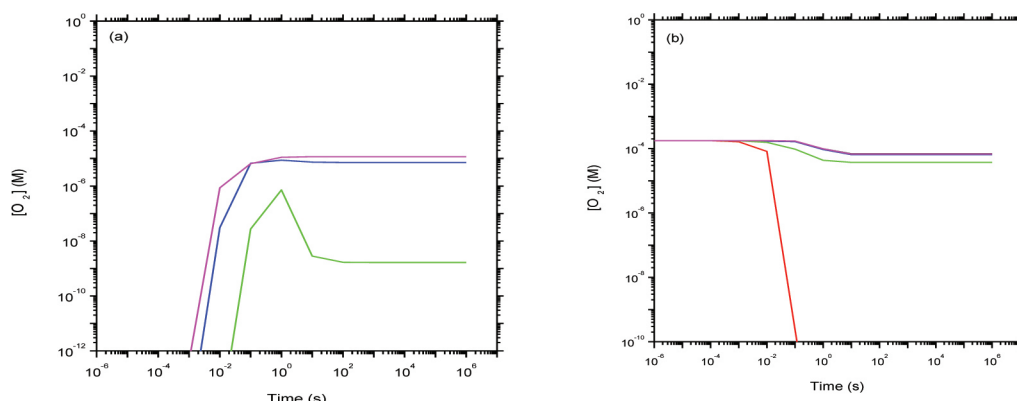


Figure 3: Time evolution of $[O_2]$ (in Molar) of pure water (black lines) and aqueous hydrazine solutions at 300 °C, calculated using our FACSIMILE in deaerated (a) and aerated (b) condition at the assumption of dose rate 10^4 Gy s^{-1} . and by varying the concentration of hydrazine added to our system under a range, 10^{-6} , 10^{-5} , 10^{-4} , and 10^{-3} M (magenta, blue, green and red lines, respectively).

whereas a slightly decrease of O_2 occurred due to the addition of 10^{-4} M hydrazine. For aerated conditions, similarly to the results at room temperature in Figure 1b, concentrations of O_2 falls down significantly at aqueous solution of 10^{-3} M hydrazine concentration.

For the case of increasing 225 centigrade temperature and above, concentrations of the O_2 reach steady state values more rapidly than those in room temperature. In other words, the higher the temperature the faster decreasing of O_2 since the reactions for O_2 consumption take faster proportionally to the temperature then O_2 production as in room temperature.

Unfortunately, regarding the water chemistry in hydrazine aqueous systems, there is however a complete lack of information on the radiolysis of water by fast neutron irradiation as the experimental data is not available in the literature to the best of our knowledge therefore we are not able to validate our results especially at high temperature.

The simulation results for room temperature, for deaerated condition, the varying concentration of added hydrazine in the range between 10^{-6} – 10^{-4} M has no effect in reaching the steady state concentration of O_2 and it is similar as in the pure water system and for 10^{-3} M hydrazine addition, a large produce of O_2 were obtained. In reverse, for deaerated condition, the concentration of hydrazine about 10^{-3} M can suppress the formation of O_2 significantly, while the addition of hydrazine in the range between 10^{-6} – 10^{-4} M is confirmed to be the same as in pure water system.

Overall, in all case, steady state concentrations of O_2 in the results of simulations for 250 and 300 °C are lower than those in room temperature both in the presence or absence of air. In deaerated condition, hydrazine addition can suppress the formation of O_2 proportionally to its concentration

4. Conclusion

In this work, FACSIMILE was used to calculate oxidator concentration, O_2 on coolant water radiolysis by fast neutrons irradiation at temperatures between 25 and 300 °C. The simulations also conducted in pure water and hydrazine aqueous solution both in the presence and absence of air. The time evolution of $[O_2]$ were obtained by taking into consideration the assumption of high dose rate conditions of fast neutron, a typical condition in reactor core (10^4 Gy s^{-1}).

The higher hydrazine concentrate, the lower O_2 . The highest concentration of hydrazine can suppress O_2 form until it becomes negligible. In aerated condition, hydrazine absent addition give the same result with 10^{-6} and 10^{-5} M of hydrazine where a slightly decrease of O_2 occurred due to the addition of 10^{-4} M hydrazine. However, experimental data are required to test more thoroughly our modeling calculations, and to specify the potential role of hydrazine to suppress of O_2 form.

References

- [1] Katsumura Y., et al., "Fast Neutron Radiolysis of Water at Elevated Temperatures Relevant to Water Chemistry", Progress Nuclear Energy, Vol.32, pp. 113-121 (1998).
- [2] Cohen P., "Water Coolant Technology of Power Reactors". La Grange Park (IL): American Nuclear Society, (1980).
- [3] McCracken D. R., et al., "Aspects of the Physics and Chemistry of Water Radiolysis by Fast Neutrons and Fast Electrons in Nuclear Reactors", Report AECL No.: 11895, Chalk River (Ontario): Atomic Energy of Canada Ltd. (1998).

- [4] Woods R.J. and Pikaev A.K., "Applied Radiation Chemistry: Radiation Processing", Wiley, New York (1994).
- [5] Research needs and opportunities in radiation chemistry workshop, Chesterton (IN), 19-22 April 1998, Report No.: DOE/SC-0003. Germantown (MD): U.S. Department of Energy, Office of Basic Energy Sciences; 1999. Available from <http://www.science.doe.gov/production/bes/chm/Publications/RadRprt.pdf>
- [6] Garbett K., et al., "Hydrogen and Oxygen Behavior in PWR Primary Coolant Water Chemistry of Nuclear Reactor Systems", Proceedings Of The 8th Conference Organized by The British Nuclear Energy Society, October 22-26, Bournemouth, UK (2000).
- [7] Ishida K., et al., "Hydrazine and Hydrogen Co-Injection to Mitigate Stress Corrosion Cracking of Structural Materials in Boiling Water Reactors, (I) Temperature Dependence of Hydrazine Reactions," Journal of Nuclear Science Technology, Vol.43, pp.65 (2006).
- [8] Sunaryo G.R. and Domae M., "Numerical Simulation on Effect of Methanol Addition on Coolant Radiolysis in Pressurized Water Reactor", Journal of Nuclear Science and Technology, Vol.45, Issue 12, pp.1261-1274 (2008).
- [9] Ishigure K., et al., "Radiolysis of High Temperature Water," Radiation Physical Chemistry, Vol.46, Issue 557, pp. 4-6 (1995).
- [10] Elliot A.J. and Bartels D.M., "The Reaction Set, Rate Constants and *G*-Values for the Simulation of the Radiolysis of Light Water Over the Range 20° to 350 °C Based On Information Available in 2008", Report AECL No.: 153-127160-450-001, Chalk River (Ontario), Atomic Energy of Canada Ltd. (2009).

Conference Paper

Analysis on the Change in Neutronic Parameters Due to Mispositioning of Fuel in the AP1000 Core

J. Susilo, I. Kuntoro, T.M. Sembiring

Center for Nuclear Reactor Technology and Safety - BATAN, Kawasan PUSPISTEK Gd. No.80, Setu, Tangerang Selatan, 15310

Abstract

AP1000 on the first cycle operation uses three types of UO₂ fuel enrichments that are 2.35 w/o, 3.40 w/o and 4.50 w/o. To compensate excess reactivity, AP1000 uses an Integrated Fuel Burnable Absorber (IFBA) and a PYREX absorber as additional compensator to the boric solution in the moderator. IFBA is a burnable absorber made from ZrB₂ which is integrated into the UO₂ fuel. Human errors, such as fuel misposition, could happen when operators load fuel assemblies into the reactor core. For evaluating the design performance of AP1000, analysis on the change of neutronic parameters due to this fuel mispositioning need to be done. Analysis was performed on the reactor at hot zero power condition (HZP), beginning of cycle (BOC), and zero xenon condition with several cases of mispositioning between two adjacent fuels. Neutronic parameters, mainly the k-eff and power factor distribution will be derived from SRAC2006 computer code module of CITATION. One of the inputs required is fuel lattice macroscopic cross-section data, which are generated by PIJ module. These calculations performed condensation energy group of 107 into 10 groups with JENDL - 3.3 library cross section data. From the analysis, it can be concluded that misposition of the fuel in the first cycle of AP1000 core will result in very small change to the neutronic parameters. This very small change cannot reduce the performance of the core.

Corresponding Author:
J. Susilo,
email: shushilo@batan.go.id

Received: 29 July 2016
Accepted: 21 August 2016
Published: 21 September 2016

Publishing services
provided by Knowledge E

Keywords: Fuel mispositioning, neutronic parameter, AP1000

© J. Susilo. et al. This article is distributed under the terms of the [Creative Commons Attribution License](#), which permits unrestricted use and redistribution provided that the original author and source are credited.

Selection and Peer-review under the responsibility of the ICoNETS Conference Committee.

 OPEN ACCESS

1. Introduction

AP1000 is a pressurized water reactor (PWR) that can produce a nominal power of 1154 MWe (3415 MWth). The reactor is designed by Westinghouse Co. based on the performance of the proven PWR. AP1000 reactor can be operated for 18 months for each cycle and has a life time of about 60 years. Today, AP1000 reactors are still under construction in several countries, such as Bulgaria, England, China, and U.S.A [1, 2].

In the frame of evaluation of the core safety system in National Nuclear Energy Agency (BATAN), a simulation calculation using computer code on safety design parameter of AP1000 core has been done. Some related researches that have been done are analysis on the criticality of AP1000 core [3], analysis on the coefficient reactivity of the 1000 MWe PWR [4], kinetic parameter calculation of AP1000 core [5, 6], and analysis of using mixed oxide (MOX) fuel on AP1000 core design [7, 8, 9].

At the first operation cycle, AP1000 core uses 3 type enrichments of UO₂ fuels, that are 2.35 w/o, 3.40 w/o and 4.50 w/o. To compensate the effective multiplication factor (k_{eff}) or excess reactivity in the beginning of cycle of the AP1000 core, borid acid which is dissolved in moderator, Pyrex absorber rod and Integrated Fuel Burnable Absorber (IFBA) are used. IFBA is a burnable absorber made from ZrB₂ which is integrated into UO₂ fuel, whereas Pyrex is an absorber rod made from B₂O₃ which is inserted into the guide tube [10,11]. In the core, UO₂ fuel, IFBA and Pyrex are arranged to form a configuration in such away that it can generate the neutronic parameters which meet the safety criteria, so the core configuration is safe and feasible to be operated. Figure 1 shows distribution of fuel and Pyrex layout on the quarter core of the AP1000 according to the inial design.

	H	G	F	E	D	C	B	A
8	2.35	3.40 88I 24P	2.35	3.40 88I 24P	2.35	3.40 28I 24P	2.35	4.45 88I 12P
9	3.40 88I 24P	2.35	3.40 88I 24P	2.35	3.40 88I 24P	2.35	4.45 72I 24P	4.45 88I 9P
10	2.35	3.40 88I 24P	2.35	3.40 88I 24P	2.35	3.40 28I 24P	4.45 112I	
11	3.40 88I 24P	2.35	3.40 88I 24P	2.35	3.40 44I 24P	4.45 112I	4.45 112I	
12	2.35	3.40 88I 24P	2.35	3.40 44I 24P	2.35	4.45 112I		
13	3.40 28I 23P	2.35	3.40 28I 24P	4.45 112I	4.45 112I			
14	2.35	4.45 72I 24P	4.45 112I	4.45 112I				
15	4.45 88I 12P	4.45 88I 9P						

w/o
IFBA
Pyrex

Figure 1: Fuel and Pyrex layout in a quarter core of the AP1000.

Part of UO₂ pellets are coated with absorbent material ZrB₂ (called with IFBA fuel) and the remaining are without absorbent material. Fuel assembly is composed by a 17×17 fuel arrangement with a certain ratio between the number of UO₂ to IFBA. Based on the UO₂ enrichment and number of IFBA, there will be 9 different types of fuel assemblies. Each fuel assembly with their respective positions are predetermined arranged to form the reactor core. Due to the possibility of human errors, misposition of fuel assemblies might happen when operators load thoes fuel assemblies into the core. Therefore, it is necessary to investigate the effects of those misposition to the AP1000 neutronic parameters.

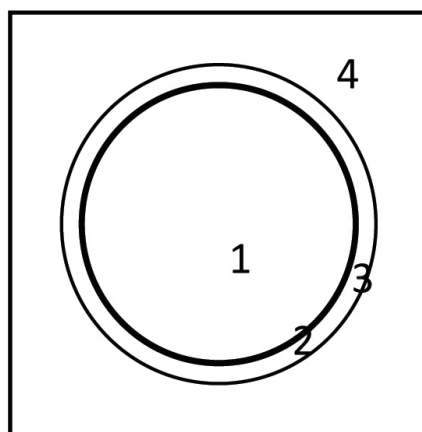
In this research, analysis of changes in the neutronic parameters of the AP1000 core due to the mispositioning of two adjacent fuels was performed. Analyze is imposed to the core at hot zero power (HWP), beginning of cycle (BOC), and zero xenon condition. Neutronic

parameters calculation was carried out by means of CITATION module of the Standard Reactor Analysis Code 2006 (SRAC2006) [12] computer code for ¼ core model in 2 dimension geometry. CITATION is a computer code, which uses diffusion theory in the multiplication factor calculation with finite different method to solve Boltzman equation. One of input data that is fuel macroscopic crosssection was prepared using PIJ module. PIJ is a computer code based on transport theory with neutron collision probability method. The CITATION module of the SRAC2006 computer code has been validated for the criticality value of conventional PWR with good results [13]. From the analysis results, it is expected to know the safety characteristics of the AP1000 core’s design.

2. Methodology

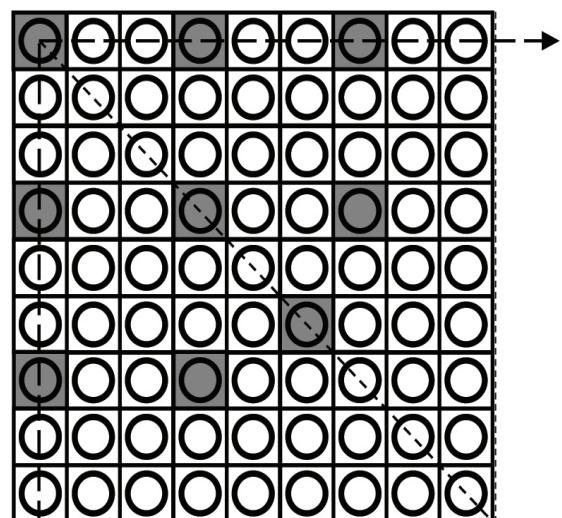
Fuel Crosssection Calculation

The homogenization macroscopic crosssection of the fuel calculation performed by PIJ module of the SRAC2006 through condensation 107 to 10 group of neutron energy. Cross section data library used in the calculation was JENDL-3.3. Input data required for those calculation is the size, dimensions and material that make up the fuel. Cross section calculations carried out on the ¼ part of the fuel lattice model in the two-dimensional geometry. Fuel lattice of the AP1000 core composed by 17×17 of fuel pin cell arrangement with water as moderator. Model of the fuel pin cell as showed at Figure 2. is composed from fuel pellets, gap, cladding and moderators in the square form with size of 1.25984 cm x 1.25984 cm. The outer part of pin cell is a moderator that consist a mixing of H₂O and boron solution with concentration of 1382 ppm. There are two sort of fuel pellet, standard UO₂ fuel and IFBA. Fuel pellets standard are UO₂ (2,35 w/o, 3,40 w/o dan 4,50 w/o) and IFBA are UO₂ fuel coated with ZrB₂. Dimension of pellet, gap of the He gas and cladding of the ZIRLO are r₁ = 0,409575 cm, r₂ = 0,426085 cm, and r₃ = 0,483235 cm, respectively. Whereas IFBA fuel is same as standard fuel which ZrB₂ coated with amount of B-10 content of 0,772 mg/cm. Composition of ZIRLO cladding are Zr 97,85 %, Fe 0,15 %, Sn 1,0 %, dan Nb 1 %.



No.1=Fuel, No.2=Gap,
No.3=Cladding, No.4=Modertor

Figure 2: Model of the fuel pin cell.



Legend: = Guide Tube Cell, = Fuel Pin Cell

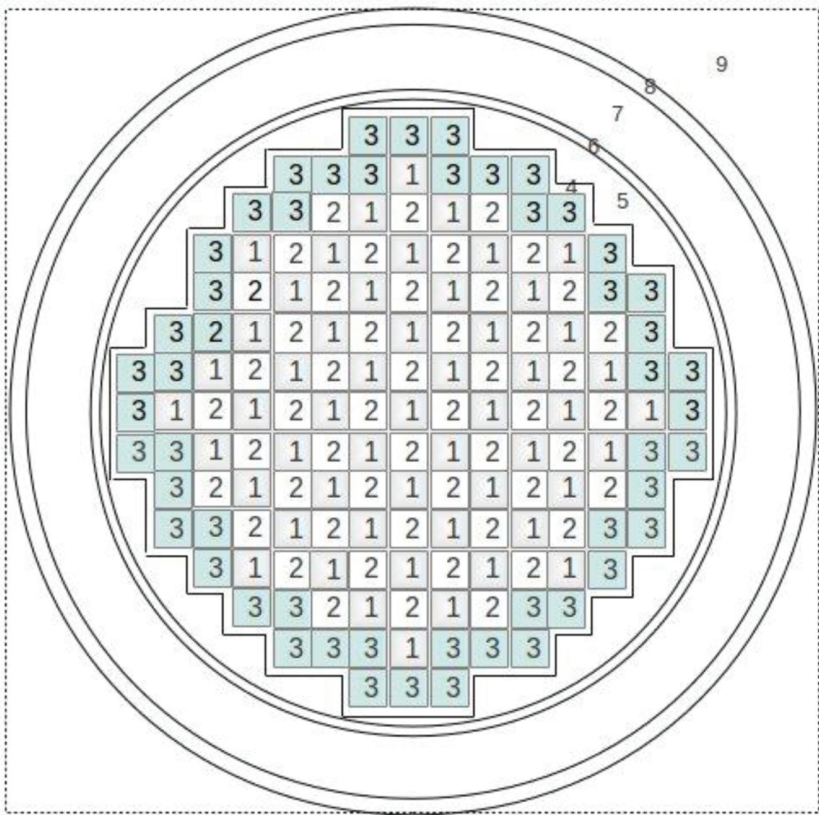
Figure 3: A Quarter geometry model of the fuel lattice.

Figure 3 shows a quarter model geometry of the fuel lattice. Whole of the fuel lattice on the AP1000 core have size 21.50364 cm × 21.50364 cm that contains 264 fuel, 25 guide tubes and with moderator H₂O. Guide tube is provided for absorber Pyrex, or Ag-In-Cd control rod, or moderator. Based on the amount of the fuel IFBA, then fuel lattice are divided into fuel lattice without IFBA, fuel lattice with 28 IFBA, 44 IFBA, 72 IFBA, 112 IFBA and 88 IFBA.

Neutronic Parameters Calculation of the AP100 Core

Neutronic parameters has been calculated for a quarter 2 dimensional geometry of AP1000 core. Input needed to core calculation using module CITATION of SRAC2006 are nuclide density of non fuel material, dimension size of the core, and homogenization macroscopic crosssection of the fuel. Output from the core calculation using CITATION are k-eff, power distribution of the fuel, prompt neutron life time and generation time, as well as delayed neutron fraction.

As shown in Figure 4, two-dimentional model geometry of the AP1000 core is built from fuel lattice of 3 type of fuel enrichment that are 2.35 w/o, 3.40 w/o dan 4.50 w/o which relates to region number 1, 2 and 3 respectively. Then, the core is surrounded by reactor baffle (no. 4), coolant (no. 5 and 7), reactor barrel (no. 6), reactor vessel (no. 8) and vacum (no. 9).



No.1,2, and 3 = Fuel Lattice 1, 2 and 3, no.4 = baffle, no.5 = coolant, no.6 = barrel, no.7 = Coolant, no.8 = reactor vessel, no.9 = Vacuum.

Figure 4: Radial core structure of the two-dimentional model AP1000 core.

Mispositioning of Two Adjacent Fuels Assumption

In this study, analysis of the neutronic parameters change due to mispositioning of two adjacent fuel has been done. Such as illustrated in Figure 5., it is assumed that mispositioning have occur of two adjacent fuel in the AP1000 core (Case 1 to 6). While the absorber rod Pyrex position was fixed, do not change from the design data. Case 1 to 6 are all located in column 8 start from the center to the edge of the core. Case 1 to 5, the mispositioning accour between UO_2 3,40 w/o 24 Pyrex 88 IFBA fuel with UO_2 2,3 w/o fuel. The mispositioning fuel in the core were G-8↔F-8, F-8↔E-8, E-8↔D-8, D-8↔C-8 and C-8↔B-8. Whereas, mispotition fuel in the case 6 was between UO_2 4,45 w/o 12 Pyrex 88 IFBA and UO_2 2,35 w/o fuel.

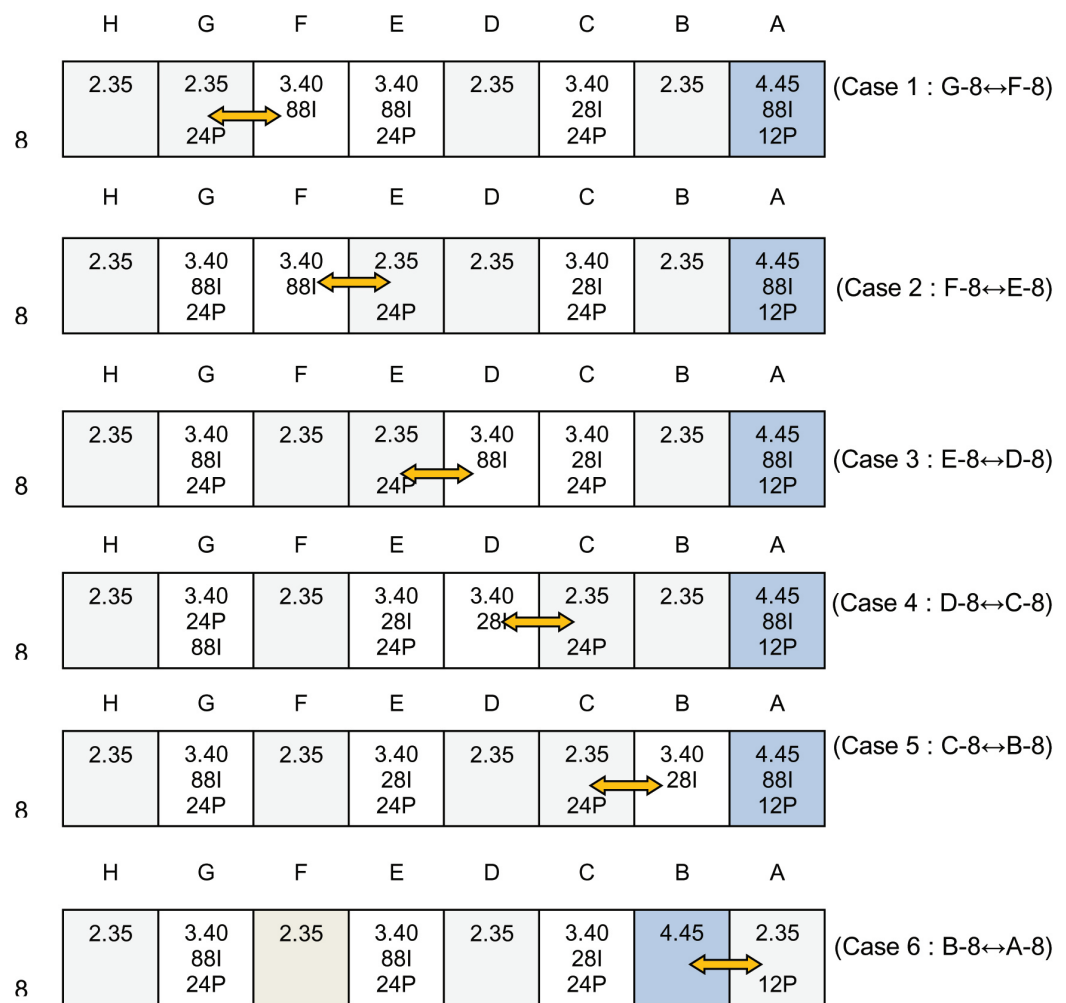


Figure 5: Misposition fuel located in column 8 of the quarter AP1000 core for case 1 to 6.

3. Results And Discussions

Change in the Effective Multiplication Factor

Calculation results of the k_{eff} value changes due to the misposition fuel of AP1000 core are shown in Table 1. The standard core that has same configuration of the fuel with design data showed that the value of k_{eff} is 1,001910. Whereas the value of k_{eff} for the first operating cycle of the AP1000 core at Hot Full Power, BOC, Zero Xenon condition in the reference data is 1,00.

Therefore, differences among calculation result with reference data is 0,001910 or 0,19%. So that, it can be said that the k_{eff} value of AP1000 core calculation result using module CITATION of the SRAC2006 computer code is about the same with references value.

TABLE 1: Change of the k_{eff} value due to the mispositioning fuel in the AP1000 core.

No	Case of AP1000 Core	k_{eff}	Change of the k_{eff} value	
			$\Delta k = k_n - k_o$	%
1	Standard Core (k_o)	1.001910	-	-
2	Case 1 (k_1)	1.004707	0.002797	0.28
3	Case 2 (k_2)	1.004228	0.002318	0.23
4	Case 3 (k_3)	1.003691	0.001791	0.18
5	Case 4 (k_4)	1.003488	0.001578	0.16
6	Case 5 (k_5)	1.004056	0.002146	0.21
7	Case 6 (k_6)	1.001718	-0.000192	-0.02

	H	G	F	E	D	C	B	A
8	1.279 1.192 0.049 (3.81)	1.154 1.081 0.026 (2.28)	1.268 1.198 0.042 (335)	1.137 1.097 0.018 (1.60)	1.254 1.246 0.037 (2.92)	1.161 1.198 0.038 (3.31)	0.957 1,006 0.069 (7.16)	0.541 0.580 0.020 (3.76)
9	1.154 1.081 0.026 (2.28)	1.273 1.194 0.045 (3.52)	1.142 1.123 0.019 (1.64)	1.250 1.218 0.032 (2.60)	1.113 1.104 0.009 (0.84)	1.168 1.123 0.045 (3.84)	0.913 0.825 0.088 (9.63)	0.436 0.406 0.030 (6.97)
10	1.268 1.226 0.042 (3.33)	1.142 1.123 0.019 (1.63)	1.250 1.221 0.029 (2.35)	1.111 1.114 -0.003 (-0.26)	1.203 1.204 -0.001 (-0.07)	1.026 1.033 -0.007 (-0.65)	0.815 0.798 (0.017) (2.13)	
11	1.137 1.119 0.018 (1.55)	1.250 1.218 0.032 (2.56)	1.111 1.114 -0.003 (-0.28)	1.193 1.201 -0.008 (-0.71)	1.033 1.071 -0.038 (-3.69)	1.041 1.105 -0,064 (-6,18)	0.561 0.581 -0.020 -3.52	
12	1.254 1.218 0.036 (2.83)	1.113 1.104 0.009 (0.77)	1.203 1.205 -0.002 (-0.13)	1.033 1.071 -0.038 (-3.69)	0.859 0.888 -0.029 -3.43	0.630 0.680 -0.050 (-7.94)		
13	1.161 1.124 0.037 (3.15)	1.168 1.125 0.043 (3.72)	1.026 1.034 -0.008 (-0.78)	1.041 1.106 (-0.065) (-6.25)	0.630 0.680 -0.050 (-7.98)			
14	0.957 0.891 0.066 (6.92)	0.913 0.827 0.086 9.43	0.815 0.799 0.016 (1.98)	0.561 0.581 -0.020 (-3.62)				
15	0.541 0.524 0.017 (3.15)	0.436 0.408 0.028 (6.40)						

Reference Value (p_{ref})
 Standard Core (p_{std})
 Differences ($p_{ref} - p_{std}$)
 Differences (%)

Figure 6: Comparison calculation result and reference value of power factor distribution of the 1/4 AP1000 core at hot full power, BOC, zero xenon condition.

From this table it can also be known that except case 6, mispositioning of the fuel in the AP100 core cause a small increment in the value of k_{eff} . As it is known that in the case 1 to 5 mispositioning of fuel occurred between UO_2 3.40 w/o 88 IFBA fuel with UO_2 2.35 w/o fuel with each position are F-8 \leftrightarrow E-8, E-8 \leftrightarrow D-8, D-8 \leftrightarrow C-8 and C-8 \leftrightarrow B-8, respectively. It causes the location of 2 absorber Pyrex and IFBA are separated with different grid position. While in the initial design, 2 absorber Pyrex and IFBA located on the same grid position.

	H	G	F	E	D	C	B	A
8	1.130	0.914	1.144	1.043	1.239	1.209	1.022	0.59
	1.148	1.014	1.147	0.947	1.224	1.191	1.009	0.58
	1.200	1.080	1.178	0.941	1.179	1.105	0.957	0.55
	1.254	1.123	1.197	1.002	1.051	0.769	0.776	0.45
	1.260	1.131	1.214	1.045	1.070	0.771	0.750	0.41
	1.169	1.063	1.189	1.108	1.293	1.278	1.320	0.49
9	1.028	1.138	1.019	1.173	1.102	1.204	0.962	0.45
	1.051	1.151	1.021	1.167	1.086	1.189	0.950	0.45
	1.092	1.199	1.068	1.162	1.028	1.129	0.905	0.43
	1.143	1.248	1.094	1.139	0.947	0.970	0.759	0.36
	1.147	1.255	1.105	1.164	0.982	0.970	0.722	0.34
	1.059	1.173	1.074	1.212	1.138	1.265	1.012	0.48
10	1.174	1.062	1.174	1.073	1.199	1.042	0.818	
	1.189	1.073	1.177	1.068	1.188	1.032	0.810	
	1.222	1.101	1.197	1.065	1.163	0.998	0.780	
	1.283	1.150	1.232	1.065	1.115	0.918	0.698	
	1.285	1.153	1.238	1.075	1.124	0.917	0.689	
	1.170	1.061	1.176	1.077	1.210	1.064	0.843	
11	1.102	1.210	1.086	1.180	1.035	1.048	0.554	
	1.110	1.217	1.089	1.179	1.030	1.041	0.549	
	1.131	1.238	1.100	1.179	1.018	1.019	0.534	
	1.195	1.303	1.143	1.200	1.007	0.979	0.501	
	1.193	1.302	1.144	1.202	1.009	0.978	0.498	
	1.067	1.173	1.057	1.155	1.022	1.046	0.558	
12	1.274	1.129	1.217	1.042	0.849	0.632		
	1.281	1.134	1.220	1.043	0.847	0.629		
	1.299	1.149	1.232	1.046	0.843	0.621		
	1.382	1.218	1.294	1.082	0.854	0.614		
	1.377	1.214	1.291	1.081	0.854	0.613		
	1.208	1.072	1.161	1.001	0.823	0.620		
13	1.238	1.230	1.060	1.060	0.635			
	1.243	1.235	1.063	1.062	0.636			
	1.259	1.250	1.073	1.068	0.636			
	1.346	1.333	1.135	1.119	0.657			
	1.339	1.326	1.130	1.116	0.656			
	1.159	1.153	0.998	1.004	0.607			
14	1.046	0.983	0.832	0.561				
	1.050	0.987	0.836	0.563				
	1.063	0.998	0.844	0.567				
	1.140	1.069	0.898	0.599				
	1.134	1.063	0.894	0.597				
	0.972	0.915	0.778	0.528				
15	0.607	0.471						Case 1 (p ₁)
	0.610	0.473						Case 2 (p ₂)
	0.617	0.478						Case 3 (p ₃)
	0.663	0.514						Case 4 (p ₄)
	0.659	0.510						Case 5 (p ₅)
	0.562	0.436						Case 6 (p ₆)

Figure 7: Power Factor Distribution in the 1/4 AP1000 Core for Case 1 to 6 in Term of The Misspositioning Fuel at Hot Full Power, BOC, Zero Xenon Condition.

Therefore, it would result in a decrease in thermal neutron absorption. Furthermore it will increase the value of thermal neutron utilization factor which by, then, rising k_{eff} value of the core. The biggest k_{eff} value changes due to mispositioning fuel in the core is 0.002797 or approximately 0.28%, that is for the case 1 (G-8 ↔ F-8). This is caused by the UO₂ fuel with 2.35 w/o enrichment without absorber material IFBA moved its position to the centre of the core. So due to the influence of the interaction of neutrons produced by the two fuel UO₂ 2.35 w/o in the centre of core resulting the increase of the neutron thermal utilization. While the case 6, mispositioning of the fuel occurs in the outer position of the core. That are mispositioning among UO₂ 2.35w/o fuel (A-8) with UO₂ 4.5w/o 88 IFBA fuel (B-8). In this case 6, the k_{eff} value decreases about -0.000192 (-0.02%), which is from 1.001718 to 1.001910. This is caused by the fuel with lowest enrichment (UO₂ 2.35 w/o) in outer position of the core (A-8) which also contained 12 absorber rods Pyrex. Thereby decreasing neutron thermal utilization factor and it will also decreasing of the k_{eff} value.

Power Factor Distribution

Figure 6 shows calculated power factor distribution at first cycle operation of the AP1000 at HFP, BOC, Zero Xenon conditions compared to the reference value. It shows that the maximum power factor from SRAC 2006 CITATION module calculation is 1.246 at position D-8. Whereas from the reference, its value is 1.279 and at position H-8. The difference of their maximum value is 0.033 or 2.58%. At position D-8, the reference value is 1.254 or 0.037 (2.92%) difference. The maximum differences of the power factor values are occurred at positions B-9 and G-14 which are amount to 0.088 (9.63%) and 0.086 (9.43%). The differences of the calculated and reference values can be resulted from the differences in the computer codes module and input data used by the reference.

Nevertheless, based on the power distribution, it can be said that the both results are in a good agreement. Fuel lattice with high power factor ($p_i > 1,2$) occurs at UO₂, 2.35 w/o enrichment without absorber IFBA or Pyrex. On the other hand, fuel lattice with small power factor (< 0.6) occurs for UO₂, 4.45 w/o enrichment. It is caused by its positions are in the outer part of the core that has lower neutron fluxes compared to that in the inner part. It can be concluded that the value of power factor depends besides on the enrichment also on the in-core position and the existence of absorber in the fuel as well.

Calculation results of power factor distribution for 1/4 core of the AP1000 due to fuel mispositioning case 1 to 6 is presented in Figure 7. From the table it is found that maximum power factors for case 1 to 5 occurs in the same position that is at H-12. Those values are 1.274, 1.281, 1.299, 1.382 and 1.377 consecutively. These maximum power factor values still lay below the predetermined safety limit of 1.6. The figure shows also that mispositioning of fuel causes slightly changes in power factor distribution compared to initially designed.

Prompt Neutron Parameter

Calculation results of prompt neutron lifetime and prompt neutron generation time of AP1000 core due to fuel mispositioning are illustrated in Table 2. The value of the standard core (20.7006 μ s) is slightly higher than the reference value (19.8 μ s) or about 4.5% difference. For all cases of fuel mispositioning (1 – 6), the maximum changes of prompt neutron lifetime and prompt neutron generation time are 2.35% and 2.06% that is for Case 1. In other words, mispositioning of fuel does not give any significant changes for prompt neutron lifetime and prompt neutron generation time.

TABLE 2: Change of prompt neutron lifetime (λ) and prompt neutron generation time (Λ) core AP1000 due to fuel mispositioning.

AP1000 Core	Prompt neutron lifetime, λ (ms)			Prompt neutron generation time, Λ (ms)		
	Calculation	Difference (%)		Calculation	Difference (%)	
Standard core	20.7006	-		20.6611	-	
Case 1	21.1862	0.4856	2.35%	21.0870	0.4259	2.06%
Case 2	20.9238	0.2272	1.10%	20.8357	0.1746	0.85%
Case 3	21.0300	0.3294	1.59%	20.9527	0.2916	1.41%
Case 4	20.7698	0.0693	0.33%	20.6976	0.0365	0.18%
Case 5	20.9406	0.2400	1.16%	20.8560	0.1949	0.94%
Case 6	20.6070	-0.0936	-0.45%	20.5716	-0.0895	0.43%

Delayed Neutron Parameter

Table 3 shows the comparison of calculation and reference value of the delayed neutron fraction (β_{eff}) for all 6 cases of fuel mispositioning at AP 1000 core. The design or reference value is 7.5×10^{-3} , so deviation of calculation result is 0.5759 or 7.68%. Then, it can be said that calculation of kinetics parameter using SRAC2006-CITATION give a good result.

It is also shown from the table that delayed neutron fraction (β_{eff}) of AP1000 core a very small change either up or down with maximum change of 5.02×10^{-6} or 0.073% for cases of fuel mispositioning.

TABLE 3: Change of delayed neutron fraction, β_{eff} core AP1000 due to fuel mispositioning.

AP1000 Core	Delayed neutron fraction, β_{eff}		
	Calculation	Difference (%)	
Standard core	6.92410×10^{-3}	--	-
Case 1	6.92046×10^{-3}	-3.64×10^{-6}	-0.050%
Case 2	6.92592×10^{-3}	1.82×10^{-6}	0.026%
Case 3	6.92028×10^{-3}	-3.82×10^{-6}	-0.055%
Case 4	6.92912×10^{-3}	5.02×10^{-6}	0.073%
Case 5	6.92391×10^{-3}	-1.90×10^{-7}	0.003%
Case 6	6.92342×10^{-3}	-6.80×10^{-7}	0.010%

Reference value of delayed neutron fraction, β_{eff} : 7.5×10^{-3}

4. Conclusion

Neutronic parameter analysis has been done due to the mispositioning of the fuel in the first operating cycle of the AP1000 at Hot Full Power, BOC, Zero Xenon condition. From the analysis, it can be concluded that misposition of the fuel in the AP1000 core insignificantly change the neutronic parameters, so it will not reduce the performance of the core.

5. Acknowledgement

Authors would like to say thank you to Prof. Drs. Surian Pinem, M.Si. for his priceless advice and also to the Head of the Nuclear Reactor Physic And Technology Division as well as the Director of the Center for Nuclear Reactor Technology and Safety for supporting this research.

References

- [1] Balendra Sutharshan, Meena Mutyala, Ronald P Vijuk and Alok Mishra, "Asian Nuclear Prospects 2010-The AP1000™ Reactor: Passive Safety and Modular Design-", *Journal of Energy Procedia* 00 (2010) 000-000.
- [2] W. E. Cummins, M.M. Corletti, T. L. Schulz, "Westinghouse AP1000 Advanced Passive Plant", *Proceedings of ICAPP '03*, Cordoba, Spain, May 4-7, 2003, Paper 3235
- [3] Jati Susilo and Rokhmadi, "Analysis of Criticality Parameter of AP1000 Reactor Core Using SRAC-CITATION", *Prosiding of Scientific Meeting and Presentation on Basic Research and of Nuclear Science and Technology*, Yogyakarta, 24-25 September 2013, pp. 94-102
- [4] T. M. Sembiring and S. Pinem, "Evaluation of Moderator Temperature Coefficient of Reactivity for The 1000 MW PWR Nuclear Plant", *Prosiding of National Seminar 17th Technology And Safety of NPP and Nuclear Facility*, Yogyakarta, October 1st, 2011, pp.164-174
- [5] Jati Susilo and Lily Suparlina, "Analysis of Kinetic Parameter As a Function of Burn up of the AP1000 Core", *Prosiding of National Seminar 19th Technology And Safety of NPP and Nuclear Facility*, Yogyakarta, September 24-25, 2013, pp.13-23
- [6] Tagor Malem Sembiring and Surian Pinem, "Evaluasi of Delayed Neutron Parameter of AP1000 Reactor", *Prosiding of National Seminar 18th Technology And Safety of NPP and Nuclear Facility*, September 29, 2012, pp. 67-75
- [7] Tukiran Surbakti, "Optimization of MOX Fuel for Core Design of AP1000 Reactor", *Prosiding of National Seminar 19th Technology And Safety of NPP and Nuclear Facility*, Yogyakarta, September 24-25, 2013, pp. 23-34
- [8] Rokhmadi, "Analisis of Control Rod Reactivity on The PWR AP1000 Design Fueled MOX", *Prosiding of National Seminar 19th Technology And Safety of NPP and Nuclear Facility*, Yogyakarta, September 24-25, 2013, pp.34-45
- [9] Tukiran Surbakti, "Evaluation of Kinetic Parameter for The Safety of The AP1000 Core Used MOX Fuel", *Prosiding of National Seminar 20th Technology And Safety of NPP and Nuclear Facility*, Pontianak, June 19, 2014, pp.859-868
- [10] Anonim, "AP1000 Design Control Document Chapter 4", from:http://www.nrc.gov/reactors/new-reactors/design-cert/ap1000/dcd/Tier%202/Chapter%204/4-1_r14.pdf, January 20, 2012
- [11] T. L. Schulz, "Westinghouse AP1000 advanced passive plant", *Journal of Nuclear Engineering and Design* 236 (2006), pp. 1547-1557.
- [12] Keisuke Okumura, Teruhiko Kugo, Kunio Kaneko and Keichiro Tsuchihashi, "SRAC2006; A Comprehensive Neutronics Calculation Code System", *JAERI-Data/Code 2007-004*, Japan Atomic Energy Agency, January 2007
- [13] Jati Susilo, " Verification of MVP-II and SRACo6 Code for the Case VERA Benchmark Reactor Core", *Journal TDM Vol.16, No.2*, June 2014, ISSN 1411-240X, No. Accreditation: 402/AU2/P2MI-LIPI/04/2012, pp.75-88

Conference Paper

Analysis of Doppler Reactivity Coefficient on the Typical PWR-1000 Reactor with Mox Fuel

Rokhmadi, Suwoto, Zuhair

Center for Nuclear Reactor Technology and Safety (PTKRN) - BATAN, PUSPIPTEK Area, Building No. 8o, Serpong, Tangerang Selatan, 15310

Abstract

Doppler coefficient is defined as a relation between fuel temperature changes and reactivity changes in the nuclear reactor core. Doppler reactivity coefficient needs to be known because of its relation to the safety of reactor operation. This study is intended to determine the safety level of the typical PWR-1000 core by calculating the Doppler reactivity coefficient in the core with UO_2 and MOX fuels. The typical PWR-1000 core is similar to the PWR AP1000 core designed by Westinghouse but without Integrated Fuel Burnable Absorber (IFBA) and Pyrex. Inside the core, there are UO_2 fuel elements with 3.40 % and 4.45 % enrichment, and MOX fuel elements with 0.2 % enrichment. By its own way, the presence of Plutonium in the MOX fuel will contribute to the change in core reactivity. The calculation was conducted using MCNPX code with the ENDF/B- VII nuclear data. The reactivity change was investigated at various temperatures. The calculation results show that the core reactivity coefficient of both UO_2 and MOX fuel are negative, so that the reactor is operated safely.

Corresponding Author:
Rokhmadi,
email: rokh_rsg@batan.go.idReceived: 29 July 2016
Accepted: 21 August 2016
Published: 21 September 2016Publishing services
provided by Knowledge E

© Rokhmadi. et al. This article is distributed under the terms of the [Creative Commons Attribution License](#), which permits unrestricted use and redistribution provided that the original author and source are credited.

Selection and Peer-review under the responsibility of the ICoNETS Conference Committee.

 OPEN ACCESS**Keywords:** Typical PWR-1000 core, MOX, Doppler reactivity coefficient, MCNPX, ENDF/B-VII

1. Introduction

Mixed oxide fuel, composing MOX, PUO_2 and UO_2 [1], is a mixture of plutonium and natural uranium or depleted uranium, which is almost similar with the enrichment of uranium used in the most of nuclear reactors. MOX fuel can be an alternative uranium fuel with low enrichment in light water reactors (LWRs). Most commercial nuclear power plants (NPPs) are of LWR type. In NPPs, about 10% of the used fuel are produced and can be used as a large number of MOX source in the world [2]. During operation, an increase in fuel temperature will cause a decrease in thermal conductivity of the fuel pellets [3-5], causing a slow down of heat flow due to fission reactions. That will result in change of absorption cross section of U-233, U-235 and Pu-239, so that at the end the reactivity will change following the temperature change. Due to the smaller thermal conductivity of MOX fuel than the UO_2 fuel, a same temperature change will result in a different Doppler reactivity coefficient among those fuels.

Fuel temperature reactivity coefficient, or better known as the Doppler reactivity coefficient, is an important parameter and a dominant factor to achieve the safe operation of the reactor by controlling the reactivity transients. The Doppler reactivity coefficient

is part of the coefficient reactivity feedback, together with the moderator temperature and density coefficient, which are designed to be negative for reactor control purpose. When the fuel or moderator temperature increase due to the increase in reactor power, the negative feedback will decrease the reactivity automatically, so that the reactor is still in safe condition. This characteristic is known as the reactor inherent safety.

The Doppler effect and the isotope U-238 ensure the negative reactivity coefficient at the beginning of the cycle (BOC) of the reactor. However, the accumulation of P-239 due to the burn up can lead to the positive reactivity or an increase in the Doppler reactivity. The existence of plutonium in the MOX fuel needs a special attention because of the shifting towards a broader spectrum of the core and the possibility of the positive reactivity coefficient [6]. The Doppler reactivity coefficient is defined as fractional change in reactivity caused by changes in fuel temperature. This coefficient is considered more important than the moderator reactivity coefficient because an increased fuel temperature is followed immediately by an increase in reactor power. The main effect is due to the Doppler reactivity resonance capture of U-238 fission and absorption ratio changes due to changes in fuel temperature [7, 8].

This paper presents the effect of the MOX fuel in a typical PWR-1000. The typical PWR-1000 is a pressurized water reactor (PWR) reactor type similar to the AP-1000 without the use of 104 Integrated Fuel Burnable Absorber (IFBA) and pyrex. The purpose of the research is to determine the effect of MOX fuel to the Doppler reactivity coefficient of the typical PWR-1000 reactor core. The research was performed using the Monte Carlo MCNPX transport program [9] to calculate the MOX fuel assemblies in the typical PWR-1000 reactor core. During that process, a Nuclear Data Library continuous energy dependent temperature of ENDF/B-VII [10] files was generated using NJOY99 code for the whole calculation. The results of the MOX fuel has been compared with the calculation of a standard UO_2 fuel also loaded in the typical PWR-1000.

2. Description of the Typical PWR-1000 Reactor

The PWR-1000 typical reactor core is designed to produce power output of 1000 MWe or 3400 MWth from the 157 UO_2 fuel assemblies. Each fuel assembly is arranged by 17×17 elements, consisting of 264 fuels rod and 25 guide tubes. The number of control rod assemblies in the core are 69 pieces consisting of 53 pieces of rod cluster control assembly (RCCA) and 16 pieces of gray rod control assembly (GRCA) [11]. Table 1 shows the design parameters and the description of the reactor core.

The core as shown in Figure 1 is surrounded by a single row of reflector assemblies of the same width as the fuel assembly containing 2.50 cm thick baffle (Fe-Cr-Ni-Mn). The outer radial boundary condition is vacuum. Each fuel assembly consists of 17×17 square pin cell lattice as shown in Figure 2. The pin cell pitch equals to 1.26 corresponding to an assembly width of 21.42 cm, which is located at the highest worth regions in the vicinity of the guide tube. Their purpose is to compensate excess reactivity of the fresh fuel.

3. Methodology

1. Design of the MOX core :

The MOX core of the typical PWR-1000 is designed from the original UO_2 core of AP 1000 [12] by replacing the UO_2 fuel with 2.35 % enrichment with the MOX fuel, as shown in Figure 3.

TABLE 1: Desain parameters of typical PWR-1000 reactor [12].

Parameter	Value
Power of reactor:	
Thermal power, MWth	3400
Electric power, MWe	1117
Active core:	
High of fuel active on first core, cm	426,7
Equivalen diameter, cm	304
Fuel assembly (FA):	
arrangement one perangkat	17×17
Number of FA on core	157
Fuel material	UO ₂ (<i>sintered</i>)
Enrichment of ²³⁵ U, w%	2,35; 3,40 dan 4,45
Enrichment of MOX, w%	2
Number of fuel <i>rod</i>	264
Number of guide tube/ <i>instrument guide thimbles</i>	24/1
Structure of core:	
Material of core <i>barrel</i>	SS304
Diameter of core <i>barrel</i> , ID/OD, cm	339,72 / 349,88
Material of <i>baffle</i>	SS304
Thickness of <i>baffle</i> , cm	2,2
Fuel UO ₂ :	
rod (<i>pitch</i>), cm	0,81915
Pelet diameter,cm	0,01645
Gap thickness,cm	0,0572
Cladding material	Zirlo
Guide tube:	1,123/1,224
Inner/outer diameter, cm	ZIRLO
Tube material	1,260

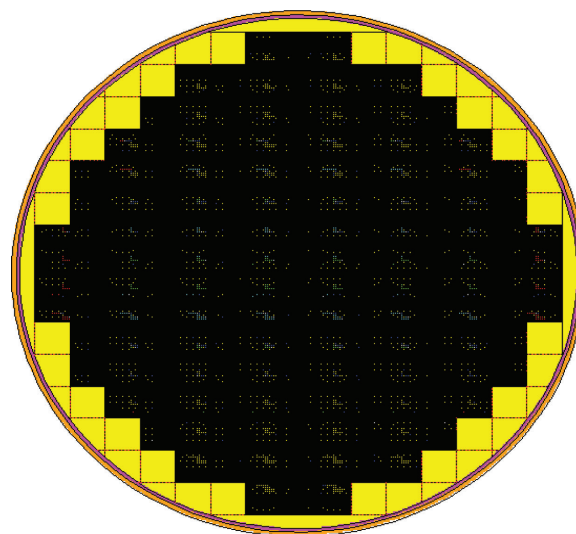


Figure 1: Typical of PWR-1000 core using VISED code.

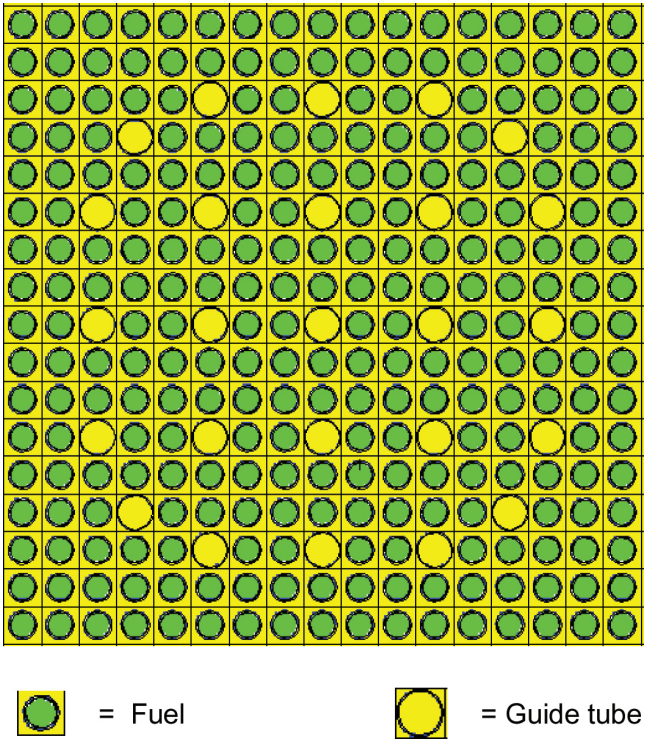
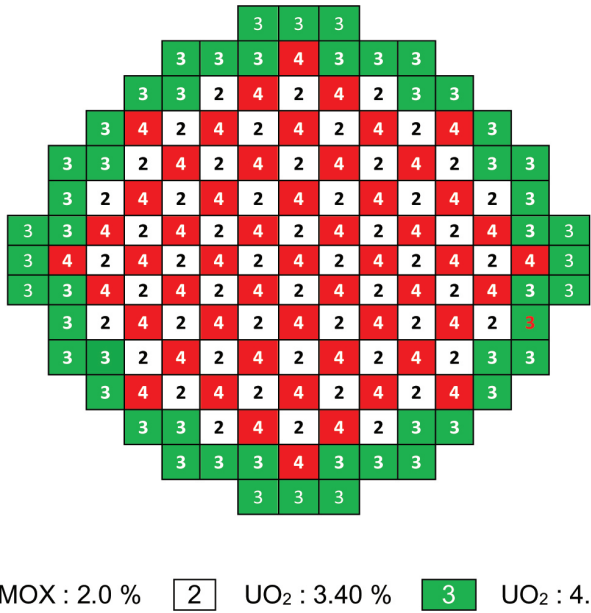


Figure 2: Fuel assembly cross section of typical PWR-1000 core (green: fuel element, yellow: guide tube).



4 MOX : 2.0 % 2 UO₂ : 3.40 % 3 UO₂ : 4.45 %

Figure 3: Design of the MOX core in the typical PWR-1000.

Based on Figure 3, the number of fuel assemblies with different fuel type and enrichment are listed in Table 2.

TABLE 2: Number of fuel assemblies in the MOX core.

Number of Fuel Assemblies		
MOX (2%)*	UO ₂ (3.40%)*	UO ₂ (4.45%)*
53	52	52

*in parenthesis is enrichment

Referring to the data from Table 1 and 2, the calculated atomic density of UO_2 and MOX fuel are shown in Table 3 and 4.

TABLE 3: Atomic Density of MOX with 2% enrichment[13-15].

No.	Nuclide	Atomic density (10^{24} atom/cm ³)
1.	U-235	3.8879e-5
2.	U-235	1.9159e-2
3.	Pu-238	8.3986e-5
4.	Pu-239	2.1706e-3
5.	Pu-240	9.9154e-4
6.	Pu-241	3.6732e-4
7.	Pu-242	2.5174e-4
8.	Am-241	1.0664e-4
9.	O-16	4.6330e-2

TABLE 4: Atomic Density of UO_2 fuel with various enrichment.

	Nuclide	Atomic Density (10^{24} atom/cm ³), enrich. (%)		
		2.35%	3.4%	4.45%
1.	U-235	1.02668e-3	1.92585e-3	1.00572e-3
2.	U-238	2.23265e-2	2.12877e-2	1.111691e-2
3.	O-16	4.67064e-2	4.64272e-2	2.42453e-2

2. Core calculation

The calculation of Doppler reactivity coefficient using MCNPX is performed step by step as follow:

1. Generation of continuous nuclear data cross section taken from ENDF/B-VII file as a function of temperature (300 K, 400 K, 500 K, 600 K, 700 K, 800 K, 900 K and 1000 K) using NJOY99 code.
2. Calculation of fuel atomic density on for UO_2 fuel with 3.40% and 5.45% enrichment and MOX fuel with 2% enrichment using the ENDF/B-VII nuclear data generated on step 1.
3. All calculation on step 1 and 2 are performed with temperature of 300 K, 400 K, 500 K, 600 K, 700 K, 800 K, 900 K and 1000 K respectively
4. Calculation of k_{eff}
5. Calculation of Doppler reactivity coefficient.

The Doppler reactivity coefficient is expressed as amount of reactivity change for a parameter change in the reactor, and defined in the following equation (1) [16]:

$$\alpha_T = \frac{(k_{eff[n]} - k_{eff[n-1]})}{(k_{eff[n]} \times k_{eff[n-1]})} \times 100\% \quad (1)$$

α_T : Doppler reactivity coefficient

$k_{eff[n]}$: k_{eff} on T temperature

$k_{eff[n-1]}$: k_{eff} on preceding T temperature

4. Result and Discussion

The core reactivity can be direct calculated after determining k_{eff} . The k_{eff} is calculated on the UO_2 and MOX core as a function of temperature respectively. The fuel temperature as the basis of calculation starts from 300 K up to 1000 K, with 100 K variation. The resulted k_{eff} calculation for UO_2 and MOX core are shown in Table 5 and depicted in Figure 3.

TABLE 5: k_{eff} calculation for UO_2 and MOX fuel.

No	Temperature (K)	k_{eff}	
		UO_2	MOX
1	300	1.41547 ± 0.00751	1.28357 ± 0.00621
2	400	1.41206 ± 0.00643	1.28314 ± 0.00829
3	500	1.40067 ± 0.00828	1.27857 ± 0.00702
4	600	1.37780 ± 0.00737	1.26473 ± 0.00779
5	700	1.37466 ± 0.00712	1.26254 ± 0.00795
6	800	1.37286 ± 0.00743	1.26135 ± 0.00764
7	900	1.37168 ± 0.00690	1.26074 ± 0.00692
8	1000	1.37021 ± 0.00601	1.25443 ± 0.00802

From Figure 4, the k_{eff} will decrease as the fuel temperature increases for the UO_2 and MOX core. In general, the k_{eff} of MOX core is lower than UO_2 core for all temperature. The results of this calculation are in good agreement with the other calculation, showing that the presence of MOX in the core will lower the k_{eff} [14]. The decrease of k_{eff} for MOX core is mainly caused by the effect of Pu-239 and Pu-241 having higher neutron absorption macroscopic (1011.3 and 1377 barn) compared to U-235 (680 barn) [2, 18].

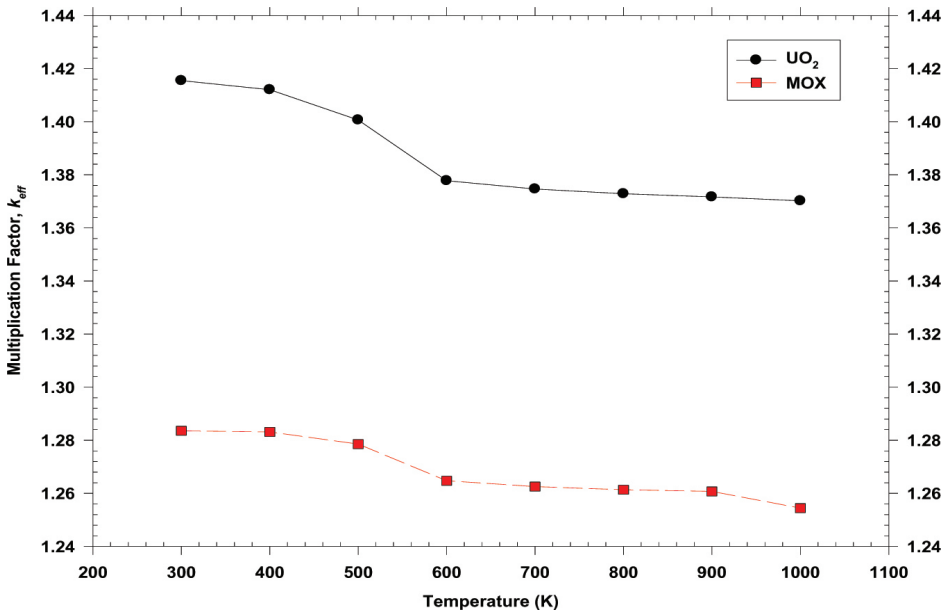


Figure 4: Relation between fuel temperature and keff in the the UO_2 and MOX core.

The effect of fuel temperature increase to decrease the k_{eff} is also caused by the increase of resonance absorption and fission capture. By referring the k_{eff} values in Table 5, the Doppler reactivity coefficient (α_T) can be determined using equation (1) as shown in Table 6 and depicted in Figure 5.

TABLE 6: Doppler reactivity coefficient α_T for UO_2 and MOX fuel.

No	Temperature (K)	α_T (pcm/K) $\times 10^{-2}$	
		UO_2	MOX
1	300 – 400	-1.71	-0.26
2	400 – 500	-5.76	-2.79
3	500 – 600	-11.90	-8.56
4	600 – 700	-1.66	-1.37
5	700 – 800	-0.95	-0.75
6	800 – 900	-0.63	-0.38
7	900 – 1000	-0.78	-3.99

Looking at Figure 5, the Doppler reactivity coefficient of the MOX and UO_2 core show a same characteristic as it decreases at temperature of 300 K – 400 K, then increases at temperatures up to 700 K, and drops again at 1000 K temperature. In overall, the Doppler reactivity coefficient of UO_2 fuels is smaller than the Doppler reactivity coefficient of MOX fuels. This phenomenon is again influenced by the presence of plutonium having a larger absorption cross section (Pu-239 = 1029 barn, Pu-241 = 1377 barn) than of uranium (U-235 = 681 barn, U-238 = 2.70 barn) [19].

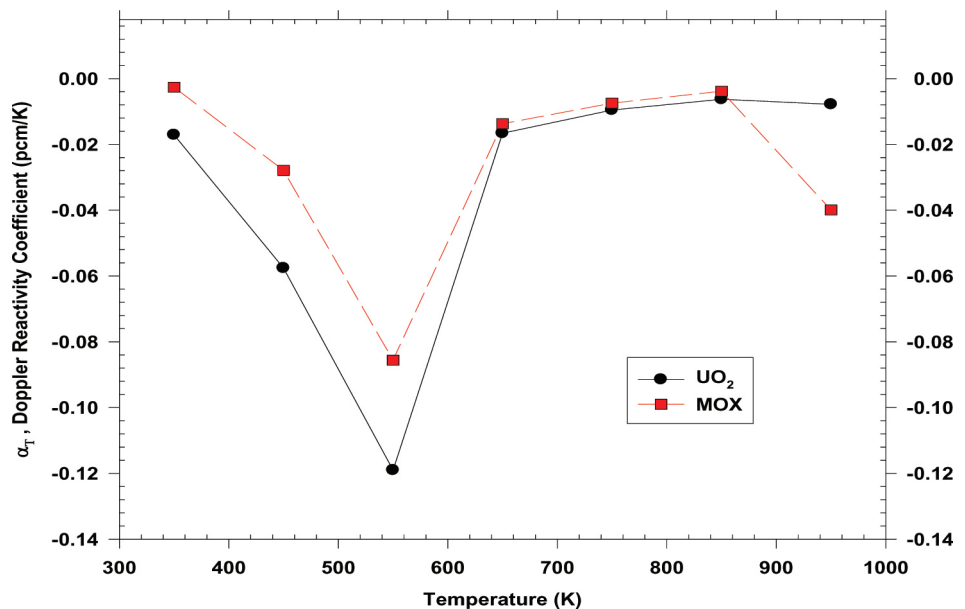


Figure 5: Relation between fuel temperature and Doppler reactivity coefficient in the the UO_2 and MOX core.

5. Conclusions

The Doppler reactivity coefficient with MOX fuel in the typical PWR-1000 reactor core has been calculated using the Monte Carlo MCNPX transport program. The results show that the Doppler reactivity coefficient decreased to a critical value as the fuel temperature increased. This is

because the presence of Pu-239 and Pu-24. Since the absorption cross section of MOX fuel is much bigger than the absorption cross section of uranium, the Doppler reactivity coefficient become negative, so that the core of typical PWR-1000 reactor core with MOX fuel is considered to be safe to be operated.

6. Acknowledgment

The authors would like to express many thanks to Division Head of Physics and Reactor Technology (BFTR) for valuable support to the writing of this paper. Moral supports from colleagues on BFTR-PTKRN are greatly appreciated.

References

- [1] SEMBIRING, TM, Analisis Pengaruh Bahan Bakar MOX Terhadap Parameter Teras Reaktor Benchmark. , J. Teknologi Reaktor Nuklir, Vol 9 No.1, Februari 2007.
- [2] MASSIH, Ali R, Model for MOX Fuel Behaviour, SKI repot 2006:10, January 2006.
- [3] STAIKU, D and BARKER, M, Thermal Conductivity of Heterogeneous LWR MOX Fuels", Journal of Nuclear Materials 442 (2013) 46–52
- [4] STAIKU, D, Thermal Conductivity of Homogeneous and Heterogeneous MOX Fuel with up to 44 MWd/kgHM Burn-up, Journal of Nuclear Materials 412 (2011) 129–137
- [5] AMAYA Masaki, NAKAMURA Jinichi, NAGASE Fumihisa, FUKETA Toyoshi, Thermal Conductivity Evaluation of High Burnup Mixed-Oxide (MOX) Fuel Pellet, Journal of Nuclear Materials 414 (2011) 303–308
- [6] TATSUMI, M, Analysis of High Moderator PWR MOX Core MISTRAL-4 with SRAC and MVP, Jurnal of Nuclear Science and Technology, Supplement 2, p 864-867, August 2002.
- [7] SEUBERT, A, et al, Solution of the Stationary State of the PWR MOX/UO₂ Core Transient Benchmark, PHISOR 2006, ANS Topical Meeting on Reactor Physics, Canadian Nuclear Society, Vencouver, September 10-14, 2006.
- [8] RIVEROLA, J, RIA Analysis for PWR at both HZP and HFP Operation and all Cycle Fuel Exposure with 3D Techniques", Proceeding of the 2004 International meeting on LWR Fuel Performance , Oriando, Florida, September 19-22, 2004
- [9] HENDRICKS, J. S., MCKINNEY, G. W., et al., MCNPX 2.6.0 Extensions, LA-UR-08-2216", Los Alamos National Laboratory, 11 April 2008
- [10] CHADWICK, M. B., OBLOZINSKY, P., HERMAN, M., et al., ENDF/B-VII: Next Generation Evaluated Nuclear Data Library for Nuclear Science and Technology, Nuclear Data Sheets, Vol. 107, pp. 2931-3060, 2006
- [11] ROKHMADI dan SEMBIRING, TM, Verifikasi Perhitungan Reaktivitas Batang Kendali Teras Reaktor PWR AP1000, Prosiding Seminar Nasional Pengembangan Energi Nuklir VI, Jakarta, 11 Juni 2013.
- [12] Westinghouse AP1000 Control Document Rev.16 [internet]. US: Westinghouse;2007. Tier 2 Chapter 4 Reactor, [cited 2010 August 3]. Available from: <http://adamswebsearch2.nrc.gov/idmws/ViewDocByAccession.asp?AccessionNumber=ML071580939>
- [13] YAMAMOTO, A, et al, Benchmark Problem Suite for Reactor Physics Study of LWR Next Generation Fuels, Journal of Nuclear Science and Technology Vol 39 No.8 p.900-912 (August 2002).

- [14] MOUSTAFA Aziz and MASSOUD Eman, Burn-up Analysis for a PWR Fuel Pin of the Next Generation, *Arab Journal of Nuclear Science and Applications*, 47(3), (93-103) 2014
- [15] KLOOSTERMAN, Program MOX A Tool for the Calculation of Nuclide Densities in MOX Fuels, NFA-ACT-95-09, December 1995
- [16] ROKHMADI, Analisis Faktor Multiplikasi Tak Hingga Bahan Bakar PWR Akibat Perubahan, Temperatur dan Data Nuklir, Prosiding Seminar Nasional Teknologi dan Keselamatan PLTN serta Fasilitas Nuklir ke13, UIN-BATAN, Jakarta 6 Nopember 2007
- [17] ROKHMADI, Analisis Reaktivitas Batang Kendali pada Desain Teras MOX PWR AP1000, Prosiding Seminar Nasional Teknologi dan Keselamatan PLTN serta Fasilitas Nuklir ke 19, Yogyakarta, 24-25 September 2013.
- [18] TUKIRAN, Menentukan Parameter Kinetik Reaktor PWR AP 600, Prosiding Laporan Tahunan P2TRR Tahun 2004.
- [19] TUKIRAN, Evaluasi Parameter Kinetik Terhadap Keselamatan Teras AP1000 Berbahan Bakar MOX, Prosiding Seminar Nasional Teknologi dan Keselamatan PLTN serta Fasilitas Nuklir ke 19, Yogyakarta, 24-25 September 2013.

Conference Paper

Sequence Analysis after Core Damage to Determine Safety Level of the AP1000


D. T. Sony Tjahyani, Deswandri

Center for Nuclear Reactor Technology and Safety – BATAN, Kawasan PUSPIITEK Gd. 80, Serpong, Tangerang Selatan 15314, Indonesia

Abstract

In safety analysis, one of important parameters is core damage as this occasion can cause fission products to release. In that regard, all possible sequences afterward must be analyzed in order to ensure that all events have been considered, because each sequence has different consequence. The objective of this research is to determine the probability of event sequences after core damage so safety level of AP1000 could be known. The AP1000 reactor is chosen as the research object because currently many units are under construction. In this research the accident sequences were analyzed by using event tree, and the probability of top event was calculated by fault tree analysis. Meanwhile, the failure rates of component or operator action were collected from IAEA documents and also published documents of the AP1000 from Westinghouse Inc. The analysis results show that probability of event sequences which causes fission product release is ranging from 10^{-2} to 10^{-26} and the total probability is $3,48 \times 10^{-2}$. Based on this analysis, it can be concluded that the AP1000 has high safety level because the probability of event sequences leading to fission product release is small. Moreover, if these results are joined with core damage probability then probability of fission product release would be less than 10^{-9} .

Keywords: safety analysis, core damage, event sequence, event tree, AP1000Corresponding Author:
D. T. Sony Tjahyani,
email: dtsony@batan.go.idReceived: 29 July 2016
Accepted: 21 August 2016
Published: 21 September 2016Publishing services
provided by Knowledge E

 D. T. Sony Tjahyani. et al. This article is distributed under the terms of the [Creative Commons Attribution License](#), which permits unrestricted use and redistribution provided that the original author and source are credited.

Selection and Peer-review under the responsibility of the ICoNETS Conference Committee.

 OPEN ACCESS

1. Introduction

Safety is the main priority in nuclear facilities, especially in power and research reactors. Therefore safety analysis to the nuclear facility design must be carried out rigorously as contained in the government regulation of Indonesia no. 54 year 2012 concerning safety and security for nuclear installation.

Based on fundamental safety principles [1], the general safety objective is to protect individuals, society, and environment from harm by establishing and maintaining in nuclear facilities effective defenses against radiological hazards. To achieve these objectives appropriate specific safety requirement is necessary and technically have three implementations. The first is to prevent accidents and to mitigate the consequences of any accidents that possibly will occur. The second is to ensure all possible accident is taken into account in the design with any risk would be minor. The third implementation is to ensure that probability of accidents with serious radiological consequences is extremely low.

There are three aspects of lessons that could be taken from the Fukushima accident [2-4]. First, it is important to develop each likely postulated initiating event in the nuclear

reactor. It would be easy to mitigate when a hypothetical event is occurred. Second, nuclear reactor which is used as energy source (Nuclear Power Plant, NPP) has complex characteristic, therefore safety design shall be provided since the beginning rather than after the accident happen. Third, all risk possibility and mitigation method shall be generally known in advance.

The fission product release to environment is a consequence of reactor existence that must get a careful attention. Fission product could be released to environment in two stages: (1) core damage and (2) containment system fail to function after the core damage happen. Therefore, these two parameters can be used as reference to find out the safety level of a light water reactor. The smaller occurrence probability means the higher level of reactor safety. There are three levels of the probabilistic safety assessment (PSA) where each has purpose in the safety analysis. Level 1 PSA is to determine core damage probability, so that it can be known the reliability level of safety system. Level 2 PSA is to establish the probability of fission product release, therefore it can find out reliability level of stage or system that issued to prevent the fission product release to the environment. Whereas level 3 PSA is to calculate risk that is accepted by public and other societal if accident happen.

The AP1000 (Advanced Passive Pressurized Water Reactor 1000) is a two-loop 3400 MWT pressurized water reactor (PWR) which is included as generation III+ and use passive system as core cooling system to prevent core damage. This reactor type is being built in some countries currently.

Several research activities related with PSA have been carried out i.e. to determine failure probability of non-safety system to prevent severe accident [5], probabilistic analysis to modify the system [6], and analysis of system failure scenario to determine severe accident probability of AP1000 [7]. As continuation of the research to determine the failure probability of AP1000 safety system, the purpose of this paper is to analyze event sequences after core damage in AP1000 by using probabilistic method. Based on this analysis, it will be known safety level of the AP1000. The analysis is done by using event tree and each probability of top event is calculated by using fault tree analysis. Failure rate of component used in calculation is based on AP1000 data that is published by Westinghouse and data from IAEA Tecdoc [8-12].

2. Level 2 PSA and Description of AP1000

To ensure that nuclear power plant is designed and operated with safe and secure, therefore it is needed safety analysis before the reactor was built as mandated on Government Regulation of Indonesia no. 2 year 2014 regarding licensing for nuclear installation and nuclear material utilization.

Probabilistic safety assessment is one of the methods that was used to the safety analysis. Within the scope of this analysis includes determining fission product release to environment if design basis accident (DBA) was occurred. It caused core damage as well as potentially release fission product. This analysis is known as level 2 PSA. The analysis is assumed that systems are included level 3 DiD (Defence in Depth) which is to overcome DBA failed. In fact, design basis accident and core damage is very small possibility.

The important insight in the level 2 PSA is to identify path of the radioactive materials released from fuel to containment that might disperse into the environment [13, 14]. Important results that will be obtained in this analysis is to prevent the accident propagation, mitigation action that is required and physical barrier that is provided. Therefore, the purpose of an evaluation of power reactor after core damage is to identify adequacy and availability these aspects. The probability of release to environment is depending on the quantity of core melt and effort to mitigation action that is done in the containment also the integrity of containment.

In the level 2 PSA is used containment event tree (CET) that is to describe accident propagation or an occurrence. The aim of analysis is to identify accident sequence which is to lead against the loss of confinement function.

AP1000 is PWR generation III+ type which all core cooling systems use passive system (passive core cooling system, PXS). These system consist of the accumulator, the core makeup tank (CMT), the passive residual heat removal system (PRHR), the automatic depressurization system (ADS), the In-containment refueling water storage tank (IRWST) and the passive containment cooling system (PCS). These systems are category of level 3 DiD that is to prevent design basis accident. Except for PCS was still needed to mitigate after core damage that is to minimize consequence [15].

The accumulator is used to inject water to the reactor core when the core pressure is low, e.g. in the event of large loss of coolant accident (LLOCA) condition. The CMT is functioned to inject water if small loss of coolant accident (SLOCA) is occurred, also other events when the core pressure is still high. The PRHR is used to remove decay and residual heat in the reactor and is operated passively. The IRWST is provided as heat sink from the PRHR. The ADS is to control pressure of the level 3 DiD systems except for the accumulator and the PCS, so these systems is operating optimally. The PCS has a function as ultimate heat sink which is operated passively. These systems diagram are illustrated in Fig. 1.

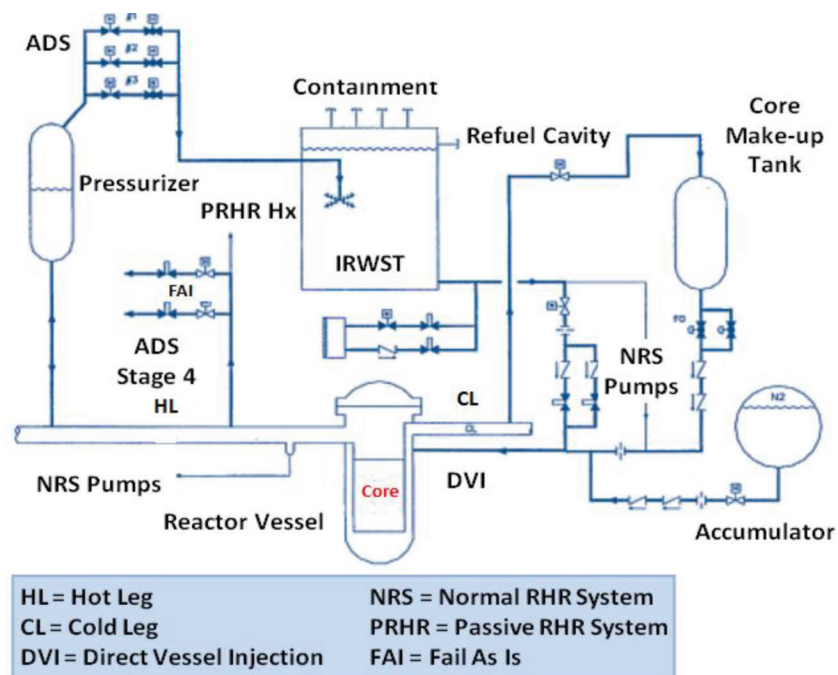


Figure 1: Diagram of AP1000 [15].

With the proper functioning of these systems, core damage is not happened caused design basis accident. However, AP1000 is strictly designed to mitigate core damage. Because core damage is significance parameter for safety level on the light water reactor. To mitigate after core damage, the operator can flood the reactor cavity as shown in Fig. 2. Water which is used for this process from IRWST. This condition will cause the lower portion of the reactor vessel become submerged. Based on an insulating structure that around the reactor vessel will configurate the water stream to reach the vessel. The water will flow around the bottom vessel head and up the vessel insulation wall annulus. In this event, to vent resulting steam from cooling the bottom

vessel from the reactor cavity, so that the reactor vessel become depressurization. This cooling process is sufficient to prevent molten core debris in the lower head caused of melting the steel vessel wall and spilling to containment. Retaining the debris in the reactor vessel provide protection the containment integrity. This process prevent severe accident phenomena, such as ex-vessel steam explosion and core-concrete interaction with molten core material.

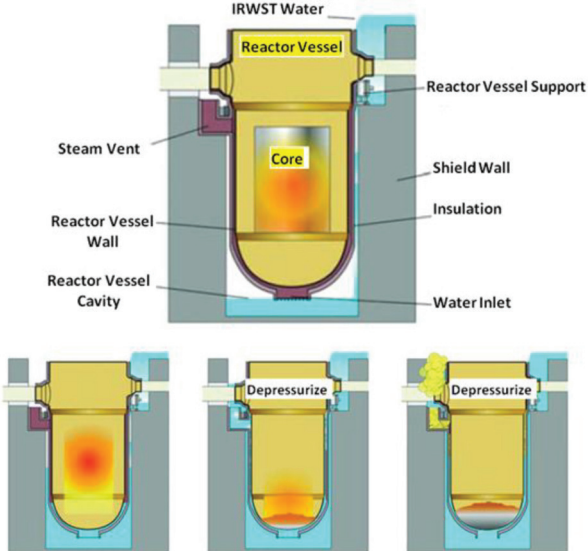


Figure 2: Cooling Phenomena on the Reactor Core Damage [16].

on the probabilistic safety assessment consider all event combination if all cooling event on the reactor vessel was failed. However based on the probabilistic theory, probability of this event is very small. Nevertheless, shall be done analysis because it have seriously consequence.

3. Methodology

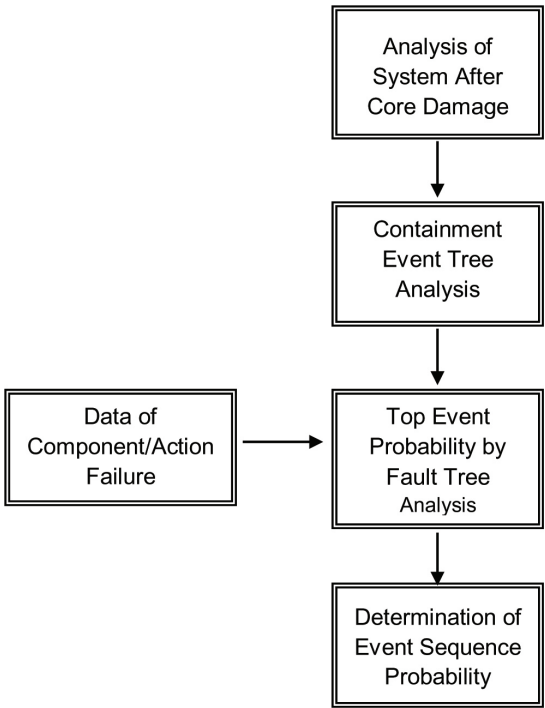


Figure 3: Analysis Stages for Calculation of Event Sequence Probability.

Analysis is carried out by constructing CET. The core melt event is assumed, several top events is selected as event sequence or event propagation by using analysis of system. The top events which is selected is to mitigate radioactive material release. Furthermore, each probability of top event is determined by using fault tree analysis. Data of component failure is adopted AP1000 data which was published and IAEA generic data [8-12]. Finally, the total probability of event sequences are calculated. Scope of event sequence analysis that is considered is based on standard mitigation system of PWR. Simply methodology diagram which is done shown in Fig. 3.

4. Result and Discussion

The analysis of system has been done and based on Fukushima accident learning, then mitigation stages which are to prevent radioactive materials release are constructed. There are ten stages that is depressurization after unroofing core (PT), Containment Isolation (IP), Reactor Cavity Flooding (PK), Core Flooding (PR), Debris drop to Cavity (DK), Containment Cooling by PCS (PC), Steam Release by Venting (PV), Containment Integrity (IS), Hydrogen Control (PH), and Fire/Explosion Control (PL). To use these top events, then it is constructed event tree as illustrated in Fig. 4. As shown in Fig. 4, there are 21 event sequences, The fission product release is not occurred in the event sequence no. 1 because all mitigations is success. The event sequence no.1 is event which is expected on the safety of power reactor. In this event, core damage is occurred but fission product is remain in the containment.

PCS is important system as shown in Fig. 4, if PCS is success, then is not needed venting and containment integrity, because cooling process is continuity, so the core damage process are not sustained. In this event would be more better if hydrogen control is success, so that it is not required fire/explosion control (event sequence no. 1, 6, 10, and 15). The PCS system is similar with containment spray (CS) on the PWR generation II that is to cool the containment and to deposition fission product. The difference is PCS including passive system so it can be operated without electric power supply, whereas CS is active system.

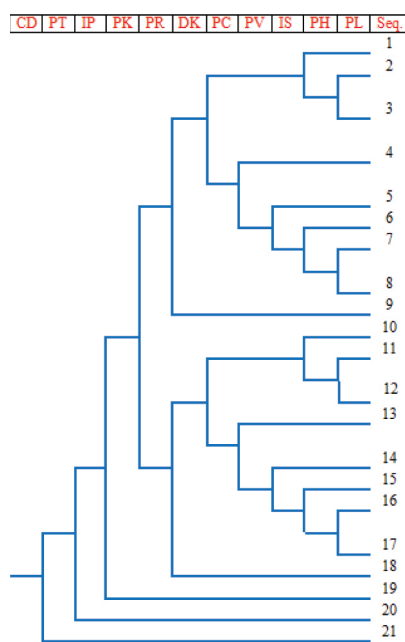


Figure 4: Containment Event Tree.

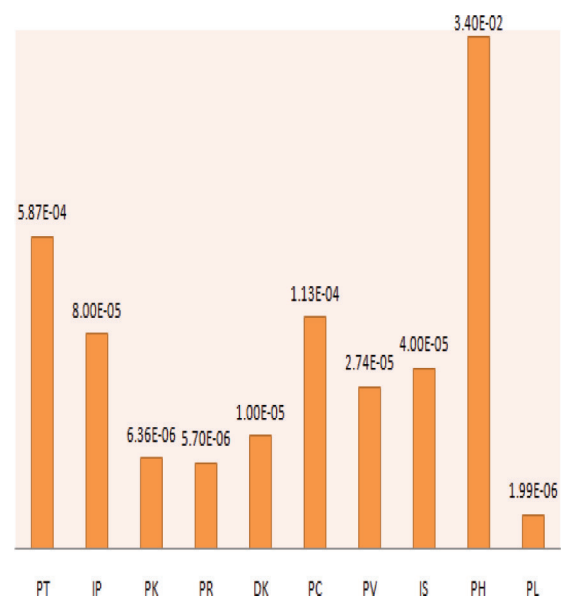


Figure 5: Probability of Top Events.

If PCS failed and then temperature will rise. In this event, pressure will increase or will be possibility produced hydrogen, then venting shall operate. If this mitigation is success, then it is not needed containment integrity, hydrogen control, and fire/explosion control (event sequence no. 4 and 13). If venting system is fail, then prevention of fission product release is depended on containment integrity, hydrogen control and explosion control (event sequence no. 5, 6, 7, 8, 14, 15, 16 and 17).

Result of event tree analysis also show if debris is not entered to reactor cavity, then PCS, hydrogen control and explosion control become not function (event sequence no 9 and 18), so it have possibility to be released fission product to environment.

Fig. 4 also show three probability of top events shall be very small that is depressurization, containment isolation, reactor cavity flooding (sequence no. 19, 20 and 21). In this case, there are not other event that can mitigate if these systems failed. If it be compared with PWR generation II, reactor cavity only seen at the PWR generation III*. This system is to contain debris or core melting.

By using fault tree analysis, probability of top event is shown in Figure 5. Failure probability of top events is enough small that is 10^{-2} to 10^{-6} because each probability of system will be multiplied with the other system or actions, so become the event sequence.

Calculation of event sequence probability is presented in Table 1. Table 1 show that the probability of event is generally small that is 10^{-2} to 10^{-26} . It means mitigation system of AP1000 could confine fission product after core damage occurred.

Probability of each sequence is not linear with quantity of fission product release or consequence. It means large probability of event sequence do not always release large quantity of fission product, so also on the contrary.

Probability of event sequence no. 2 is largest that is 3.40×10^{-2} , but quantity of the fission product released is small. In this case, all top events which assumed is success, only the hydrogen control fail. However the explosion/fire control is not occurred because fire control is success so that quantity of fission product release is small.

Probability of event sequence no. 17 is smallest that is 4.77×10^{-26} . Nevertheless if observed on this sequence, there are failure for six top events (PR, PC, PV, IS, PH and PL), then quantity of the fission product release is large. In this event, because of core unflowing so core damage is occurred. Hereafter, it is followed failure of PCS. It means core is not happened cooling process, so possibility core damage continued. Moreover, this condition is initiated with failure of venting system, then pressure and temperature increased and core damage become seriously. In this scenario, containment integrity also fail, and amount of hydrogen that is produced from core damage phenomena is increasing because hydrogen control also fail. In this event, it will initiate fire or explosion occurrence because fire or explosion control also fail. To determine quantity of each sequence is required comprehensively analysis especially deterministic analysis.

Table 1 and Fig. 4 show probability of three event sequences (no. 19, 20 and 21) that are 10^{-4} to 10^{-6} . These sequences require attention that are PT, IP and PK. If three top events is happened, then the other top events are not significantly function to prevent continually core damage and it might happen fission product release with large quantity.

Based on Table 1, quantitative of fission product release can be distinguished three levels that are minor, intermediate and major. For example, event sequence no. 2 as minor level, event sequence no. 4 as intermediate level and event sequence no. 17 as major level. To clasify all event sequences, it is required deterministic analysis with including physical phenomena for each sequence.

TABLE 1: Probability of Event Sequence.

No. Sequence	Probability
1	$9,65 \times 10^{-1}$
2	$3,40 \times 10^{-2}$
3	$6,76 \times 10^{-8}$
4	$1,13 \times 10^{-4}$
5	$3,09 \times 10^{-9}$
6	$1,20 \times 10^{-13}$
7	$4,20 \times 10^{-15}$
8	$8,37 \times 10^{-21}$
9	$9,99 \times 10^{-6}$
10	$5,50 \times 10^{-6}$
11	$1,94 \times 10^{-7}$
12	$3,85 \times 10^{-13}$
13	$6,44 \times 10^{-10}$
14	$1,76 \times 10^{-14}$
15	$6,81 \times 10^{-19}$
16	$2,40 \times 10^{-20}$
17	$4,77 \times 10^{-26}$
18	$5,70 \times 10^{-11}$
19	$6,36 \times 10^{-6}$
20	$8,00 \times 10^{-5}$
21	$5,87 \times 10^{-4}$

The total probability which have consequence (minor, intermediate and major) is 3.48×10^{-2} , if the event sequence no. 1 is omitted because no consequence. Hereinafter, If the probability of sequence no. 2 is compared with the total probability, then contribution of event sequence no. 2 is 97.69 % to the total probability. It means the contribution of other event sequences is very small. If the event sequence no. 19, 20 and 21 are assumed as important event sequences, then contribution of these event is enough small that is 1.94 % to the total probability. However on the probabilistic analysis, the event sequence which has small probability is not ignored, because each the event sequence has different consequences.

Analysis results show that the safety level of AP1000 is adequate high, because each probability of the event sequence is enough small. Furthermore, this result will be smaller, because each probability of event sequence is multiplied by core damage frequency which is about 10^{-7} . Therefore, possibility of fission product release to environment is very small which is about 10^{-9} . Based on INSAG, criteria of fission product release for power reactor generation III+ is small than 10^{-7} . This result show that the safety target of AP1000 is above IAEA criteria.

To achieve result which is more valid, it is needed more intensely research especially to determine probability of component failure on the severe accident condition.

Conclusion

Based on sequence analysis after core damage, It could be conclusion that safety level of AP1000 is adequate high because each probability of event sequence is 10^{-2} to 10^{-26} . Furthermore, probability of fission product release to environment is less than 10^{-9} , if it is joined to core damage frequency.

References

- [1] IAEA-SSR-2/1, "Safety of Nuclear Power Plant: Design, IAEA, Vienna (2012).
- [2] Rangel L. E., Leveque F., "How Fukushima Dai-ichi core Meltdown Changed the Probability of Nuclear Accidents?", *Safety Science*, Vol.64, pp.90-98 (2014).
- [3] Labib A., Harris M. J., "Learning How to Learn from Failures: The Fukushima Nuclear Disaster, *Engineering Failure Analysis*, Vol.47, Part A, pp.117-125 (2015).
- [4] Alvarenga M.A.R.B., Frutuoso e Melo P.F., "Including Severe Accidents in the Design Basis of Nuclear Power Plants: An Organizational Factors Perspective After the Fukushima Accident", *Annals of Nuclear Energy*, Vol.79, pp.68-77 (2015).
- [5] Sony Tjahyani, D. T., "Analisis Keandalan Sistem Non-Keselamatan Dalam Memperkecil Probabilitas Kecelakaan Parah AP1000", *Prosiding Seminar Nasional Pengembangan Energi Nuklir VI*, Jakarta (2013).
- [6] Sony Tjahyani, D. T., "Analisis Probabilistik Terhadap Modifikasi Sistem Untuk Meningkatkan Keselamatan Pada Reaktor Daya AP1000", *Prosiding Pertemuan dan Presentasi Ilmiah Penelitian Dasar Ilmu Pengetahuan dan Teknologi Nuklir*, Yogyakarta (2013).
- [7] Sony Tjahyani, D. T., dkk., "Analisis Skenario Kegagalan Sistem Untuk Menentukan Probabilitas Kecelakaan Parah AP1000 ", *Jurnal Teknologi Reaktor Nuklir Tri Dasa Mega*, Vol.16, No.3, pp.134-148 (2014).
- [8] Volkanovski A., "Impact of Component Unavailability Uncertainty on Safety Systems Unavailability", *Nuclear Engineering and Design*, Vol.283, pp.193-201 (2015).
- [9] Hashim M., Hidekazu Y., Takeshi M., Ming Y., "Application Case Study of AP1000 Automatic Depressurization System (ADS) for Reliability Evaluation by GO-FLOW Methodology", *Nuclear Engineering and Design*, Vol.278, pp.209-221 (2014).
- [10] Yu Y., Wang S., Niu F., "Analysis of Common Cause Failure Effect on System Reliability in Seismic PSA, *Progress in Nuclear Energy*, Vol.75, pp.158-167 (2014).
- [11] Kancev D., Cepin M., Gjorgiev B., "Development and Application of a Living Probabilistic Safety Assessment Tool: Multi-objective Multi-dimensional Optimization of Surveillance Requirements in NPPs Considering Their Ageing", *Reliability Engineering and System Safety*, Vol.131, pp.135-147 (2014).
- [12] Kamyab S., Nematollahi M., "Performance Evaluating of the AP1000 Passive Safety Systems for Mitigation of Small Break Loss of Coolant Accident Using Risk Assessment tool-II Software", *Nuclear Engineering and Design*, Vol.253, pp.32-40 (2012).
- [13] Ahn S. K., Kim I. S., Oh K. M., "Deterministic and Risk-informed Approaches for Safety Analysis of Advanced Reactors: Part 1, Deterministic Approaches", *Reliability Engineering and System Safety*, Vol.95, pp.451-458 (2010).
- [14] IAEA-SSG-4, "Development and Application of Level 2 Probabilistic Safety Assessment for Nuclear Power Plant", IAEA, Vienna (2010).
- [15] Yang J., et. All., "Simulation and Analysis on 10-in. Cold Leg Small Break LOCA for AP1000", *Annals of Nuclear Energy*, Vol. 46, pp. 81-89 (2012).
- [16] Guozhi Z., Xinrong C., Xingwei S., "A Study Using RELAP5 on Capability and Instability of Two-phase Natural circulation Flow Under Passive External Reactor Vessel Cooling", *Annals of Nuclear Energy*, Vol. 60, pp.115-126 (2013).

Conference Paper

Flexblue® Underwater Reactor: Introduction to the Concept and to the Passive Safety Strategy for a Steam Generator Tube Rupture Accident

Vincent GOURMEL, Fabien PUCETTI, François REVAUD

DCNS, 143 bis Avenue de Verdun, 92442 Issy-les-Moulineaux, France

Abstract

Nuclear power plants (NPPs), which are operating and under construction are large-scale reactors with an electrical output around 1,000 MWe. These plants do not address the needs of developing countries or archipelagos, where the grids are smaller and the investment capacities are limited. For this reason, many nuclear designers develop Small Modular Reactors (SMRs), which can generate electrical output below 300 MWe. DCNS offers a FLEXBLUE® as a solution to the problem. FLEXBLUE® is a subsea-based Small Modular Reactor and fully transportable nuclear module. A FLEXBLUE® module is designed for the single purpose of delivering electricity to the grid. Its power output is 160 MWe and is sent to the grid by submarine cables. The goal of this study is to work out an innovative strategy to handle a steam generator tube rupture with passive systems only, without releasing any radioactive elements to the environment, and without flooding the containment.

Corresponding Author:
Vincent GOURMEL,
email: vincent.gourmel@
dcnsgroup.com

Received: 29 July 2016
Accepted: 21 August 2016
Published: 21 September 2016

Keywords: FLEXBLUE®, Small Modular Reactors, steam generator tube rupture, passive safety system

Publishing services
provided by Knowledge E

© Vincent GOURMEL. et al. This article is distributed under the terms of the [Creative Commons Attribution License](#), which permits unrestricted use and redistribution provided that the original author and source are credited.

Selection and Peer-review under the responsibility of the ICoNETS Conference Committee.

 OPEN ACCESS

1. Introduction

Nowadays, most of nuclear power plants (NPPs) operating in the world or under construction are large-scale reactors with an electrical output around 1,000 MWe. This offer corresponds to the needs of large power grids like those in Europe, USA, Japan or China where electrical connections are powerful and utilities can afford a huge initial investment. However, these units are too powerful to fit in smaller grids where they would represent more than 10% of the installed capacity.

Thus, current nuclear offer does not address the needs of developing countries or archipelagos, where the grids are smaller and the investment capacities reduced. This is why many nuclear designers are developing new concepts of NPPs: Small Modular Reactors (SMRs). Electrical output of these future plants will be below 300 MWe. The financing would be eased by a more progressive capital expenditure, a shorter construction time and an accelerated return on investment [1]. The large reactors "economies of scale" are replaced by small units "economies of number" (series effect, learning effect, shared support facilities).

But the small modular reactors costs are still penalized by important civil engineering work since reactor system is sealed into large underground concrete structures. Furthermore,

there is significant energy demand in areas where land is scarce, highly populated or unsuitable for the construction of NPPs – because of the threat of natural hazards for example. Based on these two ascertainments, DCNS has imagined a solution to address the energy needs of such countries, without requiring a suitable construction land and without high civil engineering cost. This solution is FLEXBLUE[®], a subsea-based Small Modular Reactor.

DCNS is a French state-owned company, which has been designing, building, maintaining and dismantling ships of the French Navy and many foreign Navies for several centuries. DCNS engineering offices and shipyards have especially designed and built nuclear submarines and nuclear aircraft carriers during the last 50 years. Not less than 17 nuclear-propelled ships have been delivered by DCNS teams.

The goal of this study is to work out an innovative strategy to handle a steam generator tube rupture (SGTR) with passive systems only, without releasing any radioactive elements to the environment, and without flooding the containment. A SGTR is a major accident for Pressurized Water Reactors. Indeed, when a PWR is at power, the steam generator (SG) tubes form both the second and the third confinement barriers because the main steam lines at SG outlets bypass the containment. When a rupture occurs, possibly contaminated primary fluid flows out the containment to the secondary system.

2. The Flexblue[®] Concept

Location and Lifecycle

FLEXBLUE[®] is a subsea and fully transportable nuclear module. Its power output is 160 MWe and is sent to the grid by submarine cables. The module is anchored on the seabed, a few kilometers away from the shore, at an immersion depth comprised between 50 and 100 meters. The module is a 150-meter long, 14-meter diameter horizontal cylinder. Several modules can be gathered into a FLEXBLUE[®] farm. The module is remotely operated from an onshore control center. There is not permanent staff on board, only occasional presence for light maintenance. A FLEXBLUE[®] module is not a submarine: it is not self-propelled; it does not use any military devices but only civilian technologies. It is designed for the single purpose of delivering electricity to the grid.

Once set up on the seabed, the reactor starts a 40-month production cycle. Then, production stops for refueling. The module is removed and transported by a ship to a coastal support facility where the spent fuel pool is located. Then the module is sent back on production site and a new cycle begins. Major maintenance and control occur every ten years (every three fuel cycles). FLEXBLUE[®]'s lifecycle is presented in Fig. 1 and its module main characteristics are shown in Table 1.

3. Construction

FLEXBLUE[®] will be completely manufactured in factories and then assembled in a shipyard, using naval modular construction techniques that DCNS perfectly masters. Components can be made in different places in parallel, which reduces the construction time. Then, they are mounted on modular structures named 'skids'. The skids are finally inserted into the hull. Compared to a large outdoor construction site, this industrial process enables a very modular assembly, a reduced construction time and a better quality of the work (which eases the compliance demonstration). Thus, the industrial risk is reduced.



Figure 1: Artist views of a FLEXBLUE® module lifecycle: a) the subsea production site and the onshore control center; b) the ship transport; c) the support facility for refueling and maintenance; d) the transport back to the production site.

TABLE 1: FLEXBLUE® module main characteristics.

Parameter	Value
Unit power rating	160 MWe
Length / diameter	150 m / 14 m
Immersion depth	100 m
Cycle length	40 months
Lifetime	60 years

The construction cost of a SMR is supposed to be higher than the one of a large NPP, because of the economies of scale [2]. However, economies of scale are not the only ways to decrease the capital cost per MWe. There are many SMR specific factors that make the capital cost of a SMR close to the one of a large reactor:

1. Co-siting: when several units are built on the same site (like a FLEXBLUE® farm), capital cost is reduced because a lot of work is shared (geological studies, site licensing process, public acceptance, grid connection).
2. Modular design: as explained in the previous section, a modular design and a modular construction contributes to reduce the cost of a nuclear unit.
3. Series effect: because of their small output, the scheduled number of SMRs is high. Thanks to this serial production, there will be a “learning effect”: the Nth-of-a-kind will be less expensive as N is growing.
4. Shared facilities: SMRs will make possible an increased mutualisation of support functions which is cost efficient. In the FLEXBLUE® concept, the control centre operates an entire farm. The support facility (refuelling, waste management, maintenance) is shared between several modules and even several farms.
5. No civil engineering: this factor is FLEXBLUE® specific. The module does not require any expensive and time-consuming large concrete building like typical NPPs and other SMRs.

By considering the beneficial of those factors, SMRs can be competitive againts the usual large NPPs, and generally in the energy market [2].

DCNS analysis leads to the same conclusion, and shows that the levelized cost of energy produced by a FLEXBLUE[®] module will be between 100 and 120 €/MWh. This cost is slightly higher than electricity cost from new NPPs but still very competitive in the energy market. Besides, the investment required is much more progressive and make the nuclear energy accessible for utilities which have not the capacity to finance the upfront cost of a large NPP [3]. The market that FLEXBLUE[®] addresses is very large. An important share of human activity and population is located near seawater, so electricity demand is high on the coastlines. FLEXBLUE[®] is the only nuclear solution to deliver electricity at a short distance of a coastal highly populated area without compromising safety. In addition, immersion is a great protection against many natural hazards like tsunamis or earthquakes (the module will be attached on the seabed by anti-seismic studs). FLEXBLUE[®] also answers to the needs of countries eager to create local qualified jobs and to reduce their reliance on fossil fuels (to be more independent energetically or to reduce their greenhouse gases emissions, or both). For a new-comer country in nuclear energy, FLEXBLUE[®] offers the possibility of investing at one's own speed. This flexibility is a key asset in today's uncertain energy market.

Impact

The FLEXBLUE[®] concept offers valuable differentiating advantages compared with other NPPs in terms of impact. Indeed, immersion is much more an opportunity than a risk. First, there is no visual impact: the power plant is not visible. Then, there is no population in the vicinity of the module. FLEXBLUE[®] is the only solution to produce high quantities of electricity without requiring a single square meter of land and without being nearby of any population. As a consequence, no relocation of the population has to be envisaged in case of a severe accident: the land is entirely preserved.

About the environmental impact, one of the objectives of FLEXBLUE[®] early-stage design is to reduce the generation of waste. In particular, there is no soluble boron needed to control the core. It contributes a lot to the reduction of effluents production. Thus, a module does not release any radioactive liquid effluents during the fuel cycle. Storage capacities are foreseen, and liquid effluents will be collected and treated every three years by the support facility. Another great asset of FLEXBLUE[®] is its removability. The installation of modules is fully reversible because there is no large concrete structure. Thus, no dismantling is needed onsite at the end of the plant lifetime. The intact site will be quickly restored to the environment. This full removability also authorizes modules to change production site along their 60-year lifetime. Dismantling of the module will take place in an appropriated shipyard, like it has already been done for several retired nuclear submarines.

Thanks to these unique features, unmatched in the nuclear field, FLEXBLUE[®] is respectful of the environment and more easily acceptable for the population. It makes the nuclear energy more accessible to countries eager to develop their electrical production with clean, safe, reliable and low-carbon solutions.

Reactor

FLEXBLUE[®] uses the most reliable and proven nuclear technology both for electricity production and naval environment: a Pressurized Water Reactor (PWR). More than 60% of currently operated NPPs in the world are PWRs, and more than 90% of nuclear submarines host a PWR. Even though FLEXBLUE[®] is an innovative concept, it only relies on proven technologies and mostly uses offthe-shelf components. No risky development is needed. FLEXBLUE[®] PWR is a

two-loop reactor, with a pressure vessel, two horizontal recirculating steam generators (SGs), two canned coolant pumps and a pressurizer as shown in Fig. 4. Primary loops are designed to ease natural circulation. Meanwhile, FLEXBLUE® reactor characteristics are given in Table 2 [4].

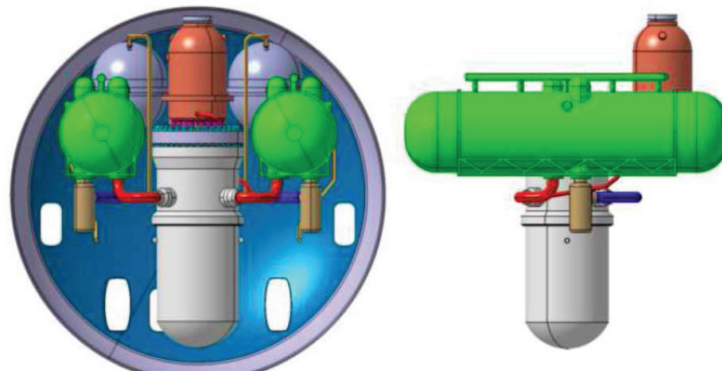


Figure 2: Cross view and profile view of FLEXBLUE® reactor. The coolant pumps (brown) are located at the outlet of SGs (green).

TABLE 2: FLEXBLUE® reactor characteristics.

Parameter	Value
Thermal power	530 MWt
Reactor core	77 fuel assemblies
Fuel assembly	17 x 17 rods, 2.15 m high
Enrichment	< 5%
Average power density	70 kW/L
Reactor coolant pressure	155 bars
ΔT core	30 °C
Steam generators	2 recirculating SGs
SGs pressure	62 bars (saturated)

The primary system and all the auxiliary and safety systems that carry primary fluid are located inside the reactor compartment of the module as shown in Fig. 3. This compartment forms the third barrier of confinement (the first one is the fuel cladding and the second one is the primary system pressure boundary). The other compartments host the turbo-generator, an on board control room, instrumentation and control panels, process auxiliaries and a living area for occasional workers.



Figure 3: Profile view of a FLEXBLUE® module.

Safety Concept and Safety Systems

FLEXBLUE® is based on a unique safety concept: a full passivity and an unlimited grace delay. It is the greatest asset of immersion: ocean around the module forms an infinite heat sink for the passive heat removal systems in case of an accidental transient. The safety systems

are designed in order to operate passively according to the IAEA passivity definition [5]. All safety functions are fulfilled without any operator action and external electrical input. The little amount of energy needed at the beginning of a transient for actuation and monitoring is supplied by on board, redundant emergency batteries.

In addition, the onshore control center hosts emergency generators that can supply active systems in the module through submarine cables in case of abnormal transients, but none of those are safety-related. Nuclear safety is fully guaranteed by the passive devices located into the module.

This safety concept is inspired by the lessons learned from previous nuclear accidents in the world, especially the Fukushima Daiichi accident. In the FLEXBLUE[®] concept, safety does not depend neither on emergency diesel generators (that have been flooded by the tsunami in Fukushima) nor on human intervention (that can lead to mistaken actions). Safety only relies on some automatic operations, and mainly on permanent natural phenomena: gravity and natural circulation of water between a heat source (the core) and a heat sink (the ocean). This makes the FLEXBLUE[®] safety concept very robust.

Reactivity control

If an emergency signal is actuated by an abnormal situation in the reactor, chain reaction can be stopped passively by two diversified devices. The first one is the control rods that drop in the core by gravity. The second one is the gravity-driven emergency boron injection system, which is actuated only in case of anticipated transient without scram. Both these devices can independently shutdown the reactor and keep it subcritical up to cold shutdown state [4].

Core cooling

The core residual heat after scram is removed by four cooling loops, each one able to transfer 50% of decay heat:

- i. Two primary chains are connected to the primary circuit: each one includes an inlet pipe connected to a hot leg, a passive primary heat exchanger (PPHX) immersed in a large safety water tank, and an outlet pipe connected to a cold leg. The intermediate heat sink formed by the safety tank is cooled by the ocean through the metallic hull.
- ii. Two secondary chains are connected to the secondary circuit: each one includes an inlet pipe connected to a main steam line, an emergency condenser (EC) directly immersed in seawater and an outlet pipe connected to a feedwater line.

Thanks to the infinite heat sink – seawater – and to the elevation difference of the heat sink with respect to the heat sources, the four chains operate passively by natural circulation. In normal conditions operation, they are closed by pneumatic valves and open to their fail safe position when electrical load is lost. The targeted long-term safe state of the reactor is a shutdown state where continuous cooling of the reactor core is achieved by natural circulation as shown in Fig. 4.

Protection against loss-of-coolant accidents is ensured by two passive safety injection trains. Each one includes a direct vessel injection line fed by three injection sources: a core makeup tank (CMT) pressurized by the primary circuit, a classical accumulator (Acc) pressurized at 40 bars by nitrogen and a large safety tank which feeds the primary circuit by gravity when primary pressure has decreased to near containment pressure. In addition, a two-train automatic depressurization system (ADS) is connected to the pressurizer (PZR) and to the hot legs to generate a controlled depressurization of the primary circuit which enables faster

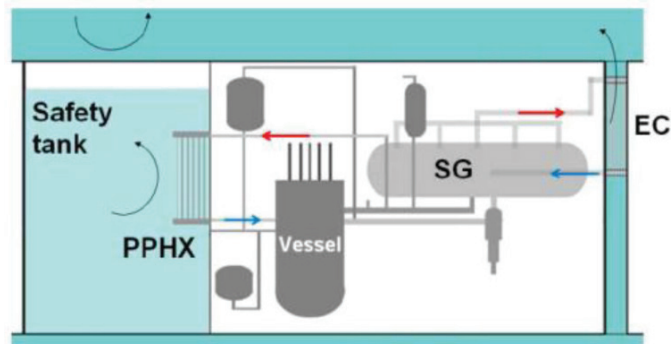


Figure 4: Targeted safe state when primary circuit is intact.

injection. Once these systems have actuated, the long-term equilibrium state is reached when the safety tanks are empty and the reactor compartment is flooded as shown in Fig. 5. At that point, a passive recirculation path is in place: water boils off the core, is released in the containment, condensates on the containment walls, collects in the sump and is injected back into the reactor pressure vessel through sump screens and direct vessel injection lines by gravity as shown Fig. 6. Decay heat is transported and removed through the metallic hull. Thanks to the unlimited heat sink (the ocean), grace period is theoretically infinite for both targeted safe states, which is a breakthrough in nuclear safety.

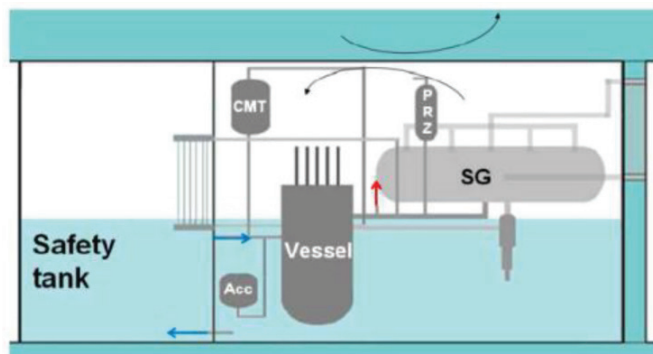


Figure 5: Targeted safe state when primary circuit has failed.

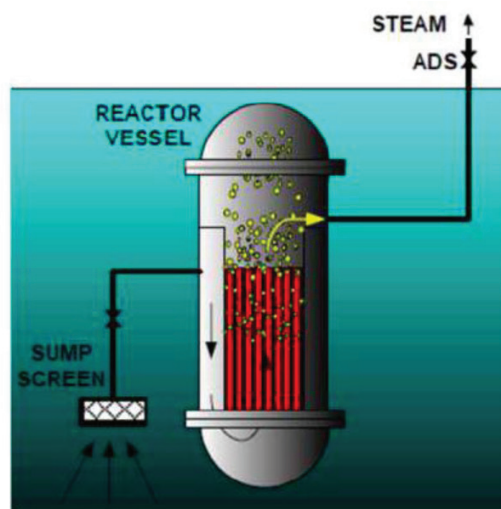


Figure 6: Core cooling by sump natural circulation [5].

Radioactivity confinement

Confinement of the radioactive isotopes is guaranteed by three hermetic barriers: the fuel cladding, the primary circuit pressure boundary and the containment boundary. The latter one is formed by the hull and the reactor compartment walls and is designed to sustain a 10-bar internal pressure. To protect its sealing against over pressurization, it is equipped with a Pressure Suppression System as shown in Fig. 7. Indeed, in case of a break in the primary or secondary systems, the pressure in the reactor compartment quickly rises. The pressurized air-vapor mixture in the drywell is passively driven to the bottom of the wetwell where the vapor is condensed. It significantly reduces the pressure in the drywell.

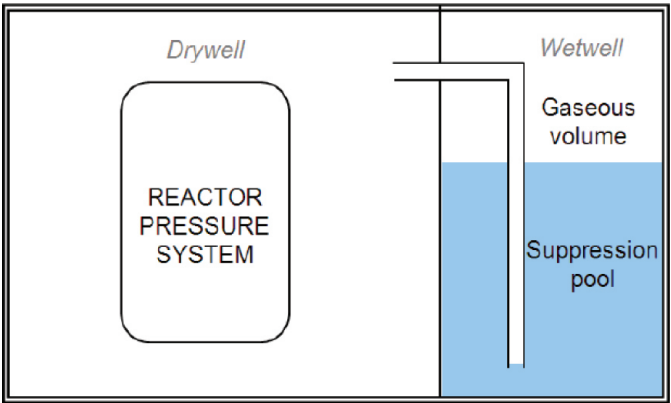


Figure 7: Diagram of the Pressure Suppression System (PSS).

Complements

The large safety tank in the reactor compartment plays three important roles: intermediate heat sink for the passive primary heat exchangers; low-pressure injection source in case of a loss of coolant accident; suppression pool to protect the containment sealing. They also act as an efficient radiation shield to protect workers and systems located in the adjacent compartment.

The capability of the hull to reject decay heat to seawater is a key point of the safety concept. It is needed to cool the safety tank and to condense vapor in the containment. FLEXBLUE® hull heat transfers have been investigated [6]. Results show the great potential of the design to remove residual power to the heat sink as shown in Fig. 8.

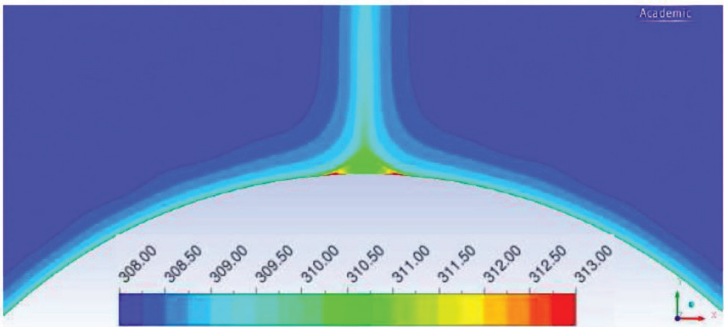


Figure 8: Seawater temperature field (K) around the top of the hull when hull internal surface temperature is 373K and initial seawater temperature is 308K [6].

Severe accidents

The availability and the infinity of the ocean around the hull make the likelihoods of core damages extremely low. Still, the reactor coolant system and the containment are designed to sustain a core melting. The mitigation strategy consists in in-vessel retention of the corium. It is possible thanks to an external cooling of the vessel by water provided by the safety tank. In a review of in-vessel retention state-of-the-art [7], the French Institute for Nuclear Safety asserts that this strategy is feasible for SMRs with appropriated cooling circuit around the vessel.

Compliance

FLEXBLUE® safety concept complies with latest international safety standards (Gen. III+): IAEA standards and guides, Western Nuclear Regulators Association and French Safety Authority technical guidelines, as well as French post-Fukushima requirements.

4. Goal of the Study

Context

FLEXBLUE® has very ambitious safety objectives: any accidental transient must be handled by passive safety systems and must end on a safe shutdown state without external electrical input and without human action. To assess the capability of the safety features to complete these objectives, the reactor and its systems have been modeled with an advanced computer code (see description in the next section). Up to now, many accidents have been simulated thanks to this model. Accident analyses of the first studied transients are [8]:

- Turbine trip accident
- Small break Loss Of Coolant Accident (LOCA)
- Large break Loss Of Coolant Accident

All of these accidents have been cumulated with a Station Black-Out (SBO), so that only the passive devices are used to mitigate the accident. The results provided by the computer code show that the systems are appropriately designed: the safety criteria are respected with significant margin and the reactor always ends on a safe shutdown state which is not limited by any given mission time. The accident analyses continued with another important transient: a steam generator tube rupture (SGTR).

Steam Generator Tube Rupture

A SGTR is a major accident for Pressurized Water Reactors. Indeed, when a PWR is at power, the SG tubes form both the second and the third confinement barriers because the main steam lines at SG outlets bypass the containment. When a rupture occurs, possibly contaminated primary fluid flows out the containment to the secondary system.

On current land-based PWRs, atmospheric steam discharge valves are used to cool down the secondary system, which is contaminated by primary water after the rupture. The affected SG is then isolated by the operator, so the radioactive leak is stopped. But one can see that radioactive elements are rejected to the environment, and their amount is highly dependent on the celerity of the operator in the control room. Regarding the safety objectives of FLEXBLUE®, this accident management is not satisfactory.

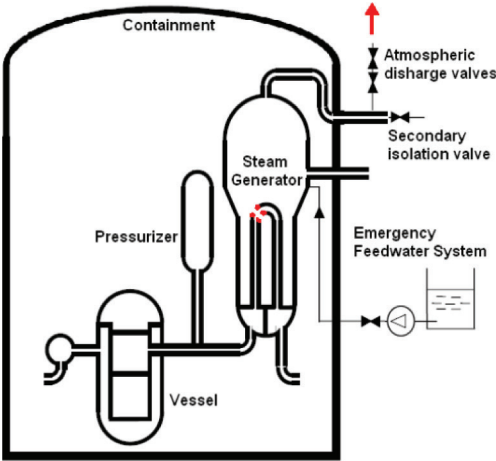


Figure 9: Steam generator tube rupture and radioactive releases to the environment on a typical land-based Pressurized Water Reactor.

The easiest strategy to manage a SGTR in the FLEXBLUE[®] reactor is to consider the tube rupture as a small break LOCA as shown in Fig. 9. The accident analysis of this transient is presented in [8]. This strategy is acceptable: all the safety criteria are respected. However, the consequences on the availability of the plant are important. The reactor compartment is flooded with primary water and it would take time to restore the operability of the plant.

5. Analysis Tool and Reactor Model

Athlet

ATHLET (Analysis of Thermal-Hydraulics of Leaks and Transients) is a thermal-hydraulic system code developed by the German technical safety organization GRS. It is applicable to the analysis of light water reactors, and has already been used for the analysis of transients involving horizontal SGs, similar to the ones of Flexblue[®]. It is composed of four main calculation modules: thermofluid dynamics, heat transfer and heat conduction, neutron kinetics, and control & balance of plant.

Modelisation

FLEXBLUE[®] reactor is modelled with ATHLET in accordance with GRS guidelines [9, 10]. The nodalization of the circuits is performed in order to get both a sufficient accuracy and an acceptable calculation time. Two core channels are modelled: an outer ring and an inner channel where power density is higher. In this latter one, the hot fuel pin is modelled to calculate peak clad and fuel temperatures. The two loops are modelled, as well as all the safety systems with the exception of the emergency boron injection system (failure of scram is not considered in the studied transients). Pressurizer and piping are considered perfectly insulated. The injection sources (tanks and accumulators) are not borated. The active auxiliary systems and the regulations are modelled for this study.

Indeed, their effect can be penalising. For example, if the chemical and volume control system is running after a SGTR, it increases the flow rate through the leak. A special attention is given to these active systems during the study, in order to ensure that only the penalising effects are considered. The diagram of the ATHLET model is showed on Fig. 10.

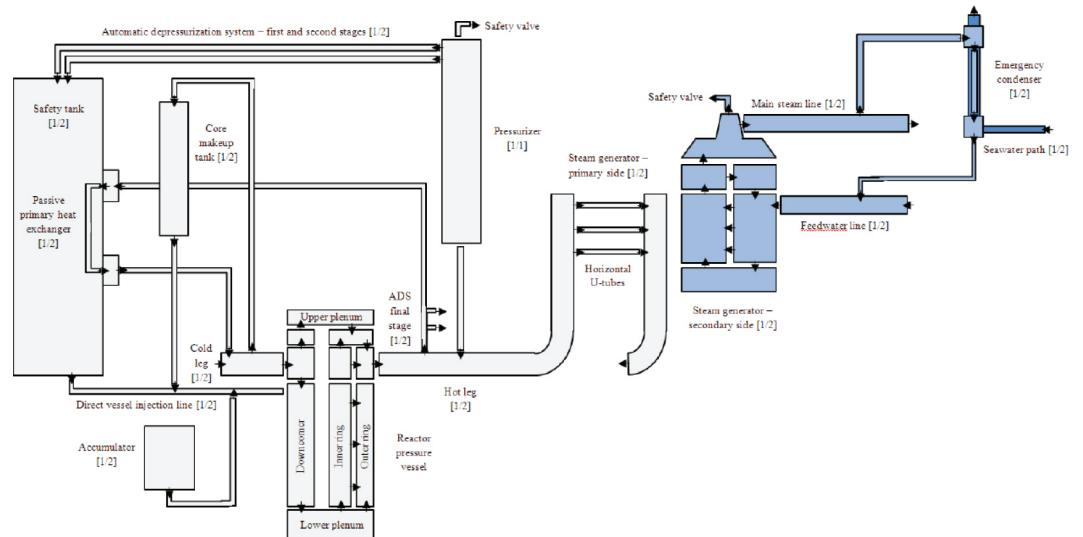


Figure 10: ATHLET model. Dimensions are not representative.

The model considers a 2.5-second delay between the scram signal and the full insertion of control rods. Decay heat calculation is based on formulas from [11], which are extracted from standards of American Nuclear Society [12], and then conservatively increased by 20% to respect NRC guidelines [13]. Fig. 11 presents the considered decay heat for the accident analyses.

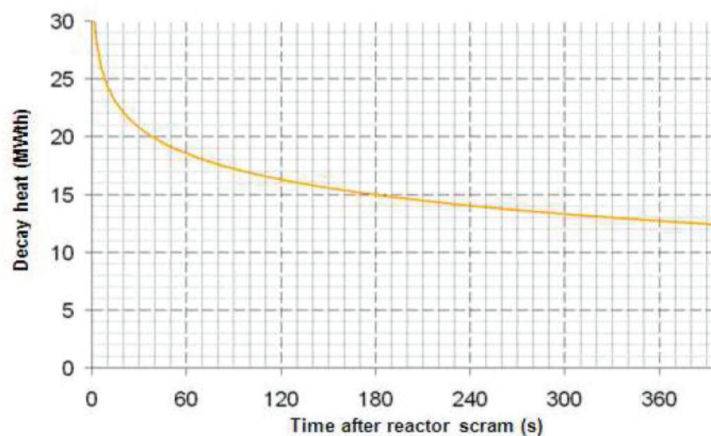


Figure 11: Decay heat of FLEXBLUE® core.

Reactor core is at 100% of its nominal power (530 MWth) at the beginning of the transient. A loss of electrical load is assumed just after the beginning of the transient. The only electrical sources available are the emergency batteries, able to monitor and control the safety systems, and to open or close some valves. The action of other active systems is considered only if they have a penalising effect. The opening time of the valves is 2 seconds. Pressurizer and steam generators safety valves setpoints are respectively 171 bars and 83 bars, with a one-second opening time. Even if it is planned to install flow restrictors in the pipes, their effects are not taken into account in the accident analysis, which is a conservative measure.

Heat transfer between safety tanks and seawater through the metallic hull is not modelled, which is conservative. None of the steam generators tubes is considered clogged. The actuation logic of emergency signals and passive systems with the treatment delays considered are presented in Table 3.

TABLE 3: Safety signals (conservative delays for actuation).

Signal	Trigger(s)	Delay
Reactor protection	High containment pressure or low pressurizer pressure	0.9 s
Reactor scram	Reactor protection or low pump speed or high pressurizer pressure	1 s
Coolant pump stop	Reactor protection or reactor scram or ADS first stage opening or low pressurizer level	3 s
Feed and steam lines isolation	Reactor protection or turbine trip	0.15 s
Core makeup tank injection	Reactor protection or low pressurizer level	2 s
Emergency condenser actuation	SG high pressure (75 bars) or passive primary cooling actuation	0.5 s
Passive primary cooling actuation	CMT injection or high pressurizer level	4 s
ADS opening	CMT injection and low level in both CMTs	20 s

6. Elaboration of a New SGTR Strategy

As stated previously, the FLEXBLUE® strategy in case of a SGTR must avoid the flooding of the containment and lead to a safe shutdown state where primary system is closed (Fig. 6). The flooding of the containment is caused by the depressurisation of the primary system and the injection of the low-pressure safety tank. These two events happen only when the low-level signal is actuated in the core makeup tanks (the first tanks that inject water in the vessel after a LOCA). To avoid the flooding, it is mandatory not to trigger this signal (see red cross on the process in Fig. 11) and then to keep the CMTs filled with water – at least partially. This is possible if the amount of coolant lost through the SG tube rupture is reduced.

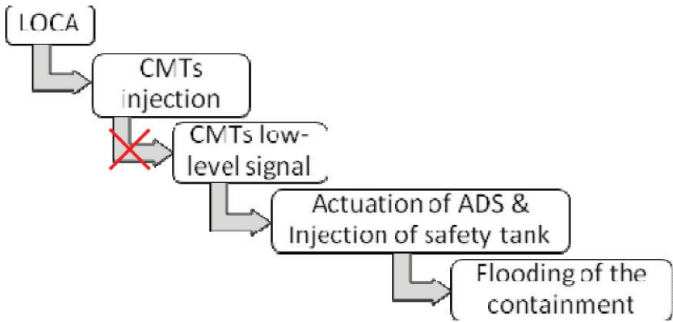


Figure 11: Logical process leading to the containment flooding.

The driving force of this leak is the difference between the primary pressure and the pressure in the affected steam generator (respectively 155 bars and 62 bars at nominal conditions). The most efficient way to reduce the loss of coolant through the leak is to eliminate as quickly as possible this difference of pressure. Two parallel actions must be implemented in the SGTR mitigation strategy:

1. Decrease the primary pressure. The opening of the depressurisation valves is not an option because the containment must not be flooded. So, the passive primary heat exchangers and the passive secondary emergency condensers will be used to remove decay heat from the primary system and decrease its pressure.

- 2. Increase the pressure in the affected SG. Usually, SG pressure is reduced by the corresponding emergency condenser (EC). If the condenser is closed, the SG pressure will increase. However, this action is limited by the SG safety valves: they will open and discharge steam in the safety tank if the pressure exceeds 83 bars.

Another concern is the detection of the accident. Unlike a large break LOCA, a SGTR is a small leak and is not easy to detect. Three signals must be closely monitored:

- a. Abnormality in the operation of the primary volume control system. This signal indicates that something is wrong in the balance of primary fluid inventory.
- b. Abnormality in the regulation of SG water level. This signal indicates that something is wrong in the balance of secondary fluid inventory.
- c. Detection of Nitrogen-16 in the secondary system. This isotope with a 7-second half-life is an activation product of primary water. It is not supposed to be present in the secondary system.

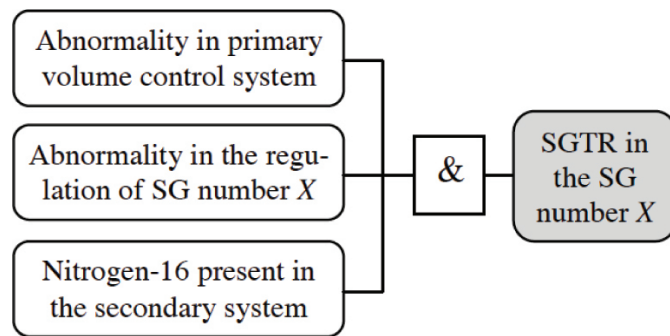


Figure 12: SGTR detection in the FLEXBLUE® reactor.

The concomitance of these three criteria (Fig. 12) points out beyond doubt that a steam generator tube rupture has occurred and that an appropriated strategy must be launched to mitigate the consequences. Three strategies are investigated in the following sections. The affected SG is always the SG number 2.

Option A

The leading idea of option A is to lock the emergency condenser of the affected SG in a closed position, as soon as the SGTR is detected.

The primary and secondary pressures are displayed in Fig. 13. The transient begins by 400 seconds of steady state at full power. Then, the computer code simulates the rupture of one tube in steam generator number 2. Fifty seconds later, the rupture is detected. It triggers automatically numerous protections measures: the chain reaction is stopped by the drop of control rods, the secondary isolation valves are closed, the CMTs injection valves are opened and the passive primary heat exchangers (PPHXs) are connected. Moreover, all the active systems (including the primary pumps) are stopped, except the ones with penalizing effect (e.g. the primary volume control system).

The closing of secondary isolation valves leads to a sudden pressurization in both SGs. When SG1 pressure reaches 75 bars, the emergency condenser n°1 (EC1) is connected, and the pressure starts to decrease. SG2 pressure continues to increase, because the emergency condenser has been locked by the SGTR signal. When the pressure reaches 83 bars, the safety valves are

passively opened. During 1,000 seconds, there are several discharges of secondary steam through the safety valves. Meantime, the primary pressure strongly decreases, thanks the combined action of the two PPHXs, the EC1 and the safety valves of SG2. At t=1800s (23 minutes after the tube rupture), the balance between primary pressure and SG2 pressure is achieved: the leaks stops.

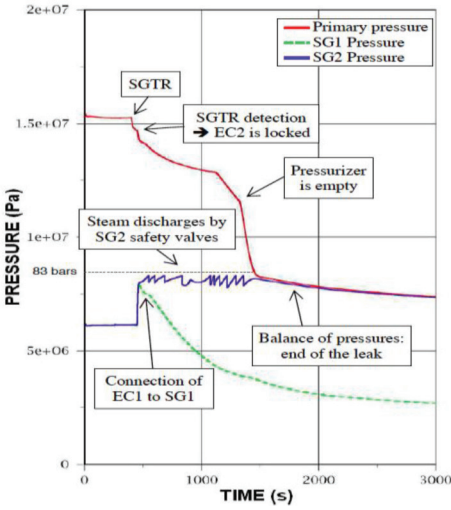


Figure 13: Primary and secondary pressures after.

This strategy fully respects the safety criteria and ends on a safe shutdown state where the primary system is closed and the containment is not flooded. But there is one major negative impact: the several discharges through the SG2 safety valves have contaminated the safety tank with 271 kg of activated steam. Indeed, the safety valves discharges are collected by the safety tank, and the fluid in SG2 is slightly activated because of the tube rupture. This consequence is not a safety issue, because the safety tank is located into the containment (the confinement is not by passed). But it is detrimental for the availability of the plant because the decontamination of a large tank is time consuming. The objective of the next options will be to handle the accident without requiring to the safety valves.

Option B

In this option, the command of the emergency condenser (EC) of the affected SG is modified. Instead of locking its opening, the state of the emergency condenser depends on the pressure in the affected SG, as shown in Fig. 14. If the pressure exceeds 80 bars, the condenser is opened and the pressure decreases. When the pressure drops below 70 bars, the condenser is closed and the pressure increases again. The cycle can repeat itself several times. The safety valves are not requested because the pressure always remains below 83 bars. The leak is quickly stopped because the pressure in the affected SG remains rather high (above 70 bars).

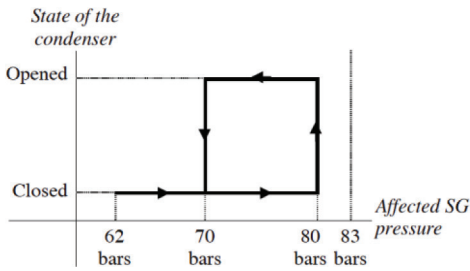


Figure 14: Option B actuation logic for the emergency condenser connected to the affected SG.

As shown in Fig. 15, the evolution of the pressures with the option B strategy is quite similar to option A (Fig. 13). The difference lies in the management of emergency condenser n°2. It is opened then closed three times before the balance of pressures is established. This balance comes a little bit later than in option A (27 minutes after the tube rupture). The objective of not requesting the safety valves is reached: there is no radioactive contamination outside the affected steam generator. Yet, a new issue is raised by option B strategy. The IAEA definition of passive systems presented in [5] and detailed in [14] specifies that “valves used to initiate safety systems operation must be single-action relying on stored energy”. The valves used to connect the emergency condenser to a steam generator rely on stored energy (on board batteries). But they are not single-action in option B strategy. They are opened and closed several times. The safety system forms by the emergency condenser and its valve cannot be called passive. A new challenge is to be addressed in the next option: mitigate the SGTR only with single-action valves.

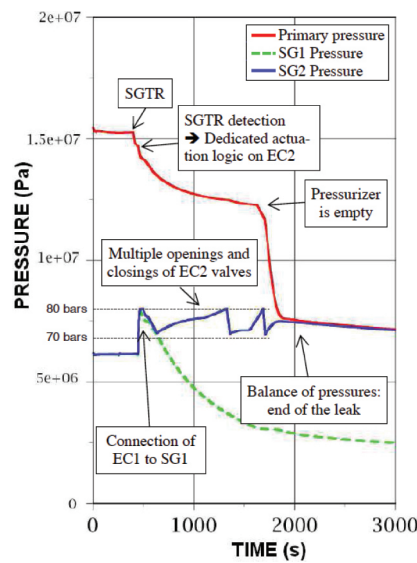


Figure 15: Primary and secondary pressures after a SGTR in steam generator n°2 with option B strategy.

Option C

Option A proves that it is impossible to avoid using the emergency condenser of the affected steam generator: the safety valves would discharge activated steam. The affected SG should be cooled and slightly depressurized in the first stage of the accident. Then, the pressure can increase again to achieve the balance of pressures. But the two parallel valves that connect the condenser to the SG (valves “A” on Fig. 19 and Fig. 20) must operate only one action. To solve this problem, a new valve - “B” in Fig. 16 and Fig. 17 - is added close to valves “A”. Valve “B” is open in normal conditions and remains open in most of accidental conditions. This valve is closed only if the two following signals are actuated simultaneously:

- a. SGTR detection in the steam generator
- b. Low-pressure in the primary system (80 bars)

This low primary pressure value has been chosen lower than the opening set-point of the SG safety valves (83 bars). Thus, it is highly unlikely that the safety valves will be required if valve “B” is closed. Valve “B” is a pneumatic valve, just like valves A. But it is not managed by the usual compressed air system: valve B is managed by a dedicated air tank (see Fig. 19). This measure is important to prevent the closing of both emergency condensers in case of compressed air system failure.

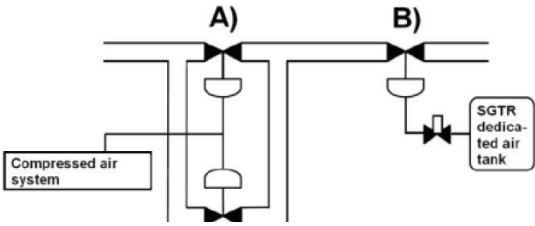


Figure 16: New layout of the emergency condenser valves.

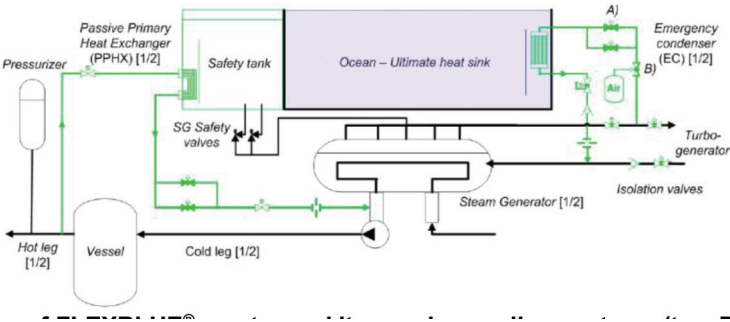


Figure 17: Diagram of FLEXBLUE® reactor and its passive cooling systems (two PPHXs and two ECs). Valve “B” is specific to option C of the SGTR mitigation strategy.

In the option C strategy as in Fig. 18, the affected SG is depressurised during the first stage of the accident by the automatic opening of valves A. When the reduction of primary pressure is considered sufficient (below 80 bars), valve B is closed. The affected SG pressure increases and the balance is done with the primary pressure. This balance comes a little bit later than in previous options (28 minutes after the tube rupture). With the new layout and the new actuation logic, each valve is single-action so the management of the accident is fully passive. The transient ends on the targeted safe shutdown state where primary system is intact, without external electrical input and without operator action. There is absolutely no radioactive release to the environment, but only a limited release to the turbo-generator before the detection of the tube rupture.

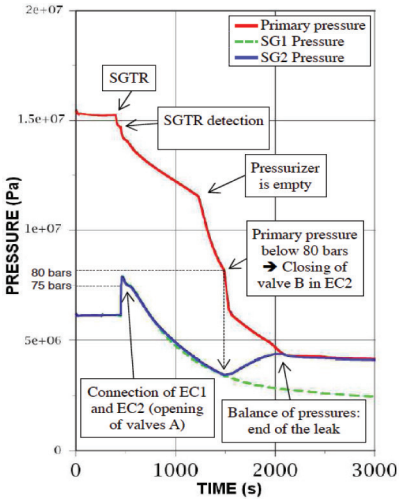


Figure 18: Primary and secondary pressures after a SGTR in steam generator n°2 with option C strategy.

7. Conclusion

The purpose of this paper was first to present an innovative nuclear concept. FLEXBLUE® is a subsea based small modular reactor with inherent advantages in terms of siting, economics, impact and safety. In particular, the immersion of the plant is a great opportunity to protect the reactor from many hazards (storm, tsunami, earthquake, plane crash, extreme air temperature) and to provide the safety systems with an infinite heat sink. This later characteristic allows the implementation of very ambitious safety objectives. FLEXBLUE® safety concept relies on a full passivity. Every single accidental transients – including core melting – can be handled with passive systems only, without external electrical input, without operator action, and without any radioactive release to the environment. These objectives are highly relevant in the post-Fukushima context. The second goal of the paper was to work out a new strategy in case of a steam generator tube rupture. Initial strategy was safe but had an important impact on the availability of the plant. It comes out of this study that a new strategy is possible: the option C strategy presented in the previous section. With a new valve on the emergency condensers inlet lines and an appropriated automatic command, it is possible to manage a SGTR with passive devices, without radioactive releases and with a very limited impact on the plant. Neither the containment nor the safety tank is contaminated. The leak of activated primary water is mostly confined to the affected steam generator and its emergency condenser. The safe state reached at the end of the transient is not limited in time because the heat sink is infinite.

8. Acknowledgments

The authors would like to thank GRS for their technical support in the use of ATHLET. The authors are also grateful for the help, the comments and the review provided by other members of FLEXBLUE® development team, especially G. Haratyk and J. Masdupuy.

NOMENCLATURE

ADS	:	Automatic Depressurization System
CMT	:	Core Makeup Tank
EC	:	Emergency Condenser
ICAPP	:	International Conference in Advances for nuclear Power Plants
LOCA	:	Loss of Coolant Accident
NPP	:	Nuclear Power Plant
NUTHOS	:	Nuclear Thermal-Hydraulic, Operation & Safety
PPHX	:	Passive Primary Heat eXchanger
PWR	:	Pressurized Water reactor
PZR	:	Pressurizer
SBO	:	Station Black-Out
SG	:	Steam Generator
SGTR	:	Steam Generator Tube Rupture

References

- [1] R. ROSNER and S. GOLDBERG, Small Modular Reactors – Key to Future Nuclear Power in the U.S., DOE technical paper, chapter 4, University of Chicago Energy Policy Institute, Illinois (2011).

- [2] L. BOLDON et al, "Sensitivity Study of the Factors Affecting First-of-a-Kind and Nth-of-a-Kind SMR Investment Costs", Proc. of ICAPP, Nice, France (2015).
- [3] G. HARATYK, C. LECOMTE and F.X. BRIFFOD, "Flexblue®: a subsea and transportable small modular power plant", Proc. of ICAPP, Charlotte, USA (2014).
- [4] J. J. INGREMEAU and M. CORDIEZ, "Flexblue® core design: Optimisation of Fuel Poisoning for a Soluble Boron Free Core with Full or Half Core Refuelling", Proc. of ICAPP, Nice, France (2015).
- [5] IAEA, "Passive Safety Systems and Natural Circulation in Water Cooled Nuclear Power Plants", IAEA-TECDOC-1624, Vienna, Austria (2009).
- [6] M. SANTINELLO et al., "CFD investigation of Flexblue® hull", Proc. of conference NUTHOS-10, Okinawa, Japan (2014).
- [7] IRSN (French Institute for Radiological Protection and Nuclear Safety), "Elements of reflection concerning corium retention in the reactor vessel", Opinions and experts reports, France (2014).
- [8] G. HARATYK and V. GOURMEL, "Preliminary Accident Analysis of Flexblue® Underwater Reactor", Proc. of ICAPP, Nice, France (2015).
- [9] GRS, "ATHLET 3.0 Cycle A - User's Manual", GRSP-1 Vol. 1, Rev. 6 (2012).
- [10] GRS, "ATHLET 3.0 Cycle A - Models and Methods", GRS-P-1 Vol. 3, Rev. 3 (2012).
- [11] N. TODREAS and M. KAZIMI, "Nuclear systems I", CRC Press (1990).
- [12] AMERICAN NUCLEAR SOCIETY, "American National Standard", Decay heat power in light water reactors, ANSI/ANS-5.1-2005 (2005).
- [13] US NRC, "ECCS Evaluation model", 10 CFR Appendix K to Part 50.
- [14] IAEA, "Safety related terms for advanced nuclear plants", IAEA-TECDOC-626, Vienna, Austria (1991).